KINETIC STUDIES IN THE ELECTROCRYSTALLISATION OF METALS

Thesis submitted to the

University of Newcastle upon Tyne

for the degree of

Doctor of Philosophy

D.J. Astley, B.Sc., A.R.C.S.

July 1968

CONTENTS

Chapter 1

Theoretical

1.1 Crystal Growth 2

1.2 Epitaxy 9

1.3 The Metal/Electrolyte Solution Interface 13

1.4 Metal Electrocrystallisation 25

Chapter 2

Experimental

2.1 Introduction 63

2.2 Potentiostat 63

2.3 Function Generators 63

2.4 Recording and Measuring Equipment 64

2.5 Preparation of Electrodes 65

2.6 Electrochemical Cell for Solid Electrodes 68

2.7 Electrochemical Cell for Mercury Electrodes 69

2.8 Reference Electrodes 70

2.9 Cleaning of Glassware 72

2.10 Preparation of Solutions 72

2.11 Electron Microscopy 74

2.12 Optical Microscopy 75

2.13 Electron Diffraction 75

Chapter 3

The Electrocrystallisation of Silver

3.1 Introduction 77

3.2 The deposition of silver upon silver 77

3.3 The deposition of silver upon silver under sweep conditions 80

3.4 The use of inert carbon substrates 89

3.5 The growth characteristics of silver on carbon substrates 91

3.6 The model for the formation of silver nuclei 92

3.7 The electrocrystallisation model 95

Chapter 4

The Electrocrystallisation of Palladium

4.1 Introduction 100

4.2 The deposition of palladium upon carbon 100

4.3 The electrocrystallisation model 101

4.4 Comparison with the silver model 105

Chapter 5

The Electrocrystallisation of Mercury

5.1 Introduction 107

5.2 The reduction of Hg_2^{2+} on Hg 107

5.3 The deposition of Hg onto carbon 109

5.4 The nucleation of Hg on carbon 112

5.5 The significance of Hg results for Ag, Pd models 113

Chapter 6

The Formation of Metal Layers

6.1 Introduction 114

6.2 The potential-sweep measurements 119

6.3 Potential-pulse measurements at short times 126

6.4 Crystal growth processes 130

6.5 A crystallographic explanation of the sweep behaviour 134

Chapter 7

The Electrocrystallisation of Cobalt on Mercury Substrates

7.1 Introduction 139

7.2 The aqueous C_o^{2+} system 139

7.3 The cobalt/thiocyanate system -sweep measurements.... 143

7.4 C_o(11)/thiocyanate - reaction control 146

7.5 C_o(11)/thiocyanate - crystal growth 150

Chapter 8

Summary

8.1 Introduction 155

8.2 Electrocrystallisation of silver on silver 155

8.3 Electrocrystallisation of metals onto carbon substrates 156

8.4 The formation of metal layers 158

8.5 The electrocrystallisation of cobalt on mercury 160

Appendix 1

A finite difference method for obtaining cyclic current/voltage curves 163

Appendix 2

Deposition of a metallic partial monolayer with reversible electron-transfer under potentiostatic conditions 166

Appendix 3

Notation 170

References 176

Chapter 1

Theoretical

Introduction

Metal electrocrystallisation may be defined as the process in which the elementary lattice is grown at a cathode by discharge of metal ions in the electrolyte. It is possible to represent the phenomenon as two consecutive processes, an electrode reaction accompanied by crystal growth. It is therefore pertinent to present short accounts of the concepts currently employed in the theories of crystal growth, epitaxy and the interfacial electrical double layer. Some of the more important theoretical work concerning metal electrocrystallisation will be reviewed. In later chapters measurements on a number of systems of metal electrocrystallisation will be discussed. An account of the processes involved in the electrocrystallisation of silver, mercury and palladium will be presented. This will be followed by a report on the phenomena occurring during the deposition of lead and thallium onto silver electrodes, and cadmium onto lead. Finally a chapter concerning the reduction of cobaltous ions at a mercury cathode will be presented.

1.1 Crystal Growth

Because of the extent of similarity between electro-crystallisation and other crystallisation phenomena, extensive borrowing from theories constructed to interpret crystal growth from melts, from vapour or from solution has occurred. The thermodynamic inequality which drives all crystal growth is the excess electrochemical potential of the reactant phase over that of the crystalline product. Where no charge transfer is involved, the electrical potential difference at the crystal surface does not contribute to the electro-chemical potential difference. In such cases the driving force is referred to more commonly as supersaturation or supercooling respectively. Their electrochemical analogue is overpotential.

Crystal growth from the vapour was first considered by Gibbs[1] (1878) from a thermodynamic standpoint, by analogy with the growth of liquid droplets from the vapour. The condition for stability of a droplet is that its surface free energy, and hence its area, is minimum. Similarly, for a crystal in equilibrium with its surroundings, the surface free energy must be a minimum for a given volume, and those crystal faces will develop which satisfy this condition.

Burton and Cabrera[2] classified crystal faces into two categories; close-packed and stepped surfaces. A close-packed surface is defined as one which, when it is as flat as possible, has all the surface molecules at the same distance from a plane parallel to the surface. All other surfaces are stepped and may be considered as being made up of close-packed layers, so that a close-packed terrace exists between each step.

The growth of a perfect crystal has been considered on the basis of the simple Kassel[3] model in which molecules are represented as cubes subject only to nearest neighbour interactions. A crystal consists of numbers of such cubes stacked face to face. It has been shown[2,4] that for a stepped surface represented by this model, the monomolecular step line is not straight but contains kink sites which represent favourable sites for lattice incorporation of surface adsorbed molecules, since these sites offer a high degree of co-ordination. Indeed a kink site constitutes a repeating stage in deposition; the incorporation of a molecule at a kink does not alter the surface free energy of the crystal. The density of kinks in a step line has been calculated by Burton, Cabrera and Frank[5] who obtained

$$\frac{n}{1-n} = \exp\left(-w/kT\right) \qquad (1.1.1.)$$

where n is the concentration of sites occupied by kinks and w is the energy of formation of a kink and was estimated as $\sim \frac{W}{12}$, where W is the evaporation energy. Since w is small, the number of kinks per unit length of step line is quite high.

Burton et al., also calculated the concentration of surface sites occupied by adsorbed molecules at equilibrium as being approximately

$$n_s = n_o \exp\left(-W_s / kT\right) \qquad (1.1.2.)$$

where Ws is the energy of evaporation from the kinks onto the surface, estimated as $\sim W/2$, and n_o is approximately the total number of sites per cm^2. Comparison of equations (1.1.1.) and (1.1.2.) shows that the concentration of kink sites is considerably greater than that of adsorbed molecules. Thus a step line may be considered as being in equilibrium with the adsorbed molecules in its immediate vicinity and on smooth parts of the surface the adsorbed molecules are in equilibrium with the vapour.

The mean displacement of an adsorbed molecule on the surface, i.e. the average distance travelled before the molecule is re-evaporated, was estimated by Burton et al., who found that the distance is large (typically 400X)

compared with the mean distance between neighbouring equilibrium sites on the surface. Growth of a step thus proceeds predominantly by the incorporation of molecules having arrived by surface diffusion and this is the slow step in the crystal growth process.

Volmer[6] concluded from the observed high growth rate of mercury crystals that adsorbed molecules must diffuse across the crystal surfaces. The overall process was proposed to follow the path: adsorption, surface diffusion to surface steps, and incorporation into the lattice at the half-crystal positions provided by the kinks.

Step lines on a perfect crystal surface will continue to advance until the edge of the crystal is reached whereupon they will disappear, leaving the crystal surrounded by low index planes. Further growth of the perfect crystal requires the formation of new surface steps. Frenkel[4,7] suggested that new steps would be formed by thermal fluctuations in the close-packed surface. However, Burton et al.,[5] calculated that the temperature required is very high and normally near the crystal melting point. Therefore further growth of the perfect crystal must occur by a surface (two-dimensional) nucleation process in which adsorbed molecules

coalesce to form a surface island monolayer. This was first realized by Gibbs.[1] According to the size of the island, it is more likely to grow or to re-evaporate. For a nucleus of radius r, we may write the Gibbs-Thomson equation

$$r = \frac{S_o \gamma_e}{kT} \left(\ln \alpha \right)^{-1} \qquad (1.1.3.)$$

where So is the area per molecule in the layer, γ_e is the specific edge free energy and α is the ratio of the pressure, p, to the equilibrium vapour pressure, p_o ($\alpha = p/p_o$). The value of r in equation (1.1.3.) is the radius of the critical nucleus, larger nuclei have a high probability of growing and smaller nuclei of evaporating.

The rate of formation of critical nuclei was calculated by Volmer[8] and by Kaischew and Stranski,[9] and the calculation was subsequently improved by Becker and Doring[10] and Volmer.[11] The nucleation rate is

$$J = Z \left(\frac{S}{S_o} \right) \exp \left(-\frac{\Delta G_{max}}{kT} \right) \qquad (1.1.4.)$$

where Z is the rate of arrival of fresh molecules at single surface lattice sites, S is the surface area of the crystal and ΔG_{max} is the free energy of formation of the critical nucleus. From this equation it was deduced that

appreciable growth rates require a supersaturation of at least 25-50% and that the nucleation rate is a very sensitive function of supersaturation.

In an attempt at verification of this result, Volmer and Schutze[12] found that the growth rate of individual iodine crystals was proportional to the supersaturation at values down to 1%. There was no abrupt fall even below this value. The inadequacy of the theory of surface nucleation to explain the growth of real crystals was thus revealed. Such growth[13] proceeds at rates proportional to the supersaturation at supersaturations much lower than the theoretical critical value.

In 1949, Frank[14] suggested that the observations of Volmer and Schutze could be explained on the basis that real crystals are in general not perfect but contain numbers of screw dislocations.[15] The points at which such dislocations are terminated in the surface provide self-perpetuating step lines at which growth occurs, thus obviating the need for two-dimensional nucleation. A single screw dislocation results in growth consisting of a rotation of the step about the point where it joins the dislocation, giving rise to a spiral growth pyramid.

Burton et al.,[5] treated the Frank mechanism in great

detail, and they obtained the rate of advance of a spiral step as

$$V = V_0 \left(1 - \rho_c / \rho \right) \qquad (1.1.5.)$$

where ρ_c is the radius of the critical nucleus and ρ is the radius of curvature of the step which initially (when straight) advances at a rate V_o. In the case of two screw dislocations with equal and opposite Burgers vectors (step heights) separated by a distance $> 2\rho_c$, the connecting terrace behaves as a growth step.

A large number of growth spirals have been observed[16,17] since 1949 as experimental evidence for the screw dislocation theory of imperfect crystal growth.

There has, until recently, been little experimental evidence in support of two-dimensional surface nucleation on solid surfaces. Recent work by Budewski[18] has shown that such a mechanism undoubtedly occurs in the electrodeposition of silver from solution onto a carefully prepared dislocation-free silver single crystal surface. An overpotential of 8-12mV was required before any growth occurred; at lower potentials the electrode was electrically cut off. The current time transients obtained after pulsing to higher overpotentials give clear indication that monomolecular layers

of silver are formed by two-dimensional nucleation and growth.

1.2. Epitaxy

The name epitaxy was first used by Royer[19] (1928) for the oriented overgrowth which occurs when a crystalline species A, grows on a foreign substrate, B, such that A bears a definite crystalline relationship to B. Royer postulated a qualitative static model for the occurrence of epitaxy, and gave a rule that oriented overgrowth occurs only when it involves the parallelism of two lattice planes which have identical networks and closely similar spacing.

The difference between the network spacings may be defined as the percentage misfit,

$$M = \frac{100\,(d_2 - d_1)}{d_1} \qquad (1.2.1.)$$

where d_1 and d_2 refer to the crystal spacings in the substrate and overgrowth respectively. Royer suggested that epitaxy should occur only if M is small (less than $\sim$15%), a conclusion deduced solely from known examples. Since the advent of electron diffraction techniques, many examples of epitaxy were observed, many with much larger misfits, extending over a range from -43% to +90%.[20] Comprehensive tables of observed cases of epitaxy and the calculated

misfits have been published by van der Merwe[21] and Pashley.[20]

Volmer[11] first suggested that low misfit between substrate and overgrowth would lead to a large reduction in the work of nucleus formation. Stranski[22] attempted to treat this problem exactly, for an ionic crystal model of the rock salt type, having equal lattice spacings along the crystal edges, with singly charged ions in the nucleus and doubly charged ions in the substrate. Assuming the formation of an adsorbed fixed monolayer at low supersaturation, which is unable to seed nuclei, Stranski found subsequent nucleus formation most likely to occur in the form of a double layer.

Frank and van der Merwe[23] proposed a simplified model to calculate the conditions necessary for the stability of an adsorbed monolayer of the type suggested by Stranski. Such a monolayer they considered to be influenced by short range forces only, so that it is homogeneously constrained to fit the substrate. They used a one-dimensional dislocation model, with a mathematical justification for its extension to two dimensions. The overgrowth is represented by a row of identical balls of natural spacing d_2 connected by a row of identical springs (force constant μ), the balls being subject to a force which varies periodically (wavelength d_1)

with the position on the substrate. The first harmonic term of amplitude $\frac{1}{2}W_1$ in a Fourier series is taken to represent the corresponding potential energy. The mathematical theory of the model then shows that the lowest energy state of the system remains one with no dislocations (i.e. the monolayer is constrained to fit the substrate lattice) up to a critical value of the misfit, given by

$$M_c = \left(\frac{d_2}{d_1} - 1\right)_{Crit.} = \frac{2}{\pi \lambda_0} \qquad (1.2.2.)$$

where

$$\lambda_0 = \left(\mu d_1^2 / 2 W_1\right)^{\frac{1}{2}} \qquad (1.2.3.)$$

Calculation with Lennard-Jones forces gives $\lambda_0 \sim 7$ and the critical misfit is thus about 9%. An activation energy for dislocation formation is required up to M = 14%, and it was deduced that a metastable monolayer fitting the substrate could exist without dislocations up to this degree of misfit.

Criticism of the theory of Frank and van der Merwe came from Smollett and Blackman[24] on the grounds that it predicts constrained monolayers which would not necessarily be stable. They considered examples of alkali halide

monolayers in parallel orientation on the (100) surfaces of other alkali halides. By estimating the elastic stability of the monolayer they deduced that in some cases where oriented growth is known to occur a monolayer constrained on the substrate would not be dynamically stable.

Frank and van der Merwe quote important examples in support of their theory as observations of 'pseudomorphic' growth (i.e. an overgrowth constrained to have the same interfacial lattice parameters as the substrate) made by Finch and Quarrell[25] for Ag on Pt and ZnO on Zn. Subsequent work by Lucas[26] has thrown considerable doubt on the validity of these results and Pashley[20] has commented that the concepts of pseudomorphism and misfit have been applied too widely in view of the lack of experimental support. However, whilst there is little or no evidence in favour of pseudomorphism, glancing incidence electron diffraction has revealed in some cases the presence of deposits which are strained in so far as their lattice spacings are slightly different from those of the bulk material (e.g. Newman and Pashley[27]).

These observations are in support of the more recent work of van der Merwe[28,29] who has developed the film stability calculations in terms of interfacial energy and has shown that the lowest energy state is one in which the

deposit film contains a homogeneous lateral strain so that the difference between lattice spacings of film and substrate is less than would be expected from bulk values.

1.3. The Metal/Electrolyte Solution Interface

It is pertinent to present a section devoted to a consideration of the metal/electrolyte.solution interface in order to ascertain the manner in which electrocrystallisation is likely to differ from crystallisation from the vapour. In the latter case a single uncharged entity traverses the entire reaction co-ordinate without substantial change in its chemical character. In electrocrystallisation the transfer of a metal species from the solution to the crystal surface is accompanied by its close association with electrons and its loss of solvent molecules. Thus the crystallisation process occurs simultaneously with ligand shedding, electrical discharge of the ion, and transfer across the high electrical fields present at the interface.

The interface between a metal electrode and a solution containing dissolved ions, generally referred to as the electrical double layer, is shown schematically in Fig.1. The excess charge in the metal phase is concentrated at the surface as is the case with charged conductors. That

fig 1 The electrical double layer

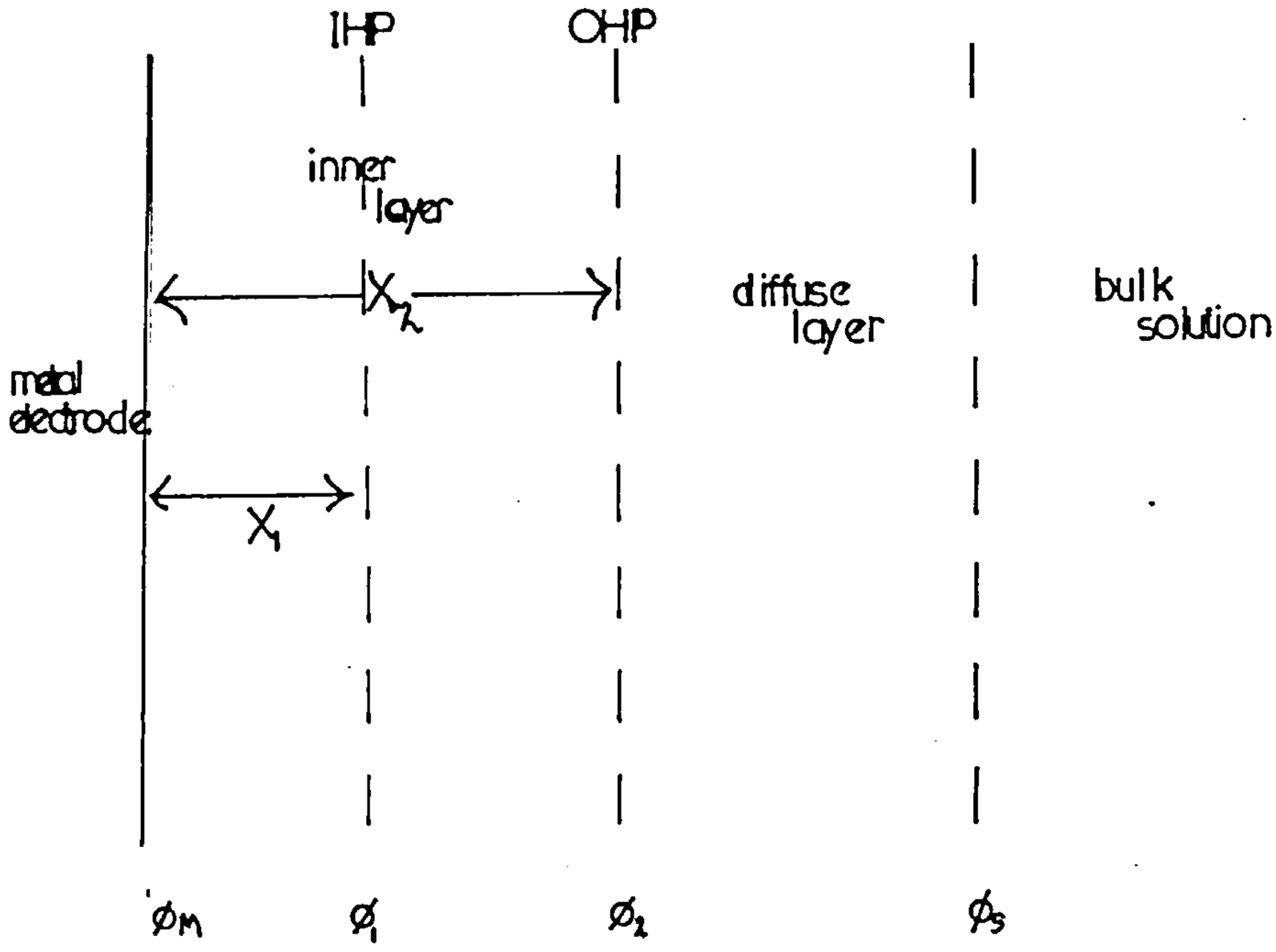

fig 2 Schematic potential-distance profiles

A : for 2 parallel planes of continuous charge

B : for " " " containing discrete charges

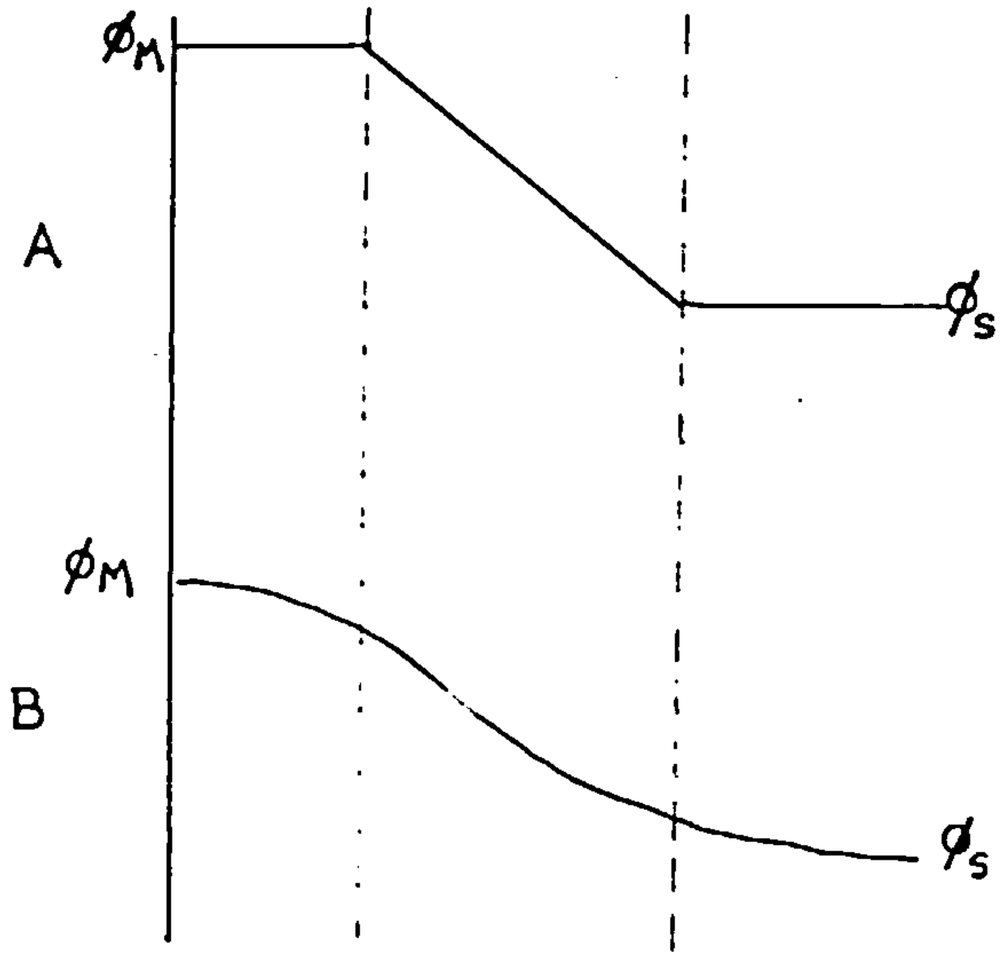

is, the charge takes the form of an excess or depletion of electrons in the layers of metal atoms which constitute the surface, probably being largely confined to the first monolayer.

However on the solution side of the interface the charge excess is concentrated less at the boundary and penetrates towards the bulk of solution. This arises because the solution is a less efficient conductor and the ions are mobile. At distances from the boundary exceeding the radius of a fully solvated ion, that is beyond the "outer Helmholtz plane" (O.H.P.) the charge distribution can be treated by the model of Gouy[30] and Chapman[31] as a one-dimensional ionic atmosphere analogous to the three-dimensional problem solved in the familiar Debye-Hückel theory. The theory assumes that the ions behave as point charges and the dielectric is a continuum having its normal dielectric constant. The potential of the O.H.P. with respect to the bulk solution, ϕ_2, is then related to the charge on the electrode, qm, by

$$\phi_2 = \frac{2RT}{nF} \sinh^{-1}\left(\frac{qm}{2A}\right) \qquad (1.3.1.)$$

where

$$A = \left(\frac{RT\,C^{*}\,\varepsilon}{2\pi}\right)^{\frac{1}{2}} \qquad (1.3.2.)$$

C^* is the bulk concentration of the solution and $\mathcal{E}$ is the dielectric constant. The equation (1.3.1.) is presented in the form which takes into account the modification by Stern[32] whereby solvated ions cannot approach the electrode beyond the O.H.P. It is therefore necessary to consider the region between the electrode and the O.H.P. in order to obtain a full description of the double layer.

The inner layer and diffuse layers may be regarded, for the purposes of evaluating the total double layer capacity, as a series combination of capacities, so that

$$\frac{1}{C_{dl}} = \frac{1}{C^i} + \frac{1}{C^d} \qquad (1.3.3.)$$

where C_{dl} is the total double layer differential capacity and C^i and C^d are the differential capacities of the inner and diffuse layers respectively. C^d may be obtained from equation (1.3.1.) by differentiation of qm with respect to ϕ_2, giving

$$C^d = \frac{nF}{RT} A \cosh\left(\frac{nF\phi_2}{2RT}\right) \qquad (1.3.4.)$$

and C^i may thus be readily obtained from the experimentally measured value of C_d . The most thoroughly studied example is that of mercury in contact with aqueous sodium fluoride, for which Grahame obtained measurements from 0 to 85°C and

from 0.001 to 0.9M NaF.[33;34] The inner layer capacity for this system was found to be virtually independent of concentration, and specific adsorption of ions does not occur, except possibly at the most positive potentials. C^i was also found to be strongly dependent on the electrode charge, qm, indicating that the inner layer cannot be treated simply as a parallel plate condenser.

Macdonald[35] proposed a theory to account for these curves based on the interplay of the two effects arising from the high electric fields in the inner layer, viz. dielectric saturation and electrostrictive compression, the former being calculated using the same treatment as proposed by Grahame[36] for the diffuse layer. The theory gives approximate agreement with experimental results only at potentials cathodic to the e.c.m., but since a C^i-qm relationship symmetrical about the e.c.m. was predicted, neither the 'hump' in the curve observed at slightly anodic potentials nor the steep rise in capacity at higher anodic potentials was explained.

The hump is observed in all mercury-aqueous electrolyte systems at low temperatures and may be due to a structural peculiarity of the water in the inner layer, as first suggested by Grahame[37] and treated quantitatively by

Watts-Tobin.[38]

When Grahame's[34] later measurements of C for mercury in aqueous sodium fluoride at a variety of temperatures became available, Macdonald and Barlow[39] improved a number of points in the original theory of Macdonald[35] by considering the inner region as a hexagonal close packed charge free monolayer of solvent physically adsorbed at the electrode surface by dipole image forces. These authors invoked a 'natural' field which gave a small amount of dielectric saturation (dipole orientation) even at the e.c.m. and allowed the maximum to occur at small positive values of qm. The high field behaviour of the original theory was improved so that a constant polarisation was achieved in the inner layer solvent molecules at sufficiently high fields.

Though the improved theory of Macdonald and Barlow gave excellent agreement with the data of Grahame at negative and small positive values of qm, it did not explain the continuous rise in capacity which occurs with increasing anodic potentials and they ascribed this effect to the specific adsorption of fluoride ions. Several other explanations for this phenomenon have been put forward and are summarised by Mott and Watts-Tobin[40] who are in general agreement with the treatment of Macdonald and Barlow, but

suggest as a possible explanation of the anodic rise in capacity the specific adsorption of hydroxyl ions. Recent work in these laboratories[41] indicates that the specific adsorption of hydroxyl ions together with the dissolution of mercury as its hydroxide constitute the cause of the anodic capacity rise.

An ion is said to be adsorbed at an electrode when it loses its hydration shell and is thus able to move closer to the metal surface than the O.H.P. Grahame[42] introduced the concept of an inner plane of closest approach or the inner Helmholtz plane (I.H.P.) located at a distance x, from the electrode and passing through the centres of the adsorbed ions, (Fig.1). The specific nature of ion adsorption is clearly demonstrated by the experimental dependence of the potential of the e.c.m., E_{ecm}, upon ionic concentration, and Parsons[43] has defined a specifically adsorbed electrolyte as one which causes a change in the co-ordinates of the e.c.m. with a change in concentration.

Esin and Markov[44] observed that the shift of E_{ecm} with change in concentration of the specifically adsorbed electrolyte was much larger than would be expected on the

basis of the Stern model of the double layer, where the specifically adsorbed ions behave as a 'smeared-out' charged sheet (Fig.2A). For this case it may be shown that for specifically adsorbed anions

$$\frac{-\partial(\phi_1 - \phi_s)}{\partial \log C^*} \ll \frac{2.3\,RT}{nF} \qquad (1.3.5.)$$

where ϕ_1 is the potential of the I.H.P., ϕ_s is the potential of the bulk solution, C^* is the bulk concentration of the anion and n is the magnitude of the anionic charge. $(\phi_1 - \phi_s)$ may be equated with E_{ecm} for this model and thus the above equation implies a maximum possible shift of E_{ecm} at 25°C of $59/_n$ mV per decade change in C^*. However, Esin and Markov[44] found experimentally that

$$\frac{-\partial(E_{ecm})}{\partial \log C^*} > \frac{2.3\,RT}{nF} \qquad (1.3.6.)$$

implying that the shift in E_{ecm} is not in fact given by $(\phi_1 - \phi_s)$ i.e. the Stern model is inadequate.

This phenomenon can only be explained satisfactorily by acknowledging the penetration of a field beyond the region bounded by the I.H.P. and the metal surface (Fig.2B). This arises because the specifically adsorbed anions are discrete charges. Esin and Shikov[45] introduced a model

based on anion-cation dipoles oriented perpendicular to the electrode surface and calculated the potential drop in this dipolar layer by the classical electrostatic method of images, with the electrode as the equipotential reflecting plane.

Erschler[46] modified the model by proposing that in concentrated electrolyte solutions the diffuse layer could be regarded as a second reflecting plane giving rise to a series of multiple reflections of the anion in the electrode surface and the O.H.P. Grahame[47] observed that Erschler's model results in the whole potential drop appearing in the inner layer and calculated its value as half that obtained from the Stern model. He also showed that the potential drop in the inner layer was approximately linear.

The major problem in the treatment of the discrete ion effect is the calculation of the actual adsorption potential, ψ_1, when the discrete nature of the adsorbed charge layer is taken into account. This potential is termed the micropotential and has been defined by Macdonald and Barlow[48] as the potential relative to the solution at the position of the centre of an adsorbed ion with that ion absent, but all other charges and image charges as they would be in the presence of the ion.

There have been recent attempts to improve the model and calculations of Erschler and Grahame, who represented the surface distribution of specifically adsorbed ions as a regular hexagonal array of point charges. This model has been further developed by Levich, Kiryanov and Krylov[49] and Barlow and Macdonald.[50] Buff and Stillinger,[51] however, have questioned the existence of a two-dimensional ordered lattice at the mercury-aqueous solution interface, they considered that only short range repulsive forces were operative. Bell, Mingins and Levine[52] have investigated the effect of temperature on a hexagonal array of point charges and find that such a lattice breaks down at small values of the adsorbed charge, q_1, of $< 22\ \mu C\ cm^{-2}$, although Barlow and Macdonald consider the hexagonal lattice to be stable down to a value of $q_1 = 8.2\ \mu C\ cm^{-2}$.

An alternative model has been developed, by Levine, Bell and Calvert,[53] based on an idea of Grahame's[47] and known as the Grahame cut-off disc model, in which two parallel planes of smeared-out charge are considered. The planes are separated by the distance between the I.H.P. and O.H.P., and a circular hole is cut from each such that the charge removed is that corresponding to one discrete

charge. The hole corresponds to an area surrounding each ion in which the mean surface charge distribution is strongly depleted. The parallel planes are circular, concentric with this hole, and of area corresponding to that of the sheets of discrete charge represented. Grahame's calculation of the micropotential from this model was shown by Levine et al., to be incorrect as a result of assigning too large a radius to the circular vacancy, and Levine, Mingins and Bell[54] have given a detailed treatment on the basis of statistical mechanics.

Many recent electrocrystallisation theories have involved the concept of adions, specifically adsorbed metallic cations. It is therefore pertinent to consider evidence for the specific adsorption of such species. Grahame[55,56] observed that the differential capacities of mercury in solutions of alkali metal fluorides increase in the order $LiF < NaF < KF < CsF$ at any given surface charge density. He attributed the differences to variations in the inner layer capacity which would be inversely proportional to the thickness of the layer; hydrated lithium ions having the largest radius, present in the outer Helmholtz plane, would produce the smallest differential capacity. Frumkin[57,58] explained the

experimental data in terms of a greater specific adsorbability of caesium ions over the lighter alkali metal cations.

Unequivocal indications for specific alkali metal cation adsorption have been obtained by Obruscheva[59] for the specific adsorption of Tl^{+}, Cd^{2+}, Pb^{2+} and Zn^{2+} on gold and platinum surfaces. The potential of a perfectly polarised platinised platinum electrode, charged to an initial potential of about 0.3v (N.H.E.) in molar sulphuric acid was found to become more positive by several hundred millivolts when those cations were added to the solution to a concentration 0.1M. Moreover electrocapillary measurements have demonstrated the specific adsorption on mercury, of Tl^{+} and Pb^{2+} ions to an extent comparable with that of bromide ions.[60]

So far in this section the double layer at perfectly polarisable electrodes has been discussed. It is necessary to consider which deviations from the equilibrium conditions are likely to occur during electrocrystallisation.

Levich[61] and Sparnaay[62] have considered the structure of the double layer under non-equilibrium conditions. Sparnaay showed that the passage of current does not seriously affect the potential distribution in the diffuse

layer. Relaxation times for the diffuse layer are of the order 10^{-7} sec. for millimolar solutions. Levich suggested that the field in the diffuse layer due to non-equilibrium retards the reduction rates of some anions. Frumkin[63] has demonstrated that specific cation adsorption retards reactions in which other cations are reactants, and accelerates those in which anions react.

The potential distribution in the double layer must have a profound effect on electrochemical reactions. The equilibrium activities of the reacting species in the reaction layer depends upon its potential according to

$$C_p = C^* \exp - \frac{nF\phi_p}{RT} \qquad (1.3.7.)$$

where C_p and C^* are the activities in the "pre-electrode layer" and in the bulk solution respectively. ϕ_p is the potential of the pre-electrode layer referred to that in the bulk.[64] The rate of any charge transfer reaction at the electrode surface depends upon the potential difference between the metal and the pre-electrode layer (which was identified by Frumkin[64]) with the O.H.P. so that ϕ_p was calculated from Gouy-Chapman theory (eqn.(1.3.1.)).

Consequently the familiar Tafel relation in electrode kinetics will not be observed for systems in which ϕ_p varies

with change in ϕ_M, the potential of the metal. In certain reactions, namely the reduction of anions and the oxidation of cations, increase in overpotential could possibly decrease the reaction rate. The potential difference, ϕ_2, across the diffuse layer may be maintained fairly constant at a relatively small value by the use of concentrated supporting electrolyte solutions (eqn. (1.3.1.)).

1.4. Metal Electrocrystallisation

The purpose of this section is to present a short review of some models which have been used for metal electrocrystallisation, and interpretation of some experimental results in the light of these models. A comparison of the suitability of the various experimental techniques available for the study of metal electrocrystallisation will be given, and the need for investigation upon inert substrates rather than the parent metal pointed out.

Theoretical interpretation of metal electrocrystallisation has been attempted by the following methods:

(a) The calculation of potential energy profiles to describe the most likely reaction paths and rate-limiting steps (Conway and Bockris).

(b) Theories of the mechanism of the electrodeposition of metals following directly from vapour phase studies.

These have adopted (i) Frank's theories of step perpetuation by screw dislocations (Vermilyea). (ii) Volmer's theories of surface diffusion of adsorbed atoms (adatoms) (Lorenz, Fleischmann and Thirsk, Bockris, Gerischer).

(c) A model of direct deposition at growth sites. (Fleischmann and Thirsk).

(d) A two-dimensional nucleation mechanism, experimentally found for dislocation free single silver crystals. (Budevski).

Following the use of potential energy profiles by Polanyi and Horiuti[65] to illustrate hydrogen ion discharge, there have been calculations of such profiles to describe the reaction paths of electrode processes by Butler[66] Parsons and Bockris,[67] and Conway and Bockris.[68] Conway and Bockris[69,70] have adopted this method to predict the most likely reaction paths and rate-limiting steps in the electrocrystallisation of copper, silver and nickel from aqueous solutions of simple cupric, argentous and nickelous ions respectively. They considered that maxima in the potential energy (and free energy) - reaction co-ordinate curves are likely to occur only for:

(i) ion transfer from the outer Helmholtz plane to a specifically adsorbed site on the surface, or at an edge,

kink, edge vacancy or surface vacancy.

(ii) ion transfer as in (i) with simultaneous discharge to form a neutral atom.

(iii) diffusion of adatoms or adions across the surface or along a step.

(iv) transfer of ad-species from the surface to a step and from a step to a kink.

(v) the reduction of polyvalent ions to monovalent ions at the outer Helmholtz plane.

Conway and Bockris computed potential energy curves for all possible reaction paths for the electrocrystallisation of the metal at its e.c.m. potential from a solution of its ions at unit molal activity. The enthalpies of the initial and intermediate stages were calculated with reference to the enthalpy of the final state. Once the heat contents of initial and intermediate stages were evaluated, it was necessary to calculate variations in P.E. with distance moved along the reaction co-ordinate in order to complete the P.E. diagrams. In the adsorption of an ion from the outer Helmholtz plane, the ion was assumed to sit down at the site so that the spatial distribution of its water dipoles minimised the potential energy. Similarly P.E. curves for

surface and edge diffusion were calculated.

To deduce the relative dominance of alternative reaction paths it was necessary to translate the P.E. reaction profiles into their free energy counterparts. Activation entropies were assumed to result from variation in degrees of translational freedom and from partial dehydration. Bockris and Conway ignored the loss of rotational freedom of an ion, necessary to achieve a favourable spatial arrangement in the process of adsorption.

Bockris and Conway estimated the margin of error in their computations to be $\pm$ 3 Kcal/mole arising from uncertainties in the published data which they employed. The weaknesses in their method which deduced the degrees of hydration of adions from space filling models and relied upon the image potential law, were also acknowledged. In fact the e.c.m. data upon which their calculation was based cannot be relied upon. The e.c.m. for copper, for example, was obtained from the e.c.m. work function relation for various metals[71] and, in consequence, is accurate to $\pm$ 0.5 volts, corresponding to an error of $\pm$ 25 Kcal/mole for the heat content of the initial state in cupric ion reduction. Bockris and Conway's prediction that at 350mV negative to the Cu/Cu^{2+} standard reversible potential a change from

rate-determining surface diffusion to rate-determining reduction of Cu^{2+} to Cu^{+}, is not borne out by the experimental measurements of Bockris and Mattson[72] who found rate control by the latter reaction over the entire potential region using electro-deposited copper electrodes.

Bockris and Conway indicated that the adsorption of metals as neutral atoms leads to prohibitively high potential energies. However Mott and Watts-Tobin[40] pointed out that neutral adatoms may become stable on a surface which is strongly polarised negatively.

Despite their numerous limitations the energy profile diagrams of Bockris and Conway do predict the order Ag $\rangle$ Cu $\rangle$ Ni for the exchange currents of the systems considered; a result in accord with reliable experimental data. The main objection to the use of energy profiles to predict rate determining steps lies in the assumption that the highest maximum represents the slowest stage. Even when the system is at equilibrium, so that the activated complexes assuredly are at equilibrium with reactants and intermediates, differences in the frequency factors operative in various steps may render such predictions inaccurate.

Clearly it is necessary to consider the origin and the concentrations of steps, kinks and adions on the surface

during electrocrystallisation. Following the theories of crystal growth from the vapour phase, Lorenz[73] used a model in which ions were discharged to adatoms which diffused across the surface to growth steps, assumed present at constant concentration.

Vermilyea[74] adapted to electrocrystallisation Frank's theories of step perpetuation by screw dislocations. The concentration of kinks and steps is expected to be high on atomically rough surfaces, so that the discharge of ions must be the rate-limiting process. In the absence of resistance and concentration contributions to overpotential then,

$$\frac{i}{nF} = \frac{k_2^o C_o a^{1-\alpha}}{N_o} \exp\left[\frac{nF\eta(1-\alpha)}{RT}\right]\left[\exp\left(\frac{-nF\eta}{RT}\right) - 1\right] \qquad (1.4.1.)$$

where i is the current density, k_2^o is the anodic reaction rate constant in sec^{-1} at the standard electrode potential, a is the activity of ions in solution, C_o the surface concentration of atoms per square cm. of surface, N_o is the total concentration of surface positions, and α is the fraction of overpotential assisting deposition.

For high currents ($i \gg i_o$) the growing steps do not maintain the linear shape associated with equilibrium. Close to the dislocation axis the angular velocity of the

step exceeds that further from the axis and eventually the step develops into a spiral. The steady state step spacing is an inverse function of overpotential. At low growth rates the step maintains its linearity.

The mean free path X_s of an adatom during its lifetime τ_s on the surface is given by Einstein's relation $X_s^2 = D_s \tau_s$ where D_s is the surface diffusion coefficient. Vermilyea derived steady state current overpotential relations for various extreme cases, assuming that electrocrystallisation occurs via surface diffusion.

(i) when $X_s \gg a_o$ (distance between two neighbouring equilibrium surface positions) and $i \gg i_o$

$$i \propto a^{\frac{1-\alpha}{2}} \exp\left[\frac{nF\eta(1-\alpha)}{2RT}\right]\left[\exp\left(\frac{-nF\eta}{RT}\right)-1\right] \qquad (1.4.2.)$$

(ii) when $X_s \gg a_o$, $i < i_o$ and $X_s \ll \ell$ where ℓ is the distance between neighbouring dislocations

$$i \propto \frac{X_s K^{\frac{1}{2}}}{\tau_s}\left[\exp\left(\frac{-nF\eta}{RT}\right)-1\right] \qquad (1.4.3.)$$

where K is the dislocation density.

(iii) when $X_s < a_o$, discharge is restricted effectively to the immediate vicinity of the kinks.

On the basis of this dislocation theory, transient effects may be expected to occur after the initiation of

electrolysis as the steady state spiral arrangement is attained. It was the suggestion of Vermilyea that this phenomenon, a "superpolarisation", would last for several minutes whereas the reattainment of true equilibrium at the completion of electrolysis may require a period of hours as smaller currents are involved. The effects of surface structure would be expected to be most noticeable at low overpotentials and short times. Vermilyea suggested that metals with low melting points which could be maintained rough by thermal fluctuations of energy would show small overvoltages. Sluggish metals[75] such as nickel would possess high surface energies, explaining their high overvoltages.

Fleischmann and Thirsk[76] chose a model of a surface possessing parallel growth steps separated by a distance 2ℓ (Fig.3). They made the assumptions that electrical fields parallel to the surface are insignificant, that diffusion of adatoms along the surface is the only mode of transport to the growth sites, that ion transfer across the double layer is first order in each direction, that the adatom concentration C is low at all points on the surface and that incorporation of adatoms into the lattice at the steps is much faster than the other stages.

fig 3 Parallel step lines model

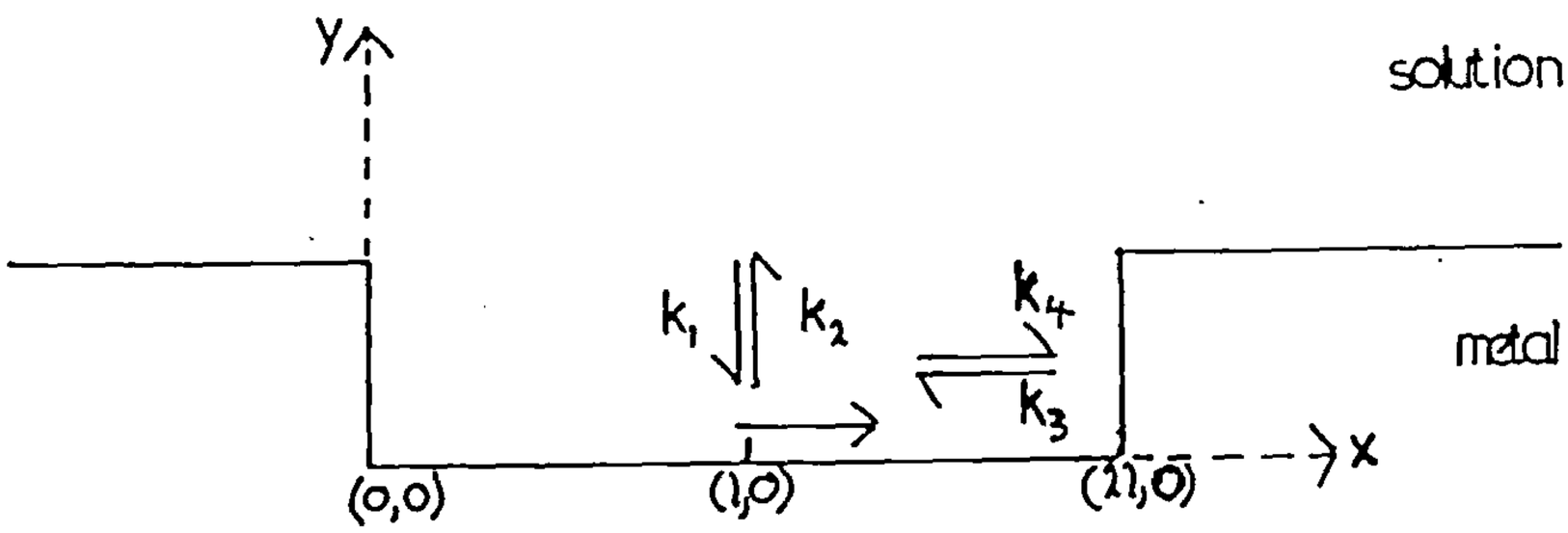

fig 4 Model of discrete nature of electrode surface at x = 0

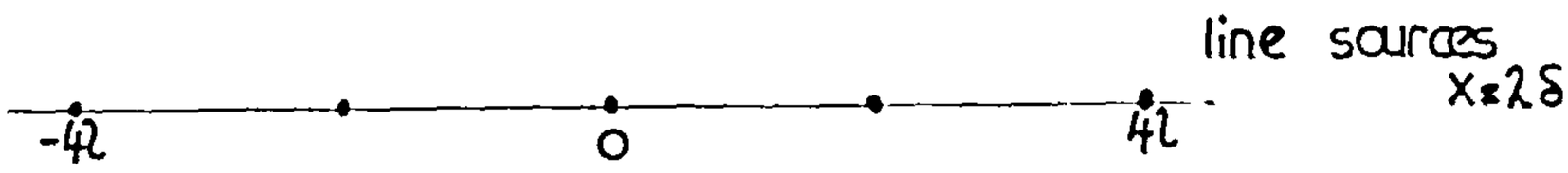

x = δ — — — — — — — — —

linear Nernst diffusion

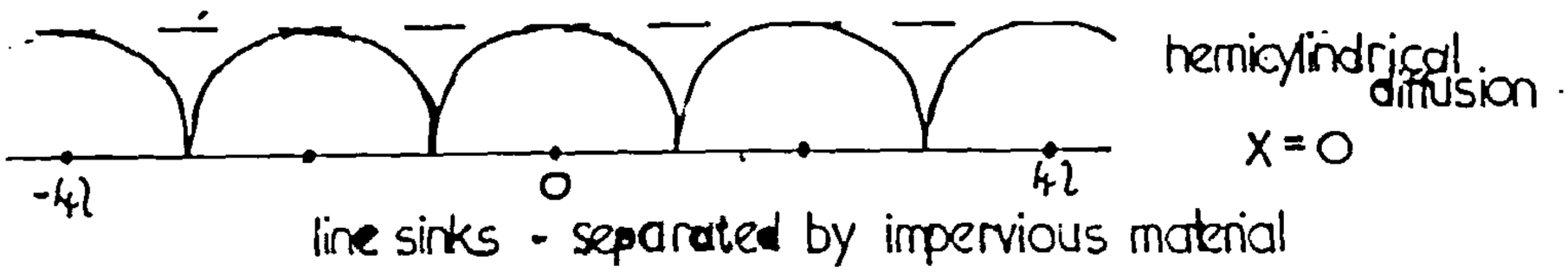

line sinks - separated by impervious material

For cathodic deposition at constant potential,

$$\frac{\partial c}{\partial t} = D_s \frac{\partial^2 c}{\partial x^2} + k_1 - k_2 c \qquad (1.4.4.)$$

where $k_1 = \frac{io}{nF} \exp\left[\frac{\alpha n F \eta_1}{RT}\right]$; $k_2 = \frac{io}{nFc_o} \exp\left[\frac{(\alpha-1) n F \eta_1}{RT}\right]$

where η is taken as positive for deposition, D_s is the adatom diffusion constant, C_o is the adatom concentration at the equilibrium potential.

They solved this equation by the haplace transform method for the boundary conditions,

$$C = C_o \qquad 0 > x > l \qquad t = 0 \qquad (1.4.5.)$$

$$C = C_o \qquad x = 0 \qquad t > 0 \qquad (1.4.6.)$$

$$\frac{\partial c}{\partial x} = 0 \qquad x = l \qquad t > 0 \qquad (1.4.7.)$$

noting that the current into unit area of surface is

$$i = \frac{nF}{l} \int_0^l (k_1 - k_2 c)\, dx \qquad (1.4.8.)$$

The solution for the case of application of an over-potential step (η_1) to the working electrode from $\eta = 0$ is,

$$i = \frac{nF(k_1 - k_2 c_o)}{l} \sqrt{\frac{D_s}{k_2}} \cdot \frac{\sinh\left(\sqrt{k_2/D_s}.l\right)}{\cosh\left(\sqrt{k_2/D_s}.l\right)} + \sum_{p=0}^{p=\infty} \frac{32 nF k_2 l^2 (k_1 - k_2 c_o) \exp -\left[\{2p+1\}^2 \pi^2 D_s + 4k_2 l^2\} t/4l^2\right]}{(2p+1)^2 \pi^2 \left[4k_2 l^2 + \pi^2 D_s (2p+1)^2\right]} \qquad (1.4.9.)$$

The first term in the R.H.S. of eqn. (1.4.9.) represents the steady state current density and the second term, which is time dependent, registers the redistribution of adatoms between the steps following the change in η. Following a change in overpotential, ζ will be time dependant as the steady state value of ζ is a function of η. Fleischmann and Thirsk estimated that ζ may be considered constant for the duration of the initial transient provided that the overpotential jump does not exceed 30mV. However the dependence of ζ upon η must be taken into account in the steady state i-η relation.

Surface steps were assumed to be the progeny of single screw dislocations in the crystal. Nowhere on the step may the radius of curvature be less than that of the critical two-dimensional nucleus. The growth spiral was assumed to follow the equation of an Archimedian Screw whose radius of curvature at its centre equals the critical radius. This second assumption requires the adatom concentration at the centre to be in equilibrium with the solution at the over-potential η. Hence the initial assumption that the adatom concentration at the steps is C_o, which requires linearity of the steps only applies far from the origin. The radius of a circular critical nucleus is shown[77] to be

$$\rho_c = \frac{V\sigma}{RT \ln \alpha} \qquad (1.4.10.)$$

where α is the supersaturation of the solution, σ is the surface energy and V is the molar volume of the metal. Now $RT\ln\alpha = n\eta F$, so that

$$\rho_c = \frac{V\sigma}{n\eta F} \qquad (1.4.11.)$$

The equation of the Archimedian screw is given in polar co-ordinates by $r = 2\rho_c\,\theta$, so the step spacing is $2\gamma = 4\pi\rho_c$ or, using eqn. (1.4.11.),

$$\gamma = \frac{2\pi V\sigma}{n\eta F} \qquad (1.4.12.)$$

As σ is a function of ρ_c, then it is also a function of γ. Thus it does not follow that $\gamma \propto 1/\eta$.

Substitution of eqn. (1.4.12.) into eqn. (1.4.9.) gives the dependence of i upon η in the true steady state. For values of $\sqrt{\frac{k_2}{D_S}}\cdot\gamma$ widely differing from unity, the resulting expression may be simplified by expansion of the hyperbolic terms.

When $\sqrt{\frac{k_2}{D_S}}\cdot\gamma \ll 1$, that is, at high overpotentials

$$i = i_o \exp\left(\frac{\alpha n F\eta}{RT}\right)\left[1 - \exp\frac{-nF\eta}{RT}\right] \qquad (1.4.13.)$$

This is the familiar Butler-Volmer relation for transfer control, corresponding to infinitely rapid surface diffusion.

When $\sqrt{\frac{k_2}{D_s}}\,l \gg 1$ the general expression reduces to

$$i = i_0^{\frac{1}{2}} \exp\left[\frac{(1-\alpha)n F\eta}{2RT}\right]\left[1 - \exp\frac{-nF\eta}{RT}\right](nF c_0 D_s)^{\frac{1}{2}}\left(\frac{nF\eta}{2\pi V\sigma}\right) \quad (1.4.14.)$$

This expression may be simplified further at very low over-potentials by expansion of the exponential terms to read

$$i = i_0^{\frac{1}{2}} \frac{(nF D_s c_0)^{\frac{1}{2}} (nF\eta)^2}{2\pi V\sigma RT} \quad (1.4.15.)$$

Fleischmann and Thirsk concluded that in cases where crystal growth proceeds at dislocation steps at low overpotentials the same mechanism will predominate over two-dimensional nucleation at high overpotentials. Those nuclei, growing at a relatively low rate because of their curvature, will be overtaken by the advancing, nearly linear, steps of the spiral.

A more interesting solution of eqn. (1.4.4.) is the one for the conditions of an experiment of the type proposed by Gerischer.[78] The experiment was used by Gerischer to obtain an estimate of the adatom concentration during the electrocrystallisation of silver. After a steady state had

been established at the overpotential η_1, for the dissolution of the electrodes, a smaller overpotential η_2 was applied such that the initial current was zero. This second over-potential was identified with the total concentration polarisation. A proportion of the polarisation was attributed to concentration changes in the solution and the magnitude was estimated from the cathodic limiting current. The amount remaining after subtraction of this component was assigned to changes in the adatom concentration on the surface of the silver.

Fleischmann and Harrison[79] obtained the solution for these conditions by reinserting the expression for C, the steady state adatom concentration at η_1, obtained by solution of eqn. (1.4.4.), into the diffusion equation (1.4.4.) as an initial condition for obtaining the solution when the overpotential was switched instantaneously to the new value η_2.

The resulting expression is

$$O = i_{t\to O} = nF\,k_2\left[\frac{k_1}{k_2} - \frac{k_1'}{k_2'} + \frac{(k_1' - k_2' c_o)}{k_2'\eta}\left(\frac{D_s}{k_2'}\right)\frac{\sinh(k_2'/D_s)^{\frac{1}{2}}\eta}{\cosh(k_2'/D_s)^{\frac{1}{2}}\eta}\right] \quad (1.4.16.)$$

where the quantities without a prime belong to η_2. By

substitution of the rate constants in terms of i_o and over-potential then

$$i_o \exp \frac{\alpha n \eta_1 F}{RT} \left(\exp \left[\frac{nF}{RT} (\eta_2 - \eta_1) \right] - 1 \right) = -i_{stat} \qquad (1.4.17.)$$

where i_{stat} is the stationary current at η_1. This consequence of the theory could be tested, after correcting the overpotentials for concentration changes in the solution, by using the known values of i_o and α and the experimental parameters. This theory applies only to very rapid reactions where at short times the double layer charging can be neglected.

An alternative interpretation of the results of Gerischer's experiment was suggested by Fleischmann and Thirsk,[76] namely, that the excess concentration polarisation could be due to hemicylindrical diffusion zones in the region of the growing edges. Fig.4 shows how this would occur. An estimate of the concentration changes in the solution due to the discrete nature of the growing surface may be made by regarding the edges as line sinks and, using the concept of the Nernst diffusion layer, taking images of the sinks in this plane. Fleischmann and Harrison[79] calculated the concentration distribution at the edges in the steady state for this model, assuming the edges to be stationary.

The method of Kasper[80] was used to obtain, in the stationary state, the relative concentration changes in the solution due to linear and hemicylindrical diffusion. The result is

$$\frac{\Delta C}{\Delta C_{Nernst}} = \frac{l}{\delta\pi} \ln \frac{16\delta^2}{\pi^2 a^2} + \frac{2l}{\delta\pi} \sum_{1}^{\infty} \ln \left\{ \frac{1 + \cosh \frac{\pi\rho l}{\delta}}{\cosh \frac{\pi\rho l}{\delta} - 1} \right\} \quad (1.4.18.)$$

where ΔC is the total concentration change in the solution and a is an arbitrary radius of atomic dimensions surrounding the line sink. If $a = 2 \times 10^{-8}$cm and $\delta = 10^{-3}$cm then $\Delta C/\Delta C_{Nernst}$ can be evaluated as a function of l/δ. The curve has a limiting value of approximately 1.3 when δ/δ is small. This would be the case for experiments on solid metals, such as silver, as step lines would probably be generated by dislocations. In agreement with this Gerischer[78] gives $\Delta\eta/\Delta\eta_{Nernst}$ (idential to $\Delta C/\Delta C_{Nernst}$ when the total overpotential is small) as 1.5. The interpretation of the excess polarisation as due solely to adatoms on the surface, is therefore not unambiguous.

A relation analogous to eqn. (1.4.17.) may be deduced for a 'Gerischer experiment' if concentration polarisation is restricted to the solution. It has the form

$$i_0 \exp \frac{\alpha n F \eta_1}{RT} \left\{ \exp\left(\frac{-n\eta_2 F}{RT}\right) - \exp\left(\frac{-n\eta_1 F}{RT}\right) \right\} = -i_{stat} \quad (1.4.19.)$$

It should be possible using eqns. (1.4.17.) and (1.4.19.), to decide whether the concentration polarisation takes place in the solution or on the surface. However these equations can equally well be deduced from any other model provided only that in one case concentration changes take place before and in the other case after electron transfer. A detailed assignment of the reaction path must therefore be dependent on a detailed fitting of the current/time transients to the theoretical expressions.

Equilibrium at step lines during metal growth is probably only achieved for metals with high exchange currents. Experimental results for the growth of thin films of nickel on a mercury substrate,[81] from solutions of the nickel thiocyanate complex, by a mechanism related to the classical model for crystal growth (nucleation and growth of two-dimensional centres) show, however, that the lattice is formed at a finite rate, comparable to the rates of surface diffusion and electrochemical discharge. The potentiostatic current time curves, corresponding by charge to the formation of a monolayer one unit cell thick, have a maximum. A symmetrical curve would be expected if the slow step is only at the edge.[82] This would arise from the variation of available area for growth on the centres, which

at first increases as the centres grow and then begins to decrease as the centres overlap. The curves are, however, unsymmetrical. This suggests that some process precedes lattice incorporation. This could be a preceding chemical reaction in the solution or the diffusion of adatoms to the growth site. The initial currents, plotted as a function of potential, show a Tafel slope corresponding to the discharge step. At higher negative potentials the initial current becomes kinetically controlled by the rate at which the preceding chemical reaction

$$Ni^{2+} + SCN^{-} \rightleftharpoons NiSCN^{+} \xrightarrow{2e} Ni + SCN^{-}$$

can produce the reducible species. In the region at lower potentials where the initial current is the discharge rate, which is followed by the effects of crystal growth, in that the curves go through a maximum, the inescapable conclusion is that these two processes are linked by adatom diffusion on the surface. The experimental fact that by switching instantaneously to more positive potentials some of the charge is removable, presumably that in transit to the growth site, lends more confidence to this suggestion.

To allow for the finite rate of lattice growth in the

parallel step line model, it is necessary to replace boundary condition (1.4.6.) by (1.4.20.)

$$D_S \frac{\partial c}{\partial x} = k_4 c - k_3 \qquad x=0 \qquad t>0 \qquad (1.4.20).$$

where k_4 is the rate constant governing growth at the step lines and k_3 that of the back reaction. Fleischmann and Harrison[83] solved eqn. (1.4.4.) with boundary conditions (1.4.5.), (1.4.20.) and (1.4.7.). The steady state term of their resulting expression for i at low overpotentials i.e. when $\left(k_2/D_S\right)^{\frac{1}{2}} \eta$ is large, was

$$i = \frac{nF}{\eta}\left(k_1 k_4 - k_2 k_3\right)\left(\frac{D_S}{k_2}\right)^{\frac{1}{2}} \frac{1}{k_4 + \left(D_S k_2\right)^{\frac{1}{2}}} \qquad (1.4.21.)$$

Two limiting cases of this can be distinguished. If $\left(D_S k_2\right)^{\frac{1}{2}} > k_4$, then deposition and diffusion are fast compared to lattice growth and eqn. (1.4.21.) becomes, on substitution for k_1,

$$i = \frac{nF}{\eta}\left[k_4 c_0 \exp\left(\frac{\eta F}{RT}\right) - k_3\right] \qquad (1.4.22.)$$

If $k_4 > \left(D_S k_2\right)^{\frac{1}{2}}$, then deposition and lattice growth are fast compared to diffusion of the adatoms and eqn. (1.4.21.) becomes

$$i = \frac{nF}{\eta}\left(\frac{D_S}{k_2}\right)^{\frac{1}{2}}\left(k_1 - \frac{k_2 k_3}{k_4}\right) \qquad (1.4.23.)$$

An explicit expression for ζ, substituted in these equations, would allow information about the mechanism to be obtained from stationary current potential curves. The opposite assumption that $(k_2/D_s)^{\frac{1}{2}}\zeta$ is small, at high over-potentials, leads to

$$i = nF\left(k_1 - \frac{k_2 k_3}{k_4}\right) \qquad (1.4.24.)$$

The current is independent of the spacing between the lattice edges and follows a Tafel-type relation.

Fleischmann and Harrison also obtained the solution for the conditions of a "Gerischer experiment". This leads when the metal deposition is relatively irreversible, i.e. $k_3 = 0$ and the potentials such that $k_2^{1} = 0$, $k_1 = 0$ (the prime signifies the state at ζ_1, k_4 is considered independent of potential) to

$$i = \frac{-2nFD_s k_2 k_4^{2} k_1'}{\zeta} \int_0^{\infty} \frac{\exp -(D_s \alpha_\rho^{2} + k_2)t}{(D_s^{2}\alpha_\rho^{2}\zeta + D_s k_4 + k_4^{2}\zeta) D_s^{2}\alpha_\rho^{2}} \qquad (1.4.25.)$$

This represents a transient due only to the removal of adatoms and the lattice continues to grow during the transient. In eqn. (1.4.25.) α_ρ is the root of the transcendental equation

$$\alpha_\rho \tan \alpha_\rho \zeta = k_4 / D_s \qquad (1.4.26.)$$

It would seem possible, by setting up calibration curves in terms of the parameters $k_4 l/D_s$ and D_s/l^2, to compare the experimental and theoretical results when adequate experimental data are available.

The equations derived from the parallel step line model so far have assumed that diffusion of adatoms along the surface is the only mode of transport to the growth sites. A more complete theory has been formulated by Fleischmann, Rangarajan and Thirsk.[84] Differential equations corresponding to eqn. (1.4.4.) can be written for potentiostatic conditions as follows

$$D\left[\frac{\partial^2 C}{\partial x^2} + \frac{\partial^2 C}{\partial y^2}\right] = \frac{\partial C}{\partial t} \qquad 0 \ll x < l \qquad y > 0 \qquad (1.4.27.)$$

$$D_s\left[\frac{\partial^2 C_a}{\partial x^2}\right] + k_1 C - k_2 C_a = \frac{\partial C_a}{\partial t} \qquad 0 \ll x < l \qquad y = 0 \qquad (1.4.28.)$$

As before x is the distance co-ordinate in the surface as shown in Fig.3. y extends into the solution. Ca, now refers to adatoms, and C,D, to the ions in solution.

The initial conditions are now

$$C(x,y,t) = C^0 \qquad t = 0 \qquad (1.4.29.)$$

$$C_a(x,t) = C_a^0 \qquad t = 0 \qquad (1.4.30.)$$

The Boundary conditions are now

$$C(x,y,t) = C^{o} \qquad y \to \infty$$

$$\frac{\partial C}{\partial x} \to 0 \qquad x = 0$$

$$C_a(x,t) \to C_a^{o} \qquad x = 0$$

$$D\left(\frac{\partial C}{\partial x}\right) = D_s\left(\frac{\partial C_a}{\partial x}\right) = 0 \; ; \quad x = \delta \; , \; y \geq 0 \qquad (1.4.31.)$$

and $$D\left(\frac{\partial C}{\partial y}\right) = k_1 C - k_2 C_a \; , \; y = 0, \; 0 < x \leq \delta$$

In order to make the problem symmetrical in both phases, Fleischmann, Rangarajan and Thirsk rewrote eqns. (1.4.27.) - (1.4.31.) in terms of a surface layer of thickness δ^{o}. It can be shown that solving the amended equations and allowing $\delta \to 0$ gives a correct solution of (1.4.27.), (1.4.28.). The transform of the solution is complicated and inversion may be accomplished using a computer. However, it is possible to discuss limiting cases.

When $D_s \to \infty$, then

$$i_{(t)} = i_o \left[\exp \frac{\alpha n F \eta}{RT} - \exp \frac{(\alpha - 1) n F \eta}{RT} \right] \exp \frac{k_1^2 t}{D} \; erfc \left(k_1 \sqrt{\frac{t}{D}} \right) \qquad (1.4.32.)$$

Eqn. (1.4.32.) is the well-known equation for semi-infinite diffusion to a planar electrode, and at long times reduces to $i \propto t^{-1/2}$.

When diffusion in the solution is neglected by allowing $D \to \infty$ the equations derived by Fleischmann and Thirsk[76] are reproduced.

In a later paper Fleischmann, Rangarajan and Thirsk,[85] relaxed boundary condition $C_a = C_a^o$ at x = 0 in (1.4.31.) by replacing it by

$$D_S \left(\frac{\partial C_a}{\partial x}\right)_{x=0} = k_4 \left(C_a - C_a^o\right)_{x=0} \qquad (1.4.33.)$$

This treats the case when equilibrium is not maintained at the step line and there is a finite rate of incorporation at the step line. Again the transform of the solution is complicated. A number of steady states are possible from the general equation which also may predict $i\eta^2$ showing that a square law dependence between i and η (eqn. (1.4.15.)) cannot prove by itself that surface diffusion is rate determining.

Bockris et al[72,86-91] have attempted to interpret their observations of metal deposition in terms of rate-limiting ion transfer, electron transfer and surface diffusion.

Bockris and Mehl[90] considered that for low coverages of adions one may write

$$\frac{i}{i_o} = \exp\frac{-\alpha n F \eta_t}{RT} - \frac{C_{\eta,t}}{C_o} \exp\frac{(1-\alpha) n F \eta_t}{RT} \qquad (1.4.34.)$$

for the instantaneous Faradaic current i where $C_{\eta,t}$ is the instantaneous mean surface concentration of adions. C_o is the quiescent value. For $\eta \ll \frac{RT}{nF}$, the exponential terms may be expanded to give

$$\frac{i}{i_o} \simeq 1 - \frac{C_{\eta,t}}{C_o} - \frac{\eta nF}{RT} \qquad (1.4.35.)$$

provided that it is assumed that $\frac{C_{\eta,t}}{C_o} \simeq 1$

But $$\frac{dc}{dt} = \frac{i}{nF} - \gamma \qquad (1.4.36.)$$

where γ is the flux of adions into the growth steps per unit area of electrode surface. Mehl and Bockris assumed that

$$\frac{\gamma_o}{C_o} = \frac{\gamma}{C - C_o} \quad \left(= \frac{D_s}{x_o^2} \right) \qquad (1.4.37.)$$

This assumes a model of parallel step lines, separated by a distance $2x_o$, in which the concentration gradients across the surface are linear. γ_o has no physical significance and is simply a constant. Eqns. (1.4.36.) and (1.4.37.) combine to give on integration at constant i,

$$C_\eta - C_o = \frac{iC_o}{nF\gamma_o}\left(1 - \exp -\frac{\gamma_o t}{C_o}\right) \qquad (1.4.38.)$$

Eqns. (1.4.35.) and (1.4.38.) lead to

$$\frac{i}{nF\gamma_o}\left(1 - \exp \frac{-\gamma_o t}{C_o}\right) + \frac{\eta nF}{RT} + \frac{i}{i_o} = 0 \qquad (1.4.39.)$$

For small values of $v_o t/c_o$ the exponential term was expanded to give

$$\frac{it}{nFc_o} + \frac{\eta nF}{RT} + \frac{i}{i_o} = 0 \qquad (1.4.40.)$$

Fleischmann and Thirsk pointed out that an exact solution of eqn. (1.4.4.) is not possible for the galvanostatic case since k_1 and k_2 then become time dependant. They solved eqn. (1.4.4.) after substituting $C = C_o$ in the final term. This corresponds to the assumption that surface diffusion is a fast process. In this way they obtained[76] eqn. (1.4.40.).

Bockris and Mehl derived the steady-state relation from eqns. (1.4.34.) and (1.4.38.);

$$i = \frac{\exp\left(-\frac{nF\eta}{RT}\right) - 1}{\frac{i}{i_o}\exp\left[\frac{(\alpha-1)\eta nF}{RT}\right] + \frac{1}{nFv_o}} \qquad (1.4.41.)$$

Eqn. (1.4.41.) may be simplified if the denominator terms are not comparable, corresponding to the cases of either complete surface diffusion control or of complete transfer control.

The theory of Bockris and Mehl was used to interpret results of silver and copper electrocrystallisation.[72,89,90] It relies upon the unlikely equation (1.4.37.) and the assumption of low coverage of adions. Moreover the time dependant relations are restricted to very low overpotentials.

Bockris found that his basic theory (eqn. (1.4.41.)) was inadequate to explain his experimental observations. Therefore he made[90] V_o potential dependant according to the purely empirical relation

$$V_o(\eta) = V_o(0) \exp \frac{-nF\eta}{RT} \qquad (1.4.42.)$$

in order to allow for potential dependance of the steady state step line density. $V_o(\eta)$ replaces V_o in eqn. (1.4.41.).

In later papers,[86,91] Bockris et al recognised the necessity of treating the surface concentration of adions as a function of their position with respect to the steps. Despic and Bockris[91] solved eqn. (1.4.4.) for the steady state $\left(\partial c/\partial t = 0\right)$ to obtain the steady state part of Fleischmann and Thirsk's eqn. (1.4.9.).

Bockris, Enyo and Kita[86] investigated the potential dependance of V_o. They chose a model in which step lines originate from pairs of screw dislocations of equal and opposite Burger's vector, an idea originally advanced by Burton et al.[5] Bockris et al assumed a random distribution of dislocations and of step lengths and that the number of steps of step length greater than the diameter of the critical nucleus was equal to $1/8\chi_0^2$. The latter assumption is unreliable as it depends upon the model for the arrangement

of steps on the surface. They derived the expression

$$v_o = 8D_s c_o N_o \exp - \left(\frac{2\sqrt{2}\, V \sigma\, N_o^{\frac{1}{2}}}{RT \ln \alpha} \right)^2 \qquad (1.4.43.)$$

where N_o is the total number of steps, V is the molar volume of the metal, σ is the surface energy and α is the supersaturation ratio for adions at the step, attributed the value c/c_o. This latter assumption means that the adion concentration at the step is equal to the mean value over the entire surface, which, in turn, implies a uniform surface coverage and therefore infinitely fast surface diffusion. In such a case considerations of step concentrations are irrelevant.

Many authors have tacitly assumed that electrocrystallisation proceeds exclusively through a surface diffusion stage. It has been shown earlier in this section that the experiments of Gerischer[78] which sought to explain excess concentration polarisation at silver electrodes in terms of changes of the adatom concentration on the surface, may be interpreted by assuming that material is incorporated into the lattice at the growing edges from hemicylindrical diffusion zones.[79] In the light of this interpretation one may consider an alternative mechanism of direct deposition at growth sites for electrocrystallisation. Fleischmann and Thirsk[76] set

up such a model considering hemi-cylindrical diffusion through the solution to each step line. If the inner radius of the hemi-cylinder is equal to the lattice spacing a, then the flux at r = a is given by

$$D\left(\frac{\partial C}{\partial r}\right)_{r=a} = \frac{i_o'}{nF} \exp\left(\frac{\alpha n F \eta}{RT}\right)\left[\frac{C_{r=a}}{C^*} - \exp\left(\frac{-nF\eta}{RT}\right)\right] \qquad (1.4.44.)$$

where D and C are the diffusion coefficient and the concentration in solution respectively and C^* is the concentration in the bulk ($r = \infty$). i_o' is the actual exchange current density at the steps. The steady state occurs when

$$\frac{d}{dr}\left(r\frac{dC}{dr}\right) = 0 \qquad (1.4.45.)$$

The solution of eqn. (1.4.45.) on the terms of eqn. (1.4.44.) leads to a value for the apparent current density i^1 given by,

$$i' = nF\frac{\pi a}{l} D\left(\frac{\partial C}{\partial r}\right)_{r=a} = \frac{\pi a D\, i_o' \exp\frac{\alpha n F\eta}{RT}\left[1 - \exp\left(\frac{-nF\eta}{RT}\right)\right]}{Dl + \left(\frac{l a i_o'}{nFC^*}\right)\exp\left(\frac{\alpha n F\eta}{RT}\right)\ln\left(\frac{l}{a}\right)} \qquad (1.4.46.)$$

A comparison of equations (1.4.14.) and (1.4.46.) shows that surface diffusion predominates over direct deposition at low overpotentials provided that

$$\sqrt{\left(\frac{D_s n F c_o i_o}{\exp\frac{(\alpha-1)nF\eta}{RT}}\right)} \rangle \frac{\pi a D\, i_o'}{D + \frac{a i_o'}{nFC^*}\exp\left(\frac{\alpha n F\eta}{RT}\right)\ln\left(\frac{l}{a}\right)} \qquad (1.4.47.)$$

If D exceeds the second term in the denominator of the R.H.S. of inequality (1.4.47.) (i.e. if rate control by diffusion through the solution is negligible) then (1.4.47.) may be rewritten;

$$\sqrt{\frac{D_s}{k_2}} \cdot i_0 \rangle a\, i_0^{1} \qquad (1.4.48.)$$

It is of interest to substitute typical values in this inequality. Suppose that

$$k_2 \sim \frac{i_0}{nFc_0} \sim 10^{5}\ \text{sec}^{-1} \left\{ c_0 \sim 10^{-12}\ \text{mole.cm}^{-2};\ i_0 \sim 10^{-2}\ \text{amp.cm}^{-2} \right\}$$

and that $D_s \sim 10^{-7}\ \text{cm}^2.\text{sec}^{-1}$

Therefore surface diffusion mechanisms predominate over direct deposition unless $i_0^{1} \rangle 100\, i_0$. Within the probable ran ges of the parameters it is clear that direct deposition is a possible mechanism and should always be considered.

The work of Budevski et al[18,92] has shown that the classical theory of two-dimensional nucleation applies to the electrocrystallisation of silver onto dislocation-free single crystals of silver. The single crystals, exposing only one single plane to electrolysis, of very small area, were grown in a capillary from a single silver crystal of suitable orientation, by an A.C. method. Under galvanostatic

conditions (0.5 - 2.5 $mA.cm^{-2}$) the overpotential rose and having attained 7-12mV began a periodic oscillation. Such oscillations were ascribed to nucleation processes. Under potentiostatic conditions, growth was not observed until an overpotential exceeding 8-12mV was exceeded. A short voltage pulse is applied to the cell held at a potential where no growth occurs, sufficient to enable a nucleus to form. The nucleus then spreads out over the electrode surface to form a two-dimensional monolayer. The current-time curves observed may be simulated by assuming definite co-ordinates for the site of formation of a nucleus of given shape and that the current is proportional to the edge area available at any instant. This latter assumption implies that the rate of lattice incorporation into the expanding edge areas is rate controlling.

From an experimental viewpoint, kinetic measurements of metal electrocrystallisation may be conducted to find the inter-relations amongst overpotential, current density and time. One must apply to the cathode a known potential-time function and observe the resulting current density-time variation or alternatively record the electrode potential during the application of a current-time profile. Observations are most easily interpreted when the applied

function is simple; that is, a sudden stepwise variation of either i or η. Upon changing from either zero current or zero overpotential to a fixed finite value, the system will eventually reach a steady state. However steady-state measurements are not applicable to metal electrocrystallisation systems. Fast processes are obscured by the rate-limiting diffusion of reactant material from the bulk solution to the growing surface. Steady-state measurements cannot provide sufficient information to permit the deduction of an unequivocal mechanism and it is necessary to perform additional transient experiments.

Under galvanostatic conditions the initial current is required to charge the double layer capacity. Thereafter the fraction of the current used for charging diminishes gradually and it is replaced by Faradaic current. Consequently the measured overpotential rises from the initial value, corresponding to the ohmic drop IR through the solution, to the steady state potential. The interpretation of experimental data is facilitated when the overpotential may be considered constant. For example Fleischmann and Thirsk[76] showed that the general solution for the problem of simultaneous charge transfer and surface diffusion is possible for the potentiostatic case, but impossible for galvanostatic

conditions. In the past, experimental difficulties encountered in the development of potentiostatic equipment have usually led to the employment of constant current techniques in metal deposition investigations. Fast electrochemical processes expose an inherent limitation in the single galvanostatic pulse method. For highly reversible systems, the charging and discharge reactions are indistinguishable by this technique. To extend the range of application of the galvanostatic approach, Gerischer and Krause[93,94] preceded the main pulse by a shorter pulse of greater magnitude. It was argued that a pre-pulse of suitable current density and duration would charge the double-layer without seriously disturbing the electrode reaction. Because of the comparative simplicity of interpretation of measurements, the potentiostatic method has been used throughout this thesis.

The foregoing accounts of models for the electrocrystallisation of metal onto bulk parent metal illustrate the difficulties encountered in attempting to explain measurements upon substrates having a complex structure. Step lines are created, advance across the surface, and interact with other step lines. This situation is difficult

to control experimentally and the surface has usually to be brought to a standard condition before the measurement by an anodic polarisation. This procedure is likely to roughen the surface and make measurements at short times unreliable.

It is clearly essential to investigate metal deposition before the complicated structure of the real metal surface has formed. An attempt has been made to do this by depositing N_i^{81} from thiocyanate solutions onto mercury, as mentioned earlier. In this thesis, metal deposition will be investigated by interpreting the phenomenon as a phase change and observing this when metal ions are deposited as metal onto an inert substrate. This has the advantage that the initial stages of growth can be studied when the nuclei may be still reasonably dislocation-free, and the currents are truly controlled by the kinetics of the electrocrystallisation reaction.

The observed current into a growing nucleus depends on the geometry and the site of the slow step.[95] The slow step is assumed to be incorporation at the edge of a growing nucleus, all transport processes to the nucleus being fast. If one considers a single hemispherical nucleus growing on a surface under potentiostatic conditions, then if V(t) is the volume of the nucleus at any time, r is the radius, and

i(t) the current

$$i(t) \propto \frac{dV(t)}{dt} \propto \frac{\partial}{\partial r}\left(\frac{2}{3}\pi r^3_{(t)}\right)\frac{dr}{dt} \propto 2\pi r^2_{(t)} \qquad (1.4.49.)$$

and $r(t) \propto t \;;\quad i(t) \propto t^2$

in the early stages of growth, before overlapping becomes important.

Another possibility is that the slow step is round the basal periphery (for instance by the movement of adatoms along the basal plane); then the rising transient can be calculated as follows

$$i(t) \propto \frac{\partial}{\partial r}\left(\frac{2}{3}\pi r^3_{(t)}\right)\frac{\partial r}{\partial t} \propto 2\pi r_{(t)}$$

and

$$r(t) \propto t^{\frac{1}{2}}\;; \qquad i(t) \propto t^{\frac{1}{2}} \qquad (1.4.50.)$$

The constant of proportionality in eqn. (1.4.49.) is obtained by equating

$$\left(\frac{n_{Fe}}{M}\right) 2\pi r^2_{(t)} \frac{\partial r}{\partial t} = n_{Fk}\, 2\pi r^2_{(t)} \qquad (1.4.51.)$$

where ρ is the metallic density, M the molar mass and k the lattice incorporation rate constant is moles cm^{-2} sec^{-1}.

Thus one obtains for one nucleus,

$$j = \left(\frac{2\eta F_{\pi} M^2 k^3}{\rho^2} \right) t^2 \qquad (1.4.52.)$$

The laws of growth for a single nucleus can be combined with the appropriate law of nucleation to give the overall current-time variation.[82] If the growth law is written

$$j = f_1(u) \qquad (1.4.53.)$$

and the nucleation law

$$N = f_2(t) \qquad (1.4.54.)$$

then the overall current is given by

$$j = \int_0^t f_1(u) \left(\frac{d}{dt} f_2 \right)_{t=(t-u)} du \qquad (1.4.55.)$$

The integral summates contributions to the overall current at time t for centres formed u ago for all u from $u = 0$ to $u = t$. If there is a uniform probability with time of converting sites into nuclei, the nucleation law is first order,

$$N = N_0 \left(1 - \exp(-At)\right) \qquad (1.4.56.)$$

where N_0 is the total number of sites and **A** is the nucleation rate constant in sec^{-1}.

Eqn. (1.4.56.) gives two limiting cases of special

interest; if A is large, all the sites are converted to nuclei virtually instantaneously:

$$N \approx N_0 \tag{1.4.57.}$$

while if A is small,

$$N \approx A N_0 t \tag{1.4.58.}$$

Upon substituting eqn. (1.4.52.) and either (1.4.57.) or (1.4.58.) into eqn. (1.4.55.), one obtains the expressions for three-dimensional (hemispherical) growth with instantaneous nucleation:

$$i = \left(\frac{2\pi F_\pi M^2 k^3 N_0}{\rho^2} \right) t^2 \tag{1.4.59.}$$

and with progressive nucleation;

$$i = \left(\frac{2\pi F_\pi M^2 k^3 A N_0}{3\rho^2} \right) t^3 \tag{1.4.60.}$$

The form of the nucleation rate constant, A, may be derived by considering the change in free energy associated with the formation of the nucleus. For the growth of a hemisphere radius r, density ρ;

$$\Delta G = -\frac{2}{3}\pi r^3 \rho \frac{F}{M} n\eta + 2\pi r^2 \sigma_1 + \pi r^2 (\sigma_2 - \sigma_3) \tag{1.4.61.}$$

where σ_1, σ_2, and σ_3 are the surface energies for the nucleus-solution, nucleus-electrode and electrode-solution interfaces respectively. The maximum value will be

$$\Delta G_{max} = \frac{[\lambda\sigma_1 + (\sigma_2-\sigma_3)]^3 M^2 \pi}{e^2 F^2 n^2 \eta^2 3} \qquad (1.4.62.)$$

ΔG_{max} may be equated to the free energy of activation for nucleation and thus one obtains,

$$A = K k_o \exp\left\{\frac{-N[\lambda\sigma_1 + (\sigma_2-\sigma_3)]^3 M^2 \pi}{RT e^2 F^2 n^2 \eta^2 3}\right\} \qquad (1.4.63.)$$

where N is the Avogadro number, k_o the growth constant at the reversible potential and K is a constant containing the number of adsorbed species and the frequency factor.

The form of the growth (lattice incorporation) rate constant, k, was suggested by Fleischmann and Thirsk,[82]

$$k = k_o \left(\prod_j a_j^{\nu_j}\right) \exp\left(\alpha n F \phi / RT\right) \qquad (1.4.64.)$$

where a_j, ν_j represent the activities and reactant orders of the reactants. This expression follows from the normal charge-transfer expression and applies provided either the discharge step is rate-controlling at higher overpotentials, lattice formation being rapid, or else discharge takes place directly at the lattice building sites.

By similar arguments to those used above one may predict

the form of the current-time rising transient observed for other combinations of geometry, reaction site, mode of transport to the growing centre and type of nucleation.[95] These equations are not, however, unique, as can be seen by reference to Table 1, in which some possible dependencies are given.

Table 1

t^3	t^2	t	$t^{1/2}$	e^t	$t^{3/2}$	
Progress-ive	Instant-aneous	Instant-aneous	Instant-aneous	Progress-ive	Progress-ive	a)
3D	3D	2D	3D	2D	3D	b)
periph-ery	periph-ery	periph-ery	basal periph-ery	Top area	basal periph-ery	c)
none	none	none	none	none	none	d)
	Progress-ive	Progress-ive	Instant-aneous		Progress-ive	a)
	2D	1D	3D		3D	b)
	periph-ery	periph-ery	periph-ery		periph-ery	c)
	none	none	planar diffus-ion		planar diffus-ion	d)

a) Type of nucleation; b) geometry; c) site of slow step;

d) transport in solution.

A knowledge of the geometry by means of electron diffraction is an advantageous prerequisite to the interpretation of experimentally observed potentiostatic rising current-time transients. Application of a double potentiostatic pulse technique often clarifies the nature of the geometry of the deposited nuclei. A large potential prepulse of short duration effectively nucleates all the available surface sites and the growth of such nuclei may be followed at the lower potentials of the second pulse under essentially instantaneous nucleation conditions, as the nucleation rate constant is generally an extremely sensitive function of overpotential, c.f. eqn. (1.4.63.).

Chapter 2

Experimental

2.1. Introduction

Electrochemical measurements reported in this thesis were obtained under conditions of controlled potential of the working electrode. Electronic potentiostats were employed in all experiments.

All measurements were obtained at room temperature, $24 \pm 1^{o}C$.

2.2. Potentiostat

A valve potentiostat (Chemical Electronics Co., Newcastle) and one with full solid stage circuitry (Chemical Electronics Co., type TR70-2A) were used on occasion. The design factors and circuit details of the valve instrument have been described by Bewick et al.[96,97] The details of the transistorized machine are similar to those described by Bewick and Brown.[98] The valve machine was capable of stabilising to within 0.1mV in a time of ~20μ sec in response to the application of a step potential function, under typical working conditions. The solid state machine required a time of ~50μ sec.

2.3. Function Generators

A block diagram of the potentiostat and associated

equipment is shown in Fig.5. The function (wave-form) generator provided either pulses, in order to superimpose rectangular potential-time profiles on the d.c. potential of the working electrode, or triangular potential sweeps which superimposed triangular potential-time profiles.

The valve-type generator provided only pulses, and is described by Bewick and Fleischmann.[97] The output consisted of two consecutive variable length pulses, the magnitudes of which could be varied independently in increments of 1mV. The solid-state generator (Chemical Electronics Co., type RB1) provided both pulses and potential sweeps, and a similar instrument is described by Brown.[99] The pulse output was similar to that described above and the sweep output consisted of independently variable forward and reverse sweeps (range 0.1 mV/sec to 10^3 V/sec) of maximum amplitude 3V, adjustable to 3 mV.

2.4. Recording and Measuring Equipment

The current flowing through the cell was measured either directly on the potentiostat microammeter, or as the voltage drop across a standard resistor in series with the cell. The standard resistors used were 10 and 100 Ω. For pulsed experiments the voltage was displayed as a function of time on a Tetronix type 503, 502 dual-beam or Telequipment

fig 5 Block diagram of potentiostatic equipment

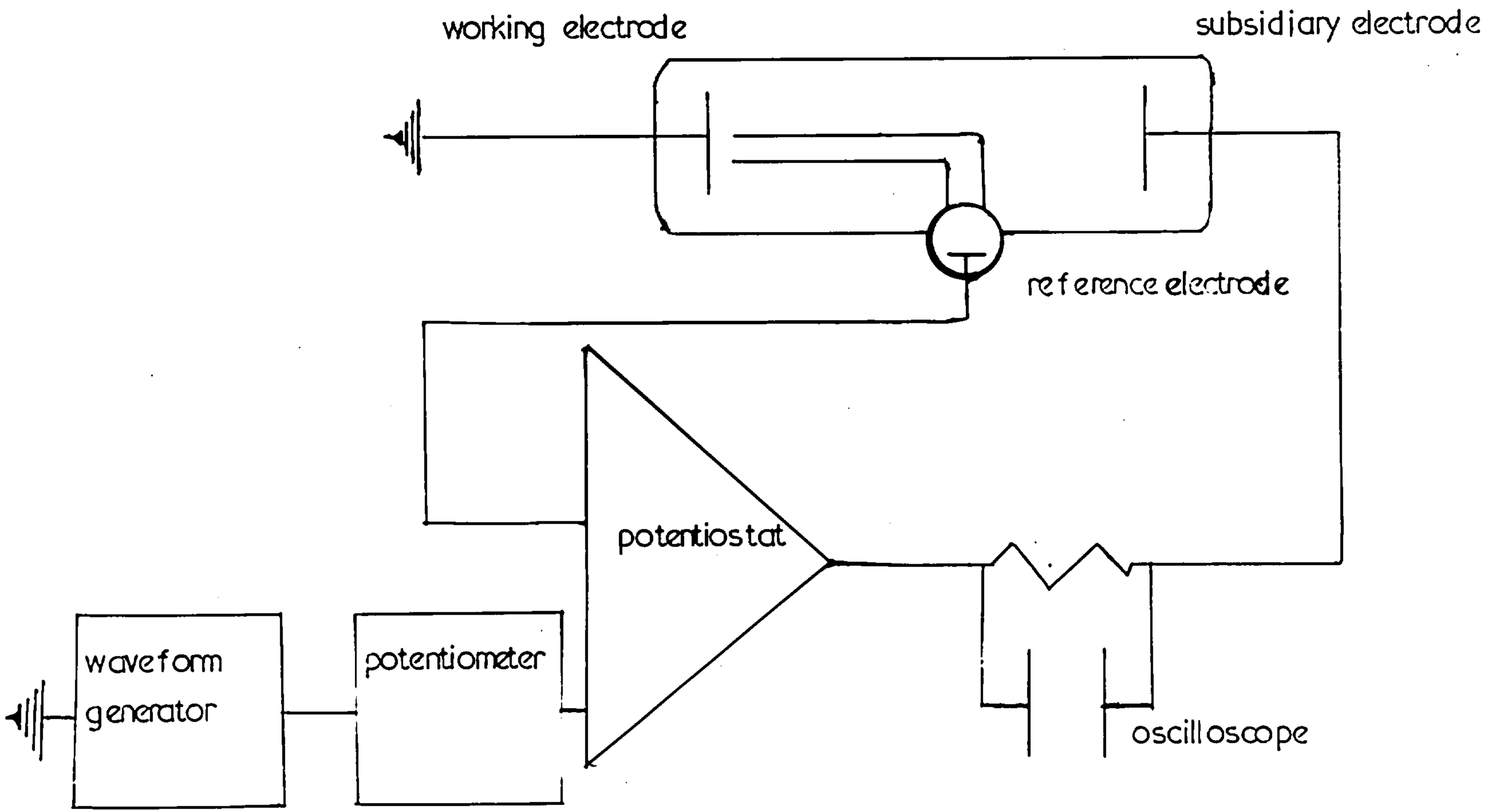

type D53 oscilloscope, which was triggered from the pulse generator. Current-time transients were then photographically recorded using a Shackman oscilloscope camera type AC2/25. Slow transients were obtained by observing the current on the microammeter as a function of time measured using a stop-clock.

For linear sweep measurements the voltage drop across the standard resistor was displayed against the voltage sweep, by connecting the horizontal deflection plates of the Tetronix type 502 dual-beam oscilloscope for external voltage amplification from the sweep generator output.

The rest (equilibrium) potentials of the working electrodes under certain conditions were measured with the aid of a Tinsley potentiometer (type 3387B).

2.5. Preparation of Electrodes

(i) Mercury.

Mercury was purified by prolonged agitation with dilute nitric acid followed by vacuum distillation.

(ii) Silver.

Rods of polycrystalline silver were supplied by Johnson, Matthey and Co. and were spectrographically standardised (99.999% purity). A silver single crystal rod offering the 111 face was supplied by Metals Research Ltd., Royston,

Herts. The rods were held in B14 cones of teflon. These rods were insulated around their length with Lacomit and the circular base surface was prepared for electrochemical measurements by electropolishing. The method used was similar to the one employed by Shuttleworth et al.[100] The polishing was carried out under potentiostatic conditions in the cell shown in Fig.6. The solution consisted of 35gm/l AgCN, 30gm/l KCN and 38gm/l K_2CO_3. The silver electrode to be polished was held at an anodic overpotential of 600mV for ten minutes, when a constant current of ca. 3 $mA.cm^{-2}$ flowed. The cell was then switched out of the potentiostatic circuit, and the silver rod immediately removed from the polishing solution and washed with distilled water. If a grey film of silver cyanide formed on the electrode surface this was removed by gentle rubbing on a selvyt cloth, and the process repeated. The silver-coated probe Pt, which constituted the reference potential for the polishing, was prepared in situ on each occasion by cathodically polarising the uncoated Pt sphere with respect to the silver subsidiary electrode for a few seconds using a 2V accumulator. It was found necessary to connect a 100 Ω resistor in series with the probe under potentiostatic conditions in order to prevent oscillation of the potentiostat.

fig6 Electropolishing cell for Ag electrodes

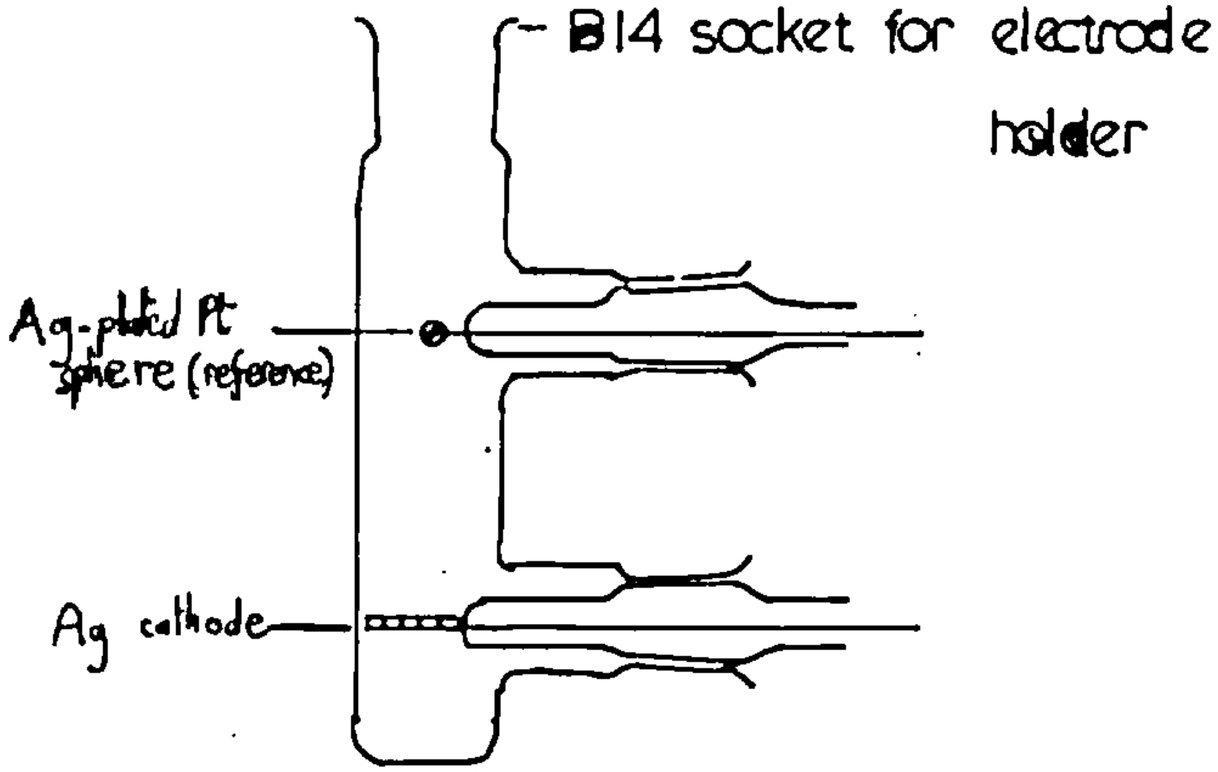

fig 8 Cell for kinetic measurements using Hg electrodes

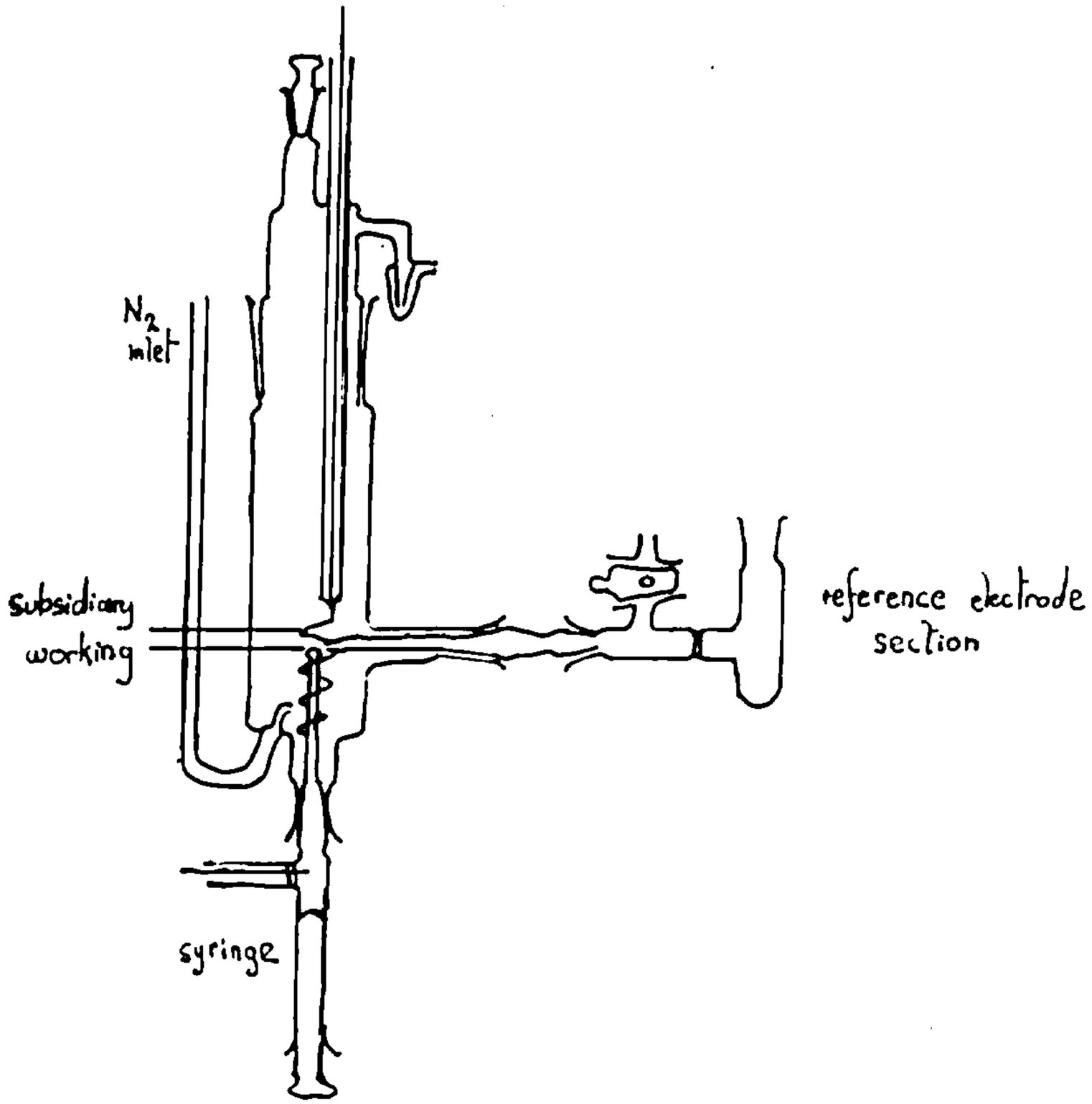

(iii) Glassy Carbon.

Rods of glassy carbon of ca. 6mm diameter were supplied by Vitreous Carbons Ltd., Bishop Auckland. Lengths of ca. 2cm. were cut off and drilled to take brass connecting rods of ca. 2mm diameter, using an ultrasonic device. The contact between the carbon and the brass was made secure with the use of thermo-setting silver cement (Johnson, Matthey and Co.). The resistance of the final assembly was ca. 0.3Ω. The electrode base surface to be used for deposition was prepared by successively polishing with all grades of S.I.A. emery paper, slow-cutting and γ-alumina on selvyt cloths and finally grades 6μ, 1μ and 0.1μ diamond pastes. The final polishing with diamond paste was conducted with the aid of a mechanical device. The sides of the carbon electrode and brass rod which was to be immersed in the cell solutions, were insulated at first with Lacomit but later on by shrink-fitting teflon tubing over them. The brass rod was held firm in a teflon B14 cone for cell measurements.

(iv) Pyrolytic Graphite.

Lengths of pyrolytic graphite of square cross-section were supplied by Le Carbone Ltd., Portslade. The lengths (ca. 2cm) were drilled to take tight-fitting brass connecting rods. The resistance of the assemblies were

ca. 2 Ω. Fresh surfaces were obtained by cleaving the carbon using a razor blade. The electrode sides and connection were insulated with Lacomit.

(v) Lead.

A square of polycrystalline lead (99.99% purity) was tapped with a brass connecting rod to form a suitable electrode assembly. Lacomit served as insulating material. The surface of the lead was prepared by electropolishing by a method similar to that used by Moulen.[101] The polishing solution employed was 40% ammonium fluoroborate and 2% sulphuric acid in water. The cathode was a Pt spade. The lead was polarised anodic to the Pt by the application of a 20V differential from a Belix power unit (type TSS 57) for 5 seconds, producing a current density of ca. 5 $A.cm^{-2}$. The surface of the lead was then washed with distilled water to remove deposited lead sulphate.

2.6. Electrochemical Cell for Solid Electrodes

The cell used for all potentiostatic kinetic experiments using solid working electrodes is shown in Fig.7. The working electrode was adjusted in the vertical direction until the electrode surface was within 1mm of the tip of the Luggin capillary, which was connected via a side arm to the reference electrode compartment. In the case of silver deposition studies on the two carbon electrodes from

fig 7 Cell for kinetic measurements using solid electrodes

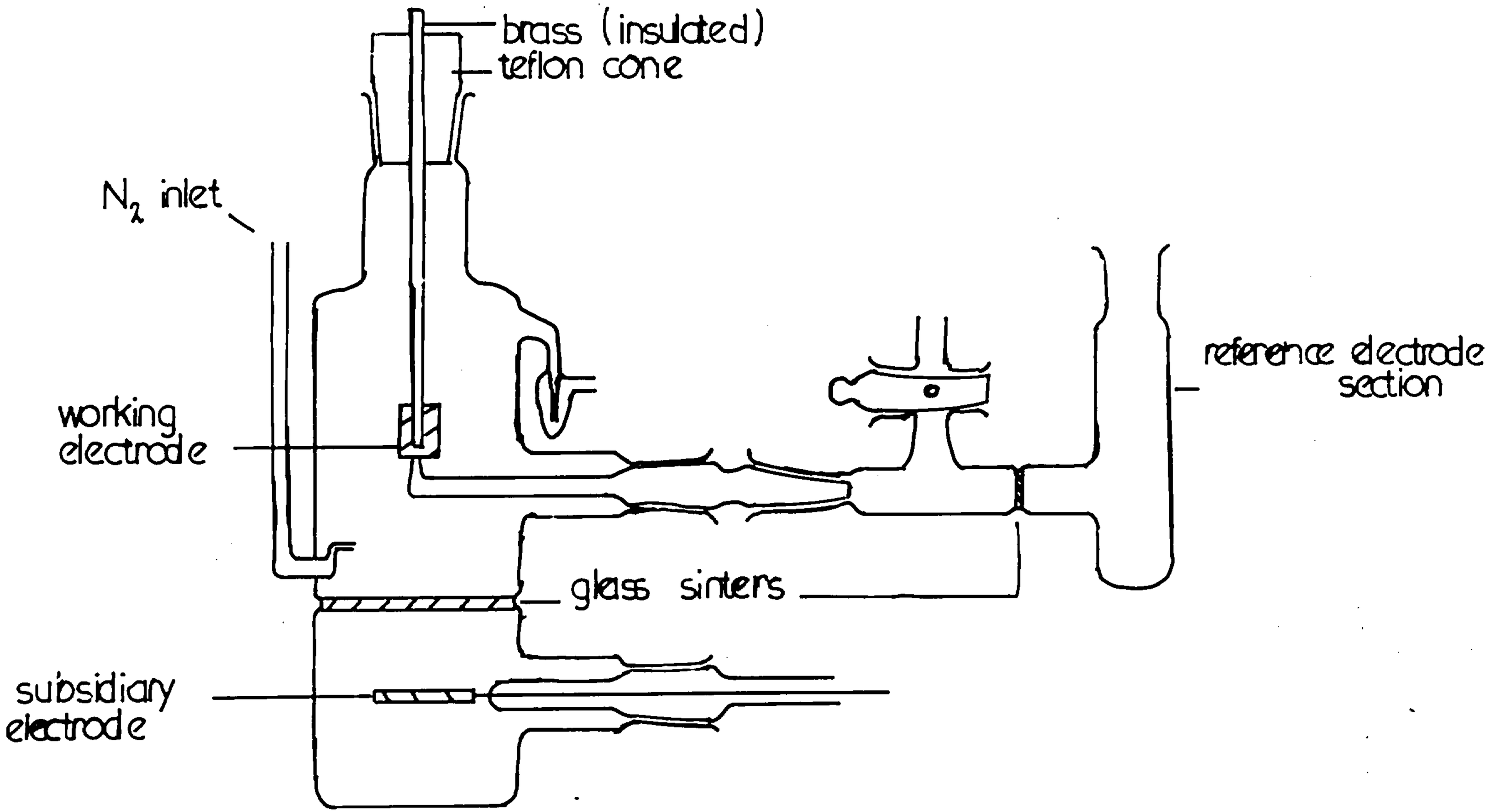

solutions of argentous ions, the Luggin capillary was replaced by a silver probe similar to that used in the silver electrode electropolishing cell (section 2.5 (ii)). The subsidiary electrode consisted of a 2 x 1 cm Pt grid placed symmetrically beneath the working electrode in a compartment separated by a glass sinter. Provision was made for bubbling of nitrogen through the cell solution. 'White spot' nitrogen (< 10 vols. in 10^6 oxygen) was used. Nitrogen was passed for 30 minutes before measurements were made.

2.7. Electrochemical Cell for Mercury Electrodes

The cell used for potentiostatic measurements was of the type shown in Fig.8. The working electrode consisted of a drop of mercury formed at the tip of a chamfered vertical capillary. A precision micrometer syringe attached to the lower end of the capillary allowed renewal of the mercury drop. The order of the drop area was 10^{-1} cm^2; the exact value was determined by measurement with a travelling microscope.

The subsidiary electrode consisted of a helix of platinum wire concentric with the upturned capillary of the working electrode. The Luggin capillary protruded horizontally through the helix, terminating within a millimetre of the mercury drop. The cell had provision for bubbling nitrogen

through the cell solution, which was passed for 30 minutes before measurements.

2.8. Reference Electrodes

(i) Ag/Ag^+

Silver-silver ion electrodes were either produced upon Pt sphere-probes (for measurements on silver deposition on carbon) or on Pt frits, the latter, sealed into a central glass tube, being attached through B14 cones so as to fit into the reference electrode compartment illustrated in Figs. 7 and 8. The Pt was first cleaned with nitric acid, and then Ag-plated by cathodic polarisation with respect to a pure Ag anode (Matthey spectrographically standardised) using a 2V accumulator for 30 minutes, in an identical cyanide solution to that used in section 2.5 (ii). For silver deposition measurements the reference electrode solution was identical to the cell solution. For mercury deposition, the solution was of the same concentration in Ag^+ as the cell solution in Hg_2^{2+}, both solutions having the same total ionic strength. (The liquid junction between the cell and reference compartment solutions was achieved with the aid of a glass sinter as shown in Figs. 7 and 8). Such electrodes differed by less than 1mV.

(ii) Calomel.

For certain measurements on palladium deposition a calomel electrode in 3M HCl was employed. The electrode was of the 'dip' type, designed to fit in the reference side arms. A platinum wire sealed into the central glass tube made contact with the mercury, on top of which was a thin layer of a paste of mercury, mercurous chloride and 3M HCl solution.

(iii) Pd/H_2

A palladium-hydrogen electrode (used for some palladium deposition measurements) was prepared by melting palladium wire so as to form a sphere which was sealed into glass, attached to a B14 cone for the reference compartment. The sphere was then 'charged' with hydrogen at 50mA by polarising cathodic for five minutes in 0.5M sulphuric acid, reversing the polarity for five minutes and finally cathodic again for five minutes, with respect to a Pt counter electrode.

(iv) PbO_2

In the case of measurements on lead dioxide deposition on glassy carbon a lead dioxide reference of the dip type was made by digesting commercial lead dioxide in 2M nitric acid at $100^{o}C$ for two days, storing the lead dioxide under dilute nitric acid and employing a reference solution identical to the cell solution.

(v) Ag/AgCl

Silver/silver chloride electrodes were prepared by chloridizing silver electrodes (prepared as in section 2.8. (i)), by passing ca. 0.4 $mA.cm^{-2}$ for 30 minutes in 0.1M HCl, using a Pt counter electrode. The reference solution employed was invariably 1M KCl. Such electrodes differed by less than 1mV.

2.9. Cleaning of Glassware

All glassware and the teflon electrode holders were rigorously cleaned with a saturated solution of potassium dichromate in sulphuric acid. Before each experiment the apparatus was rinsed thoroughly with triply distilled water.

2.10. Preparation of Solutions

Triply distilled water was used in the preparation of all solutions. This was prepared by two distillations of once-distilled water, firstly from a weakly alkaline solution of A.R. potassium permanganate and then from a solution containing a trace of A.R. orthophosphoric acid. The final distillate was collected and stored in glass-stoppered Pyrex flasks.

(i) Silver solutions.

Silver solutions were prepared by anodic dissolution of Johnson Matthey spectrographically pure silver in A.R. 1M $HClO_4$. The anode compartment, of capacity ca. 250ml, was

separated from the cathode (a Pt wire) compartment of capacity ca. 25ml, by a glass frit. A current density of ca. 200 $mA.cm^{-2}$ was employed. The stock silver solution so produced was diluted down to the required silver concentration to a constant ionic strength of 1M with perchloric acid. The solutions were standardised by titration against thiocyanate, using a ferric solution as indicator .

(ii) Palladium solutions.

Solutions of palladous chloride were prepared from B.D.H. palladium chloride and were made up to constant ionic strength with A.R. perchloric acid and constant-boiling hydrochloric acid. These solutions were standardised gravimetrically by reduction to the metal with formate.

(iii) Mercurous solutions.

Once-recrystallised A.R. mercurous nitrate was used, the solutions being made up to constant ionic strength with once-recrystallised A.R. potassium nitrate. A trace of A.R. nitric acid was added to prevent hydrolysis.

(iv) Lead solutions.

(a) acetate. Solutions of once-recrystallised A.R. lead acetate were made up to constant ionic strength with once-recrystallised A.R. sodium acetate and A.R. glacial acetic acid.

(b) chloride. Once-recrystallised A.R. lead nitrate was used in solutions of once-recrystallised A.R. potassium chloride.

(v) Thallous solutions.

Thallous solutions were made up from A.R. thallous sulphate and once-recrystallised A.R. potassium chloride.

(vi) Cadmium solutions.

Cadmium solutions were made up from twice-recrystallised cadmium perchlorate, prepared by dissolving the preciptated hydroxide in A.R. perchloric acid, and once-recrystallised A.R. sodium perchlorate.

(vii) Cobalt solutions.

(a) thiocyanate. Solutions of A.R. cobaltous nitrate were made up to constant ionic strength with once-recrystallised A.R. potassium thiocyanate.

(b) nitrate. A.R. cobaltous nitrate was used in solutions of once-recrystallised A.R. potassium nitrate.

2.11. Electron Microscopy

In order to examine the surface of solid electrodes (with or without deposit) by electron optical means, it was necessary to prepare replicas of the electrode surfaces. This was effected as follows: a 2% solution of collodion in amyl acetate was applied to the surface and when dry, the plastic film was stripped from the electrode using

'Sellotape' with an interposed 200 mesh copper grid, protected from the adhesive tape by a small piece of very thin paper. The replica formed in the plastic was then often shadowed at a known angle by vacuum deposition of a thin layer of Au/Pd alloy applied from a point source, and subsequently backed with a thin layer of vacuum deposited carbon. After dissolution of the collodion in amyl acetate the resultant negatively shadowed carbon replica of the surface was examined using an Akashi Tronscope model TRS 50E1 electron microscope.

Deposits on and surfaces of silver and carbon electrodes of suitable dimensions (length $<$ 1 cm) were examined directly by scanning electron microscopy, using a Stereoscan electron microscope (Cambridge Instrument Co. Ltd.).

2.12. Optical Microscopy

Deposits on carbon electrodes of suitable dimensions were also viewed directly by an optical microscope (Cooke, Throughton and Simms Ltd., M4080).

2.13. Electron Diffraction

Deposits of lead on silver electrodes were stripped from the electrode surface after the application of collodion, using 'Sellotape'. The film was prepared for examination by vacuum evaporation of a thin layer (~ 50 to 100Å) of

carbon on to the electrodeposit, after which they were cut into small pieces and mounted on copper electron microscope grids, plastic side down. The collodion was dissolved off with amyl acetate, leaving the deposit supported by the thin carbon film. Examination by electron diffraction was carried out by the transmission technique using a Metropolitan Vickers type EM3 electron microscope.

Somewhat less satisfactory results were obtained by the glancing incidence technique, with the solid electrode mounted in the A.E.I. type ED2 electron diffraction camera.

Chapter 3

The Electrocrystallisation of Silver

3.1. Introduction

This chapter contains accounts of measurements on the deposition of silver upon silver substrates, and upon inert carbon substrates.

3.2. The deposition of silver upon silver

It has been mentioned in Chapter 1, Section 4, that many workers have assumed that the electrocrystallisation of metals onto the parent metal involves a slow stage of adatom surface diffusion. This implies a low concentration of surface adatoms at cathodic overpotentials. It is the purpose of this section to show that potentiostatic transients for the deposition of silver onto silver may be interpreted solely in terms of semi-infinite linear diffusion of silver ions from the bulk solution, the concentration of silver ions at the interface being maintained by Nernstian equilibrium.

At the interface,

$$\left(\frac{C_{Ag}}{C_{Ag}^{*}}\right)\exp\frac{(\gamma-1)F\eta}{RT} = \left(\frac{C^{o}_{Ag^{+}}}{C^{*}_{Ag^{+}}}\right)\exp\frac{\alpha F\eta}{RT} \qquad (3.2.1.),$$

where C_{Ag} and C_{Ag}^{*} represent the active 'concentration' of 'surface' silver atoms available at any η and the reversible potential; $C^{o}_{Ag^+}$, $C^{*}_{Ag^+}$ the interfacial concentrations of silver ions at η and E^{o}, and η is taken positive for cathodic. C^{*}_{Ag} is regarded as the surface plane concentration of the silver electrode i.e. no 'additional' Ag atom concentration being present.

Thus one obtains

$$C^{o}_{Ag^+} = C^{*}_{Ag^+} + \left(C_{Ag}/C_{Ag}^{*}\right)\exp -F\eta/RT \qquad (3.2.2.)$$

Upon substitution of eqn. (3.2.2.) in the expression for control by semi-infinite linear diffusion, $i = FA\left(C^{*}_{Ag^+} - C^{o}_{Ag^+}\right)\sqrt{D/\pi t}$ one obtains,

$$i = FAC^{*}_{Ag^+}\sqrt{\frac{D}{\pi t}}\left(1 - \frac{C_{Ag}}{C_{Ag}^{*}}\exp\frac{-F\eta}{RT}\right) \qquad (3.2.3.)$$

Thus a plot of i vs. $\exp(-F\eta/RT)$ at fixed times will have a slope $= FAC^{*}_{Ag^+}\sqrt{D/\pi t}\left(C_{Ag}/C_{Ag}^{*}\right) \cdot FAC^{*}_{Ag^+}\sqrt{D/\pi t}$ will be given by the intercept on the i axis.

Fig.9 shows a plot of i vs. $t^{-1/2}$ obtained with the electropolished polycrystalline silver electrode in 1.265 x 10^{-2}M $AgClO_4$/1M $HClO_4$ solution for a series of cathodic pulses, starting from the equilibrium potential. It is

fig 9 O·01265 M $AgClO_4$/1M $HClO_4$. electropolished, polycrystalline Ag electrode. i vs $t^{-1/2}$.

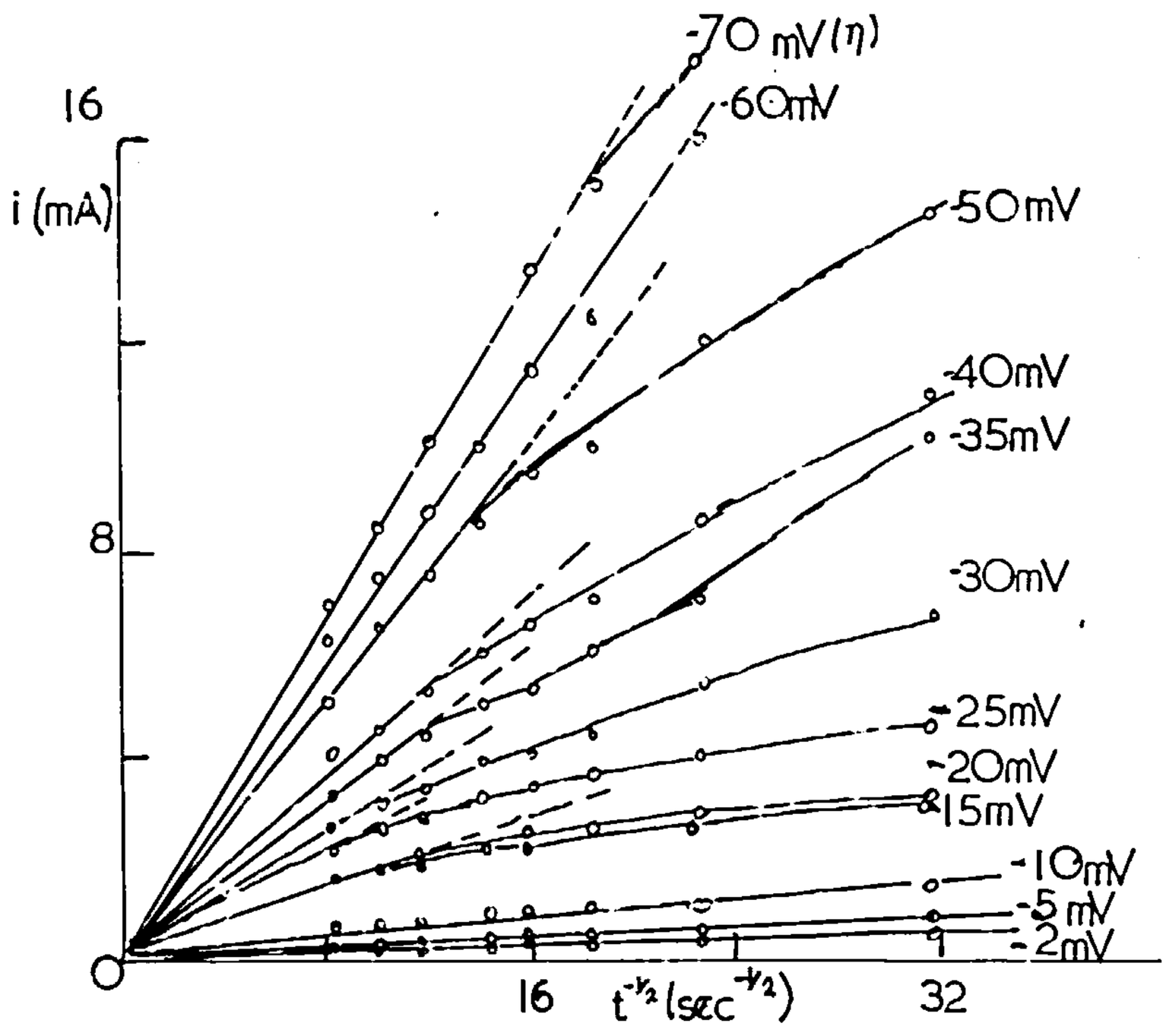

fig 10 O·01265M $AgClO_4$/1M $HClO_4$ .elpd.pdyc. Ag. i(t) vs. exp(−ηF/RT) for 1) t = 1 msec ;2) t = 3 msec ; 3) t = 7·5 msec ; 4) t = 10 msec.

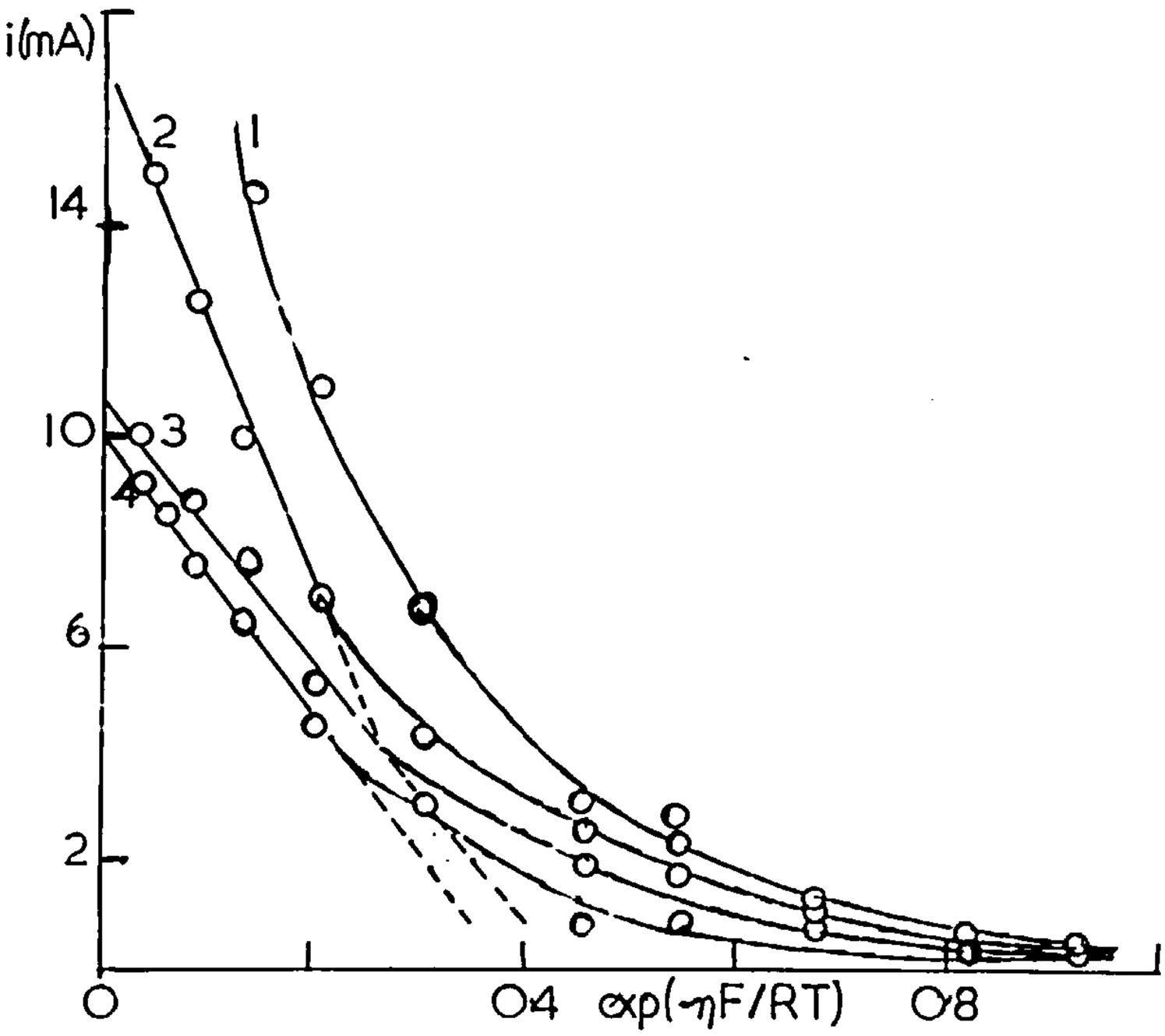

noticeable that the plots curve down from linearity at times $<$ ca. 10 m sec. Such a situation would arise if the ratio $(C_{Ag}/C_{Ag}{}^{*})$ were larger at short times. One might envisage that the electrode surface, initially rather rough, would be smoothed out by deposition as time proceeds thus causing a lowering of the 'activity' of silver surface atoms. This explanation would account for the fact that the departure from linearity of the i vs. $t^{-1/2}$ plot was restricted to shorter times as the overpotential was increased.

Fig.10 shows a plot of i vs. $\exp -F\eta/RT$ at various times. The plots are quite curved at the shorter times, though some degree of linearity is achieved at t = 10 msec when one might assume that the smoothing process had been completed. In any case because of the macroscopic irregularities of height b on the surface, measurements at short times are inaccessible. This has been discussed by De Levie[102] who suggests that only measurements at times given by

$$\sqrt{Dt} \gg b$$

are meaningful unless the exact geometry is known. Hence for b values of 1μ, only measurements at times greater than 1 msec may be considered. From such plots a value of $(C_{Ag}/C_{Ag}{}^{*})$ of ca. 2 to 3 is obtained. The concentration of

'adatoms' on a silver electrode has been estimated by Despic and Bockris[91] as ca. 10^{-11} moles cm^{-2}. C^{*}_{Ag} may be taken (since Ag has a f.c.c. lattice) as $\sim 2 \times 10^{-9}$ moles cm^{-2}. Thus any adatom theory predicts (C_{Ag}/C_{Ag}^{*}) as ca. 5×10^{-3}. As the experimental ratio obtained shows that the surface activity of the silver is essentially the geometric area, the need for the invocation of adatoms is dubious.

3.3. The deposition of silver upon silver under sweep conditions

In a recent paper by Krebs and Roe,[103] it was postulated that hemispherically shaped deposits are formed when silver is deposited on a silver substrate, these deposits being of greater reactivity than the substrate. If this is the case it is an indication that the nucleation and growth of discrete nuclei would be a controlling process in silver electro-crystallisation upon the parent metal. Such a process has been identified (though a two-dimensional nucleation) for the deposition of silver on dislocation-free single silver filaments, but not on 'ordinary' silver surfaces.

Krebs and Roe[103] used single crystal silver electrodes in the forms of spheres formed by a fusion technique. The electrode was held in a cell containing an atmosphere of helium and small areas (typically 1×10^{-4} to 3×10^{-3} cm^{2}) on the electrode surface were brought into electrical

contact with the bulk solution with the aid of a probe of small orifice. The probe tip allowed the formation and maintenance of a narrow electrolyte column between the bulk solution (and counter reference electrode) in the probe and the selected area on the crystal sphere. It was claimed that the advantage of the probe technique over conventional electrode/electrolyte assemblies was that the risk of electrode contamination was greatly reduced; the electrode area/electrolyte volume ratio being several orders of magnitude more favourable. After the completion of a series of measurements, the electrode was etched and remelted to form a new crystal sphere.

Krebs and Roe investigated the behaviour of the system under potential sweep conditions using sweeps in the range 0.05 to 1mV/sec. Starting from the rest potential they first scanned in the anodic direction, then reversed the sweep, finally scanning anodic again. They found that most of their current/voltage plots exhibited some degree of hysteresis, which in some extreme cases appeared as distinct anodic peaks on the second such sweep, as indicated in Fig.11. They argued that the consistent lack of hysteresis for cyclic scans restricted to the initial anodic scan clearly demonstrated that the deposited silver, formed on the

fig 11 Cyclic current-potential curve (from Krebs and Roe).
0·05M Ag^+; 0·57 mV/sec. electrolyte contact area, 0·0023 cm^2.

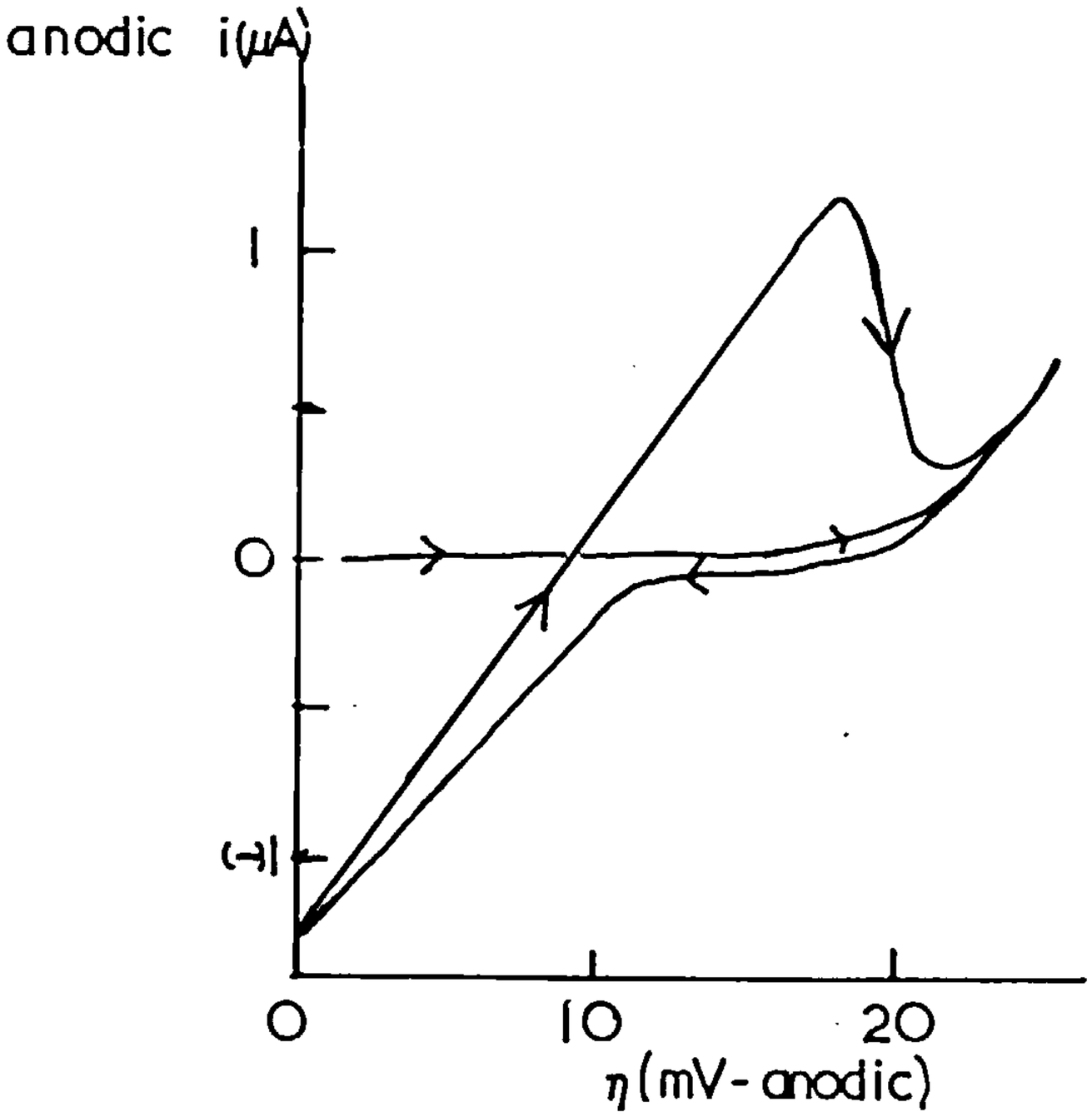

fig 12 Scheme of surface concentration-gradient variation for sweep conditions.

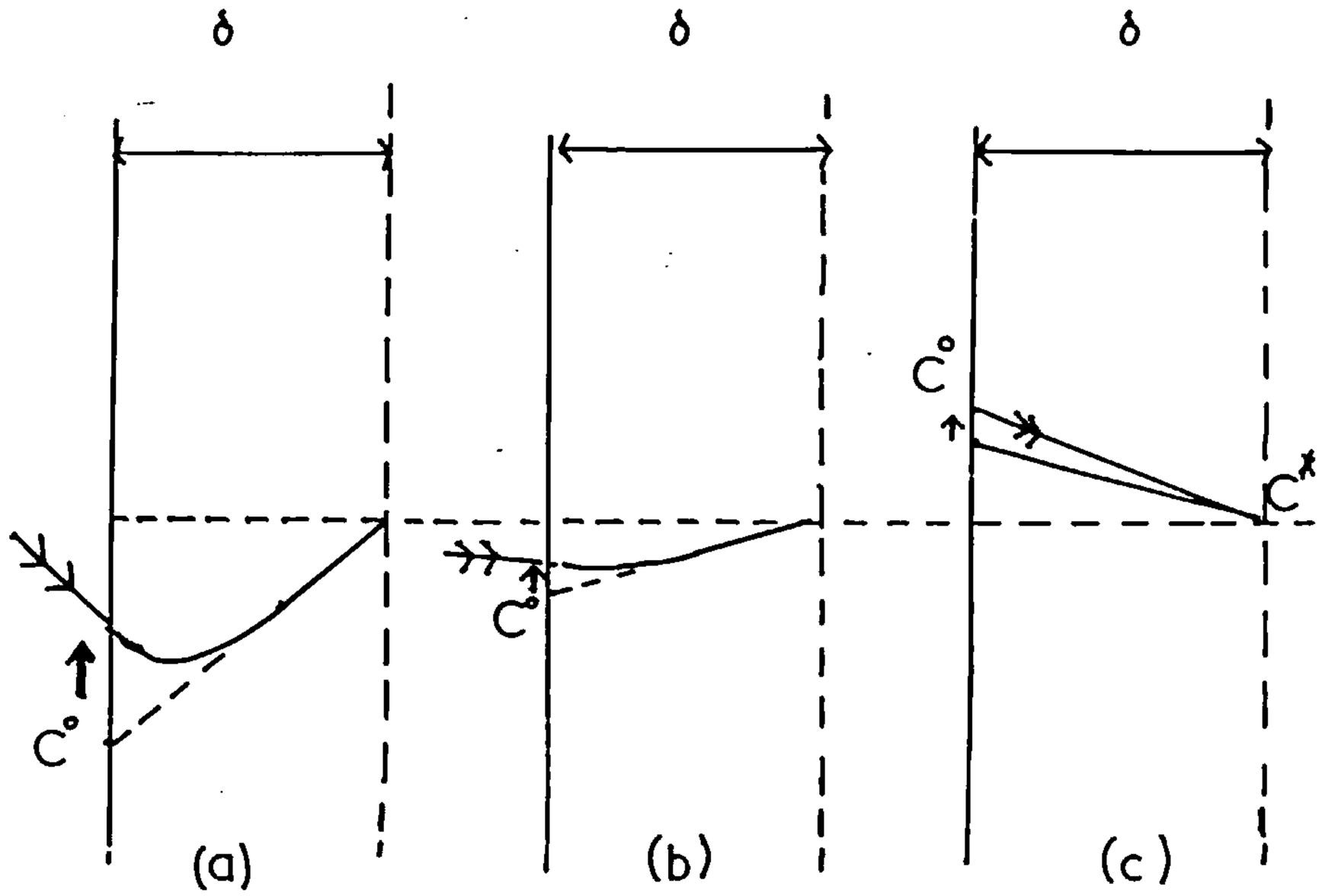

cathodic scan, was responsible for the hysteresis observed on the return anodic scans. Further evidence for this hypothesis was provided by the observed proportionality of the return anodic peak to the amount of silver deposited during a series of cyclic scans. Krebs and Roe concluded that the deposit silver was more reactive than the substrate. They presented an analysis of the situation for linear scan stripping assuming that the change of the deposit area was a controlling factor, the substrate being considered inert. They assumed that:

(i) All the deposits were of equal size and hemispherical. They presented microscopic evidence for this after extensive deposition had occurred.

(ii) The activity of the deposits was constant.

(iii) The electrolyte was homogeneous prior to the commencement of stripping.

(iv) Conditions for semi-infinite linear diffusion existed. Though diffusion to a single hemisphere is hemispherical, the linear approximation improves for many hemispheres as the degree of overlap of the individual diffusion layers increases.

The solution of Fick's second law for linear diffusion for the conditions of linear scan, assuming the electrode process to be reversible, may be differentiated to yield the flux at the interface.

$$\text{i.e.} \quad \left(\frac{\partial C_{(x,t)}}{\partial x}\right)_{x=0} = - \frac{C^{*}\left(\frac{nF\omega}{RT}\right)^{\frac{1}{2}}}{D^{\frac{1}{2}}} \exp\left(\frac{nF\omega t}{RT}\right) \operatorname{erf}\left[\left(\frac{nF\omega t}{RT}\right)^{\frac{1}{2}}\right] \qquad (3.3.1.)$$

where C^{*} is the bulk concentration, w the scan rate.

For a single hemisphere, area A,

$$A_{(t)} = 2\pi \left(\frac{3M}{2\pi}\right)^{\frac{2}{3}} Q'^{\frac{2}{3}}_{(t)} \qquad (3.3.2.)$$

where M is atomic weight/$F\rho$ and Q' is the hemispherical charge.

For N deposits, (3.3.2.) becomes

$$A_{(t)} = \gamma N^{\frac{1}{3}} Q^{\frac{2}{3}}_{(t)} \qquad (3.3.3.)$$

where

$$\gamma = 2\pi \left(3M/2\pi\right)^{2/3} \qquad (3.3.4.)$$

Now

$$D\left(\frac{\partial C_{(x,t)}}{\partial x}\right)_{x=0} = \frac{d}{dt}\left(\frac{Q_{(t)}}{FA_{(t)}}\right) \qquad (3.3.5.)$$

By substituting (3.3.3.) into eqn. (3.3.5.) and differentiating, Kreb and Roe derived

$$\left(\frac{\partial C_{(x,t)}}{\partial x}\right)_{x=0} = \frac{Q^{-2/3}_{(t)}}{3FD\gamma N^{\frac{1}{3}}} \frac{dQ}{dt} \qquad (3.3.6.)$$

Upon equating eqns. (3.3.6.) and (3.3.1.) and integrating both sides from Q_c at t = 0 (initial quantity of deposit present) to Q(t) at t = t,

$$Q(t) = \left[Q_c^{\frac{1}{3}} - FD^{\frac{1}{2}} \gamma N^{\frac{1}{3}} C^* \left(\frac{n F \omega}{RT}\right)^{-\frac{1}{2}} \left\{ \exp\left(\frac{n F \omega t}{RT}\right) \operatorname{erf}\left[\left(\frac{n F \omega t}{RT}\right)^{\frac{1}{2}}\right] - \frac{2\left(\frac{n F \omega t}{RT}\right)^{\frac{1}{2}}}{\pi^{\frac{1}{2}}} \right\} \right]^3 \quad (3.3.7.)$$

Differentiation of eqn. (3.3.7.) with respect to time leads to

$$i = -3F\gamma C^* N^{\frac{1}{3}} \left(\frac{n F \omega p}{RT}\right)^{\frac{1}{2}} \exp\left(\frac{n F \omega t}{RT}\right) \operatorname{erf}\left[\left(\frac{n F \omega t}{RT}\right)^{\frac{1}{2}}\right]$$

$$\times \left\{ Q_c^{\frac{1}{3}} - F\gamma C^* N^{\frac{1}{3}} D^{\frac{1}{2}} \left(\frac{n F \omega}{RT}\right)^{-\frac{1}{2}} \right.$$

$$\left. \left[\exp\left(\frac{n F \omega t}{RT}\right) \operatorname{erf}\left[\left(\frac{n F \omega t}{RT}\right)^{\frac{1}{2}}\right] - \frac{2\left(\frac{n F \omega t}{RT}\right)^{\frac{1}{2}}}{\pi^{\frac{1}{2}}} \right] \right\}^2 \quad (3.3.8.)$$

Krebs and Roe found close correspondence between cyclic current-voltage curves calculated by eqn. (3.3.8.) and the experimental peaks observed for the return anodic scans.

As nucleation phenomena have not been observed for electrocrystallisation on normal (with dislocations) parent metal substrates by Budevski et al,[92] it seemed possible that an alternative explanation for these phenomenon would be more likely. It is possible to envisage the situation occurring in the solution immediately adjacent to the

electrode surface during a potential scan. Fig.12 illustrates various stages during the scan as one progresses from (a) to (b) i.e. in an anodic sense. At stage (a) the surface concentration of depolariser C^o has increased by the scan, and for a scan of suitable rate the concentration in the solution will lag behind a linear concentration distribution (Nernst diffusion layer conditions). This gives rise to a concentration gradient at the interface in the opposite sense to that expected for cathodic conditions i.e. a dissolution current will occur. As the scan proceeds through stage (b), the magnitude of this 'anodic' surface concentration gradient will go through a maximum, and eventually rise again when true anodic polarisations are reached (stage (c)). In such a manner, an anodic peak similar to that observed by Krebs and Roe could occur upon anodic scan following cathodic scan.

A numerical solution of this problem is presented in Appendix 1. Fig.13 shows the computed plots derived at 1V/sec (10^{-2}M solution, δ assumed 10^{-3}cm) for a scan from +10mV (anodic) to -20mV and back, and one from zero to -20mV and back to +10mV. Both plots follow the same anodic going curve. This figure shows that computations conducted by dividing the diffusion layer into ten compartments

fig 13 Computed i-η plot. $C^* = 0{\cdot}01M$; $\delta = 0{\cdot}001$ cm ; 1V/ sec. n=50 (o, □) ; n=10 (x).

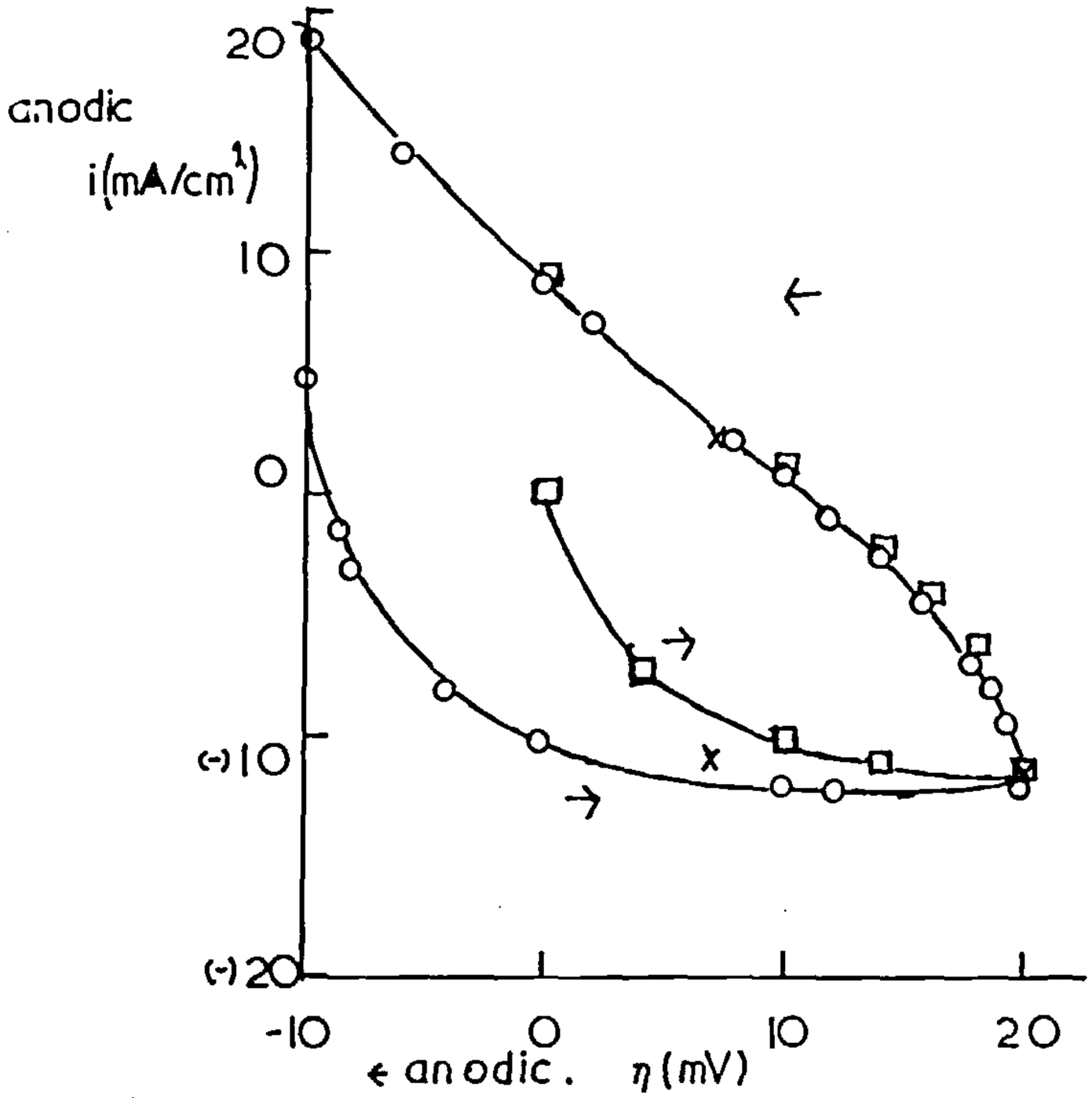

fig 14 Computed i-η plot. $C^* = 0{\cdot}01M$; $\delta = 0{\cdot}001$ cm ; 100 mV/sec ; n=10.

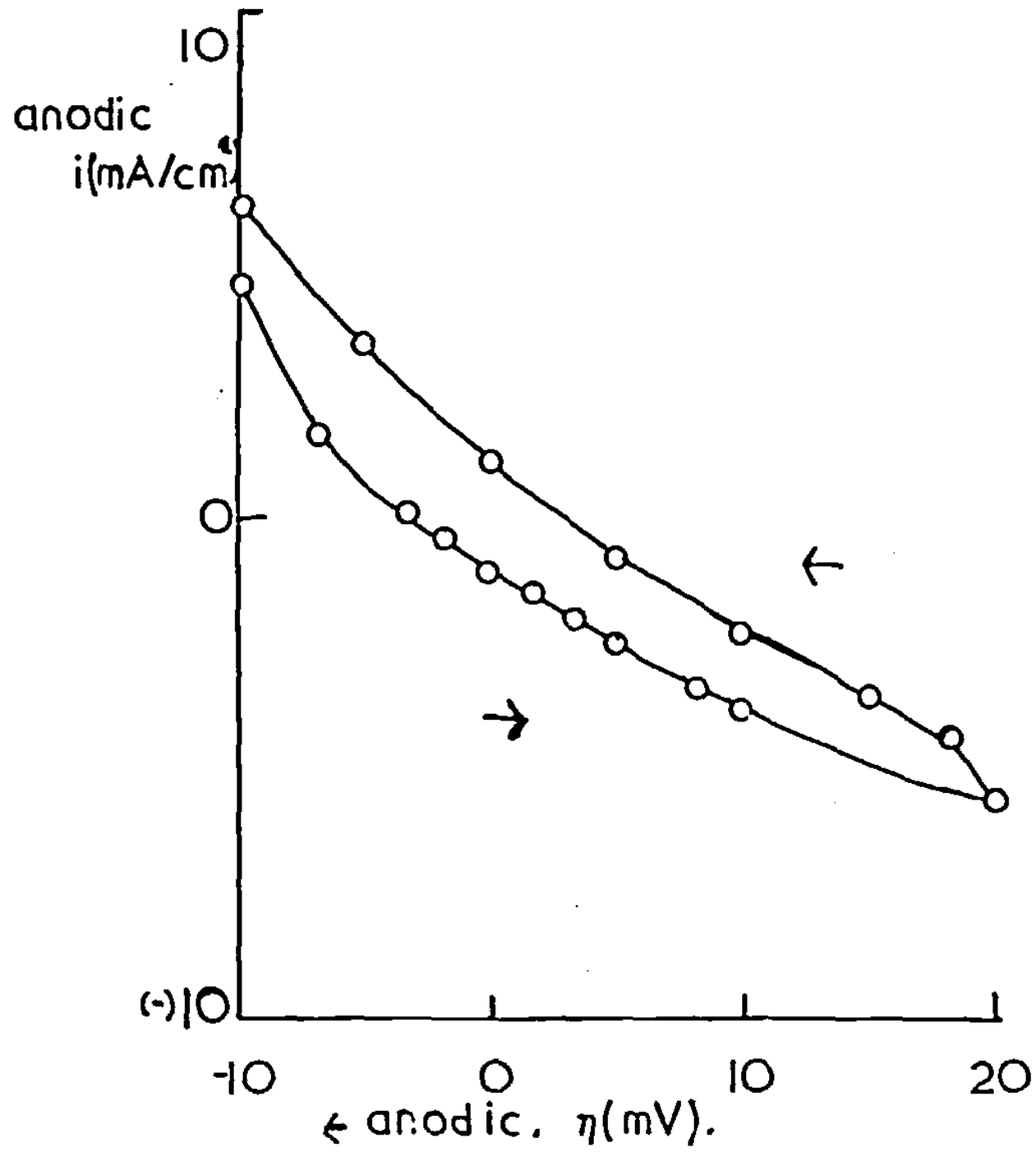

(n = 10) give essentially the same results as for n = 50. There are slight inflexions at the start of both the anodic and cathodic going sweeps as predicted by the above arguments, but no pronounced peaks were obtained. The magnitude of these inflexions are reduced as the sweep rate is decreased (as shown in Fig.14 for 100mV/sec). The computed curves always predict that the anodic and cathodic going currents at η = 0 are symmetrically placed with respect to the i = 0 axis. Figs. 15 and 16 show computed plots for sweeps of 100mV/sec and 10mV/sec for scans from +10mV to -2.5mV. At 10mV/sec the difference between the anodic and cathodic going branches is practically undetectable and the plots approximate to a single straight line passing through the i-η origin. Sweeping to more cathodic potentials produces the current/voltage peak due to the reduction of the cations (Fig.17) as predicted by the analysis of Berzins and Delahay[105] for the reversible deposition of an insoluble substance under sweep conditions, starting from the equilibrium potential. After the maximum the current is that due to diffusion in the constant diffusion layer with the interfacial concentration zero.

Similar measurements to those of Krebs and Roe[103] were made employing the electropolished silver single crystal as

fig 15 Computed i-η plot. $C^* = 0{\cdot}01M$; $\delta = 0{\cdot}001$ cm; 100 mV/sec; n=10.

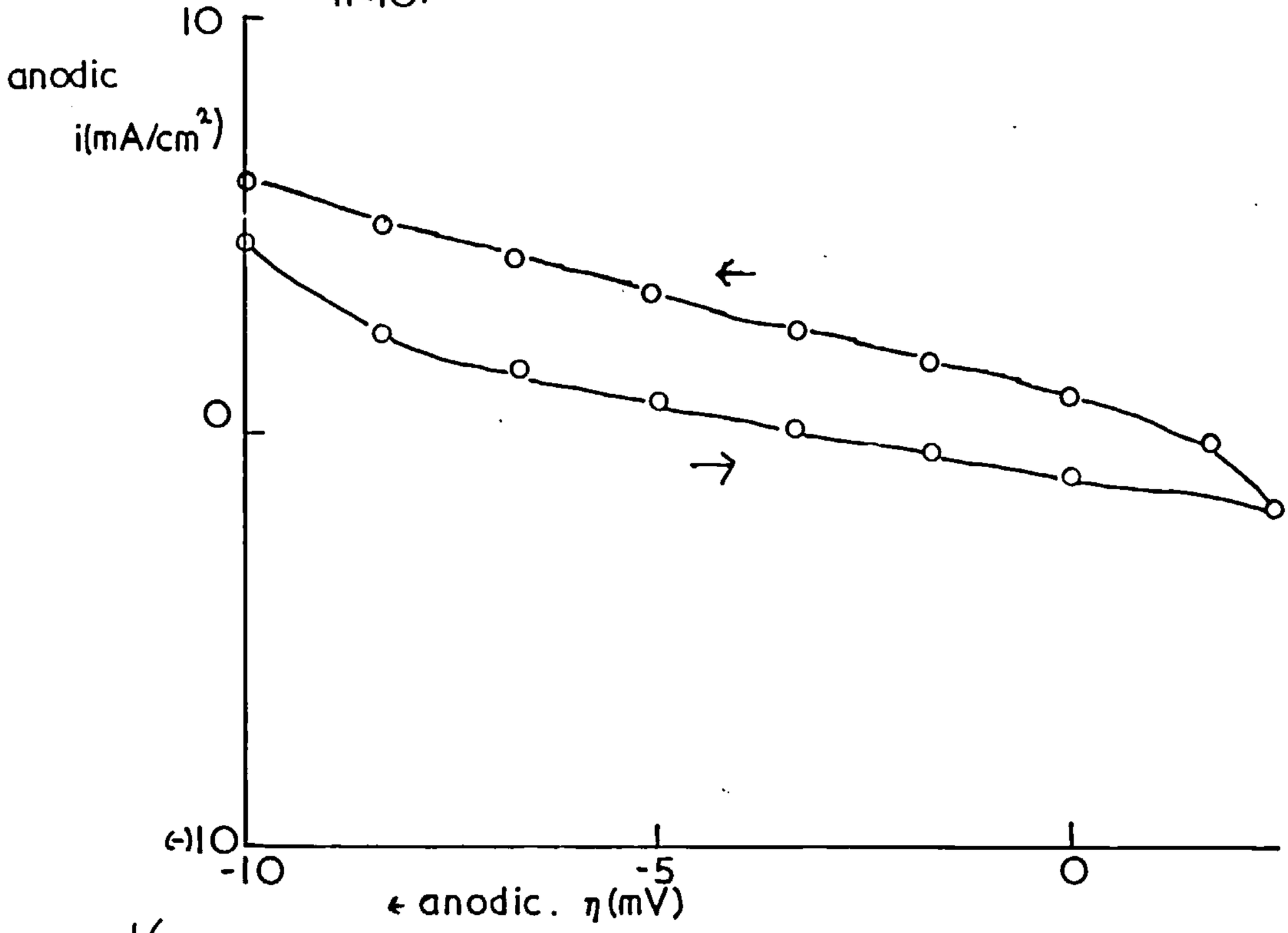

fig 16 Computed i-η plot. $C^* = 0{\cdot}01M$; $\delta = 0{\cdot}001$ cm; 10 mV/sec; n=10. o→ ; x← .

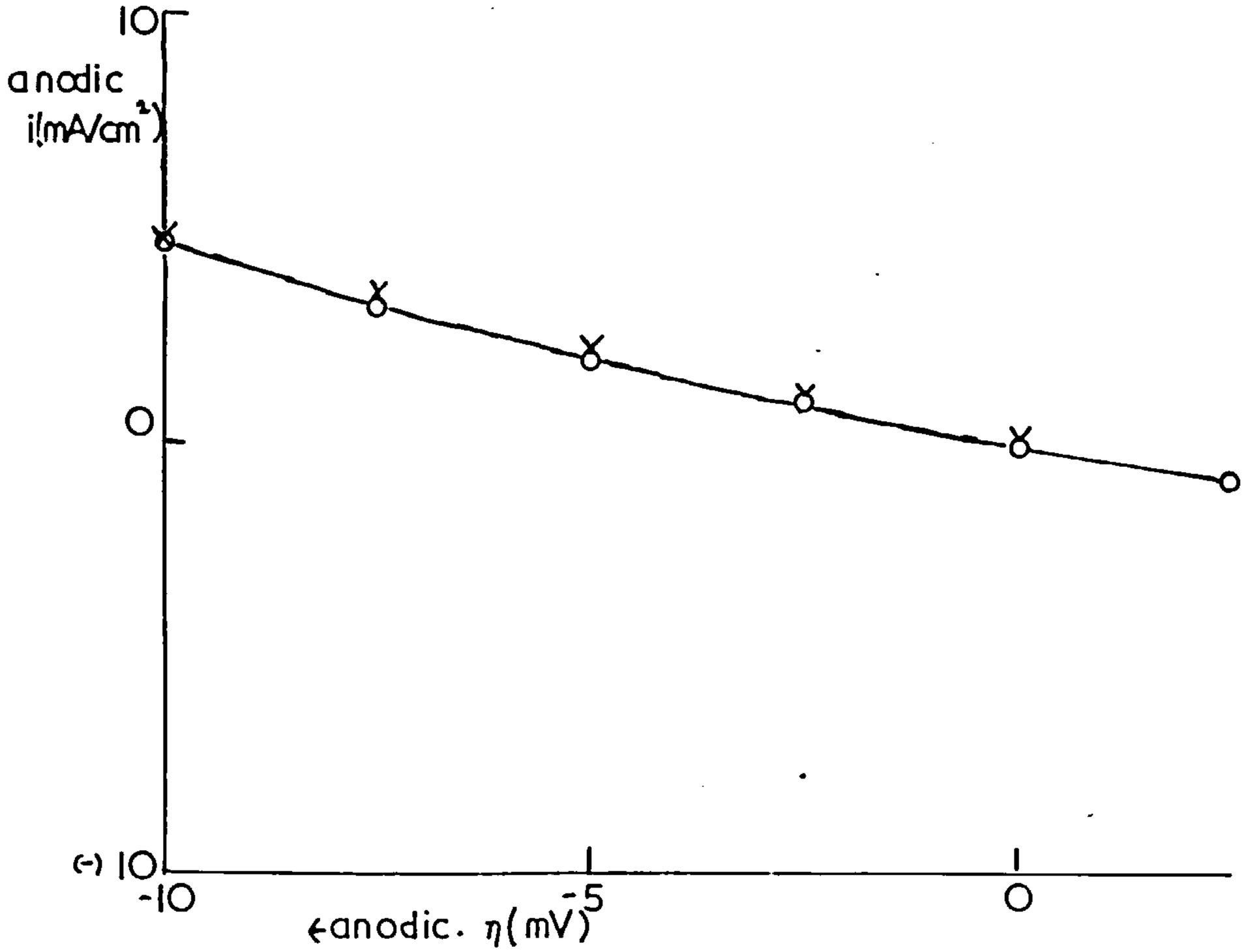

fig 17 Computed i vs η for 1V/sec ; $C^* = 0{\cdot}01M$; $\delta = 0{\cdot}001cm$; $n = 10$.
$o \rightarrow$; $x \leftarrow$.

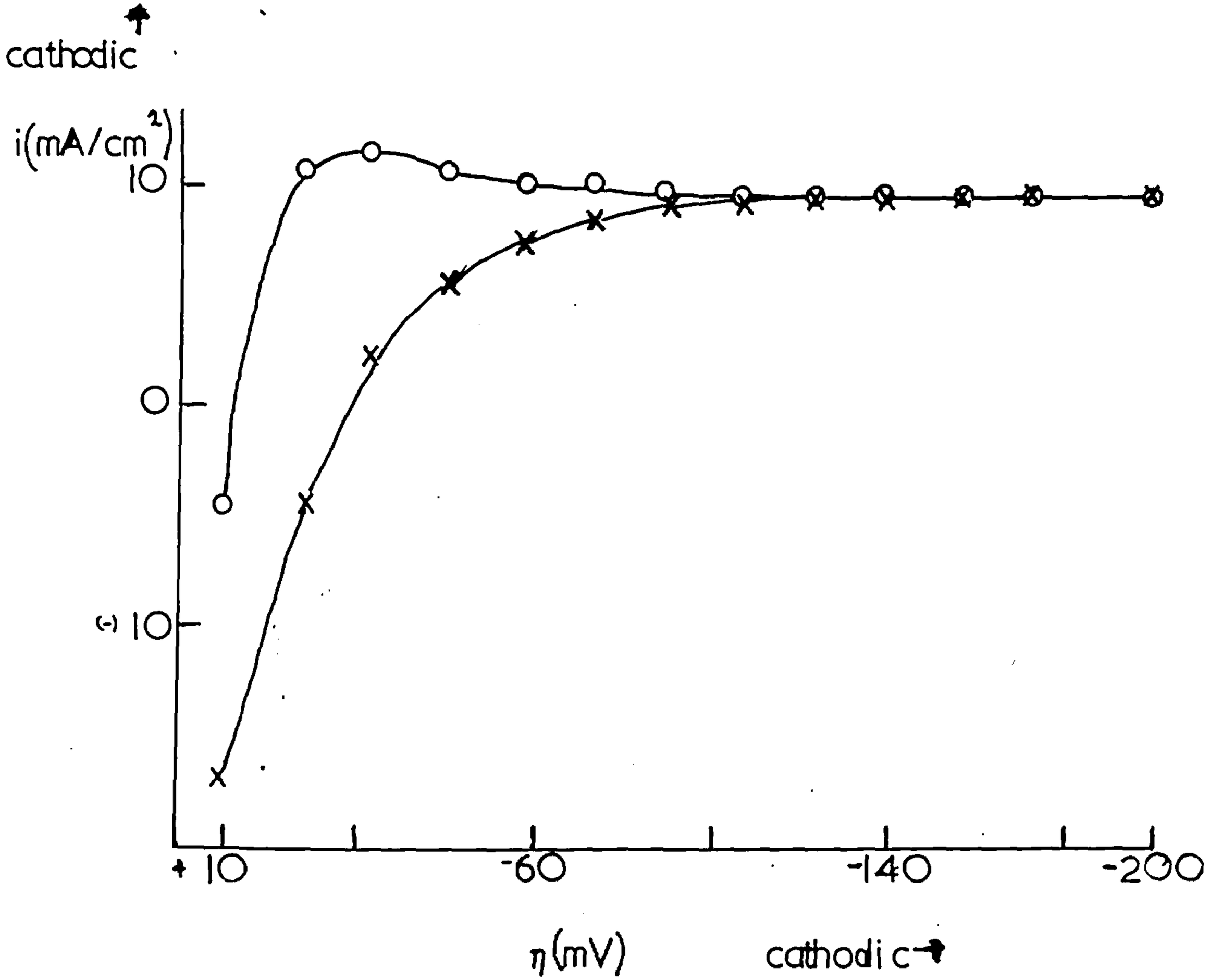

electrode. In order to obtain small scan ranges (of the order of ca. 30mV) the output from the waveform generator (maximum 3 volts) was dropped in the ratio of $1:33.^{1}/3$ with the aid of a potential divider between the generator and earth using precision 1% Welwyn resistors of 50 KΩ and 1.5 KΩ . The function generator could not supply triangular waveforms of amplitude $<$ 100mV normally. The measurements were taken from an initial potential of η = 10mV (anodic). The intended purpose of such a technique was to ensure an uncontaminated electrode surface during the subsequent sweep by always starting with a surface freshly prepared by slight anodic dissolution. The measurements were carried out with vigorous stirring by nitrogen gas bubbling through the solution in an effort to ensure Nernst diffusion layer conditions. The anodic current at η = 10mV predicted δ = 2.16×10^{-3}cm for the electrode used, area = $0.28cm^{2}$.

Current/voltage plots from n = +10mV to -20mV and back again at 100mV/sec and 10mV/sec are shown in Figs. 18 and 19 as the continuous lines for a 0.01M $AgClO_4$/M$HClO_4$ solution. The computed values for these conditions are shown on the same graphs. The experimental curves reproduce the slight maxima after the switching of scan directions predicted above. These curves are fairly closely approximated by the

fig 18 $0{\cdot}01\,M\,AgClO_4/1M\,HClO_4$ · single Ag crystal · i vs η for 100 mV/sec. (–).
x – computed values, ($n = 10$; $\delta = 0{\cdot}00216$ cm - from i at $\eta = 10$ mV, anodic)

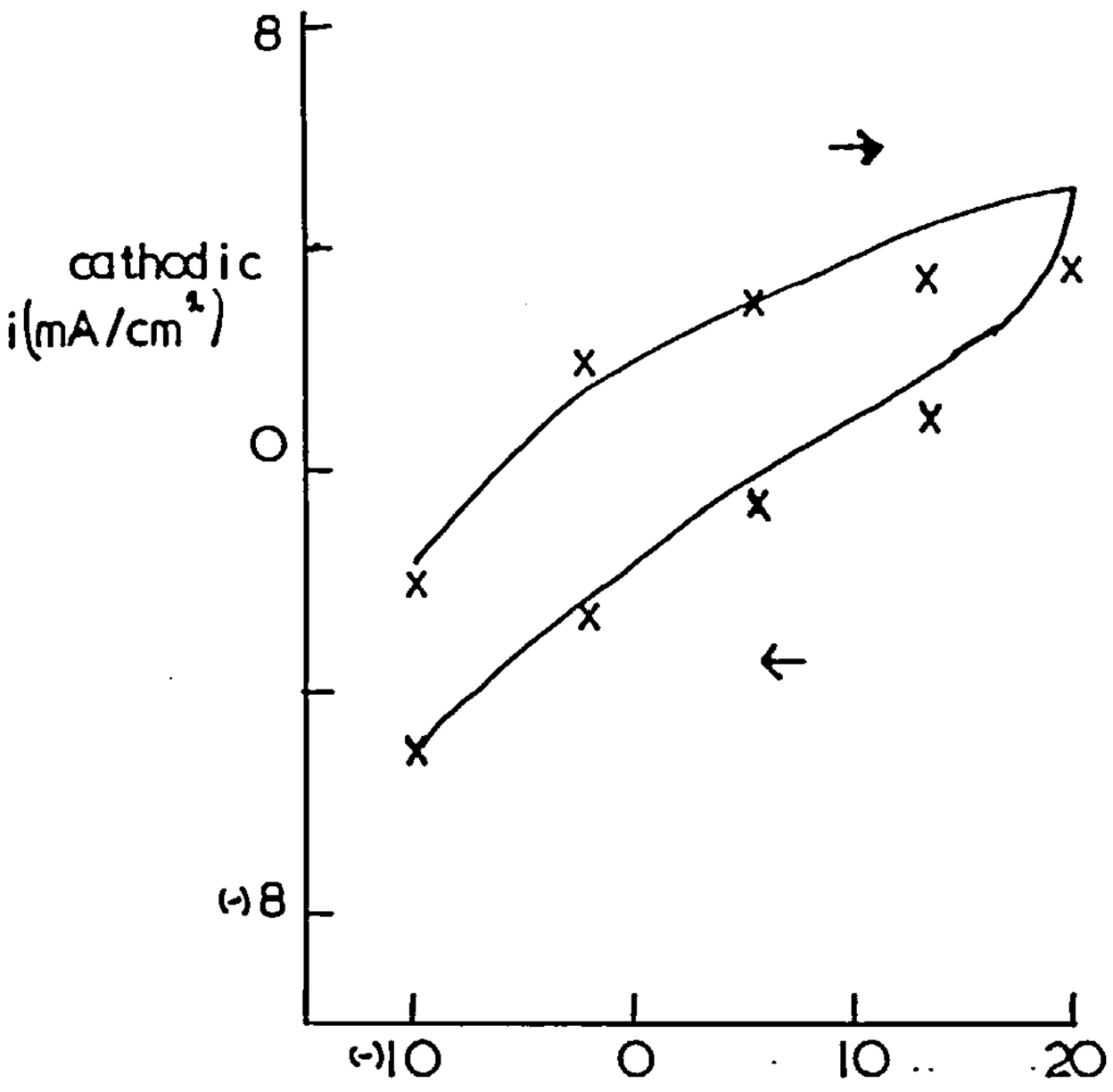

fig 19 As above, 10 mV/sec. x – computed values ($n = 10$; $\delta = 0{\cdot}00216$ cm)

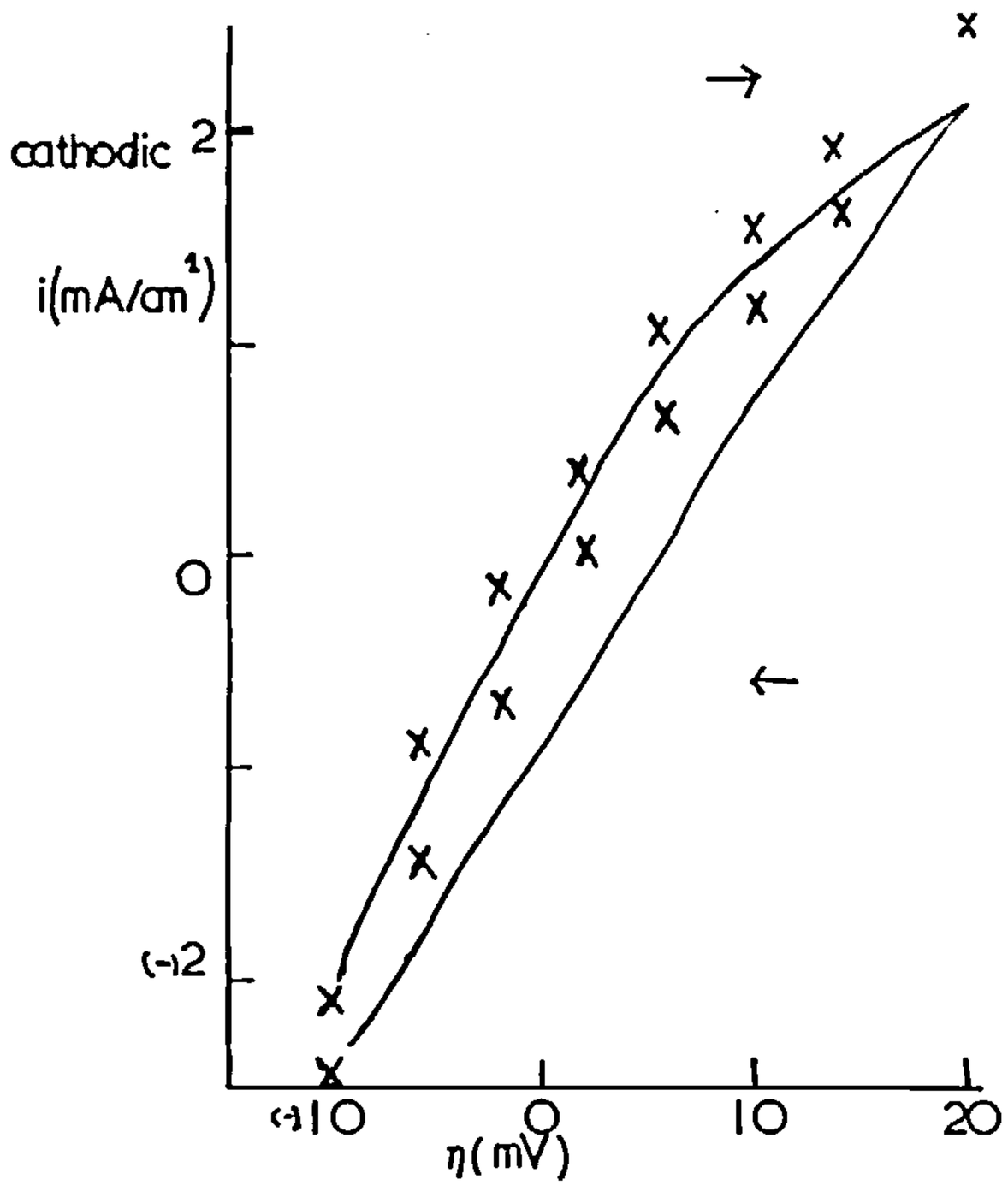

computed values, giving some justification to the hypothesis that diffusion processes to a planar electrode are the predominant ones for the electrocrystallisation of silver onto silver under these conditions. At ca. 1mV/sec the experimental plots become single lines for the forward and reverse sweeps, i.e. at the sort of sweep rates employed by Krebs and Roe.[103] Such plots pass through the i-η origin.

No pronounced maxima as observed by Krebs and Roe were observed for the system investigated. The essential difference between these measurements and those of Krebs and Roe is that their electrode was only in contact with a small drop of electrolyte solution. It would seem that this arrangement is liable to changes in contact angle and consequently electrode area, with change in potential. It is also not clear how oxygen was removed from their electrolyte solutions, its presence may have an activating role during a cathodic sweep. At low sweep rates the currents observed should pass through the i-η origin, this is not the case for the Krebs and Roe measurements.

A comparison of the computed curves with the data of Krebs and Roe shows that, assuming $\delta = 10^{-3}$cm, their currents are very much lower. For examples, at 0.5mV/sec Krebs and Roe observe an anodic current of ca. 0.5mA cm^{-2} at η = +15mV

(anodic); the calculated value is ca. 5mA.cm^{-2} for the same conditions. Extensive passivation, especially in the anodic region, is thereby indicated for their electrode. Two possibilities may explain this behaviour; either the surface has few dislocations in it or the active sites at dislocations have become blocked by adsorption of impurities. It seems unlikely that few dislocations could be achieved by melting. In any case dissolution at dislocations to form etch pits and the reverse process on deposition would only affect the above theory by making the curves increase more steeply with time during the anodic sweep with no maximum. The second possibility would require nucleation during the cathodic sweep. On the assumption that the phenomena observed by Krebs and Roe were an electrode surface effect, it must be concluded that their surfaces were untypical and severely inhibited.

3.4. The use of inert carbon substrates

It has been pointed out in Chapter 1, section 4, that in order to be able to investigate metal deposition in a manner uncomplicated by the surface structure of the solid metal, one may grow the metal as nuclei on inert substrates and study the phenomenon as a phase change during the initial stages of growth. Of all substrates, liquid mercury has the

advantage of completely reproducible surfaces and ease of purification. However the equilibrium potential for Hg/Hg_2^{2+} is only 10mV cathodic to the Ag/Ag^+ potential, added to which there is the complication of amalgam formation. Of the solid inert electrodes available platinum has been used,[106] but this has the disadvantage that the silver nuclei may not be anodically redissolved without the formation of platinum oxides. Carbon electrodes do not undergo chemical changes under these conditions, and were chosen as inert substrates. As mentioned in Chapter 2, Section 5, the glassy carbon surfaces were prepared by polishing, those of the pyrolytic graphite by cleavage.

In order to test the suitability of glassy carbon as an inert electrode surface, it was used as substrate in the deposition of PbO_2 from a lead acetate solution - a system whose potentiostatic growth characteristics have been extensively studied on platinum substrates.[4] Fig. 20 shows the growth transient obtained at +150mV (reference PbO_2 electrode) in a 10^{-1}M lead acetate solution in 1M sodium acetate, 1M acetic acid. Such a transient was obtained by Fleischmann and Liler[107] for the platinum substrate and was attributed to the three-dimensional growth of nuclei, with an induction period before nucleus formation

$$\text{i.e.} \quad i \propto (t - t_0)^3 \qquad (3.4.1.)$$

fig 20 transient for deposition of PbO_2 on glassy C at +150mV (ref. PbO_2).
0·1M $Pb(OAc)_2$, 1M NaOAc, 1M AcOH. no prepulse.

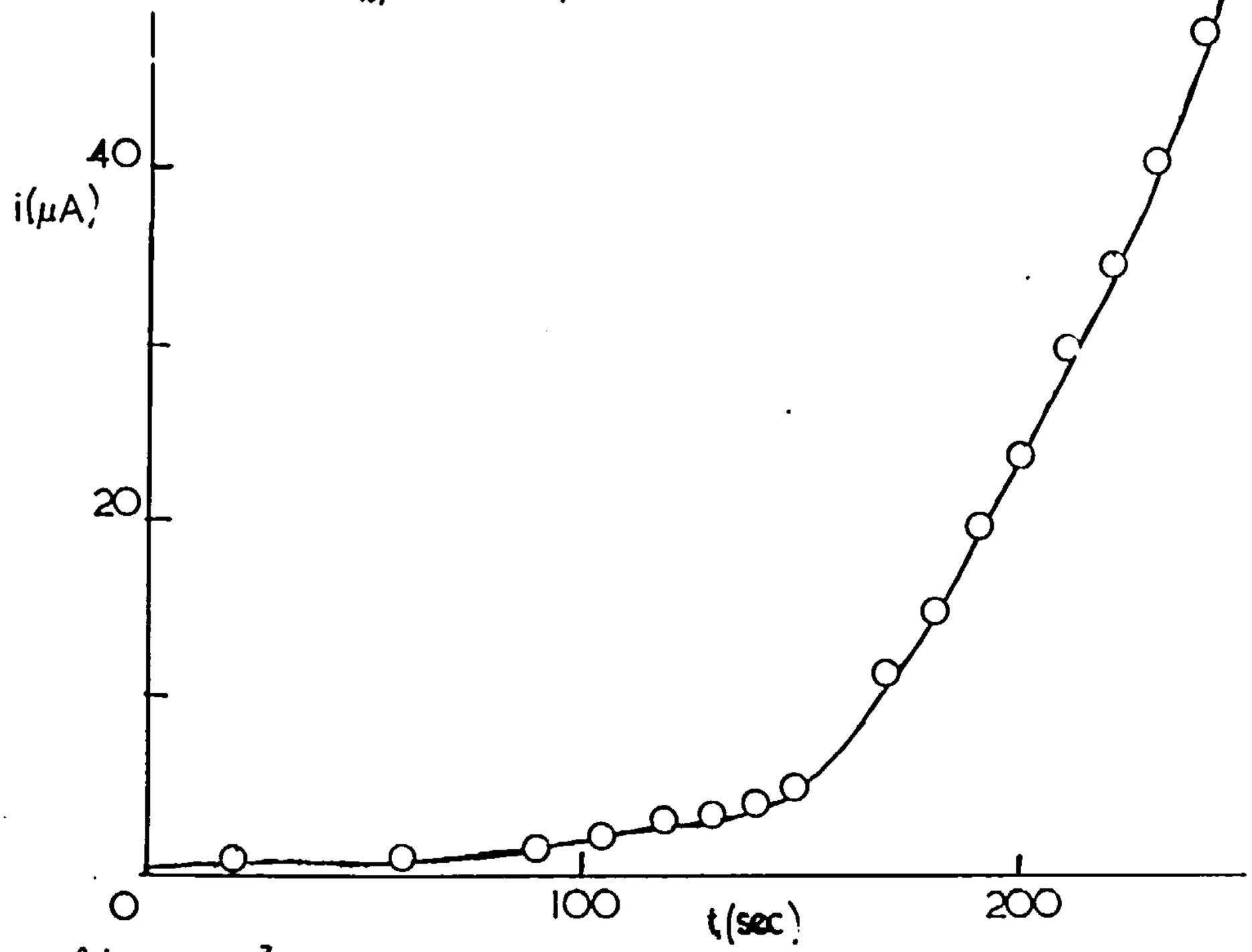

fig 21 i vs t^3 for above conditions.

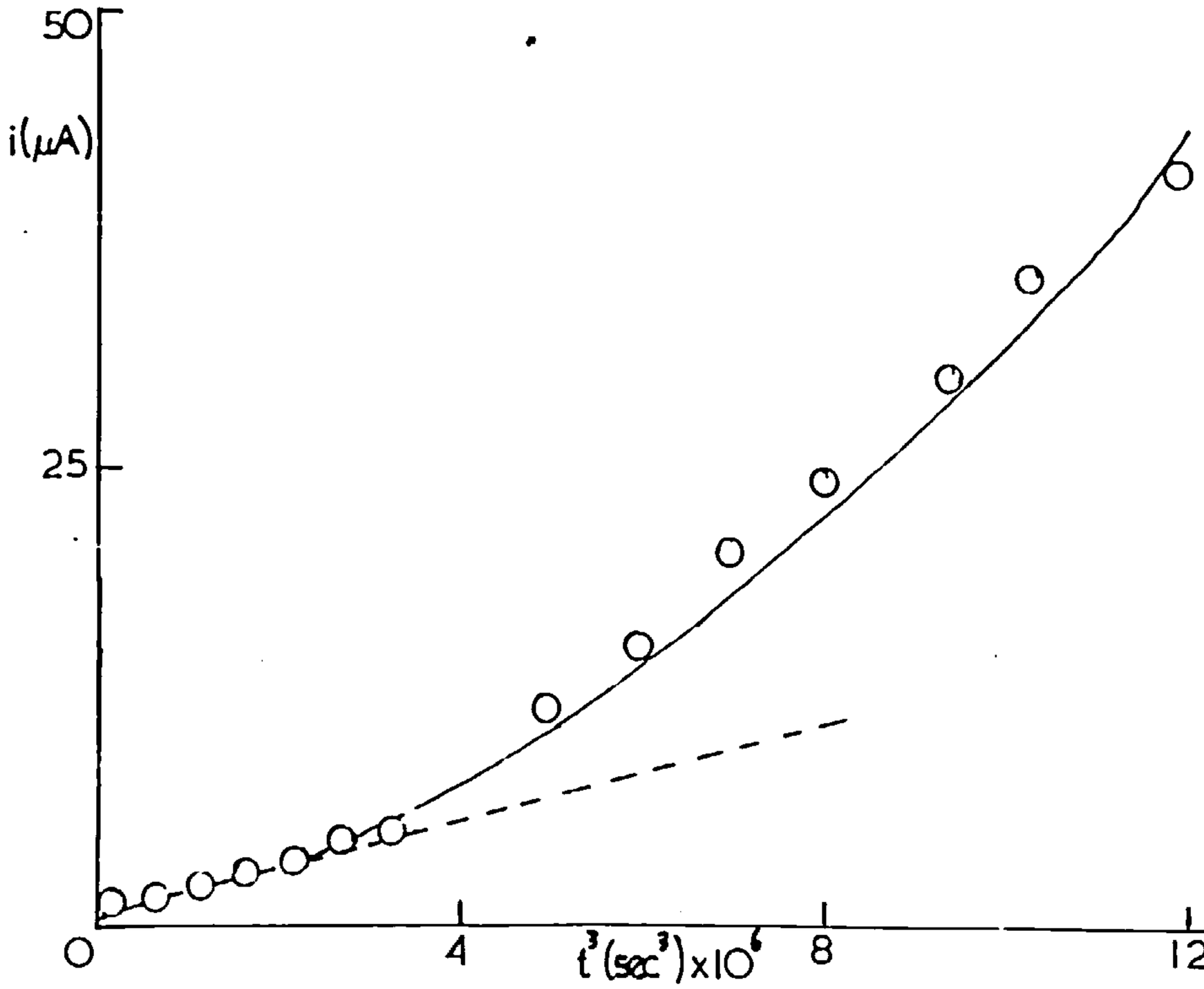

where t_o is the induction period. Fig.21 shows the plot of i vs. t^3 which illustrates the induction period affect of suggesting a higher time dependence than i vs. t^3.

3.5. The growth characteristics of silver on carbon substrates

It was mentioned in Chapter 1, section 4, that the nucleation and growth of metal nuclei, deposited onto a substrate, must be separately controlled. This can be achieved by applying double potentiostatic pulses to the electrode. The first pulse (prepulse) is large and of short duration and determines the number of nuclei formed on the surface. The second pulse is small and controls the rate of further growth. Fig.22 shows the result of applying such a combination of pulses to a glassy carbon electrode in an $AgClO_4$ solution. The initial 'sitting' potential was +100mV (η), sufficiently anodic to allow the Ag nuclei to dissolve off again.

Without a prepulse or when it is very short, the current-time characteristic observed during the second pulse is approximately $i \propto t^2$. The shape of the curve depends on the smoothness of the carbon surface. A more highly polished substrate gives the better i vs. t^2 dependence. As the prepulse width increases the dependence becomes $i \propto t$ and eventually the curves become independent of width. This means that all the nuclei are formed during the first pulse provided it is longer than about 100 msec. This is

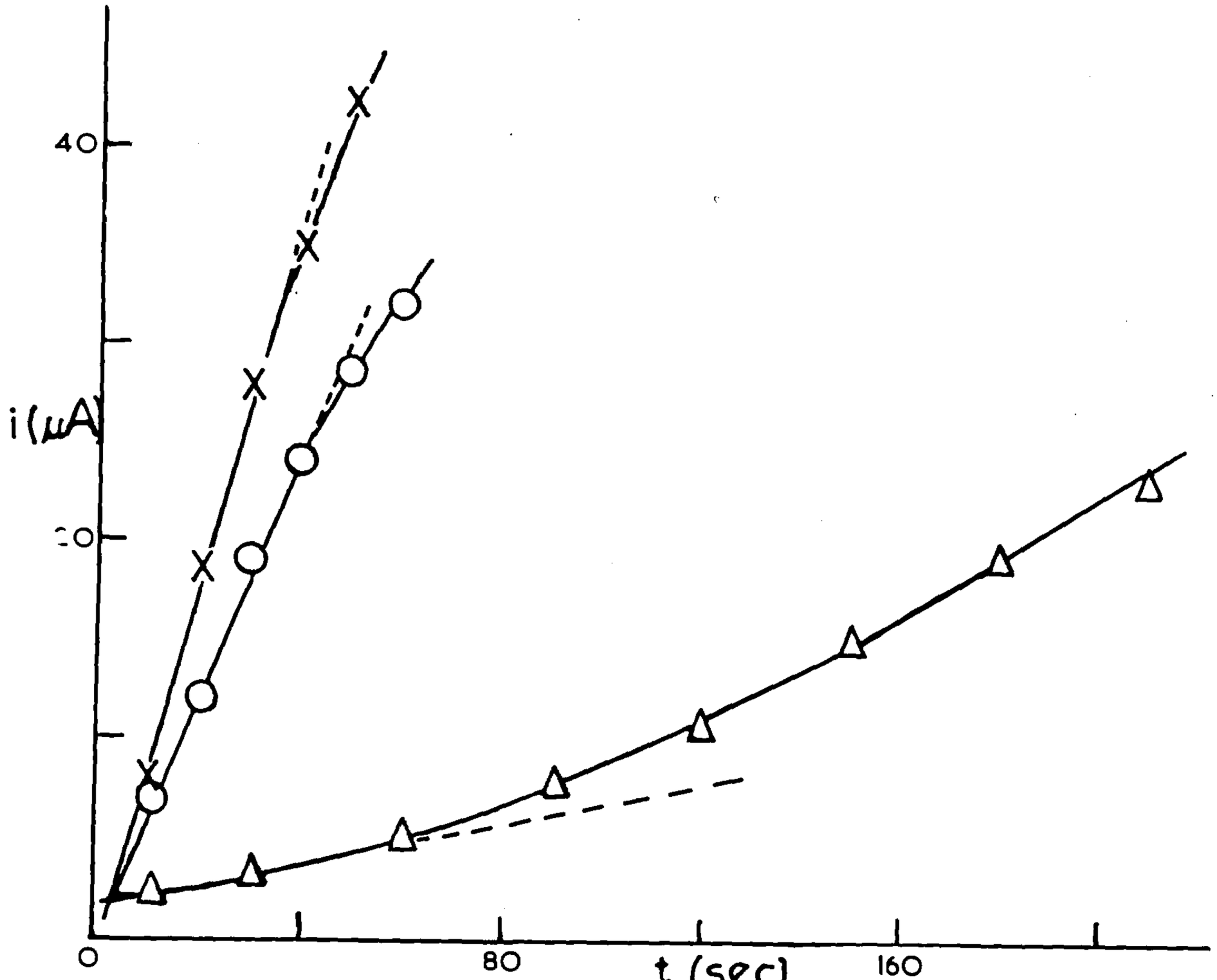

fig 22 0·05M $AgClO_4$, 1M with $HClO_4$, glassy C. dependence of transient at −10 mV (Ag/Ag^+) on prepulse at −100 mV. Δ, 9 msec ; O, 43 msec; X, 90 msec.

supported by optical micrographs. Fig.23 and Fig.24 shows silver nuclei grown for 1 min. and 2 min. respectively at η = -10mV, after a prepulse of -100mV for 200 msec. Though the nuclei have apparently grown larger in Fig.24, there is no apparent increase in their number.

Fig.25 shows that the $i \propto t$ dependence is observed at various potentials of the second pulse, using a prepulse of -100mV for 100 msec, in a solution of 1×10^{-2}M $AgClO_4$/1M $HClO_4$. Overpotentials $>$ 60mV were not used in order to avoid ohmic control with these electrodes of moderate resistance.

3.6. The model for the formation of silver nuclei

Possible combinations which might give rise to an $i \propto t$ dependence are:

(a) progressive formation and growth of nuclei which grow as needles;

(b) instantaneous formation and growth of two-dimensional nuclei;

(c) progressive formation and growth of two-dimensional clusters of separate nuclei, which then overlap, as growth proceeds on preferred sites in the carbon surface;

(d) progressive formation of nuclei the growth of which is controlled by hemispherical diffusion in the solution -

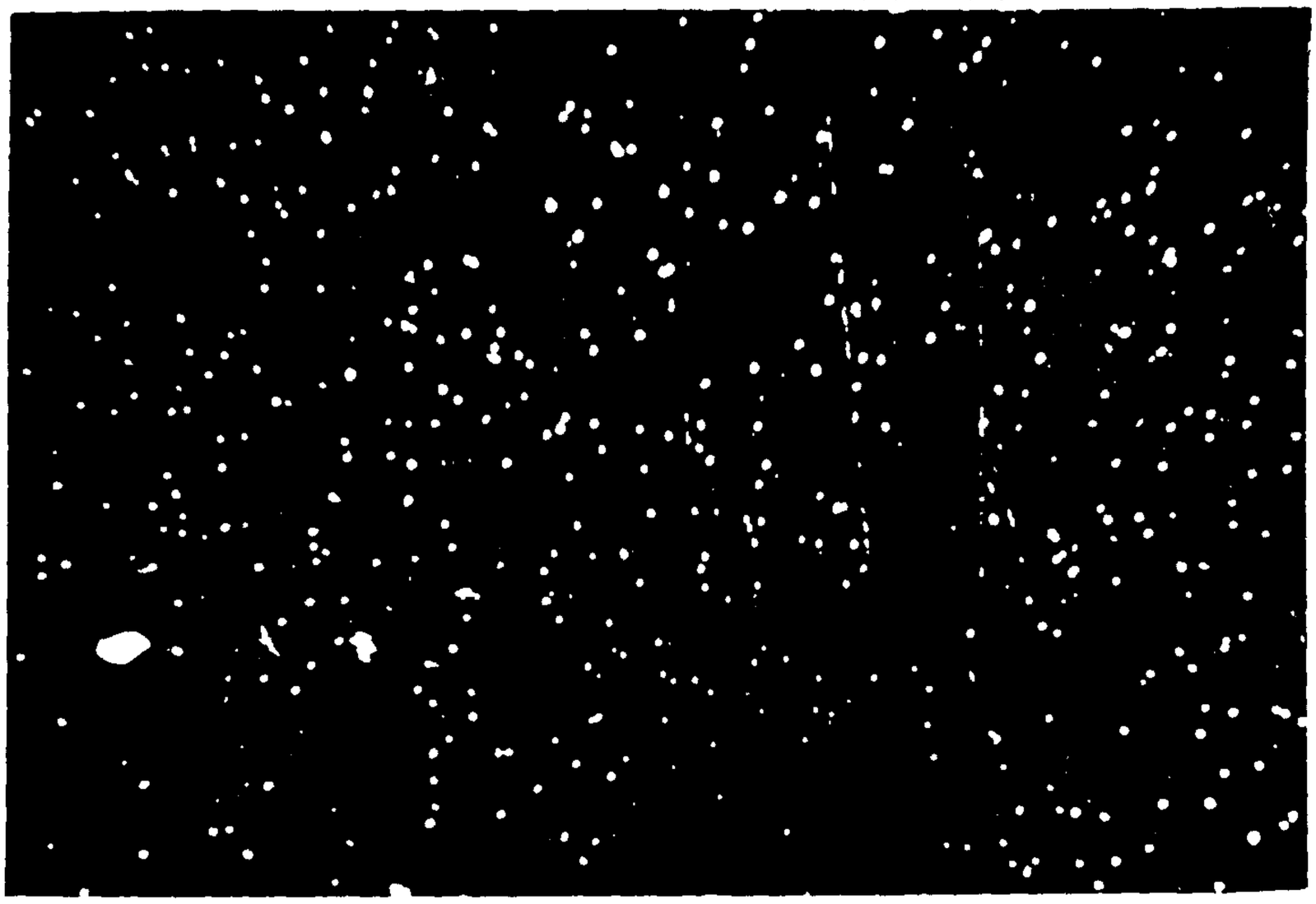

fig[13] optical micrograph Ag nuclei on glassy C formed at η -100 mV, 200msec ; then -10 mV, 1 min ; in 0·05M $AgClO_4$ / 1M $HClO_4$. magnification X 200.

fig[14] As above but -10 mV, 2 min .

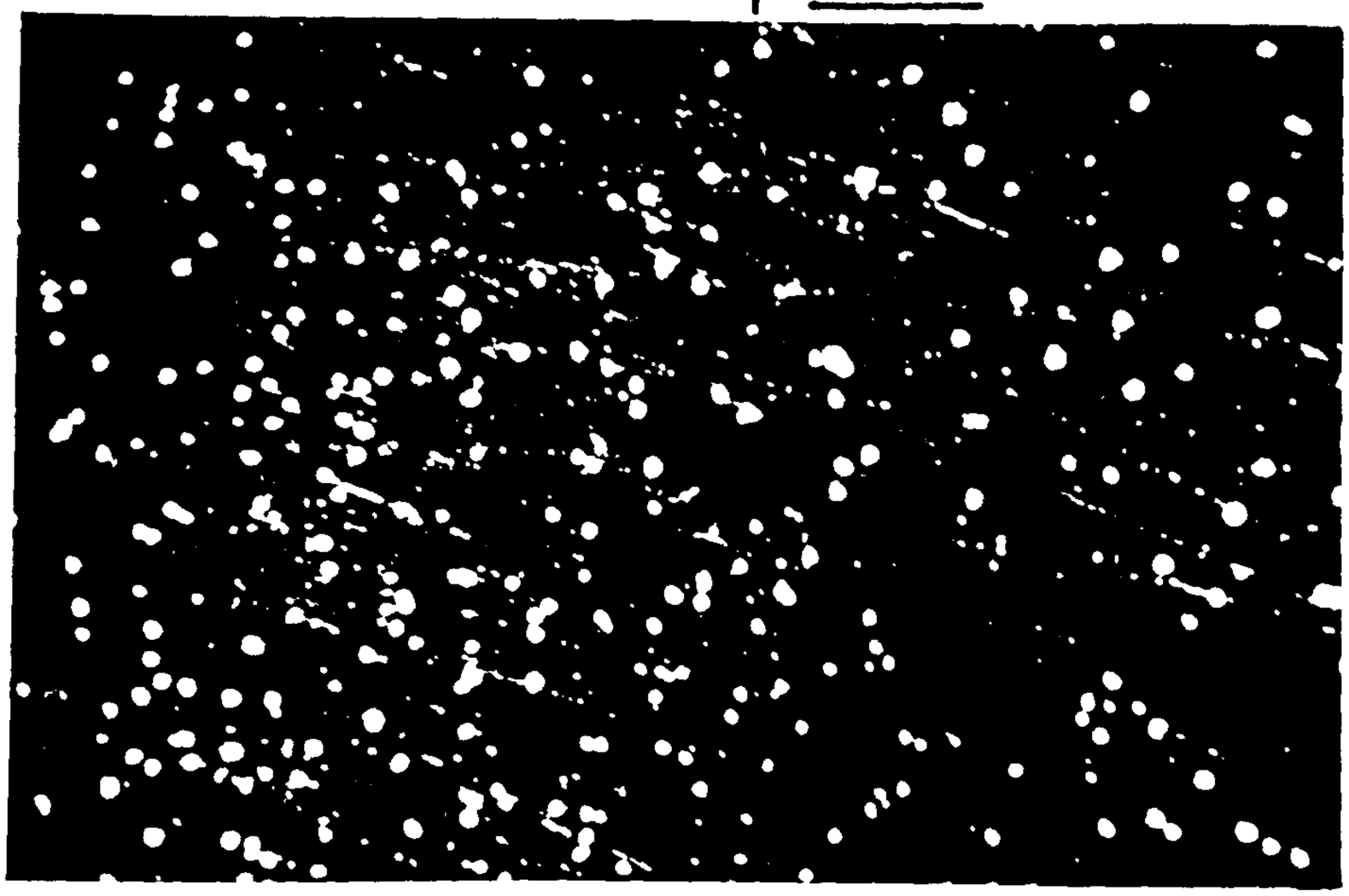

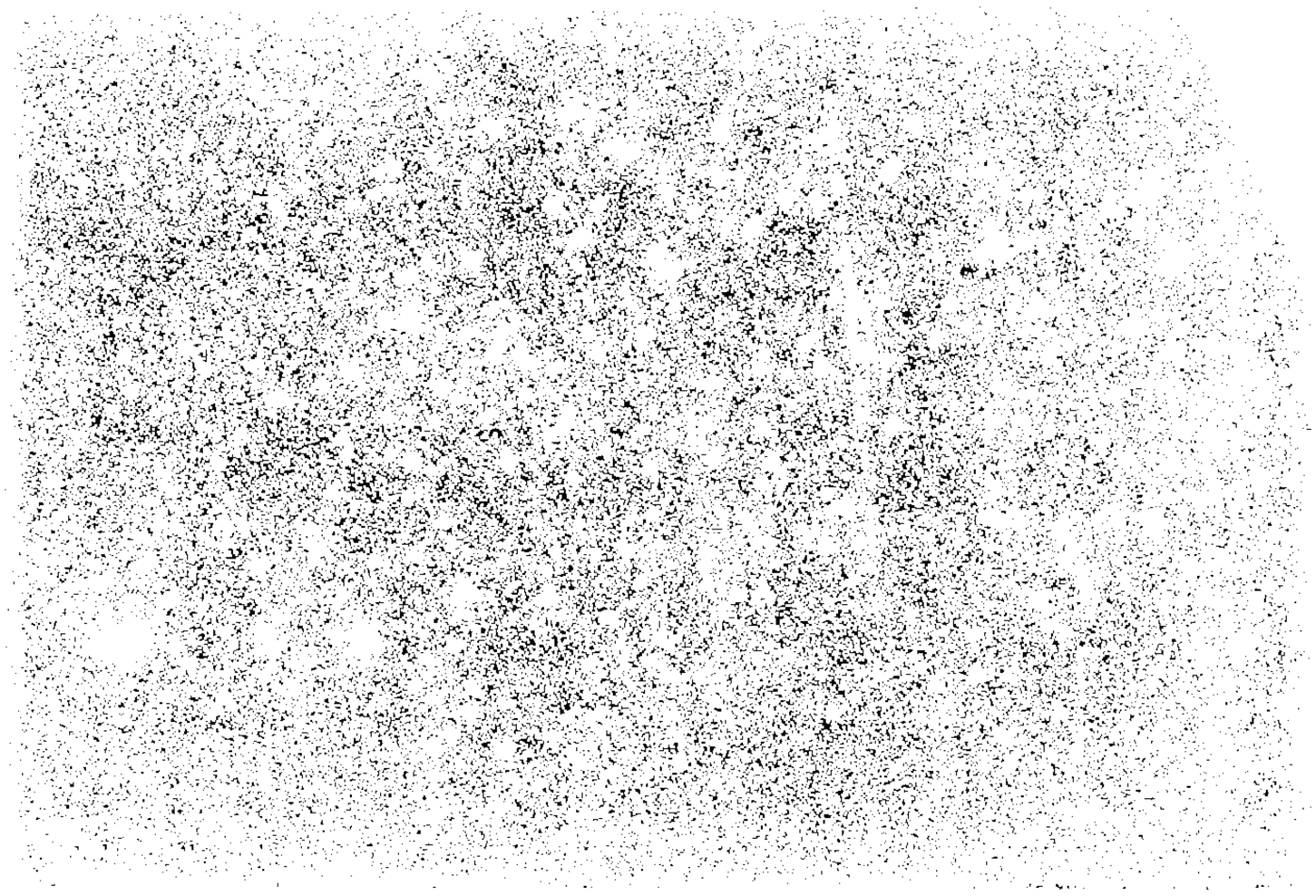

Fig. 3 Cyclic voltammetry of [illegible] in 0·05M $AgClO_4$/MeCN-CH_2Cl_2. Magnification X 250.

Fig. 4 [illegible]

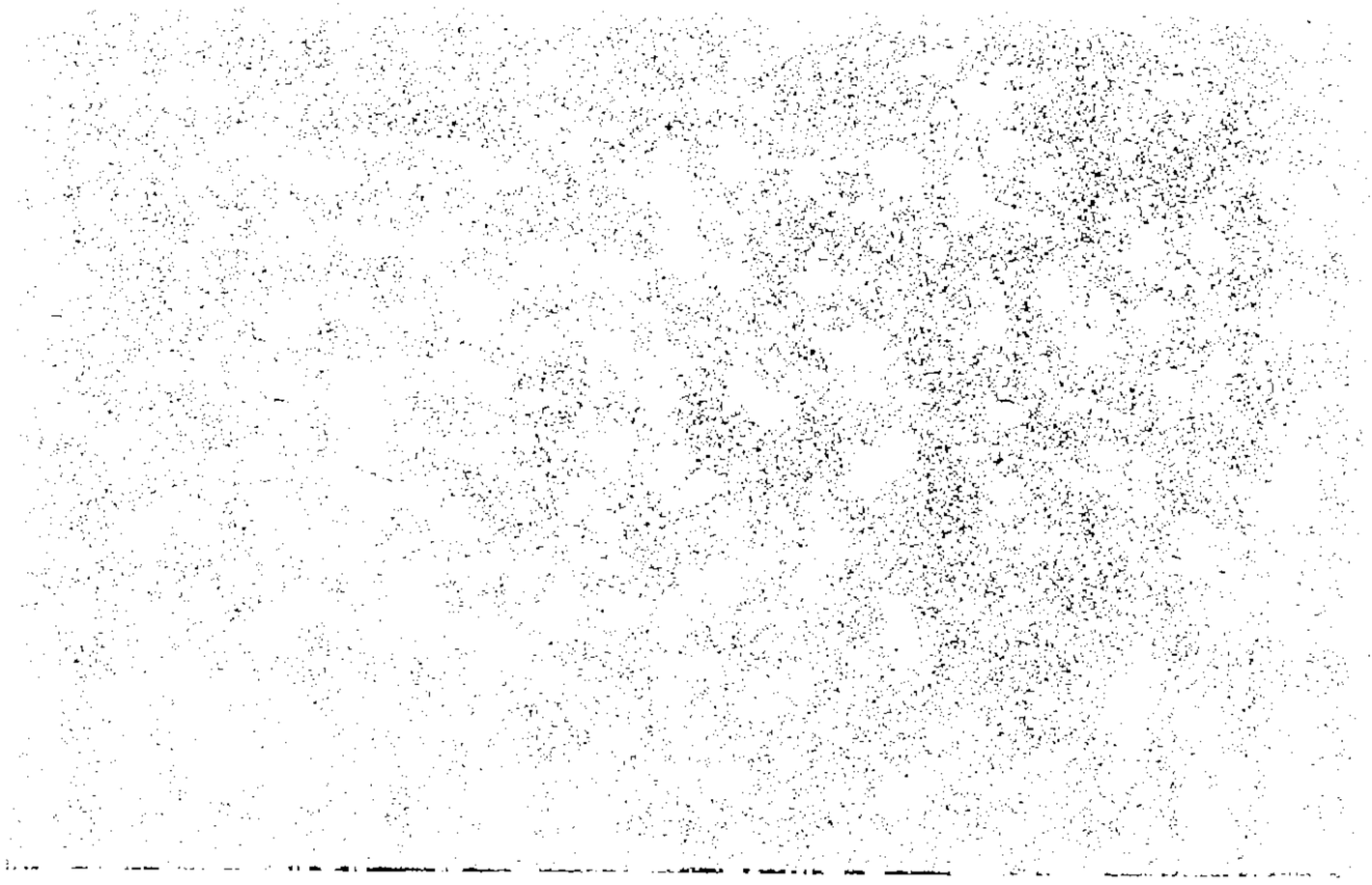

fig 15 0·01 ivi $AgClO_4$, I = 1M, $HClO_4$; glassy C . cathodic i vs t for, 1, 10 mV; 2, 15 mV; 3, 20 mV; 4, 25 mV; 5, 30 mV; 6, 40 mV; 7, 50 mV; 8, 60 mV. (Ag/Ag^+)

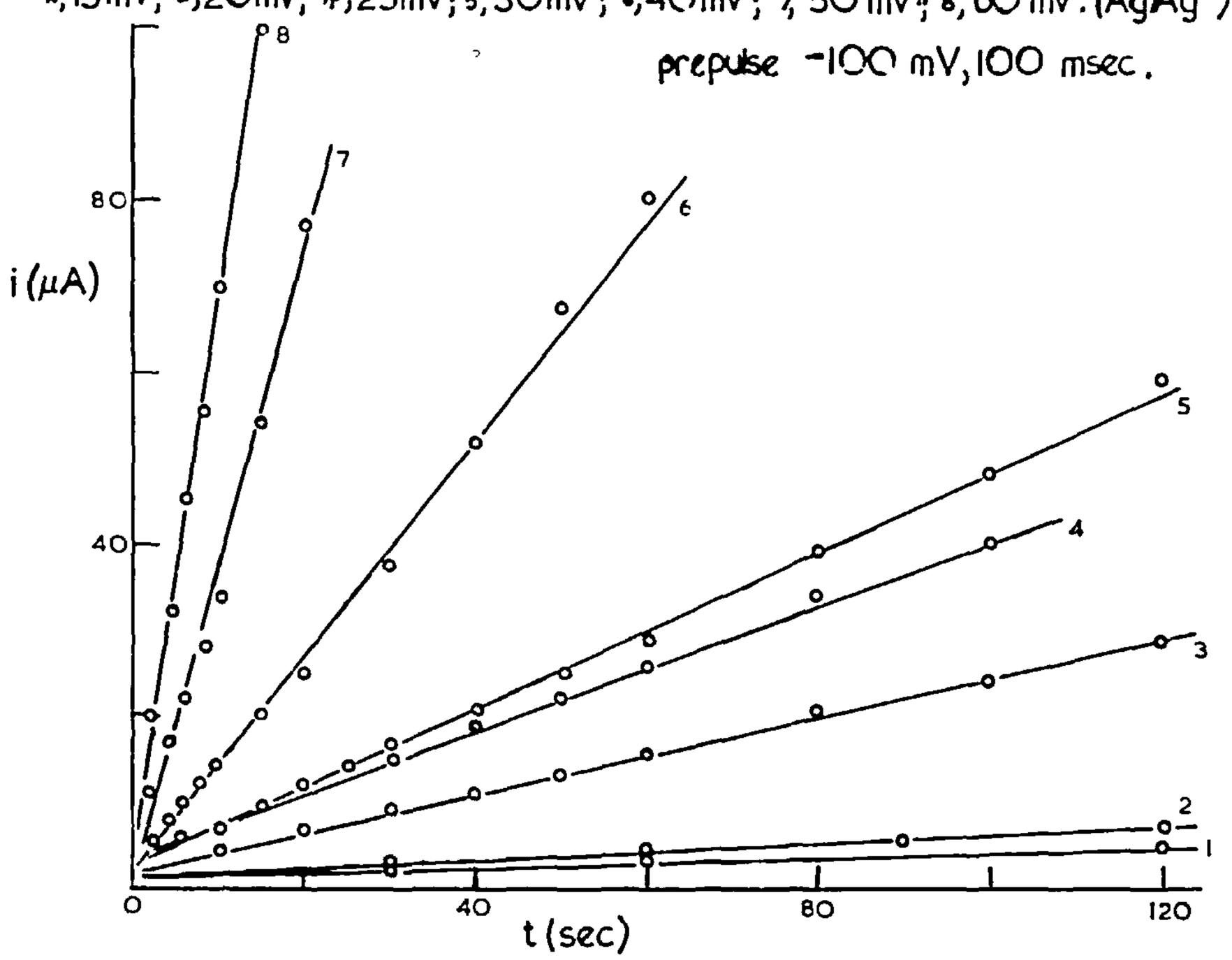

fig 16 0·01M $AgClO_4$ / 1M $HClO_4$ · glassy C · i vs t. prepulse; η - 100mV, 90msec.

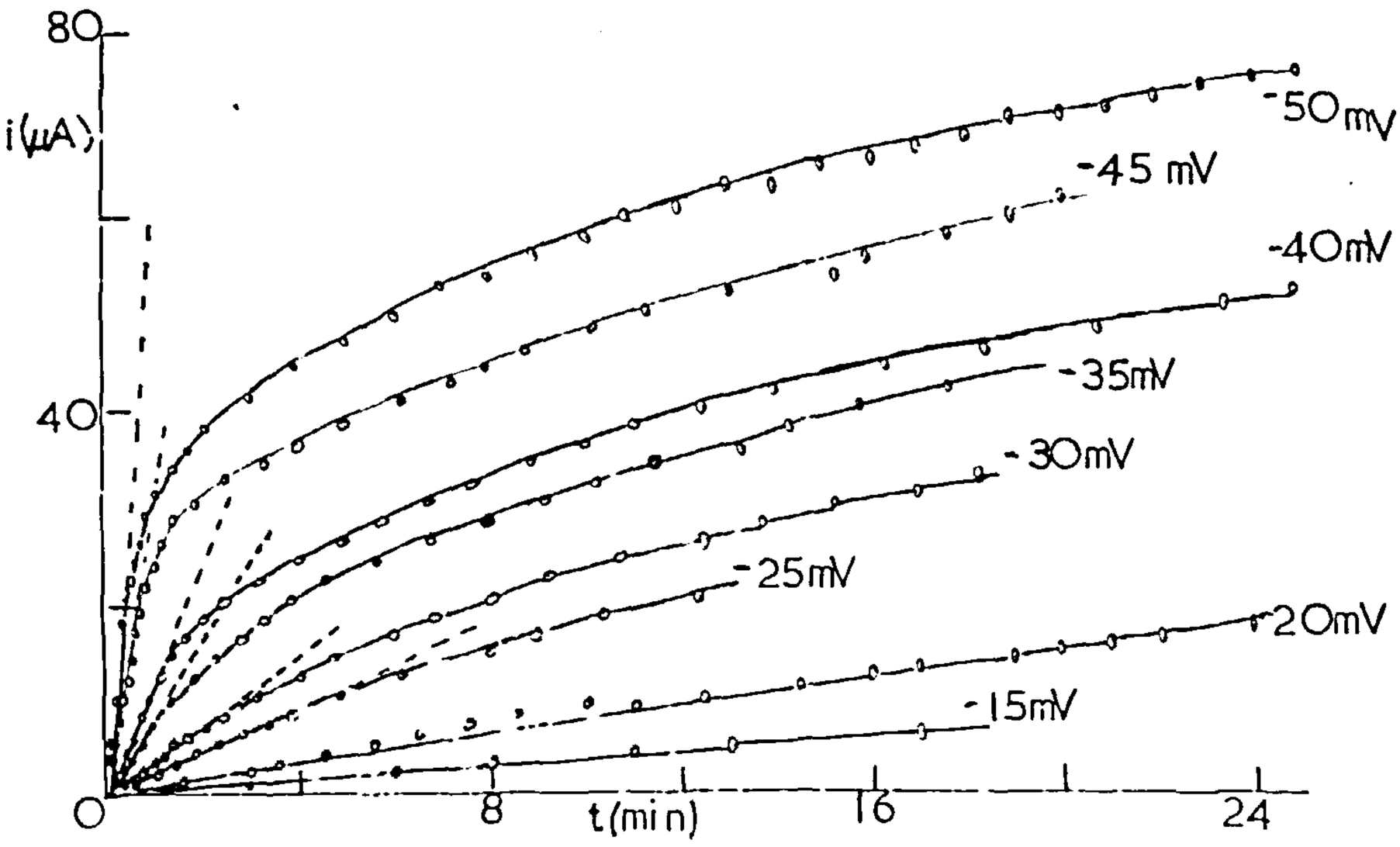

the flux in this case would be constant for each nucleus and independent of nuclear geometry;

(e) progressive nucleation and growth of needles caused by the dissolution of some nuclei during the double-layer charging transient which occurs, in a potentiostatic experiment, when the prepulse switches to the growing potential.

Fig.26 shows seeded transients for silver up to 25 min, though the transients bend over, probably due to diffusion, no maxima due to nuclei overlapping are observed.

Progressive nucleations are virtually ruled out by the use of a double pulse, and (e) seems unlikely as the observed charge needed for the double layer is not excessive. (b) is thus the most likely, particularly as without a prepulse a typical two-dimensional progressive $i \propto t^2$ dependence (probably instantaneous initially plus progressive) is observed.

Figs. 27 and 28 show electron micrographs of deposits. Probably the larger nuclei are formed by overlap as the times of deposition are long and the elementary units are particles of about 1μ across. The nuclei are too thick for electron diffraction by transmission.

The formation of single crystal nuclei, under similar

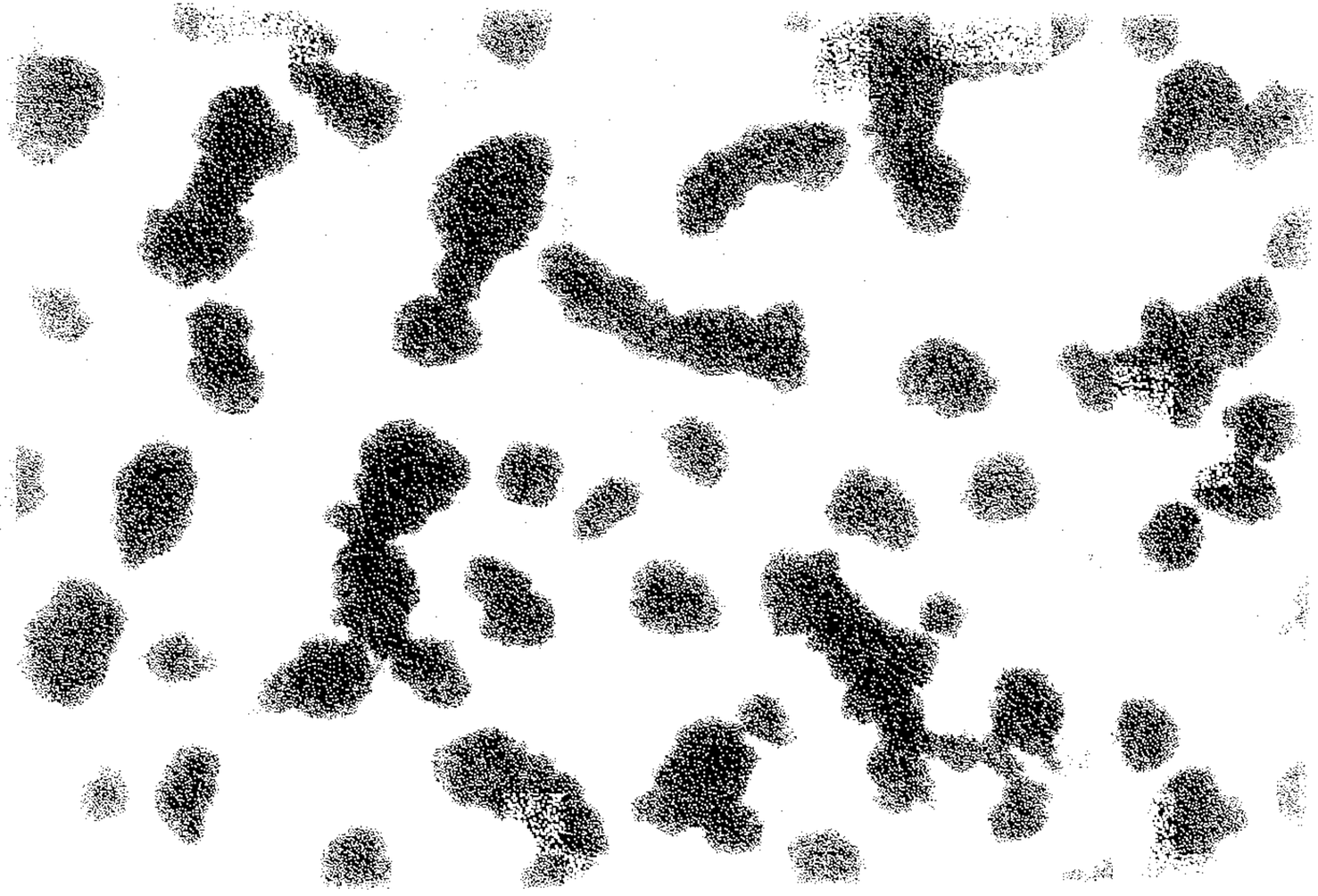

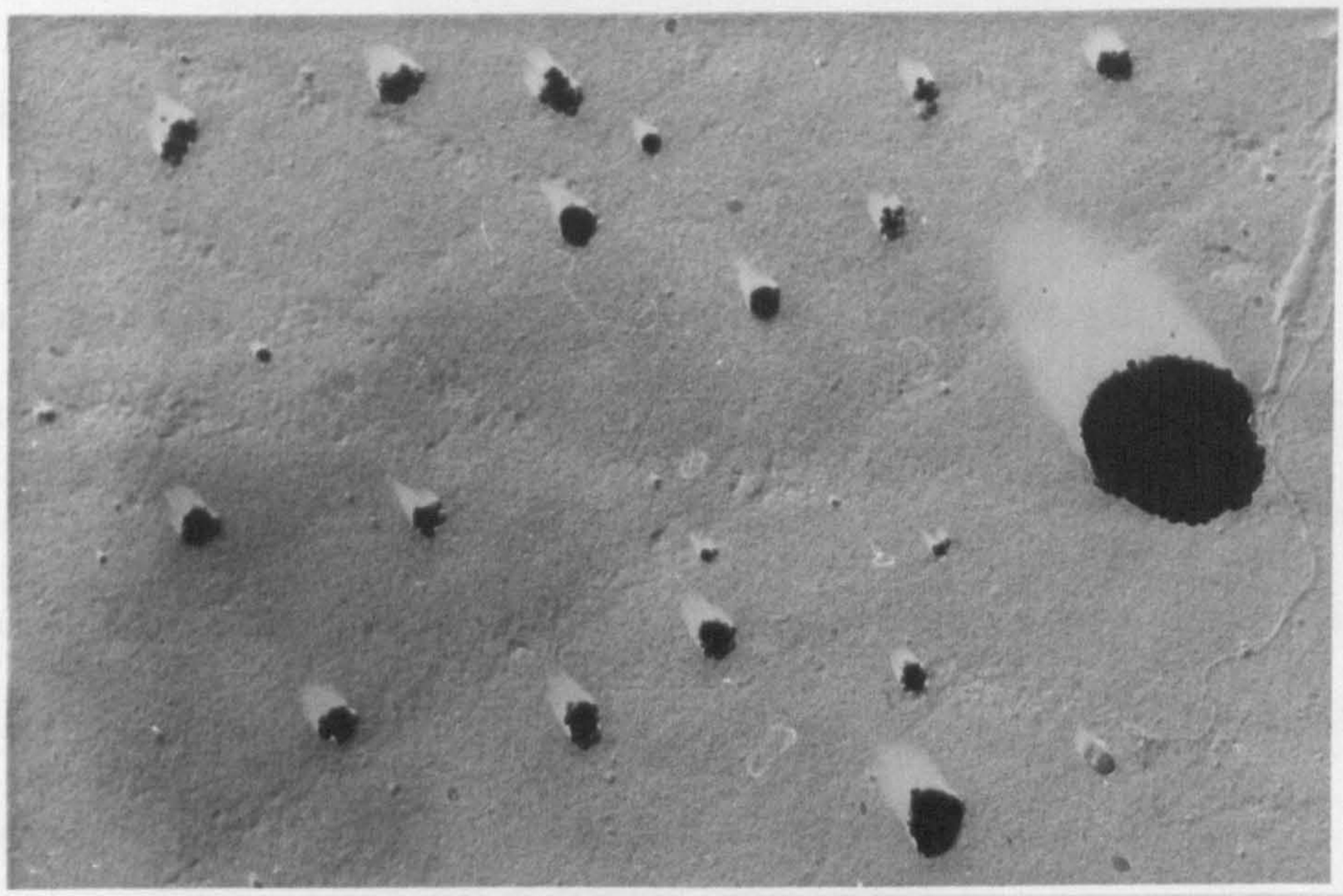

fig[29] electron micrograph Ag nuclei on glassy C formed at η -100mV, 43 msec; then -20 mV, 10 sec; in 0·015 M $AgClO_4$/1M $HClO_4$. shadowed cot^{-1} 2. mag. x39,000.

fig[28] electron micrograph Ag nucleus on glassy C formed at η -100 mV, 200 msec; then - 20 mV, 2 min; in 0·05M $AgClO_4$/1M $HClO_4$. mag. X 4500

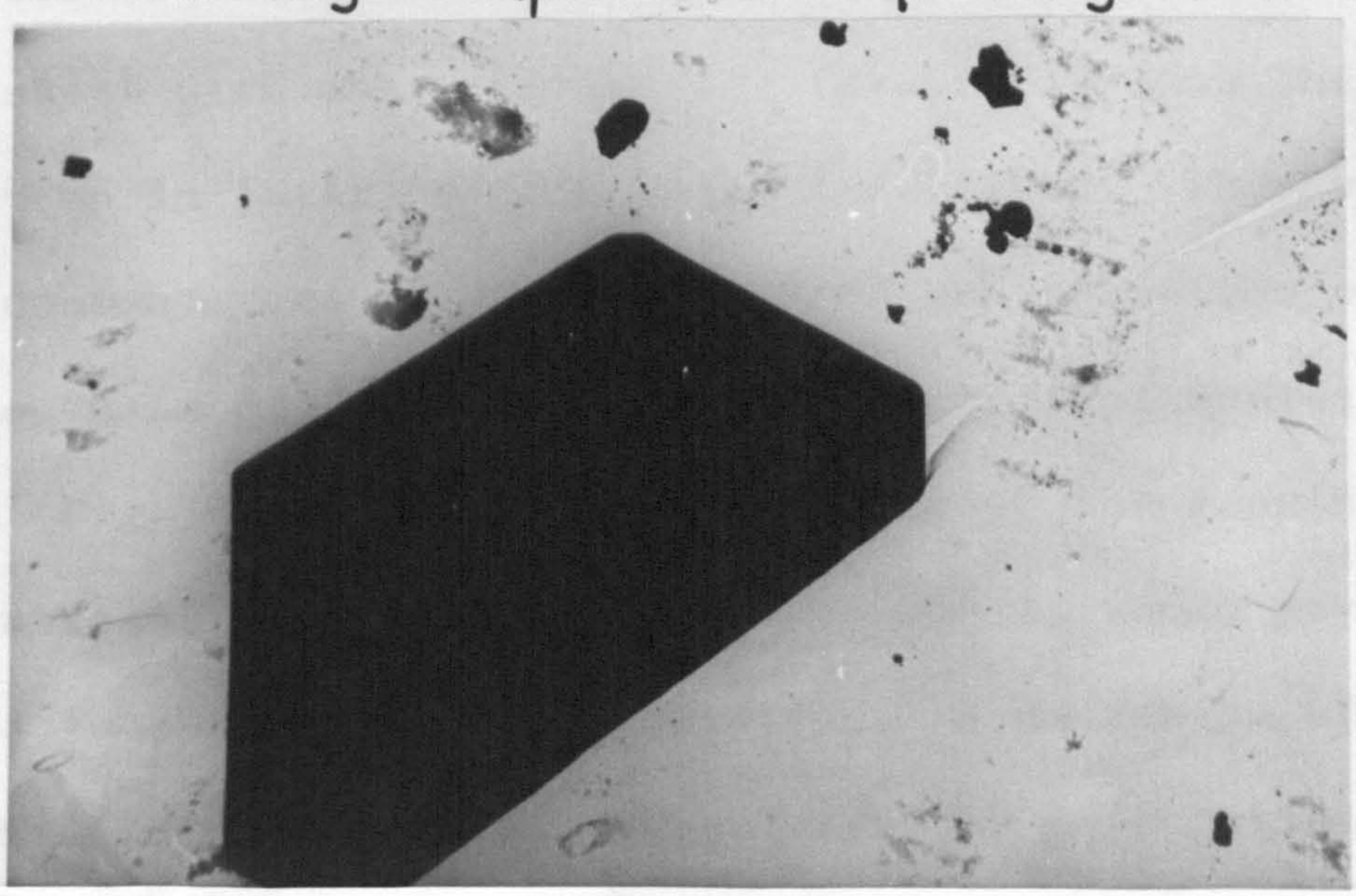

conditions, have been reported by Polukarov and Feklistov.[108] They report structural data on the orientation of silver nuclei electrodeposited onto a carbon covered platinum substrate. They consider that in the initial stages of deposition, silver is produced in a metastable modification with a close-packed hexagonal lattice. When the crystals reach a definite thickness, they undergo conversion into the stable cubic face-centered lattice modification.

A comparison of the charge which has flowed into the electrode during deposition, with the size and number of nuclei on an electron micrograph indicates that the nuclei are three-dimensional. Shadowed electron micrographs (Fig.29), and stereoscan electron micrographs (Fig. 30(a),(b)) give clear proof of this indication. The only explanation which is consistent with the experimental results is that the nuclei are built up in layers of monomolecular height. These would have to commence growth at random times and positions on the nuclei so as to produce the almost hemispherical nuclei observed (Fig.30) and the $i \propto t$ dependence. The growth of two-dimensional plates on top of one another, would give rise to a 'saw-tooth' i vs. t relation. A mechanism of two-dimensional layer formation agrees with the postulation of Budewski et al.[92] Presumably the crystals, as they are

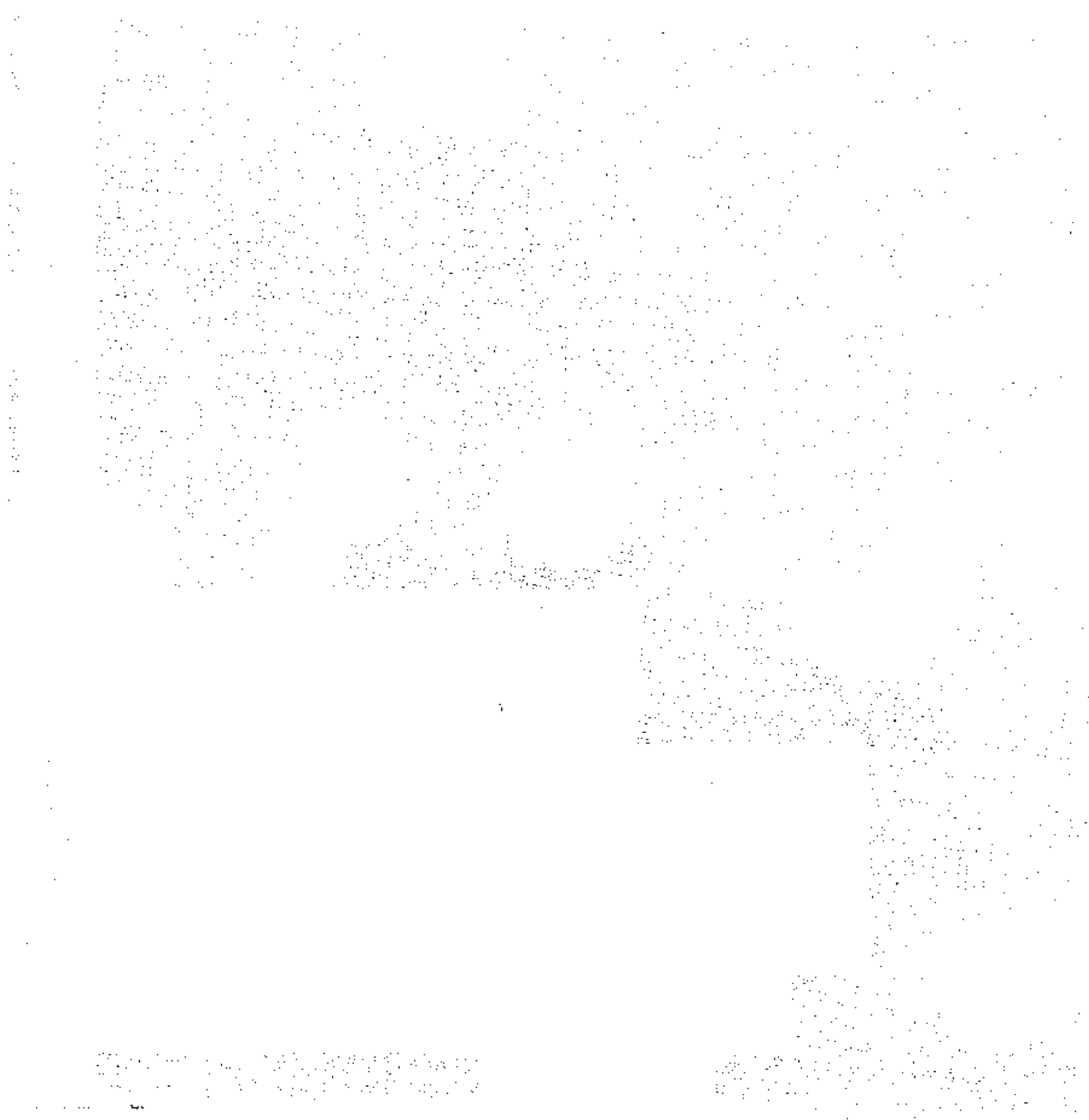

fig 30a s[illegible] ing assy C formed [illegible] 300[illegible] [illegible] ; [illegible] 30 m[illegible] 2 min; in 0.0[illegible] AgClO[illegible] M HClO$_4$. magnification x [illegible]400

fig 30b magn[illegible] 400

grown at very low current densities during the second pulse, develop few dislocations.

3.7. The electrocrystallisation model

Fleischmann and Thirsk[82] have shown, in a manner similar to that used in Chapter 1, section 4, that when N_o two-dimensional nuclei grow with the slow step at the periphery then

$$(i/t)^{\frac{1}{2}} = (2nF\pi Mh N_o/\rho)^{\frac{1}{2}} k \qquad (3.7.1.)$$

where k is the crystal growth rate constant in moles. cm^{-2} sec^{-1}, h is the height of the two-dimensional growth centres, M is the molecular weight, ρ is the density, N_o is the number of nuclei on the electrode surface, and the other symbols have their usual significance.

A plot of $(i/t)^{\frac{1}{2}}$ vs. η is therefore equivalent to a plot of k against η. Fig.31 shows such a plot. The Tafel slope of such plots is ca. 60mV at cathodic over-potentials greater than 20mV. Below this overpotential the plots become steeper.

A plot of current at constant charge vs. η shows similar behaviour and is shown in Fig. 32. Current at constant charge (q) is essentially the same as current at constant interfacial area for a growing nucleus. For true

fig 31 0·01M $AgClO_4$, 1M $HClO_4$, glassy C. $(i/t)^{\frac{1}{2}}$ vs η. prepulse -100mV, 100msec

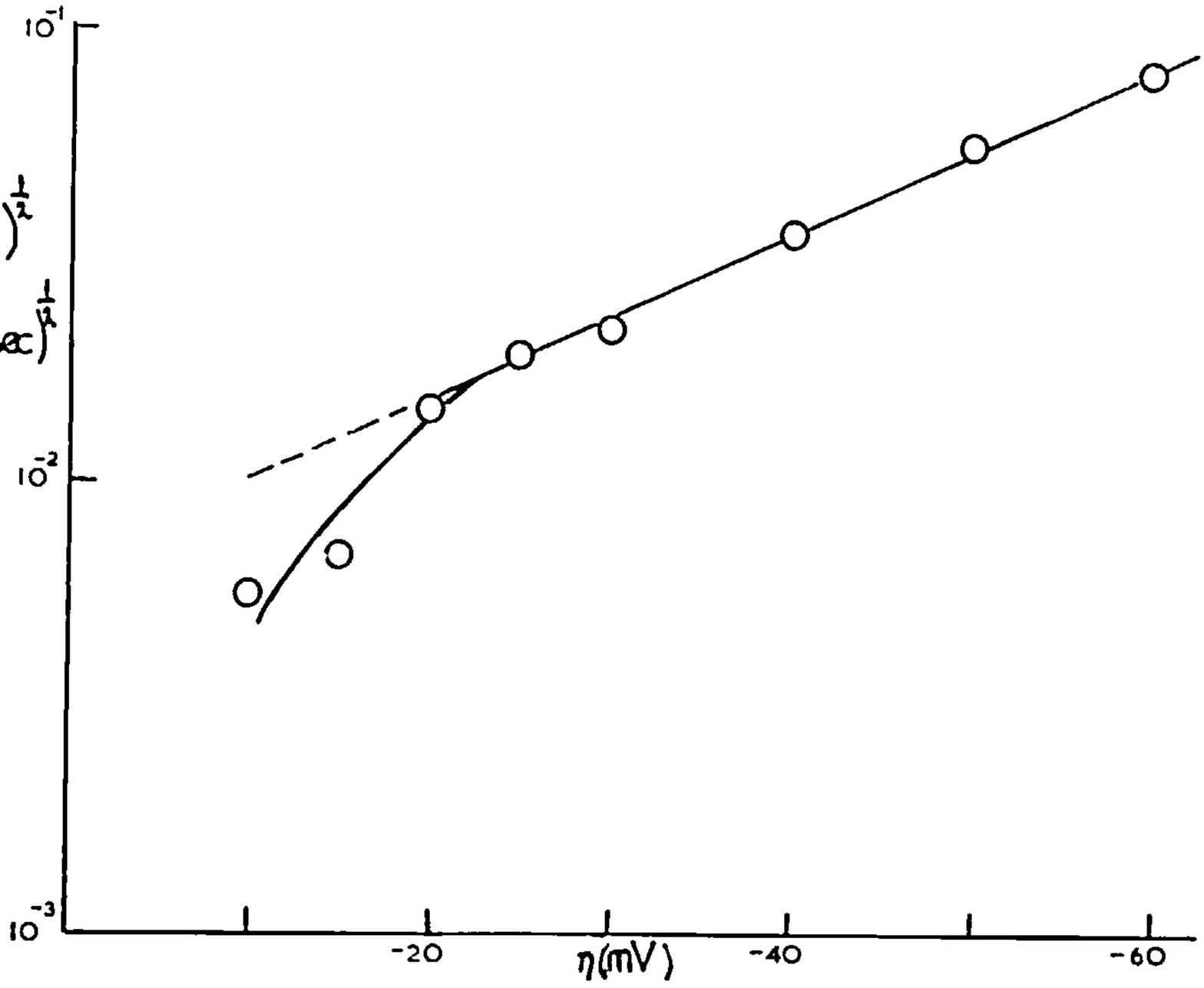

fig 32 0·01M $AgClO_4$ / 1M $HClO_4$. glassy C. i(q) vs η. prepulse -100mV, 100 m.sec.
q = 100 μC (x); q = 200 μC (o); q = 300 μC (Δ).

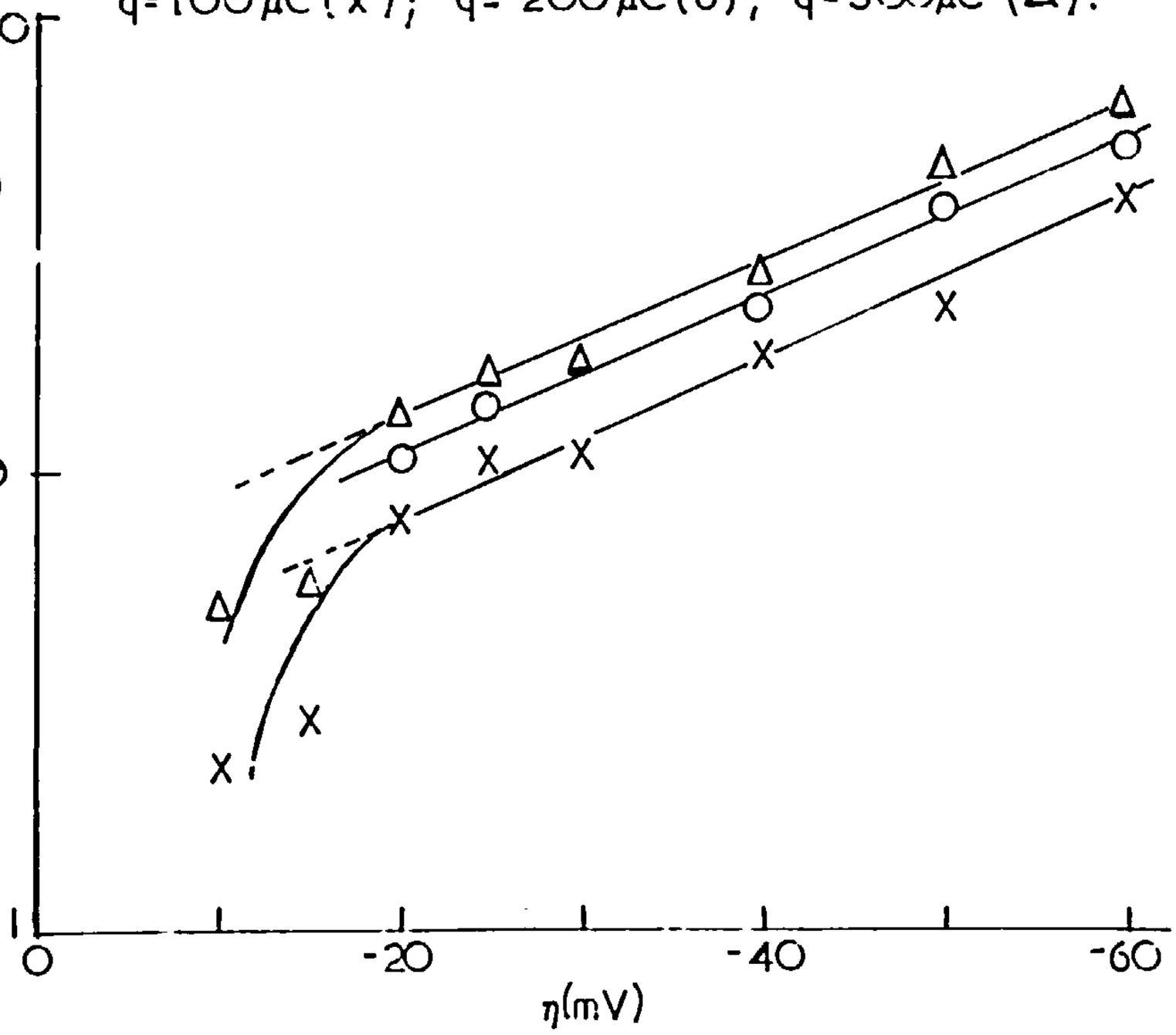

three-dimensional and two-dimensional nuclei, one would expect current (at constant η) to be proportional to $q^{2/3}$ and $q^{1/2}$ respectively. In this case, the nuclei are known to be three-dimensional of two-dimensional layered growth origin - so such plots are of little value.

A Tafel plot of 60mV (for both $(i/t)^{\frac{1}{2}}$ and i(q)) is not compatible with a lattice growth constant of the form suggested by Fleischmann and Thirsk[82] (Chapter 1, section 4). For a one electron transfer, with $\alpha = 0.5$, one would expect a slope of 120mV for normal electrochemical transfer control. Though it is possible to obtain a 60mV dependence for a reversible electron transfer, it seems likely that such conditions of rapid transfer would lower the surface concentration of cations at the surface of the growing centres to such an extent that diffusion would set in. It has already been stated in Chapter 1, section 4, that diffusive flux control into a growing three-dimensional nucleus, under instantaneous nucleation conditions, shows a $i \propto t^{\frac{1}{2}}$ dependence. With a two-dimensional centre, one would expect the current to be independent of time.

It is therefore necessary to invoke a mechanism involving a reversible process, to give the 60mV slope, but yet still show growth control at the periphery. A possible mechanism

is

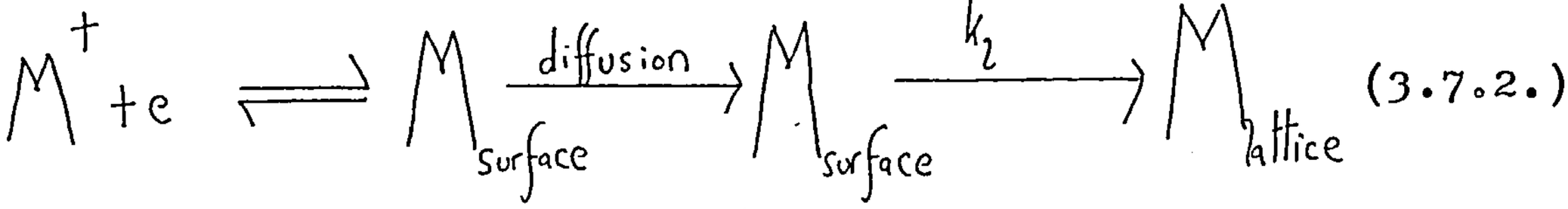

$$M^{+} + e \rightleftharpoons M_{surface} \xrightarrow{\text{diffusion}} M_{surface} \xrightarrow{k_2} M_{lattice} \qquad (3.7.2.)$$

The electrochemical equilibrium follows the applied potential according to the Nernst equation. At the equilibrium potential,

$$E^{r} = E^{\circ} + (RT/F) \ln (C_{Ag^+} / C_{Ag}{}^{r}) \qquad (3.7.3.)$$

where $C_{Ag}{}^{r}$ is the adatom concentration at the reversible potential E^{r}, and $C_{Ag}{}^{+}$ the bulk concentration of silver.

At an overpotential η,

$$E^{r} + \eta = E^{\circ} + (RT/F) \ln (C_{Ag^+} / C_{Ag}) \qquad (3.7.4.)$$

where C_{Ag} is the adatom concentration at η. $C_{Ag}{}^{+}$ is assumed to remain unchanged throughout the potentials.

Hence

$$C_{Ag} = C_{Ag}{}^{r} \exp(-F\eta / RT) \qquad (3.7.5.)$$

and the observed rate of reaction $k_\eta C_{Ag}$ becomes

$$(i/F)^{\frac{1}{2}} \propto k_\eta C_{Ag} = k_\eta C_{Ag}{}^{r} \exp(-F\eta/RT) \qquad (3.7.6.)$$

This equation shows a 60mV slope. The slight curvature at

low cathodic potentials seen in Figs. 31 and 32, could be due to dissolution of atoms, once in the lattice, directly into the solution.

Extrapolation to the equilibrium potential allows calculation of the rate of lattice incorporation by eqn. (3.7.1.). Using a value of $N_o = 360\ cm^{-2}$ (from optical micrographs) and $h = 4.09\text{Å}$, then $k = 5.1 \times 10^{-5}$ moles cm^{-2} sec^{-1} for $C_{Ag}^{+} = 1.5 \times 10^{-2}M$. Counting the number of nuclei from optical micrographs is a weakness in this calculation.

The concentration dependence of the $(i/t)^{\frac{1}{2}}$ against η plots is shown in Fig.33. If one assumes that C_{Ag}^{r} is independent of C_{Ag}^{+}, which is a somewhat rash assumption, one would expect that the k against η curves should be independent of C_{Ag}^{+} also (from eqn. (3.7.6.). Fig. 33 shows this to be approximately true; k x 2 when (C_{Ag}^{+}) x 10. It is a problem to keep the number of nuclei formed during the prepulse constant when the bulk concentration is changed. In Fig.33 an attempt was made to do this by reducing the width of the prepulse inversely proportional to the concentration. This assumed that the rate of growth during the prepulse was $\propto (C_{Ag}^{+})t$. An approximately $i \propto t$ relationship was observed on the oscilloscope at the potentials of the prepulse. The concentration dependence at the

fig 33 $(i/t)^{\frac{1}{2}}$ vs η , glassy C; O, 0·005 M $AgClO_4$, I=1M, $HClO_4$, prepulse -100 mV, 90 msec ; X, 0·01 M $AgClO_4$, I=1M, $HClO_4$, prepulse -100 mV, 45 msec ; Δ , 0·05 M $AgClO_4$, I=1M, $HClO_4$, prepulse -100 mV, 9 msec .

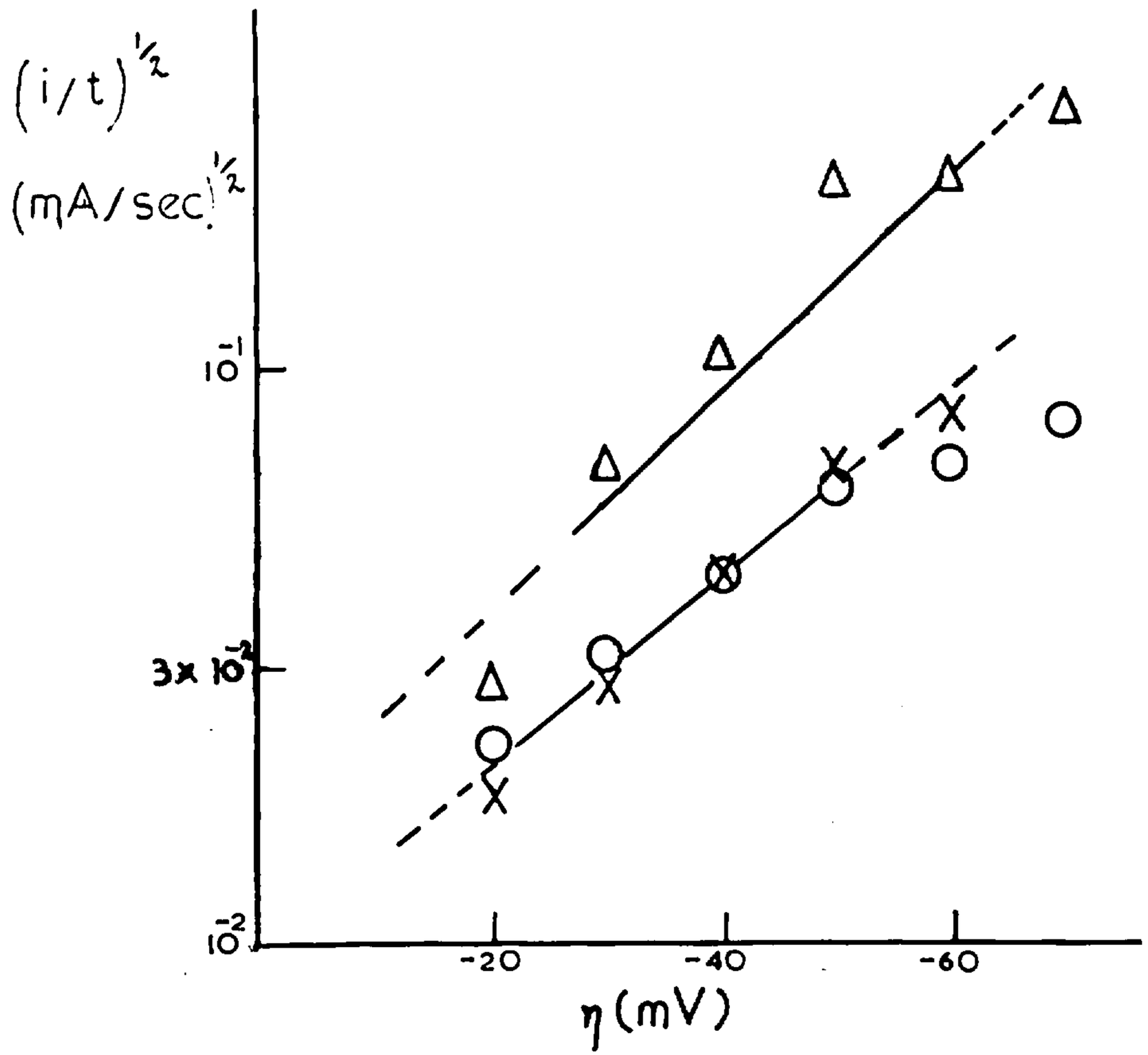

prepulse potential might be ascribed to a change over in mechanism at this high overpotential, from a reversible pre-equilibrium to an irreversible electron transfer.

Mechanism (3.7.2.) is in direct conflict with previous suggestions as the electrochemical stage is fast and in equilibrium, the slow step being the lattice incorporation of uncharged adatoms with a rate independent of potential. The measurements can no longer be interpreted in terms of α and i_{o_h}. Gerischer and Tischer[78] give an i_o equivalent to 1.75×10^{-5} moles cm^{-2} sec^{-1} (taking $i_o = nFk$) for measurements on solid silver at the same concentration. This might be interpreted as a k value in the light of these measurements, although the agreement may be fortuitous. The adatoms probably have some free existence on the silver nuclei before they are incorporated into the lattice. As a diffusion wave does not appear before the rising transients, then it would seem that silver adatoms do not exist on the carbon surface itself, but the nucleation starts directly at favourable sites on the carbon surface.

Chapter 4

The Electrocrystallisation of Palladium

4.1. Introduction

In order to test whether the i $\propto$ t transients (obtained for silver deposition) were affected by the geometry of the nuclei, it was decided to deposit other metals on carbon and see if a change of mechanism occurred. Palladium was chosen as a higher melting-point, noble metal which could be dissolved off the surface again before each measurement without forming oxide. Clearly if mechanism (3.6.(d)), involving progressive nucleation inside a hemispherical diffusion zone of constant flux explained the silver transients, one would never see any difference in the behaviour of metals having nuclei of different geometry.

4.2. The deposition of palladium upon carbon

The initial (sitting) potential in potentiostatic pulse experiments was +750mV (3MHQ/calomel electrode), sufficiently anodic to allow complete dissolution of the deposited metal after each measurement. The ratio of chloride to palladium in the solutions was kept at 3, and the total ionic strength 0.44 to achieve 96% of the palladium as the $PdCl_2$ complex.[109] There are a generation of palladous chloride complexes from $PdCl^+$ to $PdCl_4^{2-}$.

Fig.34 illustrates the time dependence of unseeded

fig 34 0·0272 M $PdCl_2$, I = 0·44 M with $HClO_4$, HCl ; $Cl^-/Pd^{2+} = 3$, glassy C,
i vs t^3 at +250 mV. (Pd/H_2)

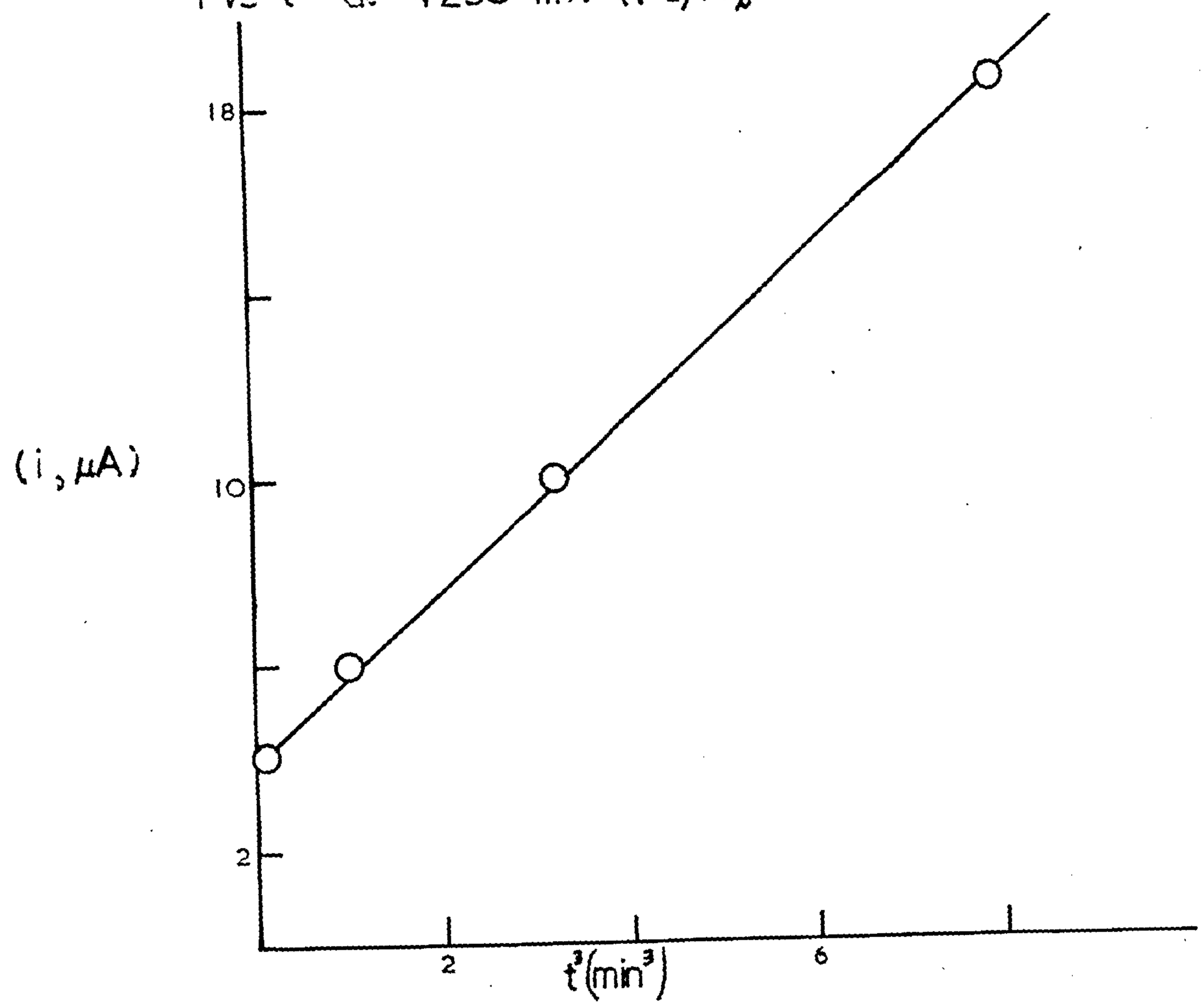

(i.e. without prepulse) transients for Pd on glassy carbon. This $i \propto t^3$ relationship changes to $i \propto t^2$ (Fig.35) upon pre-seeding. These dependencies would be obtained for three-dimensional nucleation and growth (Chapter 1, section 4). Fig.36 shows an electron micrograph of Pd nuclei grown on pyrolytic graphite. Some overlapping of nuclei is observed which may account for the seeded transients cutting off from $i \propto t^2$. More probably diffusive flux control into the growing nuclei takes over at a certain rate of growth.

4.3. The electrocrystallisation model

For instantaneous three-dimensional growth,

$$\left(i/t^2\right)^{\frac{1}{3}} = \left(2nF\pi M^2 N_0 / \rho^2\right)^{\frac{1}{3}} k \qquad (4.3.1.)$$

Thus a plot of $\left(i/t^2\right)^{\frac{1}{3}}$ against η is comparable to one of k against η. Fig.37 shows such plots for 2.56×10^{-2}M $PdCl_2$ and 5.12×10^{-2}M $PdCl_2$ solutions. The length of the prepulse was adjusted proportionally as the inverse square of concentration, assuming that material comes in by planar diffusion at the higher potential of the prepulse. The slope of these plots was ca. 50mV. The equilibrium potentials were measured in each solution with Pd deposited on the electrode surface. They were found to be +603mV, +595mV

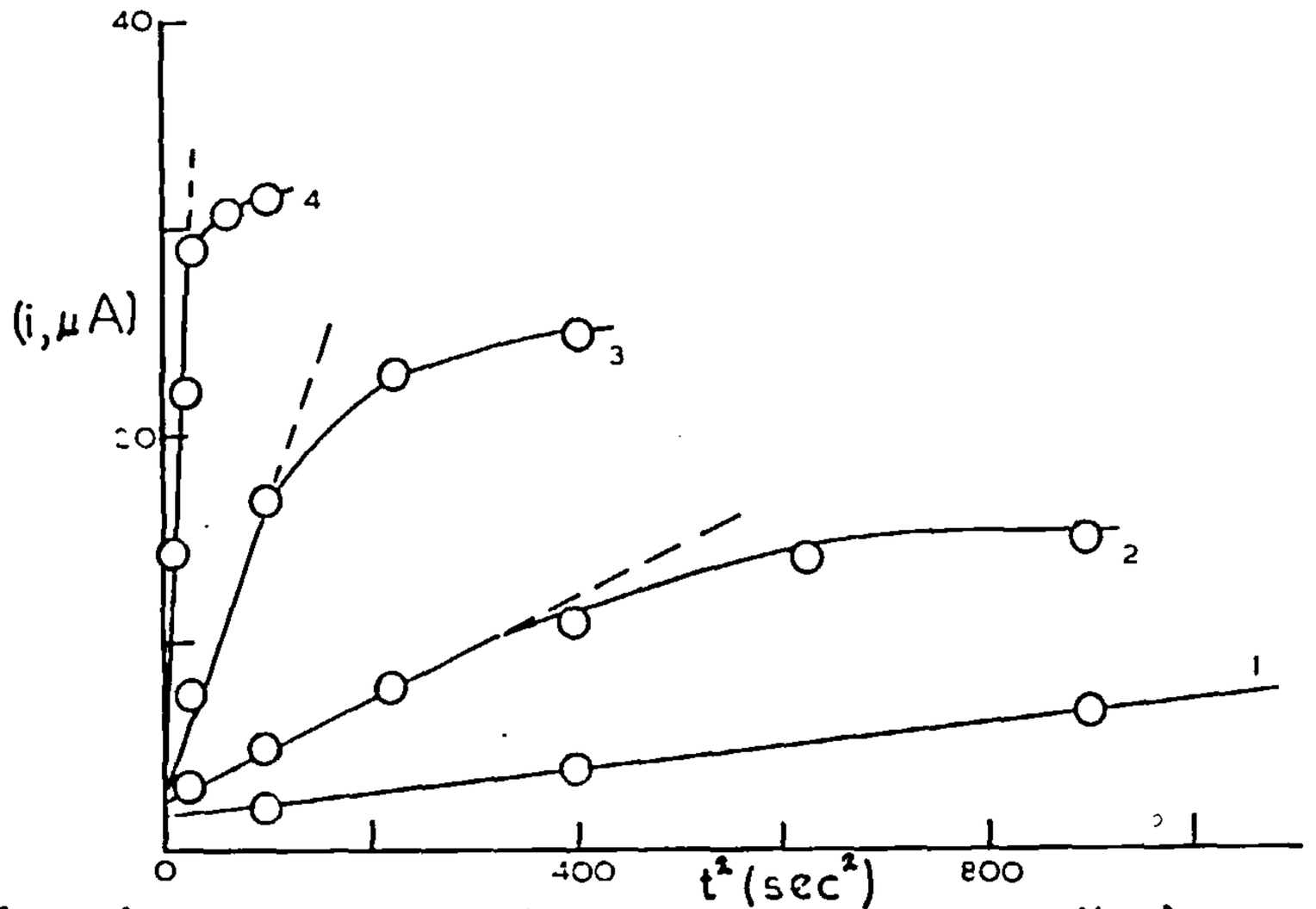

fig 35 i vs $t^{\frac{1}{2}}$, 0·0512 M $PdCl_2$ (I=0·44M, $HClO_4$, HCl, Cl^-/Pd^{2+}=3), pyrolytic graphite, prepulse +400 mV, 25 msec (ref. 3M HCl / calomel).
1, +510 mV; 2, +500 mV; 3, +490 mV; 4, +480 mV.

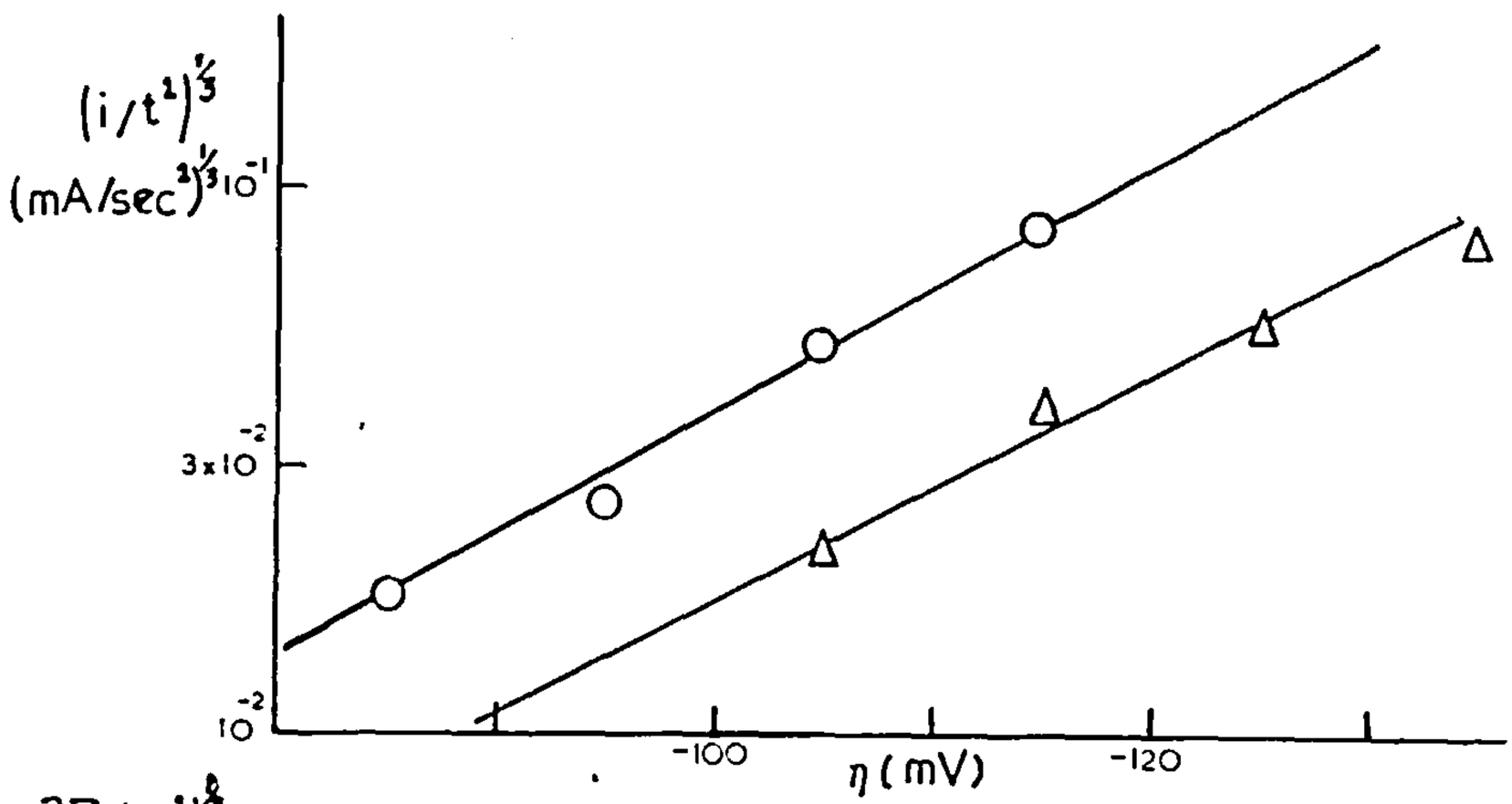

fig 37 $(i/t^{\frac{1}{2}})^{\frac{1}{3}}$ vs η, pyrolytic graphite. Δ, 0·0256 M $PdCl_2$, prepulse -200 mV, 100 msec; O, 0·0512 M $PdCl_2$, prepulse -200 mV, 25 msec; solutions to I=0·44 M, $HClO_4$, HCl; Cl^-/Pd^{2+} = 3.

with reference to the calomel/3M HCl potential, i.e. +367mV, +357mV (ref. Normal Hydrogen electrode (N.H.E.)); for the 5.12×10^{-2}M, 2.56×10^{-2}M $PdCl_2$ solutions respectively. Templeton et al[110] have measured the equilibrium potentials for the $PdCl_4^{2-} + 2e \rightleftharpoons Pd_{(s)} + 4Cl^-$ couple. Their results predict potentials of +582mV, +573mV (N.H.E.) for these solutions. No information about the equilibrium potentials involving the $PdCl_2$ complex is available.

The potential dependence observed is consistent with a two-electron transfer with a slow electrochemical step. This follows the postulated lattice growth constant form of Fleischmann and Thirsk[82], as mentioned in Chapter 1

i.e. $$k = k_0 \left\{ C_{(Pd^{II})}{}^{r} \right\} \exp\left(\alpha n_\gamma F / RT\right) \qquad (4.3.2.)$$

This expression implies that discharge takes place directly at the lattice building sites. To obtain a 50mV slope α is taken as 0.6. It is probably physically unrealistic to envisage an actual transfer of two electrons simultaneously. Two consecutive one-electron transfers of comparable rates would satisfy the results and provide a more realistic explanation. Measurements of N_o from electron micrographs gave a value of 4×10^4 cm^{-2} which led to a value for k of 3.3×10^{-9} moles cm^{-2} sec^{-1} for a 5.12×10^{-2}M Pd^{II} solution

at the reversible potential. This shows that the rate of lattice incorporation for Pd is a factor 10^4 x slower than that for Ag.

As the majority species in the palladous solutions used was controlled to be almost completely $PdCl_2$, and Fig.3 shows that k is increased two-fold for a two-fold increase in concentration ; the Pd^{II} complex involved in eqn. (4.3.2.) must be $PdCl_2$, with r = 1. A similar conclusion was drawn by Kravtsov and Zelenskii[111] from measurements under galvanostatic conditions using palladium electrodes formed by electroplating onto platinum wires sealed into glass. They used solutions of H_2PdCl_4 in 3M H_2SO_4 with various HCl concentrations, in which they considered the complex $PdCl_4^{2-}$ to predominate. From polarisation curves obtained at various chloride and Pd^{II} concentrations they obtained the reaction orders of chloride ions to be -2 and Pd^{II} ions as +1.

i.e. (rate of cathodic process) $\propto$

$$[PdCl_4^{2-}]\,[Cl^-]^{-2}\exp(\alpha nF\Psi/RT) \qquad (4.3.3.)$$

Their Tafel slopes were ca. 80 $\pm$ 7 mV. They attributed the retardation of the cathodic process by chloride ions to the direct participation, in the cathodic process, of $PdCl_2$

molecules formed by the dissociation of $PdCl_4^{2-}$ ions.

$$PdCl_4^{2-} \rightleftharpoons PdCl_3^- + Cl^- \qquad (4.3.4.)$$

$$PdCl_3^- \rightleftharpoons PdCl_2 + Cl^- \qquad (4.3.5.)$$

The $PdCl_2$ molecules were then assumed to be completely reduced to palladium.

$$PdCl_2 + 2e \rightleftharpoons Pd + 2Cl^- \qquad (4.3.6.)$$

Under the assumption that (4.3.4.) and (4.3.5.) take place under almost reversible conditions and that the rate of the entire cathodic process is determined by the subsequent slow stage (4.3.6.) Kravtsov and Zelenskii obtained eqn. (4.3.3.). They suggested that the slow stage in this case may be the process of activation of adsorbed $PdCl_2$ molecules, associated, for example, with an increase in the length of the bond between the central metal ion and the ligand.

Extrapolation of the cathodic polarisation curves to the reversible potential in a solution of 10^{-1}M H_2PdCl_4, 1M HCl, 3M H_2SO_4 gave a mean value for i_o of 4.8×10^{-5} A.cm^{-2}. This is dimensionally corresponding to a value for k (taking $i_o \equiv nFk$) of 2.4×10^{-10} moles cm^{-2} sec^{-1}. This is a factor

10 down on the value obtained for a 5.12×10^{-2}M Pd^{2+} solution in this work.

4.4. Comparison with the silver model

As palladium shows a different current-time dependence under potentiostatic pulse conditions to silver, it seems that the explanation of progressive growth of nuclei in a constant flux for the i vs. t relationship found for silver under 'seeded' conditions is unlikely. If this explanation were true, i vs. t relationships would be found for all metals under similar conditions irrespective of their nuclear geometry. The i vs. t^2 'seeded' relationship obtained for palladium is clear indication of the three-dimensional nature of the palladium centres, the rate determining step being into the periphery of the centres. It also indicates the correctness of the geometric model postulated for the growth of the silver nuclei.

Palladium has a higher melting point ($1552^{o}C$) than silver ($960^{o}C$). This would mean that the surface atoms of silver would be more mobile than those on the 'harder' metal. This would lend stability to any intermediate 'adatom' state in the electrocrystallisation process, a postulation made by the adherents of the 'adatom-surface diffusion' mechanism for solid metals, as mentioned in Chapter 1 This tends to support the model postulated for silver

electrocrystallisation (Chapter 3, Section 7) involving an intermediary surface atom state. Such a state is energetically unfavourable in the case of the higher-melting palladium metal, and lattice incorporation would tend to occur directly from the metal ion in solution. It is suggested that this type of mechanism will always occur for higher melting-point metals, and that the electrocrystallisation route will modify to the silver-type mechanism for the 'softer' metals.

Chapter 5

The Electrocrystallisation of Mercury

5.1. Introduction

In order to test the appropriateness of the models suggested in Chapters 3 and 4 for the electrocrystallisation of the solid metals, silver and palladium, it was decided to deposit a metal which is liquid at room temperature, i.e. mercury, and therefore has no crystalline lattice. Clearly one could not allow mercury to have a slow lattice-incorporation step and one would expect, in view of the reported literature[112-115] high values for i_o for the Hg/Hg_2^{2+} couple (ca. 0.46 $A.cm^{-2}$)[112] obtained mainly by the faradaic impedance method, that the growth of mercury nuclei on foreign electrodes would be controlled by bulk diffusion of mercurous ions into the growing centres. Before reporting the measurements for the deposition of mercury onto carbon, a section will be presented on the reduction of Hg_2^{2+} at a mercury electrode under potentiostatic conditions in order to show that the electron transfer is completely reversible, following the Nernst equation.

5.2. The reduction of Hg_2^{2+} on Hg

Fig.38 shows a plot of i vs. $t^{-\frac{1}{2}}$ for pulses from a

fig 38 O·005M $HgNO_3$ / 1M KNO_3 on Hg. i vs $t^{-1/2}$. E° taken +35mV (Ag/Ag^+), i = O.
o; experimental values. x; i calculated from $i = FAC^*\sqrt{D/\pi t}\left(1-\exp\left[-\eta F/RT\right]\right)$.

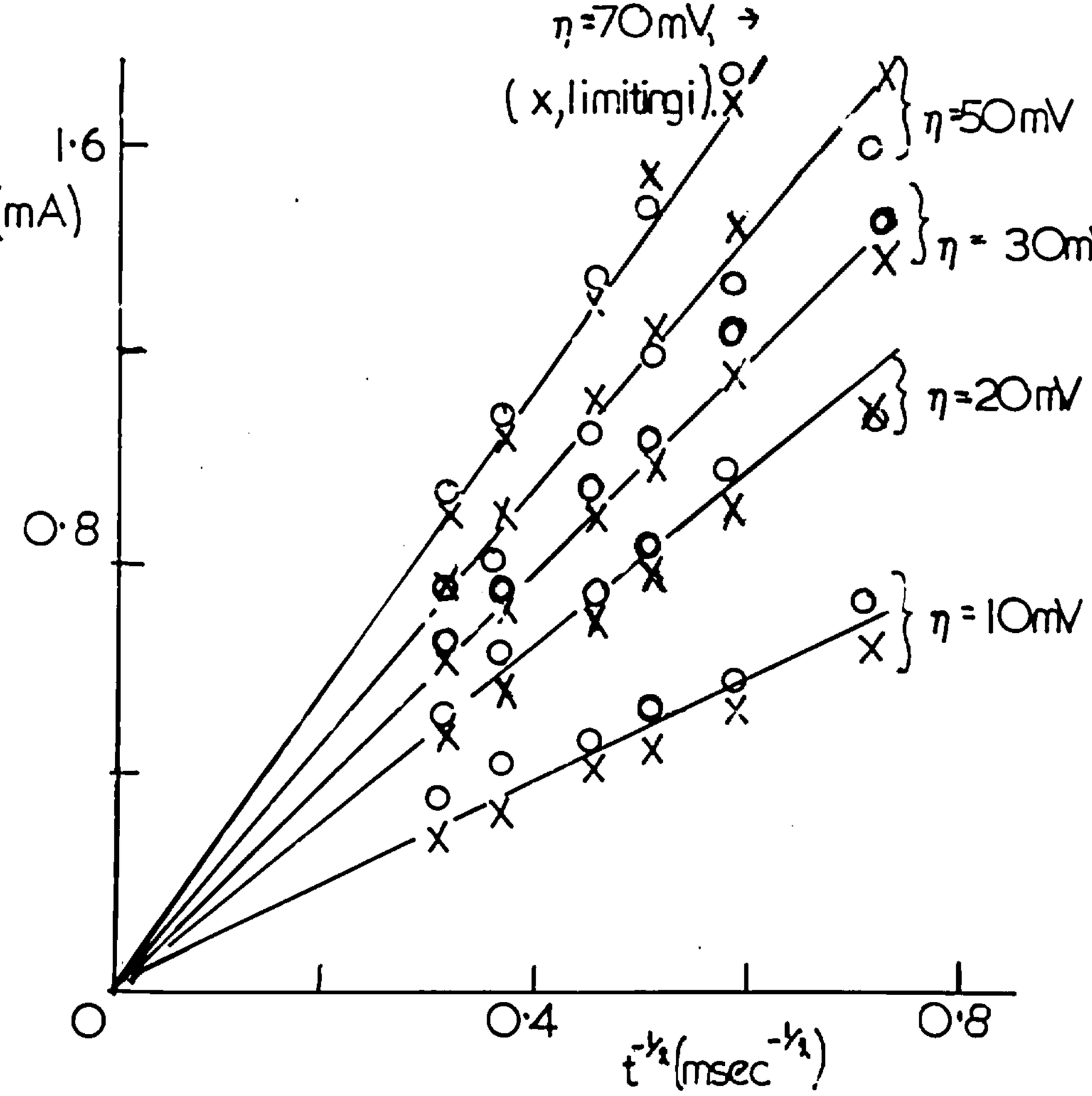

sitting potential of +35mV (ref. Ag/Ag^+ (5×10^{-3}M)), when the current passing through the cell was zero, for a 5×10^{-3}M $HgNO_3$/1M KNO_3 solution. The sitting potential was regarded as the equilibrium potential for the Hg/Hg_2^{2+} electrode. The literature values for E^o for Ag/Ag^+ are +799mV (N.H.E.)[116] and for Hg/Hg_2^{2+}, +792mV (N.H.E.).[117] This means that, from the literature values, E^o Hg/Hg_2^{2+} is -7mV (Ag/Ag^+). The large difference between the potential at zero current and the literature E^o (42mV) is difficult to explain, but could be due to the presence of Hg^{2+} in solution. The drop area used was $0.1cm^2$, and was renewed after each pulse measurement. Plotted alongside the experimental points in Fig.38 are the current values predicted assuming the concentration of Hg_2^{2+} at the interface is controlled by the Nernst equation, and Hg_2^{2+} diffuses in by planar diffusion.

i.e. $$C^{o}_{Hg_2^{2+}} = C^{*}_{Hg_2^{2+}} \exp -\eta F/RT \qquad (5.2.1.)$$

and $$i = FA\sqrt{D/\pi t}\; C^{*}_{Hg_2^{2+}}\left(1 - \exp -\eta F/RT\right) \qquad (5.2.2.)$$

The close agreement between experimental and predicted points gives clear support for eqn. (5.2.2.) and the assumption involved therein that the electron transfer is truly

reversible. At an overpotential of 70mV the concentration of Hg_2^{2+} at the interface becomes essentially zero, so that further increases in overpotential have little or no effect on the current values at given times i.e. the limiting diffusion current is achieved.

5.3. The deposition of Hg onto carbon

As no slow lattice incorporation step can be involved in the growth of mercury nuclei on an inert substrate and the electron-transfer reaction is fast (from the literature and section 5.2), one must consider that diffusion into the expanding three-dimensional mercury nuclei is probably rate determining. If we consider a freely growing mercury hemisphere radius r, volume V, in a solution of mercurous ions concentration C, the current, assuming material is transported to the surface by planar diffusion and the concentration at the interface is taken to be zero, will be given by

$$i = 2F\pi r^2 C\sqrt{D/\pi t} \qquad (5.3.1.)$$

This equals the current required for the growth of the hemisphere,

$$i = (Fe/M)(\partial V/\partial t) \qquad (5.3.2.)$$

Hence

$$r = (2MC/e)\sqrt{Dt/\pi} \qquad (5.3.3.)$$

and $$i = (8FM^2C^3D^{\frac{3}{2}}/\rho^2\pi^{\frac{1}{2}})t^{\frac{1}{2}} \qquad (5.3.4.)$$

Thus, with N_o sites and nucleation rate constant A in sec^{-1}, for progressive nucleation,

$$i = (16AN_oFM^2C^3D^{\frac{3}{2}}/3\rho^2\pi^{\frac{1}{2}})t^{\frac{3}{2}} \qquad (5.3.5.)$$

and for instantaneous nucleation,

$$i = (8N_oFM^2C^3D^{\frac{3}{2}}/\rho^2\pi^{\frac{1}{2}})t^{\frac{1}{2}} \qquad (5.3.6.)$$

Measurements for Hg deposition on carbon were made starting at a sitting potential of +100mV (Ag/Ag^+), sufficiently anodic to allow dissolution of mercury after each pulse experiment. Fig.39 illustrates how Hg deposition transients follow i vs. $t^{\frac{3}{2}}$ without pre-seeding for a 4.5 x 10^{-2}M mercurous nitrate solution, as predicted by eqn. (5.3.5.). Fig.40 shows how the transients time dependence switches to i vs. $t^{\frac{1}{2}}$ when a sufficiently large prepulse (-180mV (Ag/Ag^+), 20 msec) is employed, as required by eqn. (5.3.6.). The unseeded transients also cut off to $i \propto t^{\frac{1}{2}}$ after some growth has occurred.

The seeded transients of Fig.40 are virtually independent of potential and this point is illustrated by a plot of the gradients $i/t^{\frac{1}{2}}$ against potential shown in

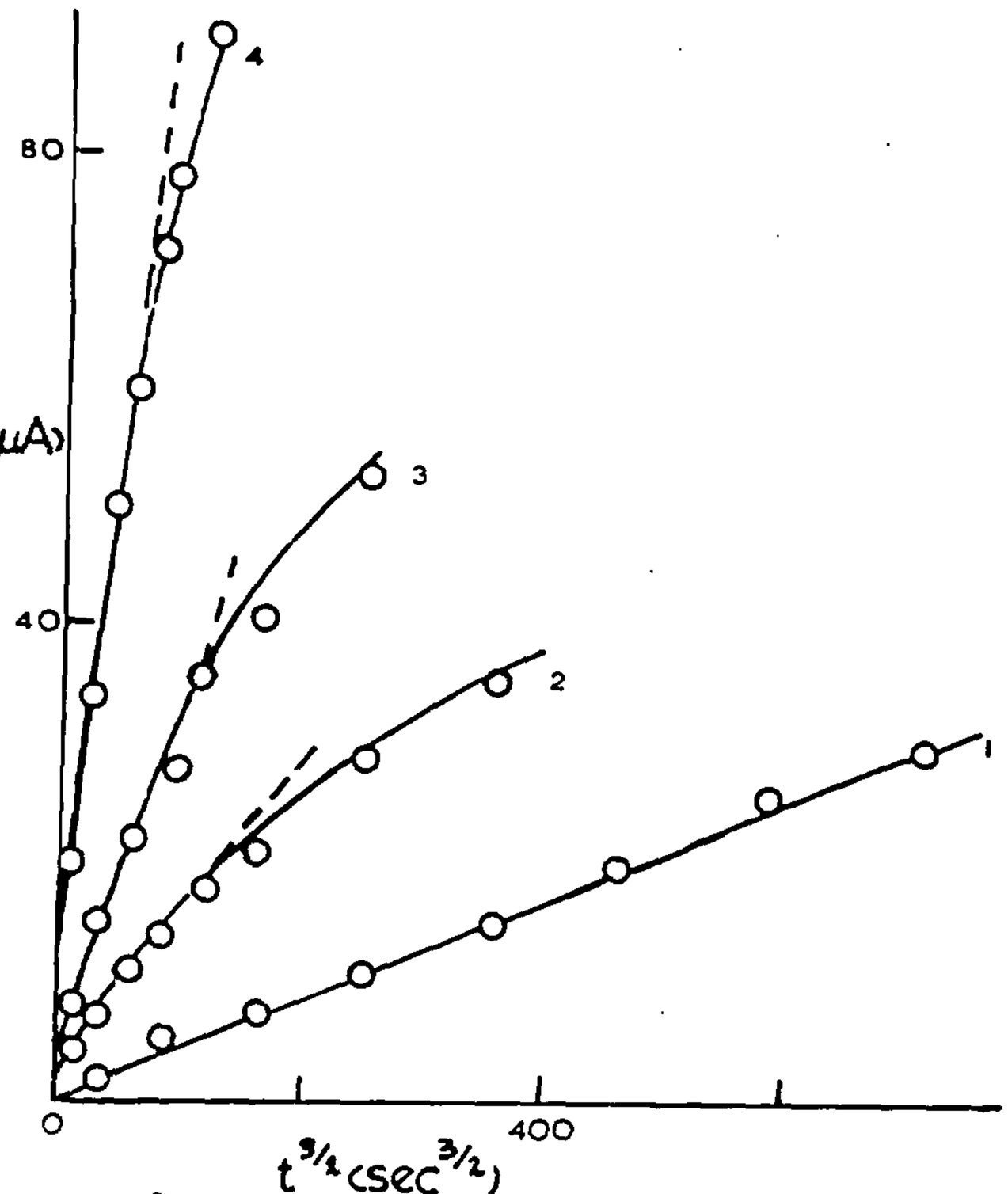

fig 39 0.045M $HgNO_3$, 1M KNO_3; glassy C; i vs. $t^{3/2}$ for (1) -30mV; (2) -35mV; (3) -40mV; (4) -45mV. (Ag/Ag^+)

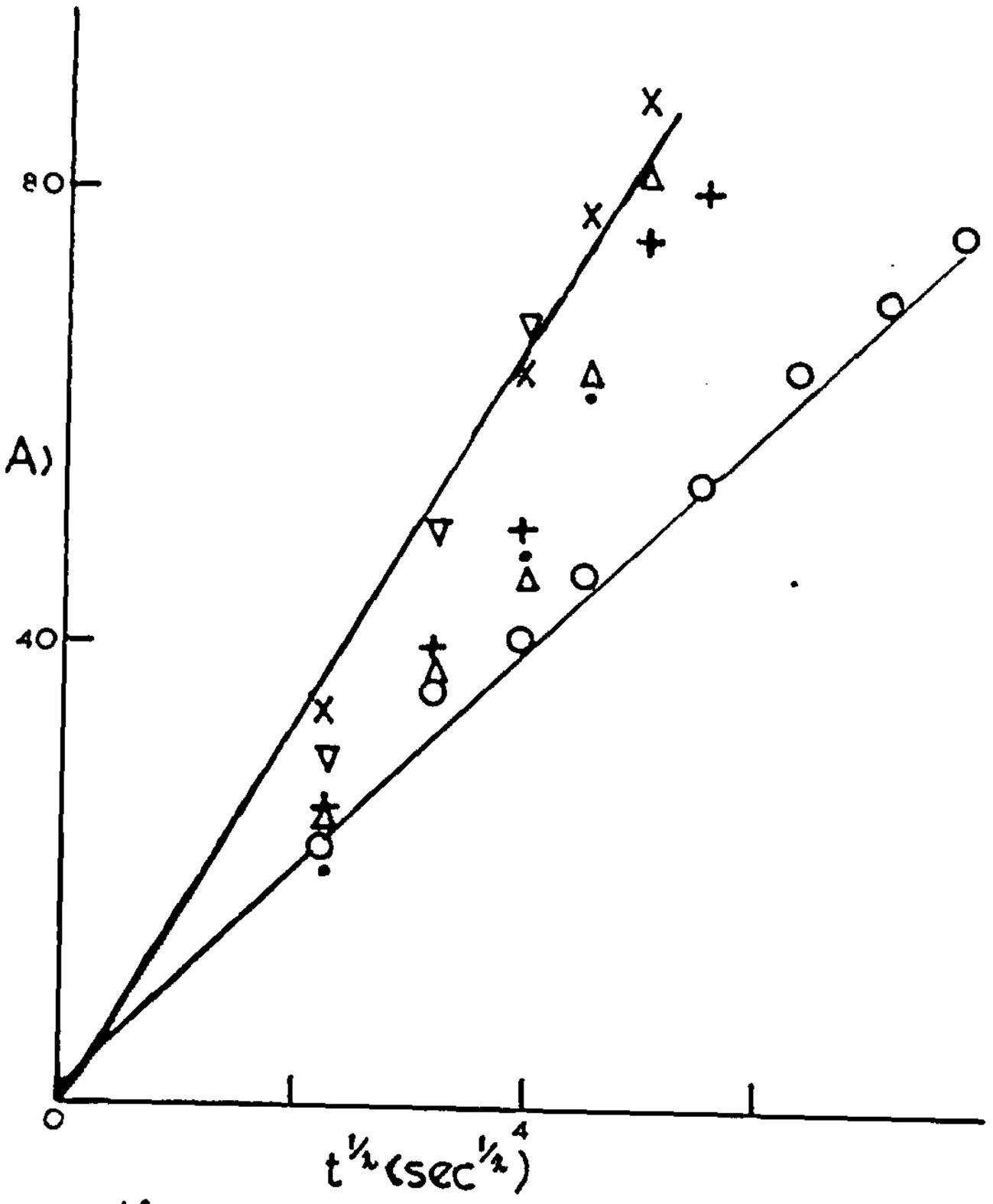

fig 40 0.045M $HgNO_3$, 1M KNO_3; glassy C; i vs $t^{1/2}$ for range -40mV to -100mV, all with prepulse -100mV, 20msec. (Ag/Ag^+)

Fig.41. There is some indication of potential dependence below ca. -60mV (Ag/Ag^+), after which the plot is essentially potential independent. In view of the results discussed in section 5.2, one would not expect total diffusion limiting control until an overpotential of ca. 70mV (i.e. when the concentration of Hg_2^{2+} at the interface may be taken as zero). In view of the fact that E^o in section 5.2 was considered 35mV positive to the Ag/Ag^+ potential, the potential at which potential independence is found in Fig.41 is of the right magnitude. At overpotentials slightly less than ca. 80mV, the potential dependence which would be observed (say in the range η, 55-80mV) would be quite insignificant owing to the nature of the exponential function controlling the concentration at the interface (eqn. 5.2.1.).

It is found that the potential at which mercury growth first starts shifts slightly to more negative potentials as time progresses. Liquid mercury is probably sensitive to contaminants on the electrode surface as these will greatly affect the surface energy terms involved in the nucleation process, and over a period gradual absorption of the trace solution contaminants would cause the observed potential shift.

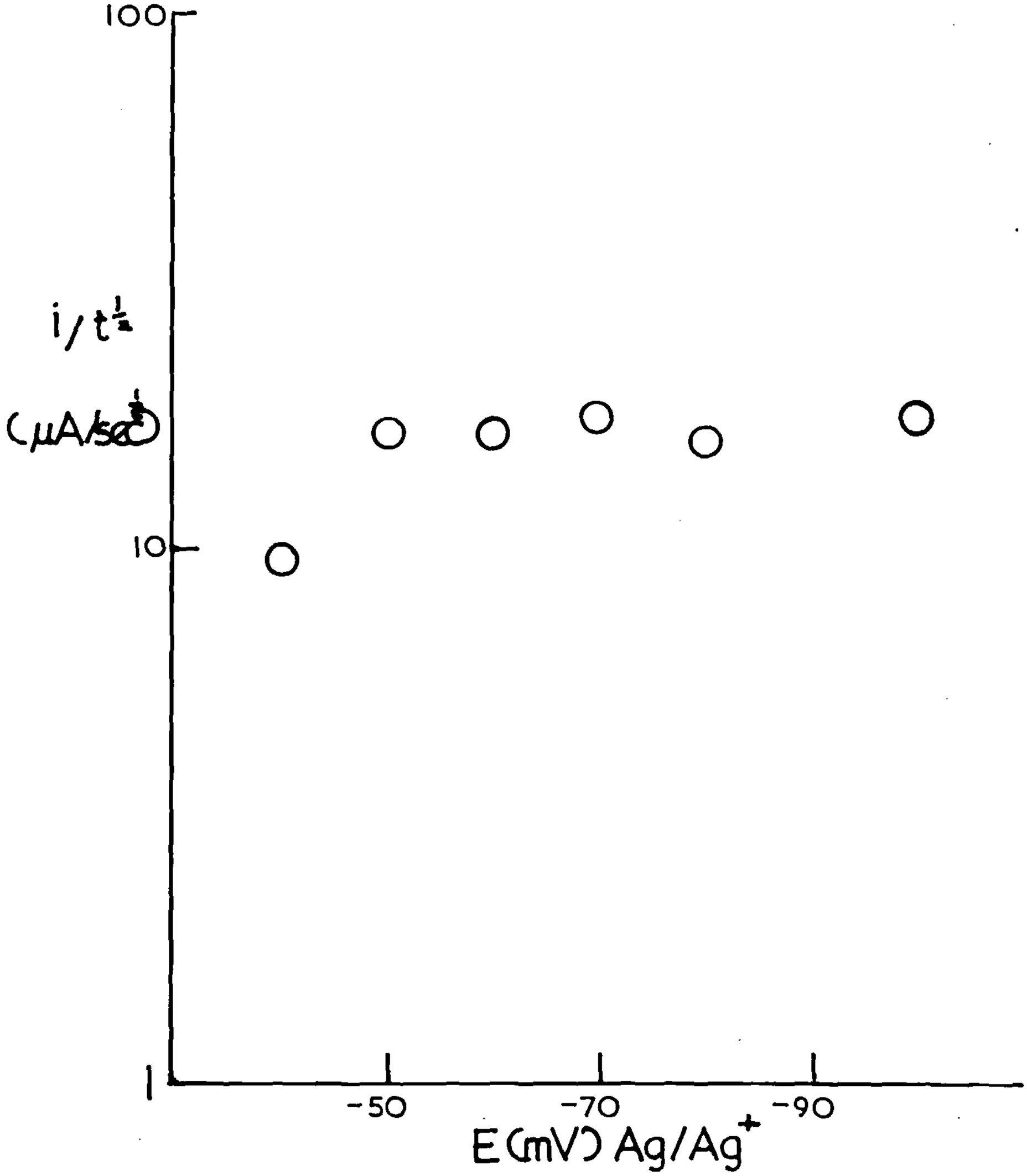

fig 4 0.045M $HgNO_3$, 1M KNO_3; glassy C; dependence of $(i/t^{\frac{1}{2}})$ on E ; prepulse -180 mV, 20 msec.

$(i/t^{\frac{1}{2}})$ by eqn. (5.3.6.) should be 2.3×10^{-10} A. $sec^{-\frac{1}{2}}$ using a value of $N_o = 2 \times 10^3$ cm^{-2} obtained from an optical micrograph. The experimental value is ca. 10^{-5} $A.sec^{-\frac{1}{2}}$. The large difference is undoubtedly due to the difficulty in handling mercury-coated electrodes and the nuclei, which must be grown appreciably larger than in the transient measurements to be optically visible, are probably the result of much smaller nuclei coalescing.

5.4. The nucleation of Hg on carbon

Using eqn. (5.3.5.) and the i vs. $t^{\frac{3}{2}}$ plots, values for the nucleation constant A were calculated. A typical value for A was 3.5×10^4 sec^{-1} at -30mV (Ag/Ag^+). It was shown in Chapter 1, section 4 that for the nucleation of hemispheres,

$$A = K k_o \exp\left\{\frac{-N[2\sigma_1 + (\sigma_2 - \sigma_3)]^3 M^2 \pi}{R T \rho^2 F^2 n^2 \eta^2 3}\right\} \qquad (5.4.1.)$$

where σ_1, σ_2, σ_3 are the surface energy terms for the nucleus-solution, nucleus-electrode, and electrode-solution respectively. Thus a plot of $\log_{10} A$ vs. $1/\eta^2$ should give a straight line, from whence an estimate of the surface energy interactions may be made. A straight line was only in fact obtained for such a plot when E^o (Hg/Hg_2^{2+}) was taken as +70mV (Ag/Ag^+); this is even more anodic than

the potential required for zero current in section 5.2 using the mercury electrode (i.e. +35mV). With such an arbitrary adjustment, the parameters obtained from such a plot cannot be regarded as too significant. A value for $\left[2\sigma_1 + (\sigma_2 - \sigma_3)\right]$ of ca. 260 erg.cm^{-2} is predicted.

5.5. Significance of Hg results for Ag,Pd models

The results obtained for mercury deposition on carbon in so far as they predict different time dependencies than for silver and palladium, which can be interpreted in terms of growth dominated by diffusion in solution owing to the absence of a lattice incorporation step; reinforce the idea that the silver $i \propto t$ dependence, and palladium $i \propto t^2$ dependence (under seeded conditions) are due to kinetic control and consequences of these metals having crystal structures.

The results also show that the proposal of section 3.6(d), chapter 3, that the growth of silver may be due to progressive nucleation inside a constant diffusion flux must be incorrect, as did the palladium results, as a different dependence than $i \propto t$ is found for mercury.

Chapter 6

The Formation of Metal Layers

6.1. Introduction

Schmidt and Gygax[118-121] have recently reported phenomena observed under potential sweep conditions when one reduces various metallic cations at inert metal electrodes. They used a chamber-type cell in which the volume of solution from which the metallic cations diffused to the electrode surface was contained inside a cylinder with insulating polyvinyl chloride walls and whose length (essentially the diffusion thickness δ) could be controlled by a piston of polyvinyl chloride containing a capillary for electrical connection to the main solution in which was placed the reference and subsidiary electrodes. δ could be adjusted within the limits $0 < \delta <$ 0.2mm; they could thus control the rate of cation diffusion in their experiments.

They used various combinations of depositing metal and metal substrates i.e. bismuth onto silver; lead onto silver and copper; tin onto bismuth; thallium onto gold, silver, copper and tin; and cadmium onto bismuth, lead and tin. They obtained either two or one current/voltage 'peaks' under potential sweep conditions according to the system

chosen. Measurements reported in a later section will confirm these results. Interpretation of the results was in terms of adsorption of metal governed by Langmuir isotherms.

They solved the diffusion equation (Fick's second law)

$$\partial C/\partial t = D\,\partial^2 C/\partial x^2 \qquad (6.1.1.),$$

where C represents the concentration of the metallic cations in the solution, with the boundary conditions relevant to their experiments,

$$\text{i.e.} \quad \left.\begin{aligned} C &= C^* \quad , \quad t = 0 \\ \partial C/\partial x &= 0 \quad , \quad x \to \delta \\ (\partial C/\partial x)_{0,t} &= i/nFAD \end{aligned}\right\} \qquad (6.1.2.)$$

The second boundary condition in (6.1.2.) follows from the fact that the piston face is completely insulating. Schmidt and Gygax were then able to derive the expression for current in terms of the surface concentration, y of deposited metal, and its activity a,

$$i(y) = nFA\frac{dy}{dt} = \frac{n^2F^2Aw}{RT}\left[(C^*\delta - y)^{-1} + d\ln a/dy\right]^{-1} \qquad (6.1.3.),$$

where w is the sweep rate. Sweep rates of between 1.67 and 3.34mV/sec were used by Schmidt and Gygax. From eqn. (6.1.3.)

the first derivative of i against y, $^{di}/dy$, follows,

$$\left(di/dy\right) \propto \left(C^{*}\delta - y\right)^{-2} + d^{2}\ln a/dy^{2} \qquad (6.1.4.)$$

The derivative will be zero for a maximum of the i/y and hence current/voltage plot. Schmidt and Gygax then presented the Langmuir isotherms for low coverage,

$$a \propto y \qquad (6.1.5.)$$

and the full isotherm

$$a \propto y/y_{a=1} - y \qquad (6.1.6.)$$

and obtained the points of intersection for the derivative $d^{2}\ln a/dy^{2}$ vs. y for these isotherms with the hyperbola $f(y) = -(C^{*}\delta - y)^{-2}$; such points corresponding to the current/voltage maxima.

The linearized isotherm (6.1.5.) implies $d^{2}\ln a/dy^{2}$ continuously falls with increasing y and there is but one point of intersection for the derivative with $f(y)$, which is a continuously rising function over the same y range. Hence such a simple isotherm predicts one current/voltage peak. Conversely, $d^{2}\ln a/dy^{2}$ for the full isotherm (eqn. 6.1.6.) shows a minimum and a maximum for the same y range and produces three points of intersection with the function. This predicts two maxima and a minimum in the

current/voltage profile. Thus the full isotherm predicts two current/voltage peaks. From the positions of the points of intersection on the y axis for this isotherm, Schmidt and Gygax argue that the first peak corresponds to adsorption of a partial monolayer and at the second peak a full monolayer is formed. Such a double-peaked current/voltage profile has also been explained by Hale and Greef[122] in terms of adsorption processes, with the particular case of hydrogen atom adsorption on noble metals in mind. They rejected the earlier restricted approach of Srinivasan and Gileadi,[123] who employed Langmuir isotherms i.e. they considered the energy of activation for the electrode reaction to be independent of coverage. They regarded this situation to be unlikely in view of mutual interaction among adsorbed species, and the fact that there must be sites of widely differing electrochemical activity on solid electrode surfaces. Hale and Greef derived the shape of the 'pseudocapacitance curves' (essentially the same as the current-voltage plot under sweep conditions; they defined pseudocapacitance C_a as $^{i}/(dV/_{dt})$, which is also identical to $q(d\theta/dV)$, where q is the charge density at unit coverage and θ is the fractional coverage) using no restriction upon the dependence of activation energy with surface coverage.

They introduced an arbitrary function $g(\theta)$ into the activation energy expression for the electrode process and showed by noting the stationary values of the subsequently derived C/V functions, that some coefficient of a θ term of order greater than or equal to three should be non-zero in order that multiple-peak behaviour could be observed, with $g(\theta)$ expressed as a polynomial in integral θ powers. This necessitated invocation of higher order interactions than first order or 'Temkin'-type interactions. Hale and Greef suggested that it would be more likely that the non-uniformity of electrode surface would be responsible for the shape of the double-peaked curves. Following a proposal of Breiter,[124] they argued that if there were two independently adsorbing 'Langmuir' sites sharing the total surface area with such different properties that the standard electrode reaction rate constants differ markedly on both sides, then two peaks could be expected.

There is considerable evidence that whenever new phases are formed, one must expect nucleation and growth to take some part. Evidence from the field of anodic film formation (e.g. the formation of calomel[125] on mercury; of thallous chloride on tallium amalgam,[126] the anodic oxidation of silver sulphate to silver oxide,[127] the deposition of lead

dioxide on platinum[107] etc.), and also from metal deposition studies (e.g. the deposition of nickel on mercury,[81] the deposition of silver, palladium and mercury on carbon (this thesis)) gives strong indication that the nucleation and subsequent growth of centres of the new phase are nearly always the predominant processes involved in the formation of the anodic film or metal deposit. Such crystallisation processes, therefore, must be involved in the phenomena observed by Schmidt and Gygax. The technique used by these authors (potential-sweep) could not identify crystal growth behaviour as such. The potentiostatic pulse method is really the only method which can be used in order to observe such behaviour. Measurements will be reported in which both the potential sweep and pulse techniques are used in an attempt to clarify the processes involved in the deposition of metal onto inert metal substrates in the case of three of the combinations studied by Schmidt and Gygax; i.e. lead onto silver, thallium onto silver and cadmium onto lead.

6.2. <u>The potential-sweep measurements</u>

Stereoscan and electron micrographs of the electro-polished polycrystalline silver and lead electrode surfaces respectively are shown in Figs. 42 and 43. The effect of applying a triangular potential wave-form from a suitable

initial potential, anodic to the reversible potential for the cation involved, for the deposition of lead onto silver from a chloride solution is shown in Fig.44. The formation of two peaks is a characteristic feature of this system. The anodic removal peaks are shifted a matter of ca. 90mV more anodic than the formation peaks. It is found that the charge under the first peak for a polycrystalline silver substrate decreases with increasing sweep rate but is of the order one would expect for a two-dimensional monolayer of Pb (ca. 280μ C.cm^{-2}). In the case of the single silver crystal substrate this charge is quite constant up to a sweep rate of 3V/sec and is ca. 370μ C.cm^{-2}. This fact is illustrated in Table 2 which shows charges under both peaks and their peak positions for the deposition of lead onto the silver single crystal, from a 3 x 10^{-3}M $PbCl_2$/1M KCl solution.

Table 2

Charges under and Positions of Peaks for Pb onto Ag (single crystal, 111 face)

Sweep rate	Position (Ag/AgCl)		Charge (μC. cm^{-2})	
(V/sec)	First	Second	First	Second
0.1	-480mV	-560mV	385	3,500
0.3	-460mV	-530mV	362	1,500
1	-460mV	-550mV	378	740
3	-480mV	-580mV	350	560
10	-490mV	-580mV	280	520

fig 44 0·003M $PbCl_2$ / 1M KCl. single Ag crystal (111 face, electropolished). sweep rate 3V/sec. E wrt. Ag/AgCl.

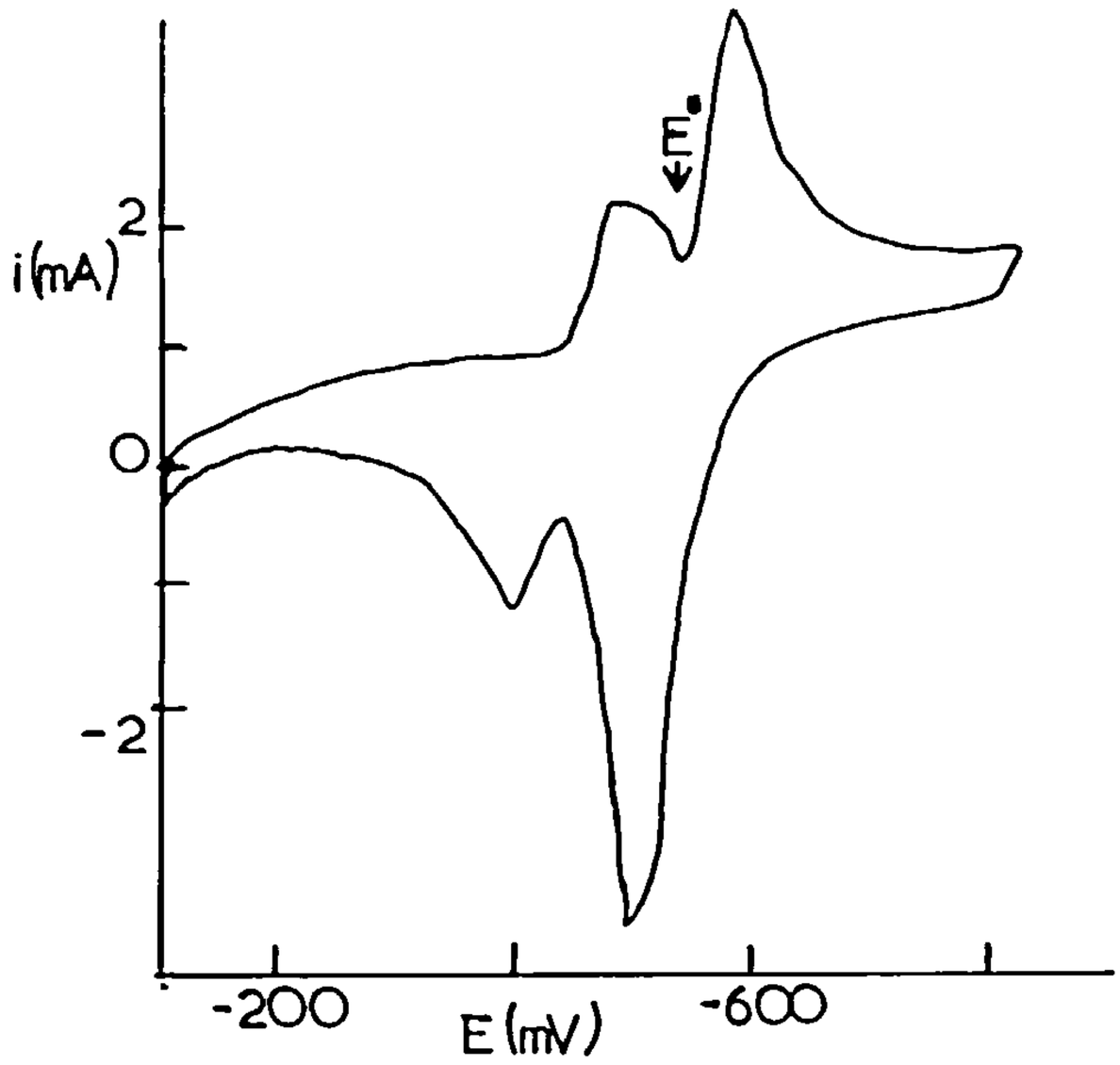

fig 45 0·03M $Pb(OAc)_2$ / 1M NaOAc / 0·1M AcOH. dpd., polyc., Ag. sweep rate 300 mV/sec. E w.r.t. Ag/AgCl.

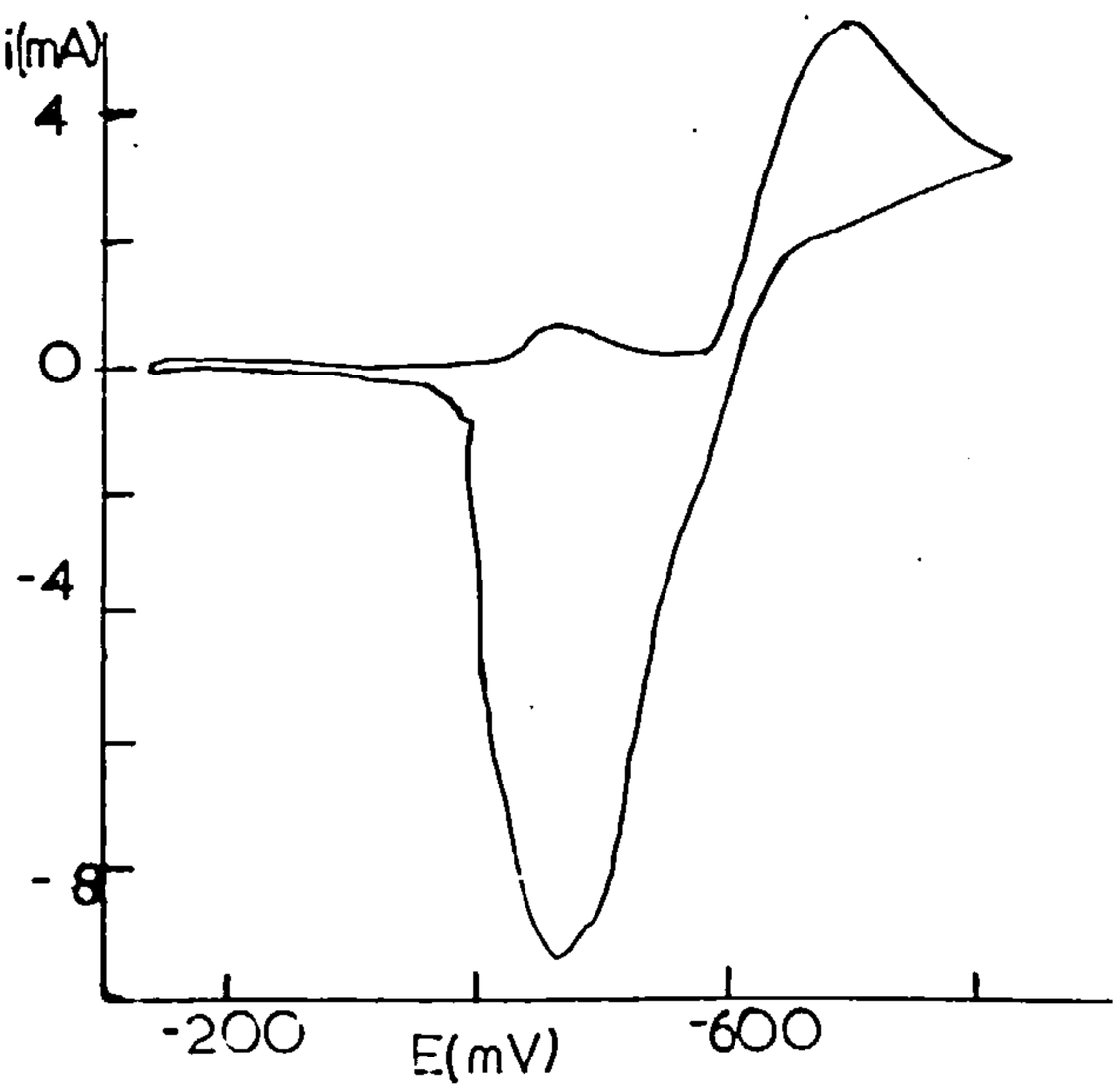

The charge under the second peak is a few times larger than under the first peak, clearly corresponding to multi-layer formation. The effect of using an acetate electrolyte in place of chloride (Fig.45), is to decrease the magnitude of the peak currents, though the charge under the peaks seems little affected. The formation of two peaks is thus a function of the depolarising ion and not the anion medium in which the reduction is conducted. If crystal growth processes are involved in the formation of two peaks for the deposition of metal onto solid metal inert electrodes, they cannot be controlling in the case of reduction of metal cations at mercury electrodes, for metals which are soluble in mercury. In such a case only one peak could be expected under sweep conditions and this has been reported[128] for the reduction of Pb^{2+} at Hg (and for Tl^{+} on Hg) which result was confirmed using a 10^{-1}M lead acetate solution (Fig.46), the mercury drop area was ca. 0.1 cm^2. Such sweep profiles show an abrupt fall of current from the rising current/voltage dependence at ca. -950mV (Ag/AgCl). There is a similar sharp rise of current on the anodic going cycle at ca. -600mV. An apparent explanation for these phenomena is that a passivating film of some description is formed at -950mV on the mercury surface, which is removed at the anodic potential.

fig 46 O·1M $Pb(OAc)_2$ / 1M NaOAc / O·1M AcOH. Hg electrodes. sweep rate 100 mV / sec. E w.r.t. Ag/AgCl.

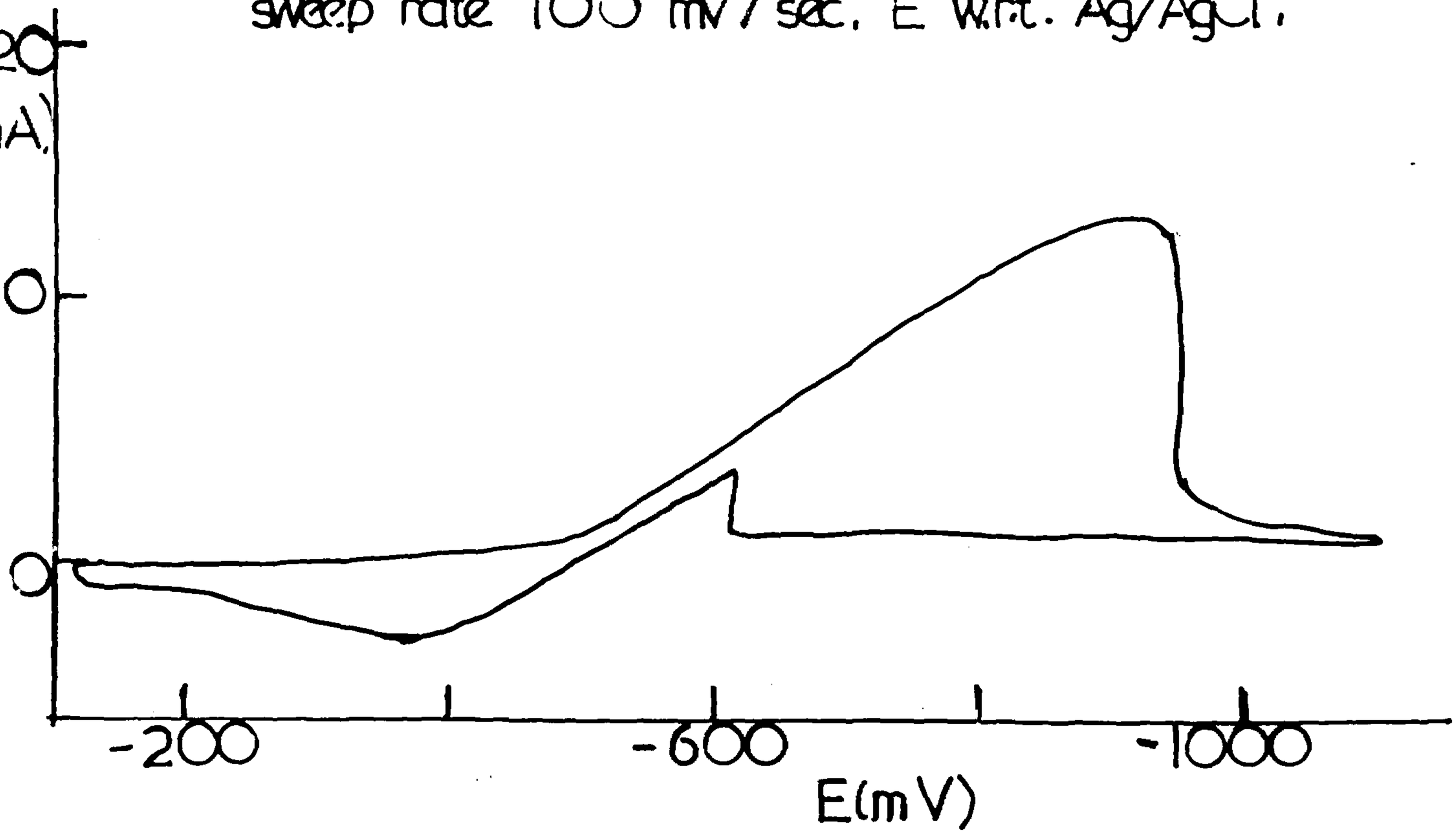

A possible film would be one due to hydrogen adsorption formed at -950mV, stabilized by some form of interaction with the lead-amalgam. This could be re-oxidised at ca. -600mV and the predominating Pb^{2+} reduction process possible at this potential would give rise to a cathodic current as found. The current would then fall to anodic values with increasing anodic potentials as the lead is redissolved into solution as Pb^{2+}.

A second system in which two peaks are observed under sweep conditions for the deposition of metal onto inert metal substrate is that for the reduction Tl^{+} on silver (Fig.47). The charge under the first peak is again equivalent to that due to a two-dimensional monolayer (ca. 200μ $C.cm^{-2}$), the second peak being the multilayer formation with charge a factor four larger. A system which gives rise to only one peak under potential sweep is that of cadmium onto lead (Fig.48). The charge under this peak is equivalent to about ten to thirty two-dimensional monolayers.

The thermodynamic reversible potentials for the systems are marked on graphs as E^{o}. The value for the Pb/Ag case was measured for the bulk lead electrode in the same solution as used for deposition. The values for $Tl_{(s)}/TlCl$ and $Cd^{2+}/Cd_{(s)}$ were obtained from the literature.[116]

fig 47 0·0000875 M TlCl / 1M KCl. electropolished, polycrystalline Ag. sweep rate 300 mV/sec. E w.r.t. Ag/AgCl.

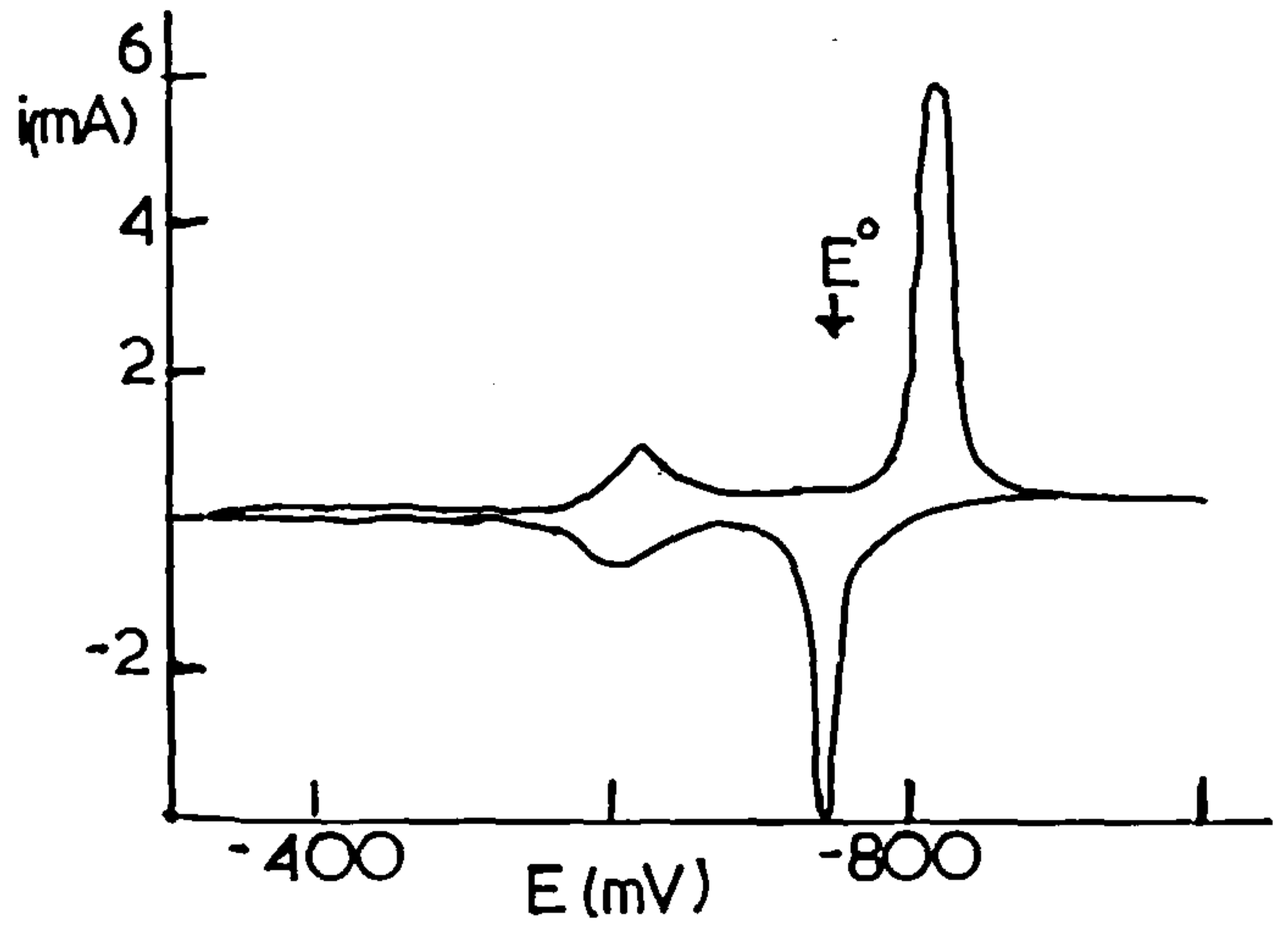

fig 48 0·0083 M $Cd(ClO_4)_2$ / 1M $NaClO_4$. elpd., polyc., Pb electrode. sweep rate 30 mV/sec. E w.r.t. Ag/AgCl.

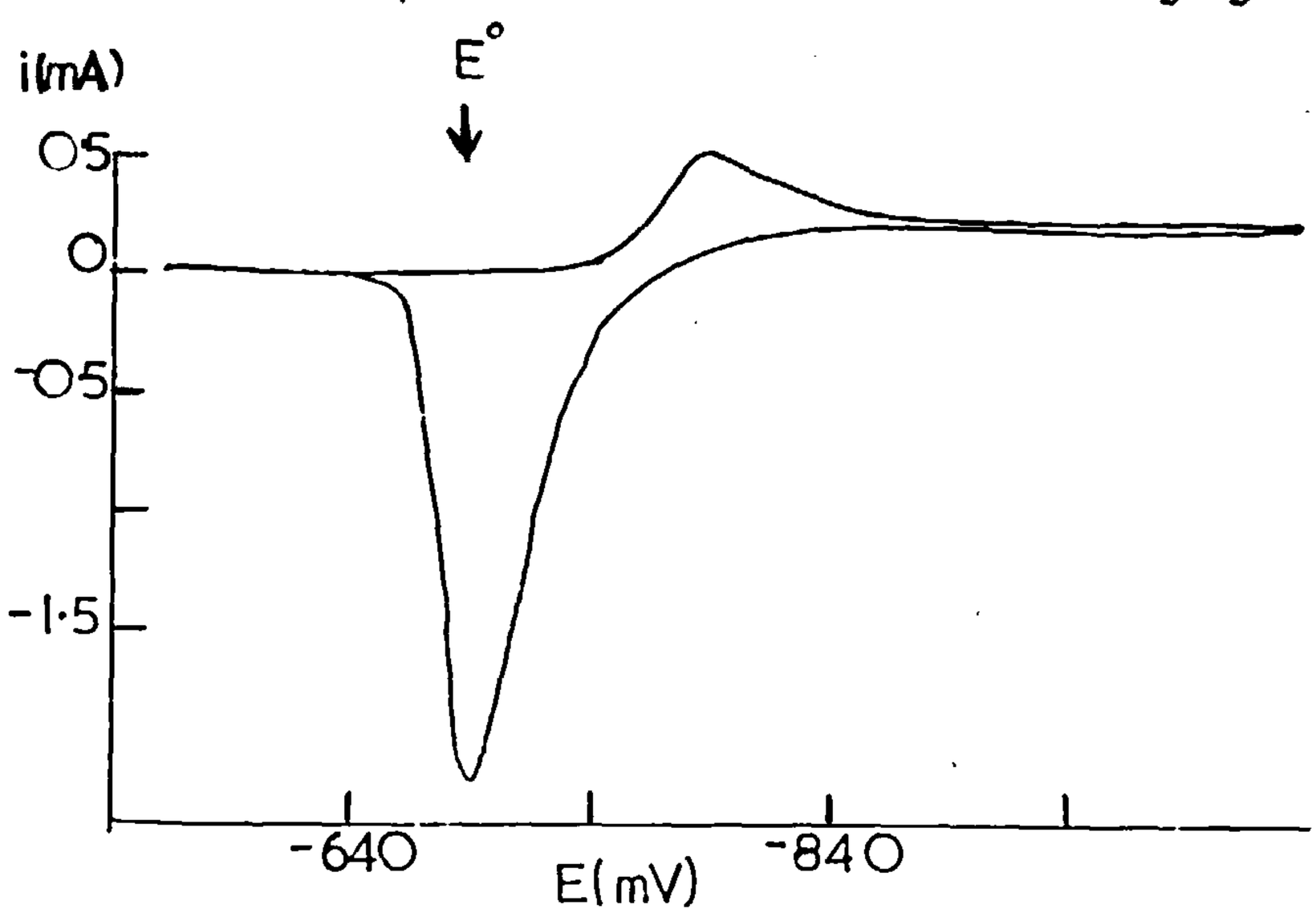

The monolayer peaks form anodic to E^o. There is evidence in the electrochemical formation of mercury salts that the reversible potential of a monolayer occurs cathodic to the thermodynamic reversible potential for the bulk salt. For example, in the formation of Hg_2HPO_4 the first monolayer occurs approximately 40mV cathodic to the thermodynamic reversible potential.[129] It would seem likely that when a metal is deposited on an inert substrate a similar effect could occur and there is no reason to suppose that the first layer is the adsorption of discrete atoms rather than the formation of a crystalline phase.

The potential difference between the peaks is large, about 120mV for Pb/Ag and 200mV for Tl/Ag. It seems unlikely that these magnitudes could be explained in terms of adsorption isotherms.

The capacitative contribution to the currents observed under sweep conditions, which may be taken as the current necessary to charge and discharge the double-layer given by

$$i_c = A \times C_{dl} \times dV/dt \qquad (6.2.1.)$$

where C_{dl} is the double-layer capacity, was estimated by carrying out sweeps with the substrate electrodes in the supporting electrolytes alone. The currents observed were

at no time larger than ca. 5% of the currents in the presence of the depolarising metal ions. Figs. 49 and 50 show plots of C_{dl} vs. potential calculated from such sweep measurements using eqn. (6.2.1.) for 1M potassium chloride and 1M sodium acetate/0.1M acetic acid solutions using the polycrystalline silver electrode. The apparent decrease in C_{dl} with increasing sweep rate may be ascribed to the decrease in available area of electrode as the potential scan rate increases; the electrode area approaching the macroscopic value at fast sweeps. The observed maxima for these plots are difficult to explain. One would expect chloride ion adsorption on the Ag electrode to decrease negative to the Ag/AgCl potential. There is evidence for adsorption of the free halogen radical on silver[130] in halide electrolytes and reduction of this to the anion might justify the rising part of the C_{dl}/potential plot.

Berzins and Delahay[105] have obtained the solution to the diffusion equations with boundary conditions involved in the reversible deposition of an insoluble reductant with constant activity under sweep conditions. Their solution for ip (peak current, Amp) in terms of sweep rate (w) at 25°C is

$$i_p = 3.67 \times 10^5 \times n^{\frac{3}{2}} \times A \times C^* \times D^{\frac{1}{2}} \times \omega^{\frac{1}{2}} \qquad (6.2.2.)$$

fig 49 1M KCl ; electropolished, polycrystalline Ag · Capacity $\{C = i/(dV/dt)\}$ vs E.

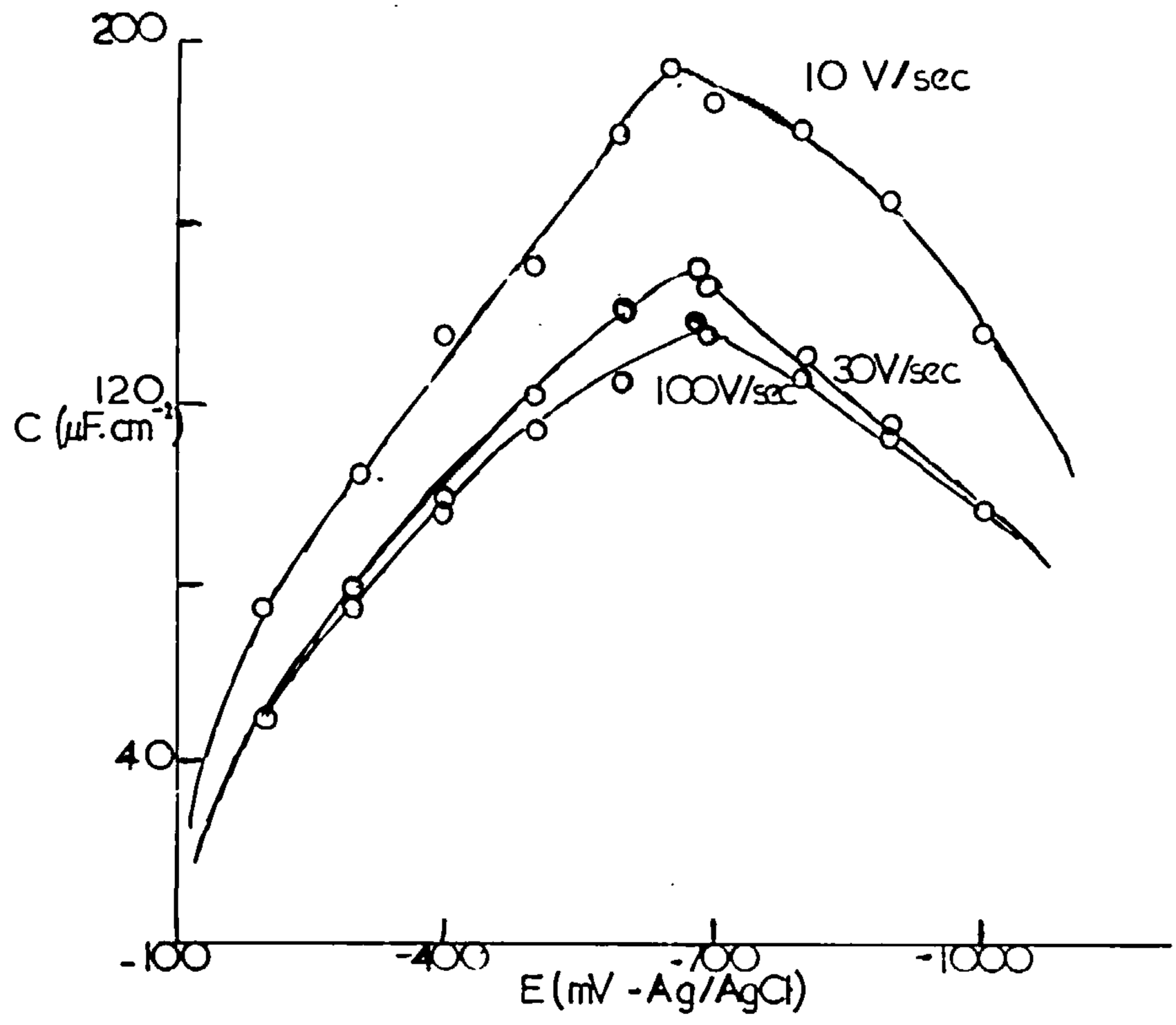

fig 50 1M NaOAc/0·1M Ac OH ; elpd. polyc. Ag . C vs E.

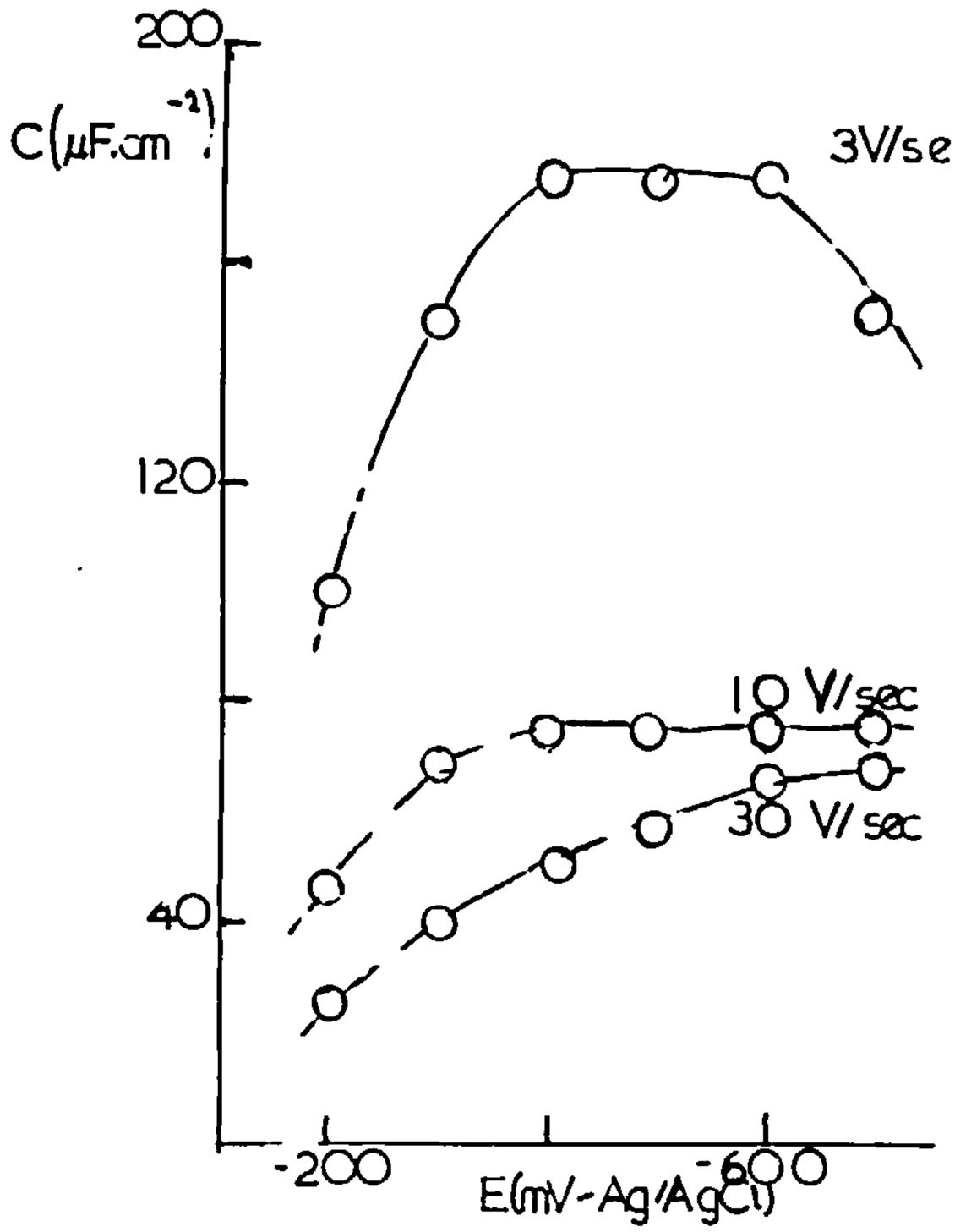

Hence plots of ip vs. $w^{\frac{1}{2}}$ are predicted linear. Figs. 51, 52 and 53 show such plots for Pb and Tl onto Ag, and Cd onto pb. In the case of Pb and Tl onto Ag, linearity is only achieved for such plots for the second peaks, but a higher dependence of ip on w is suggested for the first peaks. Assuming that the electrode processes involved may be considered reversible the only other major assumption of Berzins and Delahay's analysis with regard to these measurements is that the reductant (deposit) activity may be considered constant. The assumption is probably justified for the second peaks involved when a full monolayer of deposit has already formed. However in the case of the first peak, deposition starts at zero reductant activity. A mathematical analysis of the formation of a partial monolayer under sweep conditions with this initial condition is possible, but has not been attempted. The ip vs. $w^{\frac{1}{2}}$ plot for Cd onto Pb does not follow the pattern of the plots for the first Pb and Tl peaks, the profile falling down from linearity. In this case growth does not stop after the formation of one monolayer, a multilayer being formed and the peak current is essentially due to deposition on deposit of constant activity.

fig 51 $0.003M\ PbCl_2$ / 1M KCl. electropolished, polycrystalline Ag. ip vs $\omega^{\frac{1}{2}}$. (a) first peak (b) second peak.

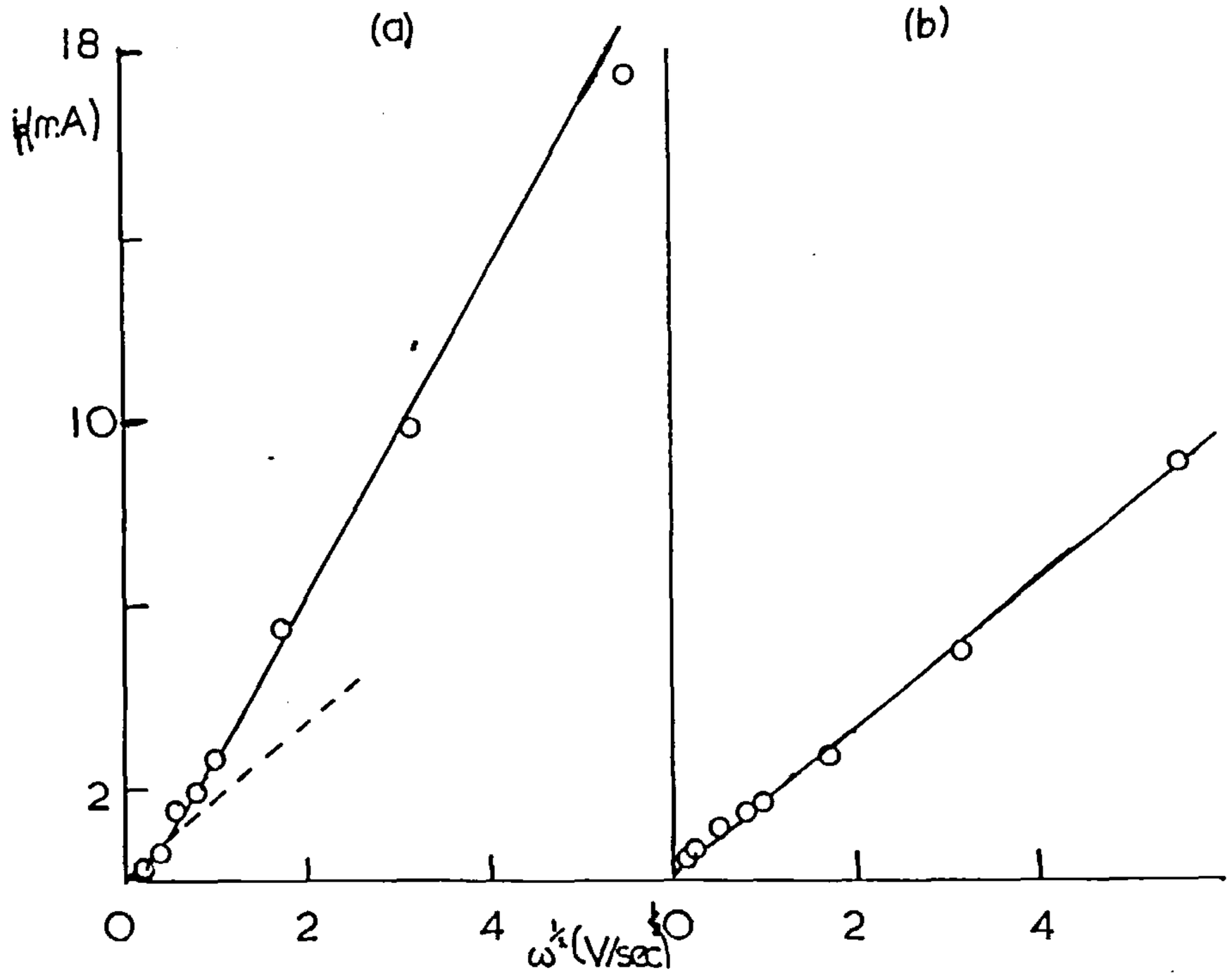

fig 52 0.000875M TlCl / 1M KCl. elpd, pdyc, Ag. ip vs $\omega^{\frac{1}{2}}$.
(a) first peak . (b) second peak.

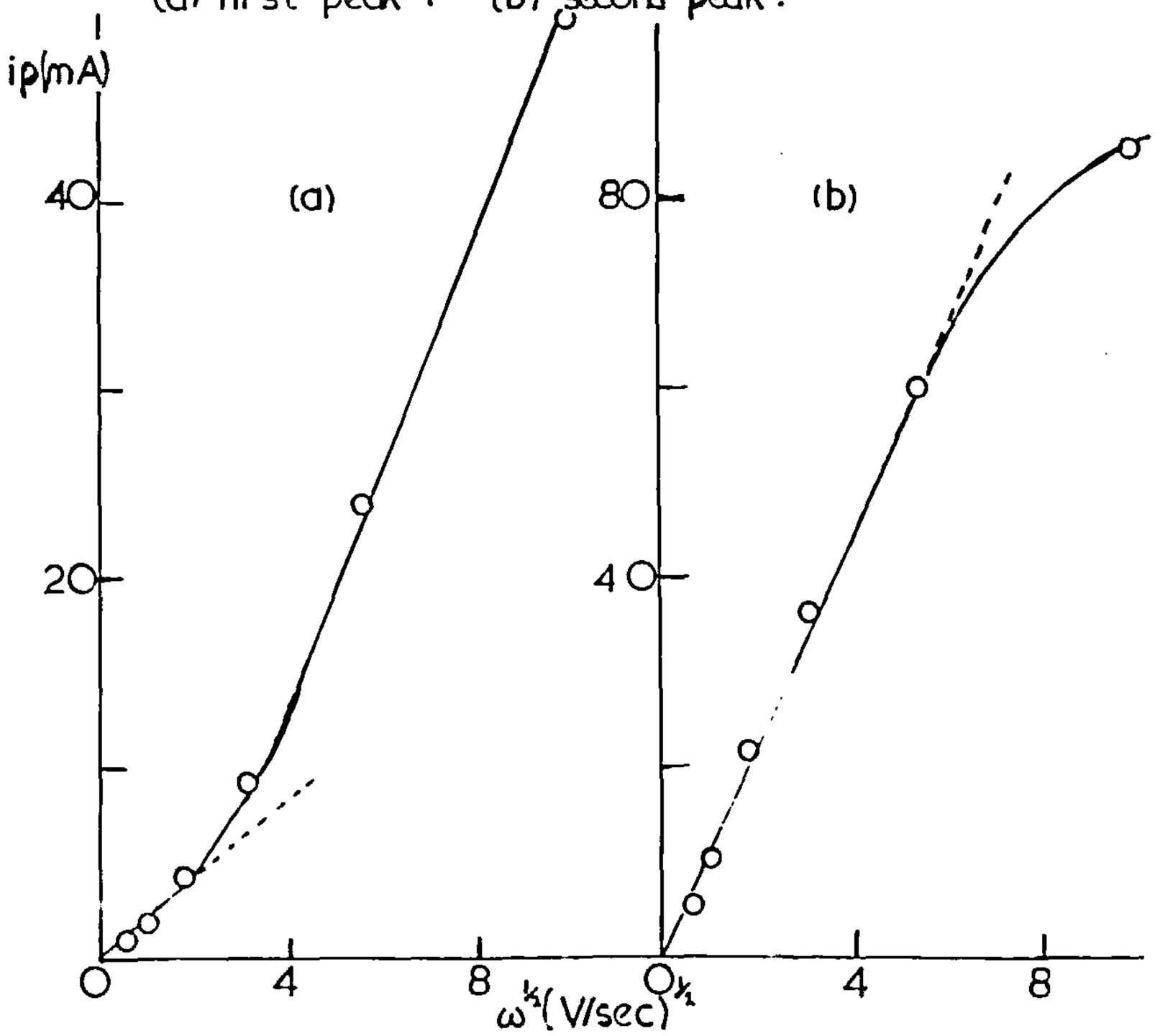

fig 53 0·0083M $Cd(ClO_4)_2$/1M $NaClO_4$ on electropolished Pb.ip vs $\omega^{1/2}$.

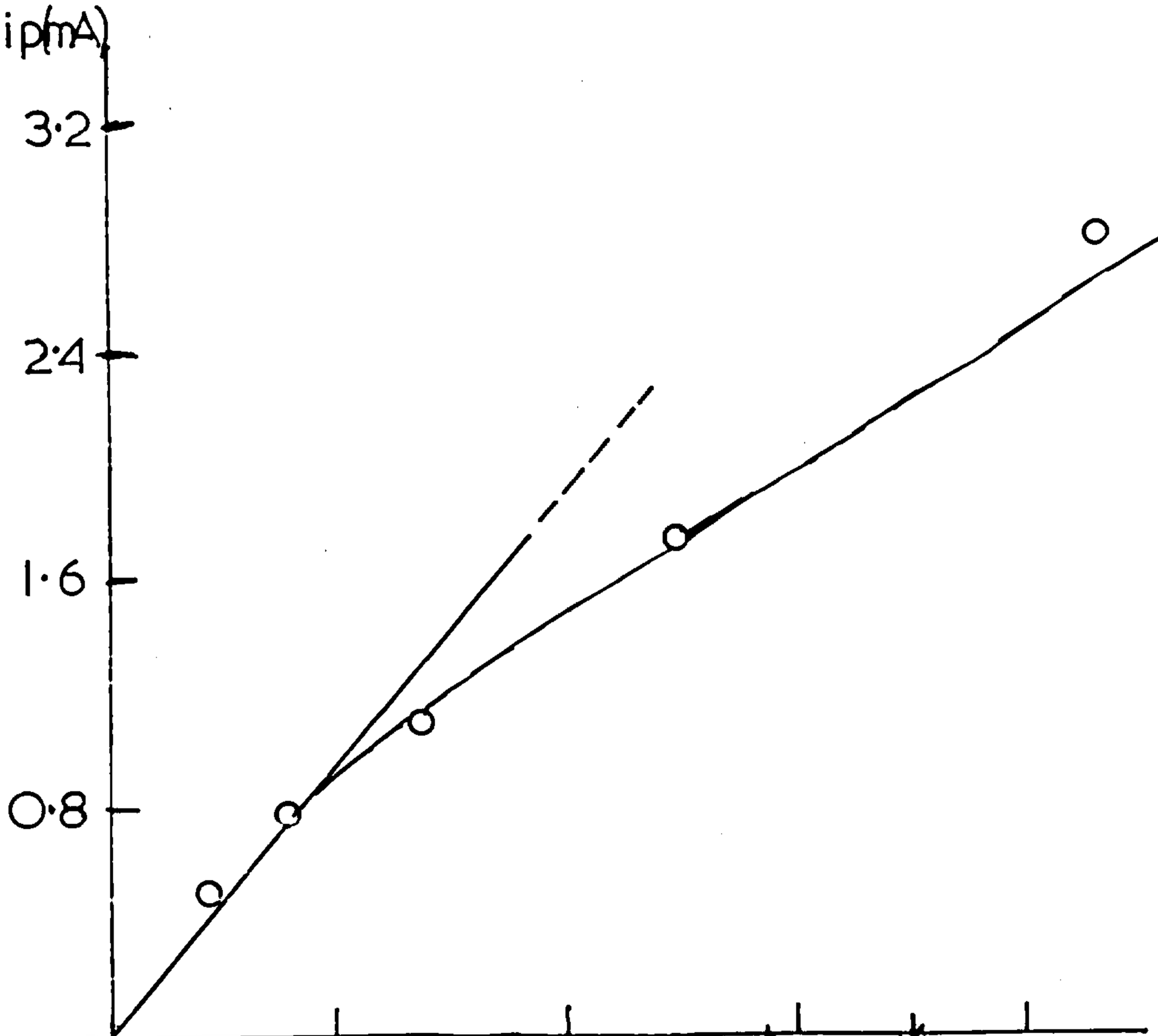

6.3. Potential-pulse measurements at short times

It might be suspected from the values of the charges under the peaks, representing either a monolayer or multilayer, that typical nucleation and growth processes are involved in these sweep regions. To test this, potentiostatic pulses were applied, starting from potentials well anodic to the reversible potential of the cation in solution and jumping to various positions within the sweep range. In this section measurements involving short time transients (up to 25 msec) will be described, and in the next section the identification of crystal growth transients (times up to ~3 minutes) will be presented.

The results of applying pulses at various potentials to the polycrystalline silver electrode for a 3×10^{-3}M $PbCl_2$ solution from an initial potential of -100mV (Ag/AgCl), are shown in Fig.54 as i vs. $t^{-1/2}$. The potentials extend through the monolayer and multilayer regions. Similar plots are shown in Figs. 55 and 56 for the deposition of Tl onto Ag (6×10^{-4}M TlCl; initial potential -100mV (Ag/AgCl)), and Cd onto Pb (8.3×10^{-3}M $Cd(ClO_4)_2$; initial potential -500mV (Ag/AgCl)). In the case of Pb and Tl deposition, the monolayer region curves are essentially diffusion controlled, but with two striking differences. The curves do not pass

fig 54 0·003M $PbCl_2$ / 1M KCl . electropolished, polycrystalline Ag. i vs $t^{-1/2}$.

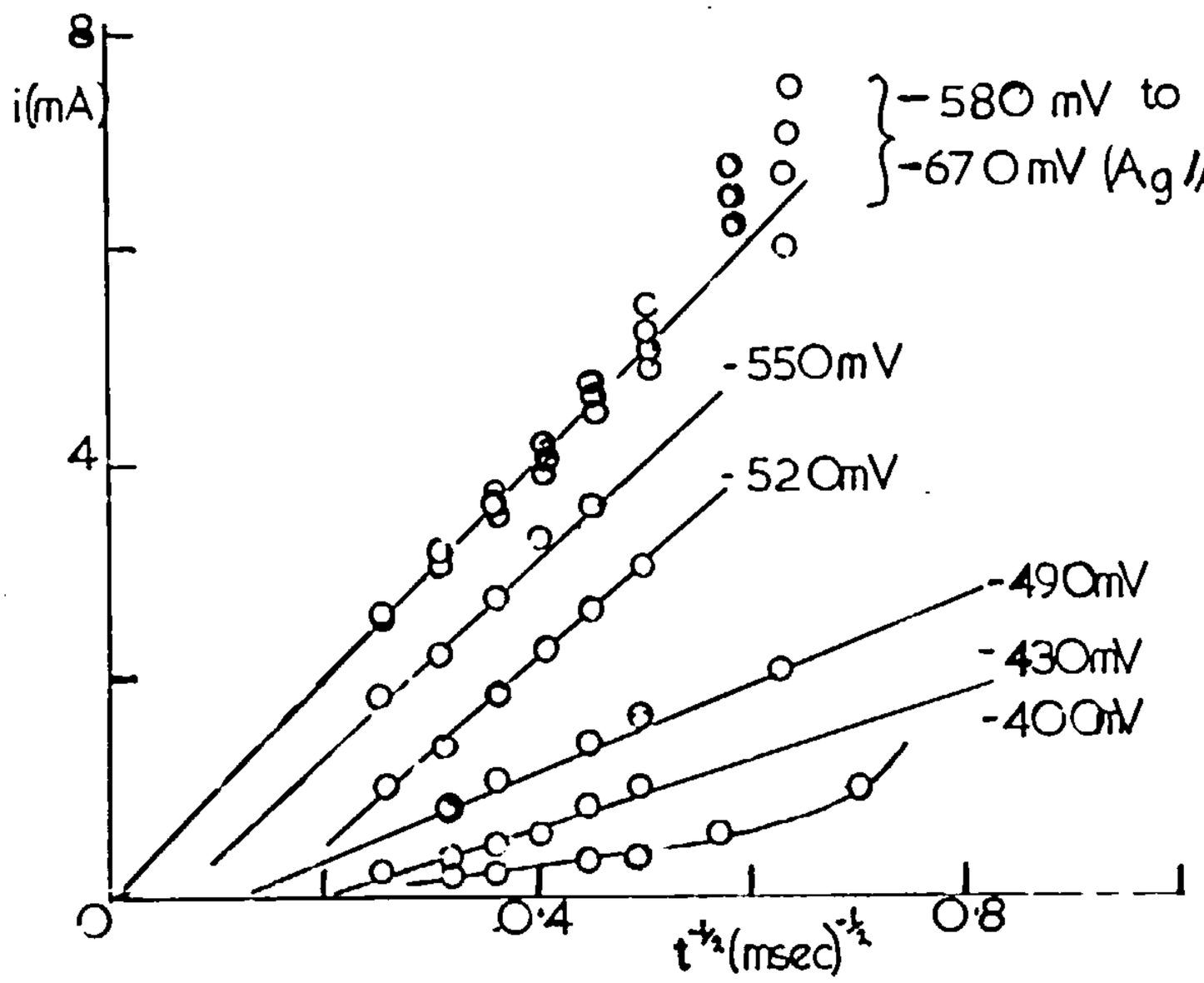

fig 55 0·0006M TlCl / 1M KCl . elpd., polyc. Ag. i vs $t^{-1/2}$.

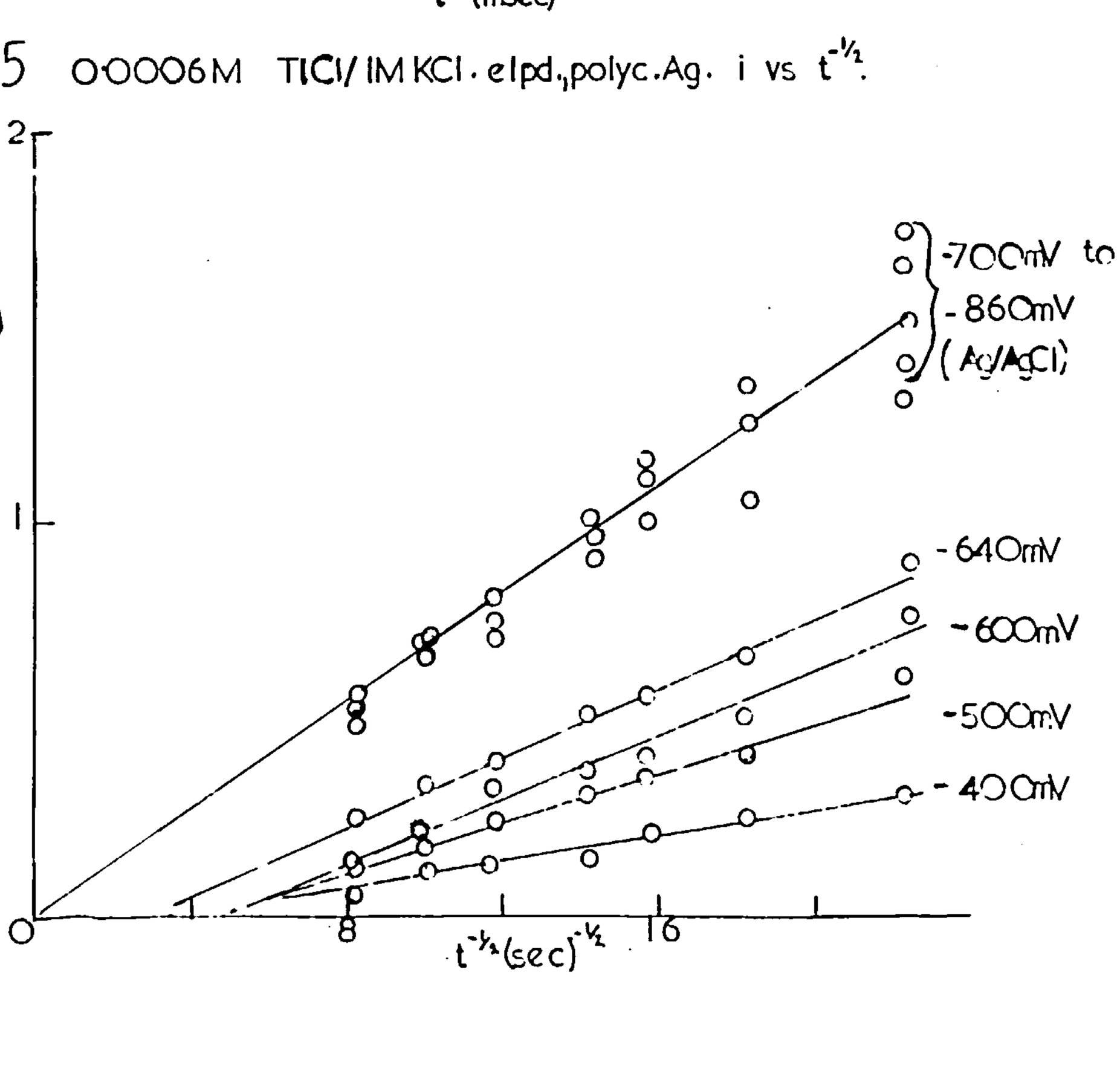

fig 56 0·0083 M $Cd(ClO_4)_2$/1M $NaClO_4$. electropolished Pb.
i vs $t^{-1/2}$. 1)-700mV; 2)-720mV; 3)-740mV; 4)-760 mV; 5)-800mV;
6)-850 mV. (Ag/AgCl).

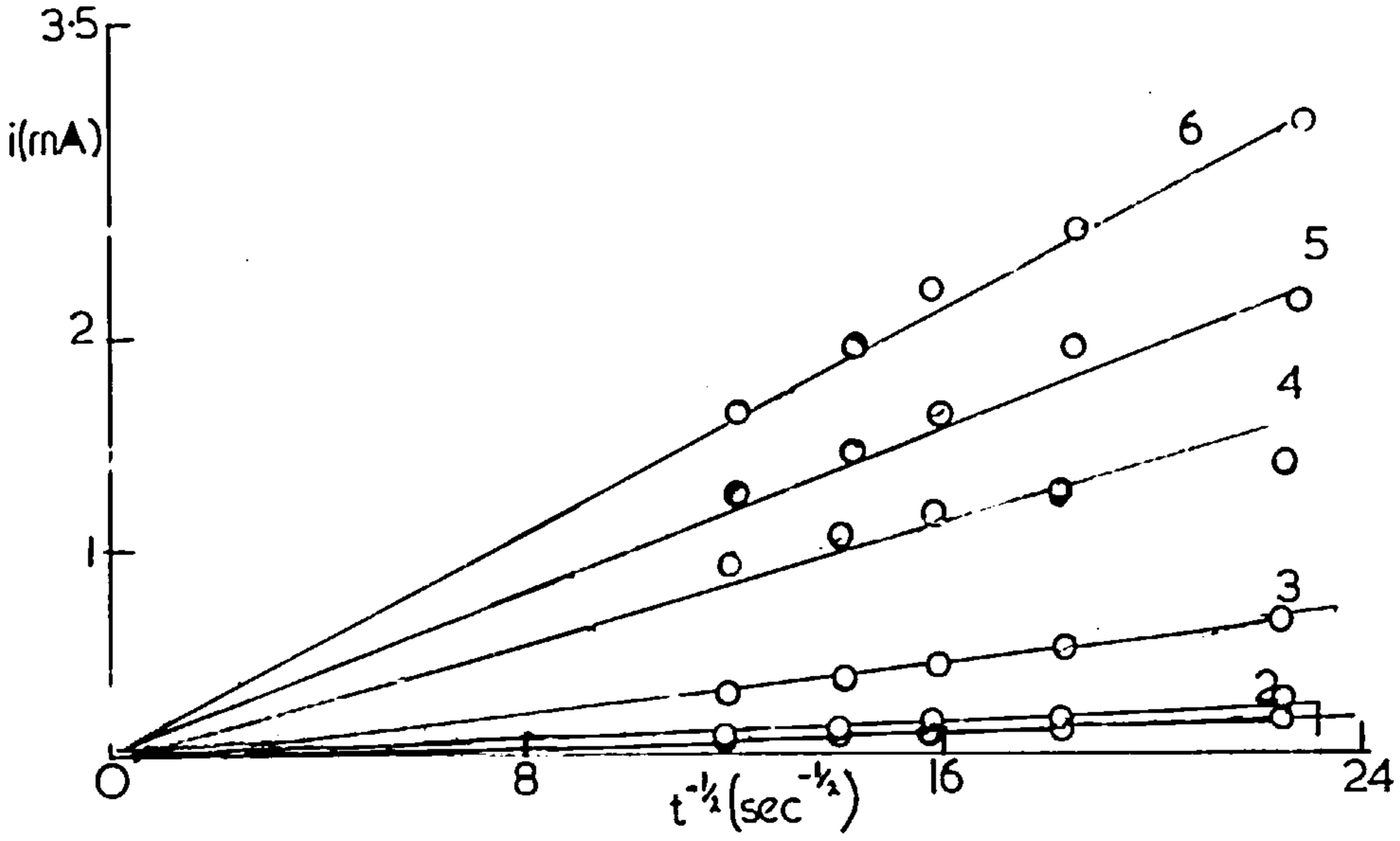

fig 66 As above. Unseeded growth transients. 1)-720 mV ; 2)-722mV;
3)-724 mV ; 4)-730 mV. (Ag/AgCl)

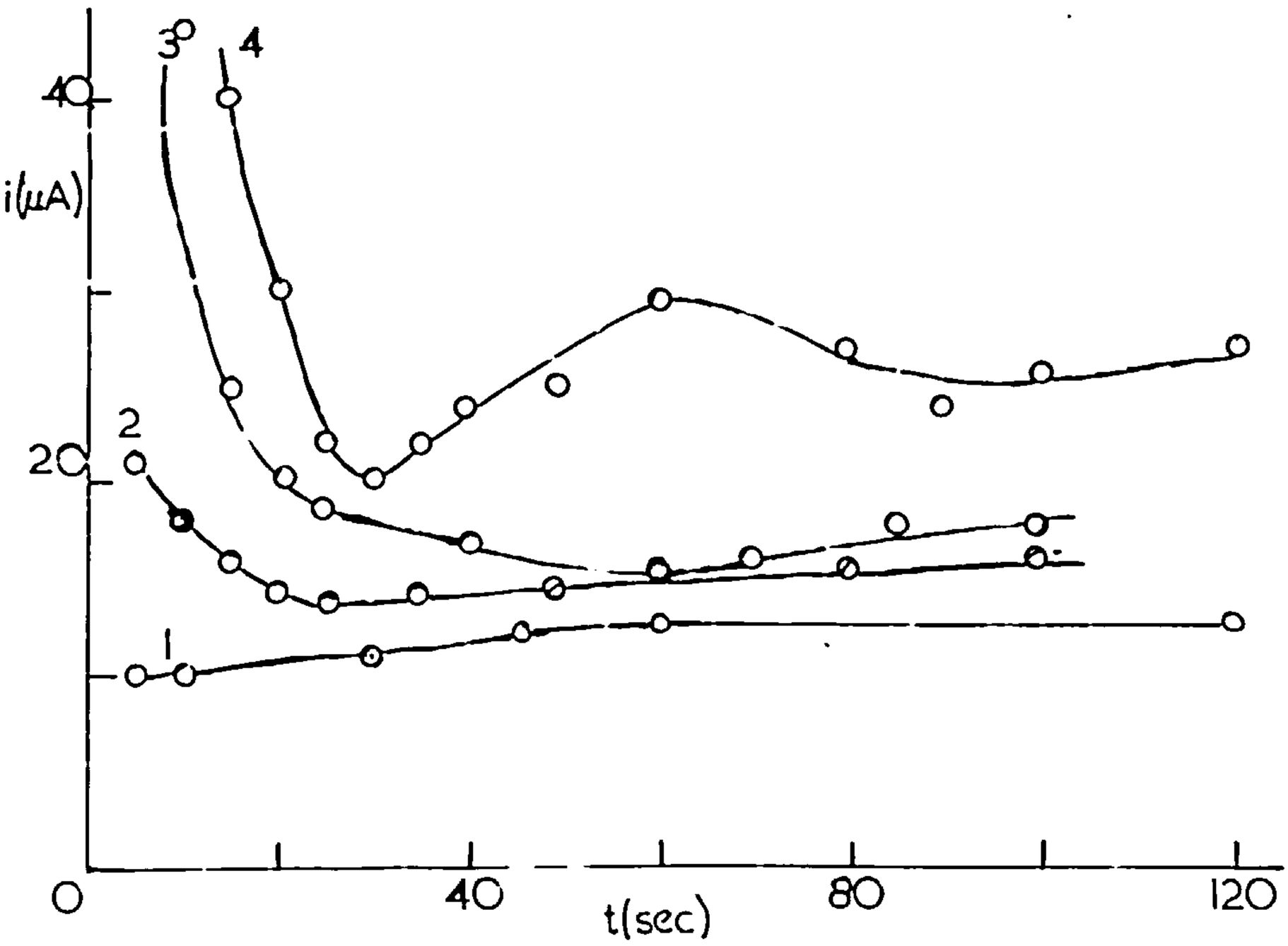

through the $i/t^{-1/2}$ origin but at $i = 0$, cut the $t^{-1/2}$ axis at finite times. At low overpotentials the plots show curvature. In order to explain this behaviour, a model of deposition of a partial monolayer is considered.

Appendix 2 contains an analysis for a model of reversible deposition of a partial monolayer under potentiostatic conditions. This predicts (eqn. A.2.1.7.), i.e.

$$i = nFAC^*\sqrt{\frac{D}{\pi t}} - \left[\left(nFA^2(C^*)^2 D/m\right)\left(\exp - nF\eta/RT\right)\right.$$

$$\left.\times \exp\left[\left\{(C^*)^2 D\left(\frac{A^2}{m^2}\right)\exp\left(-2nF\eta/RT\right)\right\}t\right] \times \operatorname{erfc}\left\{\left[C^* D^{\frac{1}{2}}\left(\frac{A}{m}\right)\exp\left(-nF\eta/RT\right)\right]\sqrt{t}\right\}\right] \quad (6.3.1.)$$

where m is the number of moles of deposit at monolayer coverage, and η is the overpotential defined with respect to normal thermodynamic equilibrium. The form of the transients predicted by eqn. 6.3.1. is shown in Fig.57 for four potentials up to the diffusion limited current with the conditions: $n = 2$, $C^* = 3 \times 10^{-3}$M, $A = 0.28$ cm^2 and $m = 1.9 \times 10^{-10}$ moles. The form of the i vs. $t^{-1/2}$ plots predicted for these parameters (corresponding to some Pb onto Ag measurements) is shown in Fig.58. Totally diffusion controlled currents are much more rapidly achieved by this equation for increasing cathodic overpotentials than those reached for the deposition of Pb onto Ag. (Fig.54). Nevertheless

fig 57 Transients predicted for reversible formation of ½ partial monolayer. $n = 2e^-$; $C^* = 3 \times 10^{-3} M$; $A = 0{\cdot}28 cm^2$; $ms = \underline{1{\cdot}9} \times 10^{-10}$ moles.

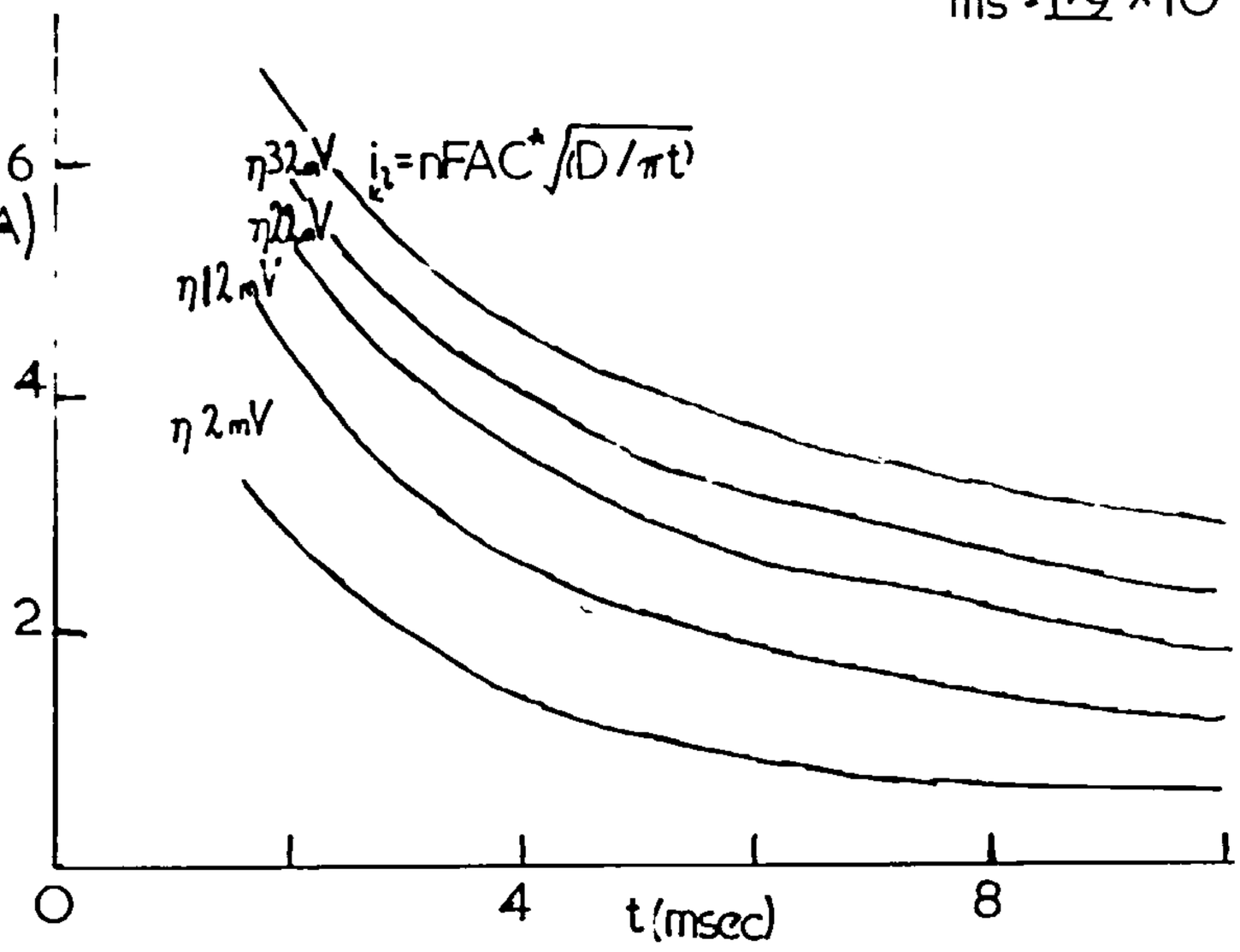

fig 58 i vs $t^{-½}$ predicted as above.

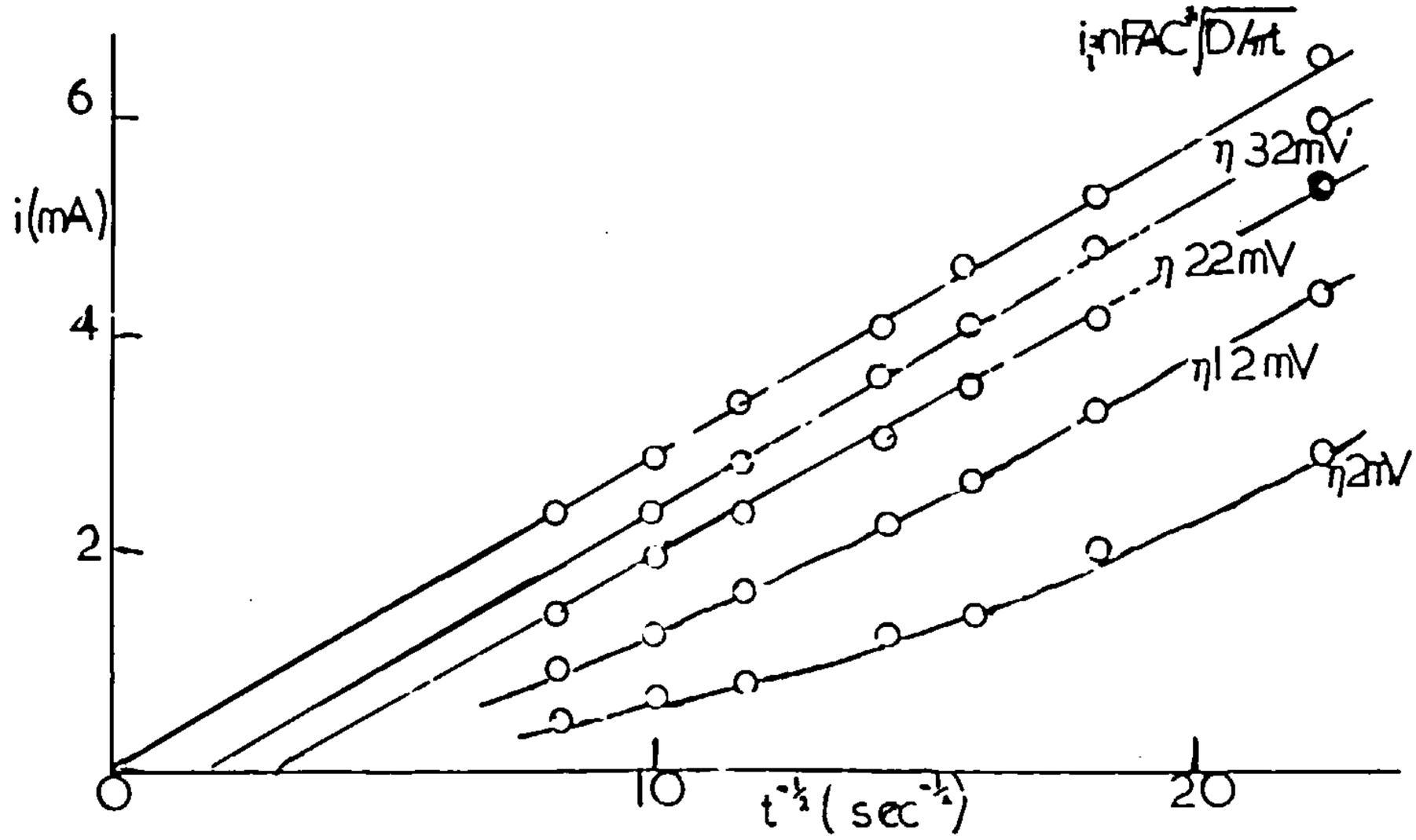

the curves reproduce qualitatively the characteristics of the experimental curves. The theoretical plots are curved at low overpotentials and intersect the $t^{-1/2}$ axis. The parameter which can be varied in eqn. (6.3.1.) is m. The value of m chosen in calculating Figs. 57 and 58 is the one expected for a two-dimensional plane of lead atoms packed as the basal plane of the close packed cubic lattice. Figs. 59 and 60 show plots of i vs. $t^{-1/2}$ predicted for the same conditions as Fig.58 save that in Fig.59, m is a factor 2 down i.e. 0.95×10^{-10} moles and in Fig.60, m is two times larger i.e. 3.8×10^{-10} moles. Clearly when m is decreased the overpotential required to approximate the currents to the diffusion limited value goes up (to ca. 50mV for 0.95×10^{-10} moles); and conversely when m is increased it decreases (to ca. 30mV for 3.8×10^{-10} moles).

There is some evidence in the case of thallium deposition that reaction control may be involved in the electrode process. Fig. 61 and Fig.62 show plots of i vs. $t^{-1/2}$ and i vs. $t^{+1/2}$ respectively for the deposition of Tl onto Ag from a 8.75×10^{-4}M TlCl solution. The i vs. $t^{-1/2}$ curve off appreciably from linear dependence at lower times for some potentials, and indeed these potentials (e.g. -670mV, -700mV (Ag/AgCl)) show a linear i vs. $t^{+1/2}$ dependence.

fig 59 i vs $t^{-\frac{1}{2}}$ predicted for reversible formation of partial monolayer. $n=2e^-$; $C^*=3\times10^{-3}M$; $A=0{\cdot}28\ cm^2$; $ms=\underline{0{\cdot}95}\times10^{-10}$ moles.

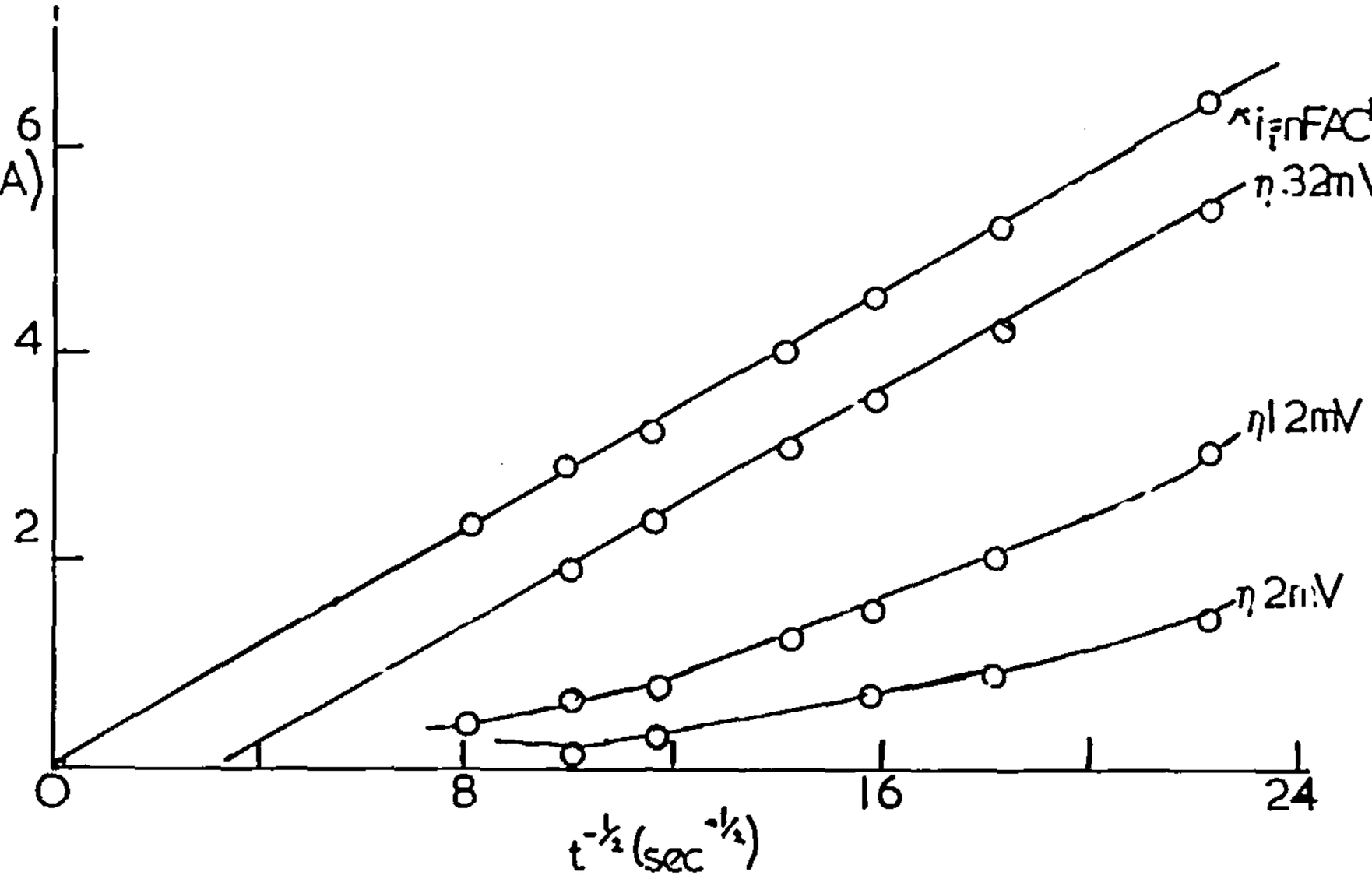

fig 60 i vs $t^{-\frac{1}{2}}$ predicted as above, with $ms=\underline{3{\cdot}8}\times10^{-10}$ moles.

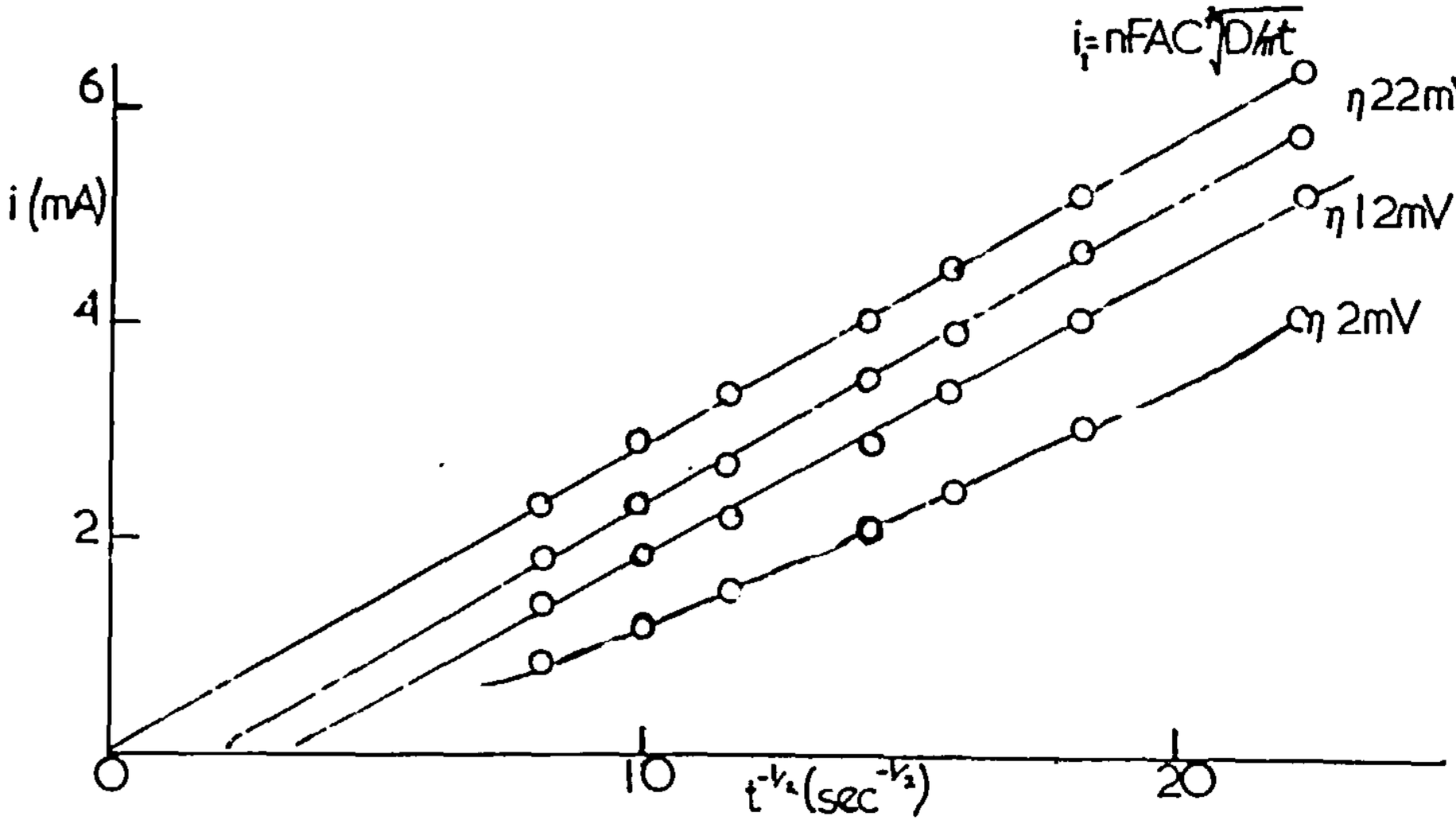

fig 61 0·000875 M TlCl / 1M KCl on elpd-polyc. Ag · i vs $t^{-1/2}$.

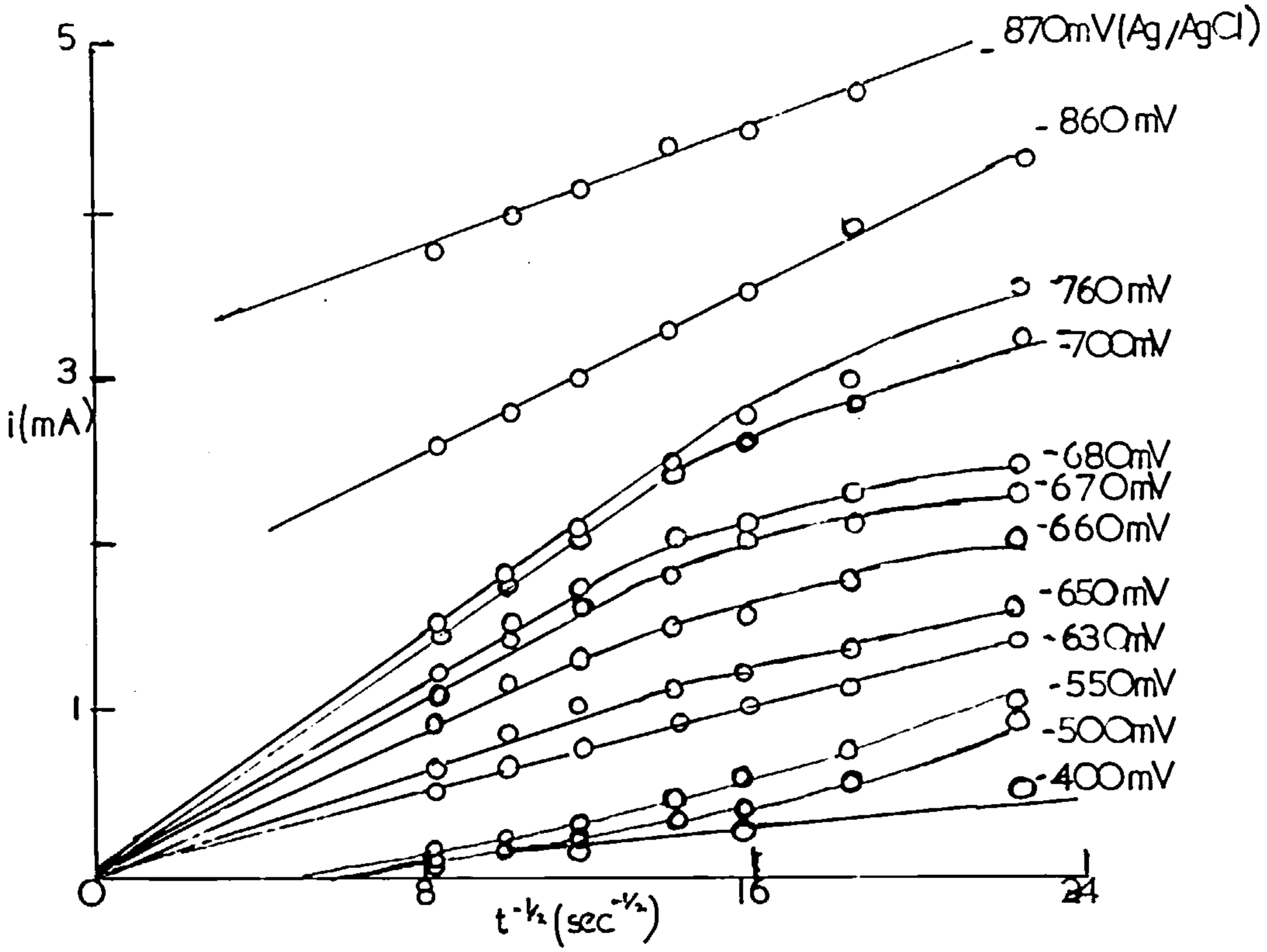

fig 62 As above. i vs $t^{+1/2}$

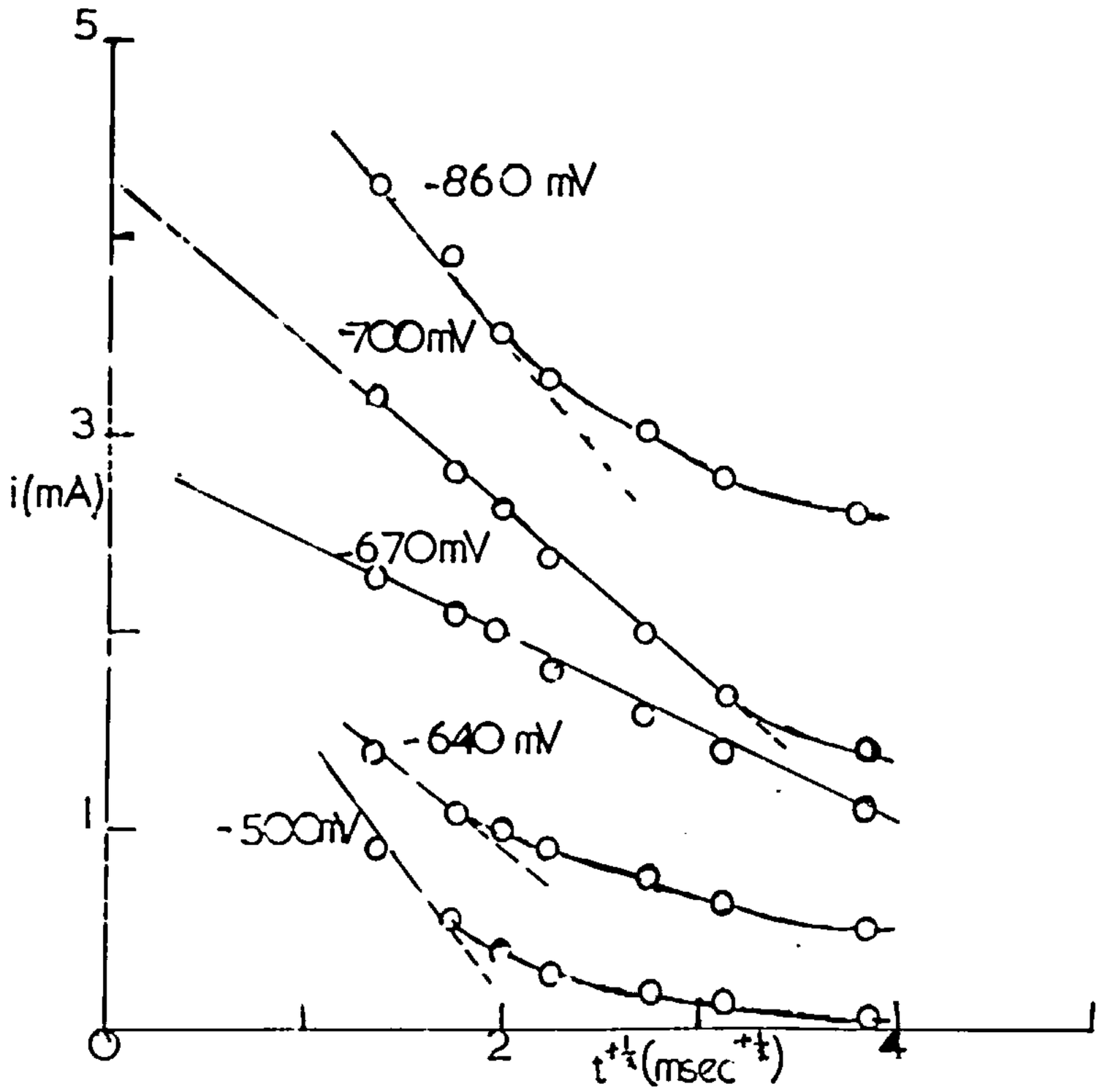

The i vs. $t^{+1/2}$ dependence may be explained by assuming reaction control to be involved and following the argument of Delahay.[133] Delahay considered a scheme

$$X \rightleftharpoons Y \xrightarrow[\text{fast}]{e} \text{products} \qquad (6.3.2.)$$

when $[Y] \ll [X]$, and the electrode process would be controlled by the rate at which Y is provided by the preceding chemical reaction. The change in X in dt

$$k\,C_{(o,t)}\,dt = D(\partial C/\partial x)_o\,dt \qquad (6.3.3.)$$

Delahay solved Fick's second law of diffusion with eqn. (6.3.3.) and derived,

$$i = nFAC^*\,k\,\exp(k^2t/D)\,\mathrm{erfc}\left(k\sqrt{t/D}\right) \qquad (6.3.4.)$$

At low times, this expression predicts a linear dependence of i on $t^{+1/2}$. At zero time, eqn. (6.3.4.) predicts $i = nFAC^*k$, which is the intercept on the i axis at t = 0. If such reaction control occurs in the thallous solutions (chloride media) used, a possible scheme may be

$$TlCl \rightleftharpoons Tl^+ \xrightarrow{e} Tl \qquad (6.3.5.)$$

Literature values[134] for the thallous/chloride system predict

for a 10^{-3}M total Tl^+ concentration in 1M Cl^-: $[Tl^+] \approx 0.15 \times 10^{-3}$M; $[TlCl] \approx 0.5 \times 10^{-3}$M; $[TlCl_2^-] \approx 0.35 \times 10^{-3}$M. Clearly the difference in $[TlCl]$ and $[Tl^+]$ is not very great.

6.4. Crystal growth processes

Pulsing into the multilayer regions and at longer times for Pb/Ag, Tl/Ag and Cd/Pb produces rising transients. Such transients (without a prepulse) are shown in Fig.63 (Pb/Ag; 3.4×10^{-3}M $PbCl_2$/1M KCl), Fig.64 (Pb/Ag; 3×10^{-2}M $Pb(OAc)_2$/1M NaOAc/0.1M AcOH), Fig. 65 (Tl/Ag; 8.75×10^{-4}M TlCl/1M KCl), Fig. 66 (Cd/Pb: 8.3×10^{-3}M $Cd(ClO_4)_2$/1M $NaClO_4$). Rising transients are characteristic features in the formation of new phases being due to nucleation and crystal growth processes.

These transients are extremely potential dependent and plots of current at constant time (and charge) against potential show steep Tafel slopes. Such a plot for currents at constant time for an unseeded Pb/Ag transient is shown in Fig.67(a). The slopes for the transients on the polycrystalline electrodes are 4-6mV; for the deposition of Pb onto the single silver crystal the slope is less steep, 12mV.

The form of the lead deposit on the polycrystalline

fig 63 0·0034M $PbCl_2$/1M KCl. electropolished, polycrystalline, Ag. i vs t. no prepulse.

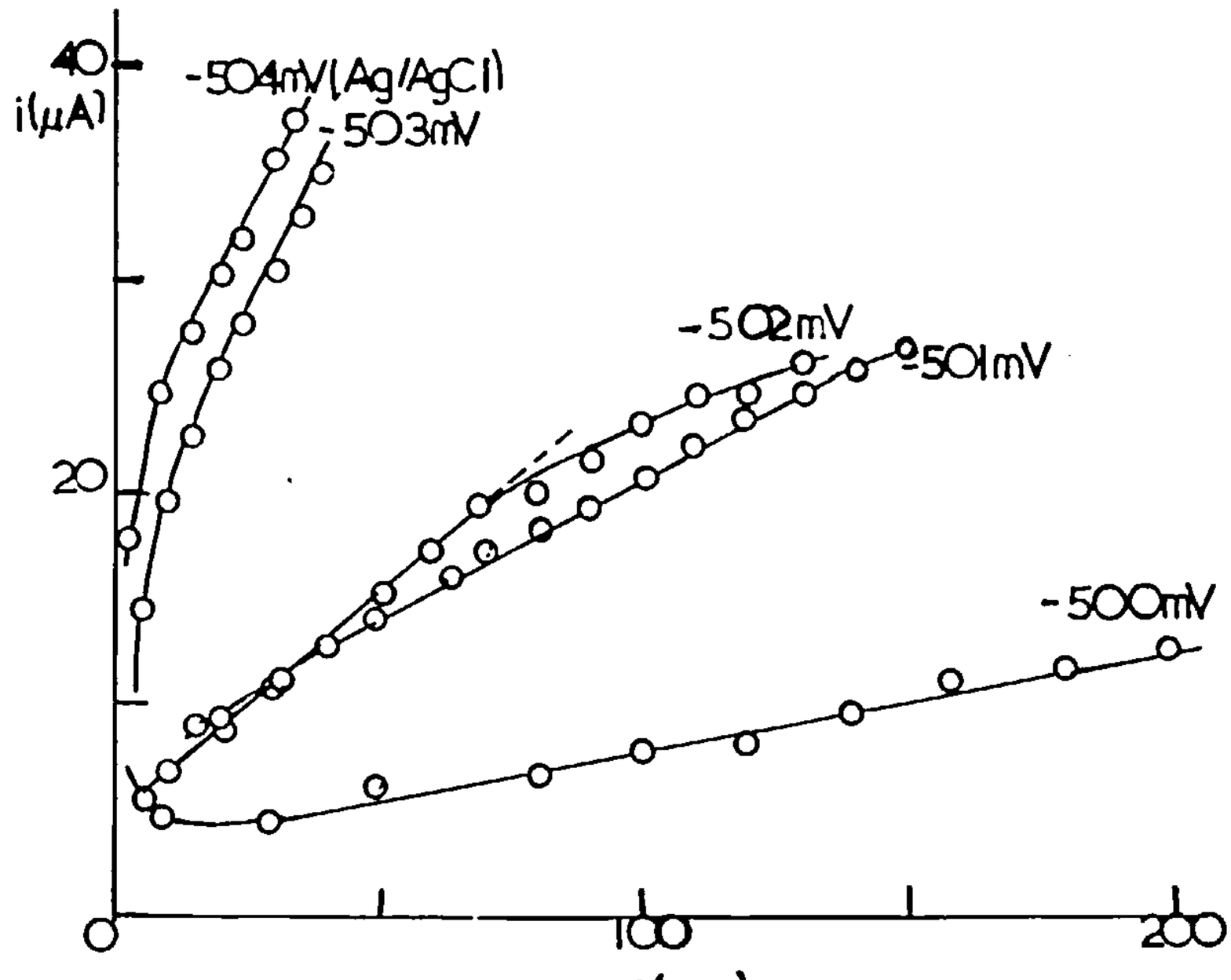

fig 70 Above conditions. prepulse -700 mV, 10 msec (Ag/AgCl).

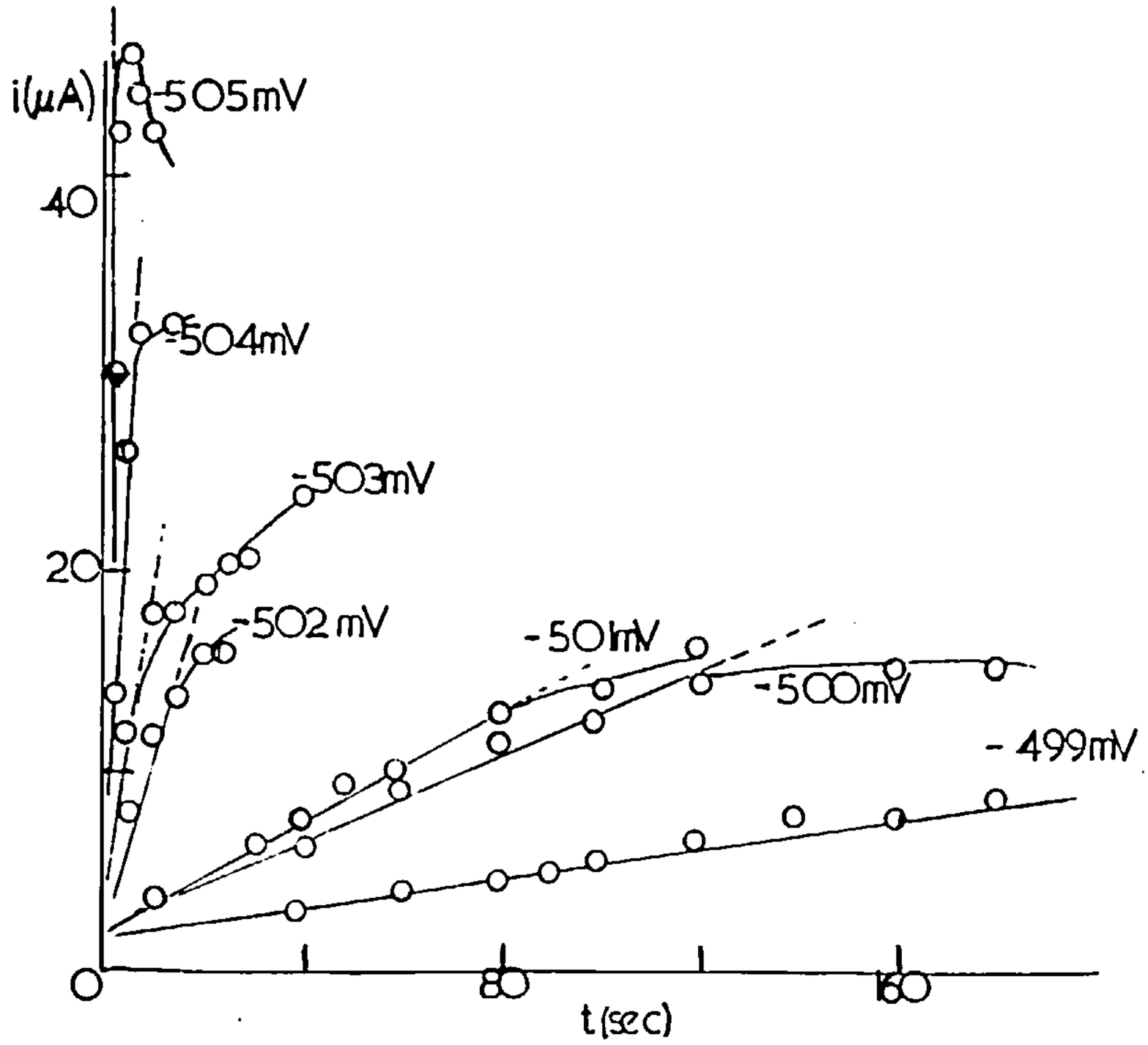

fig 64 0·03M $Pb(OAc)_2$, 1M NaOAc, 0·1M AcOH. electropolished, polycrystalline Ag. i vs t. no prepulse.

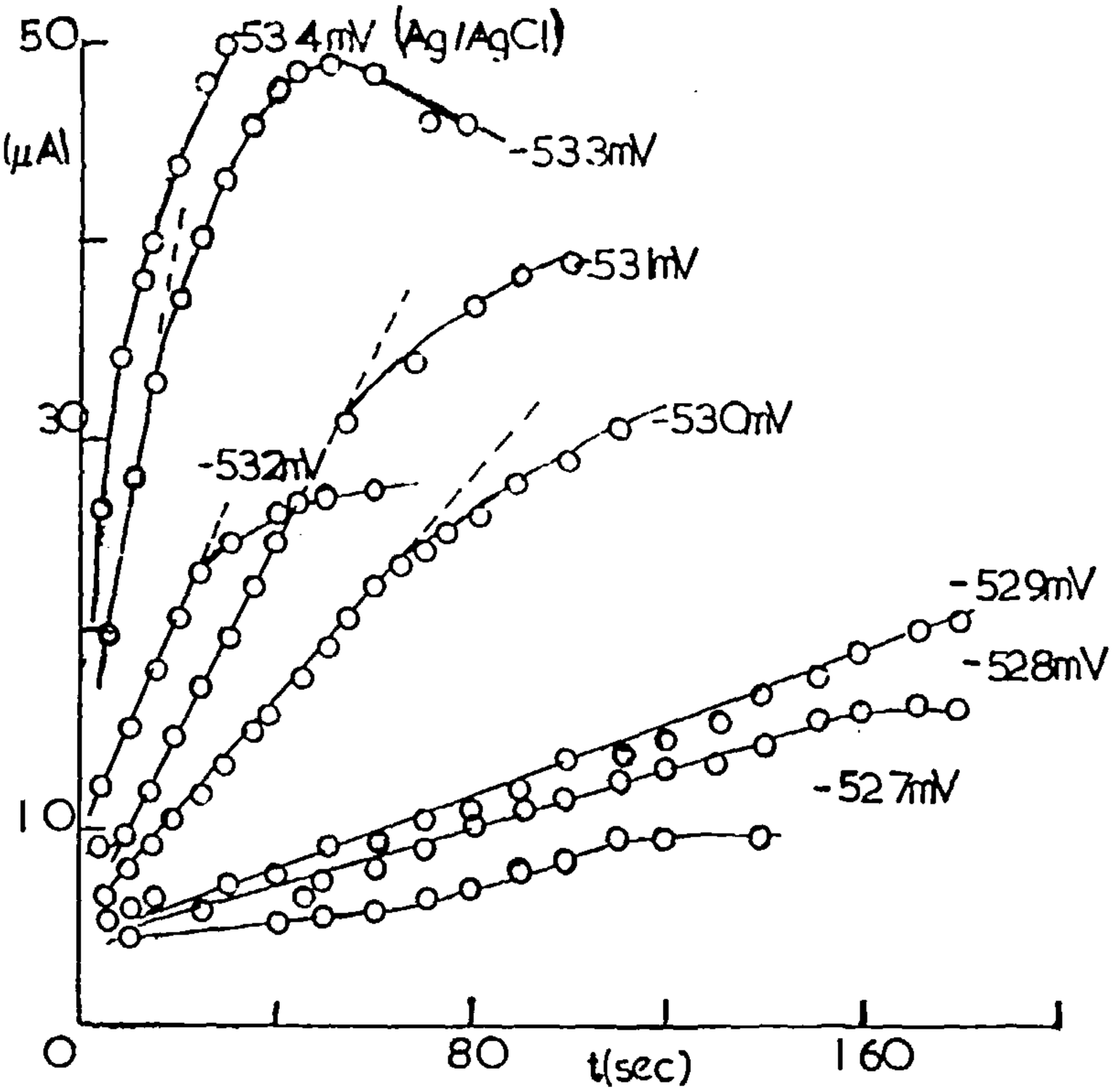

fig 65 0·000 875 M TlCl / 1M KCl. elpd, polyc., Ag. i vs t. no prepulse.

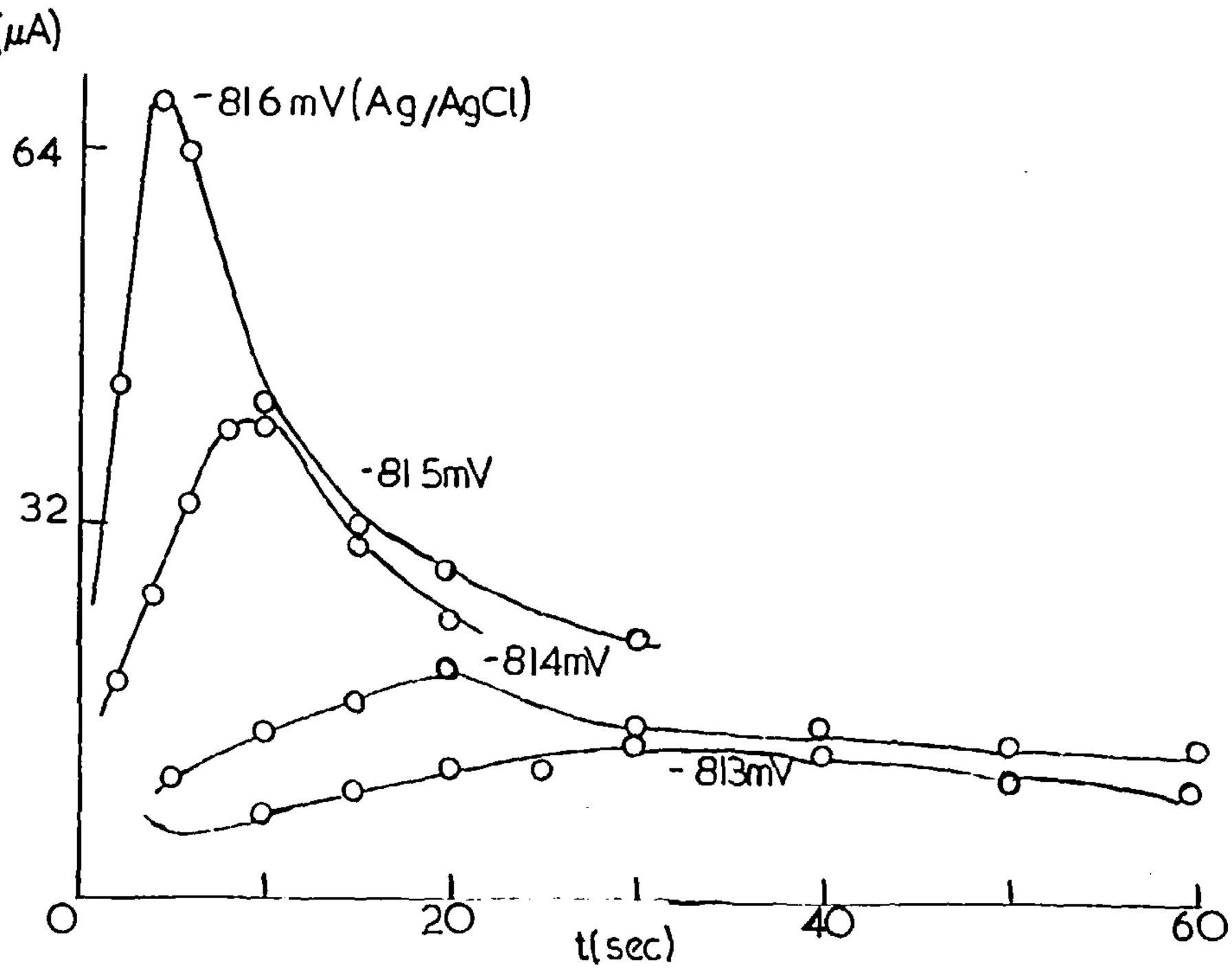

fig 67 O·003M $PbCl_2$/1M KCl. electropolished, single Ag crystal (111).
i(t) vs E. t = 15 sec (o); t = 10 sec (x). (a) no prepulse.
(b) prepulse -700mV, 30 msec (Ag/AgCl).

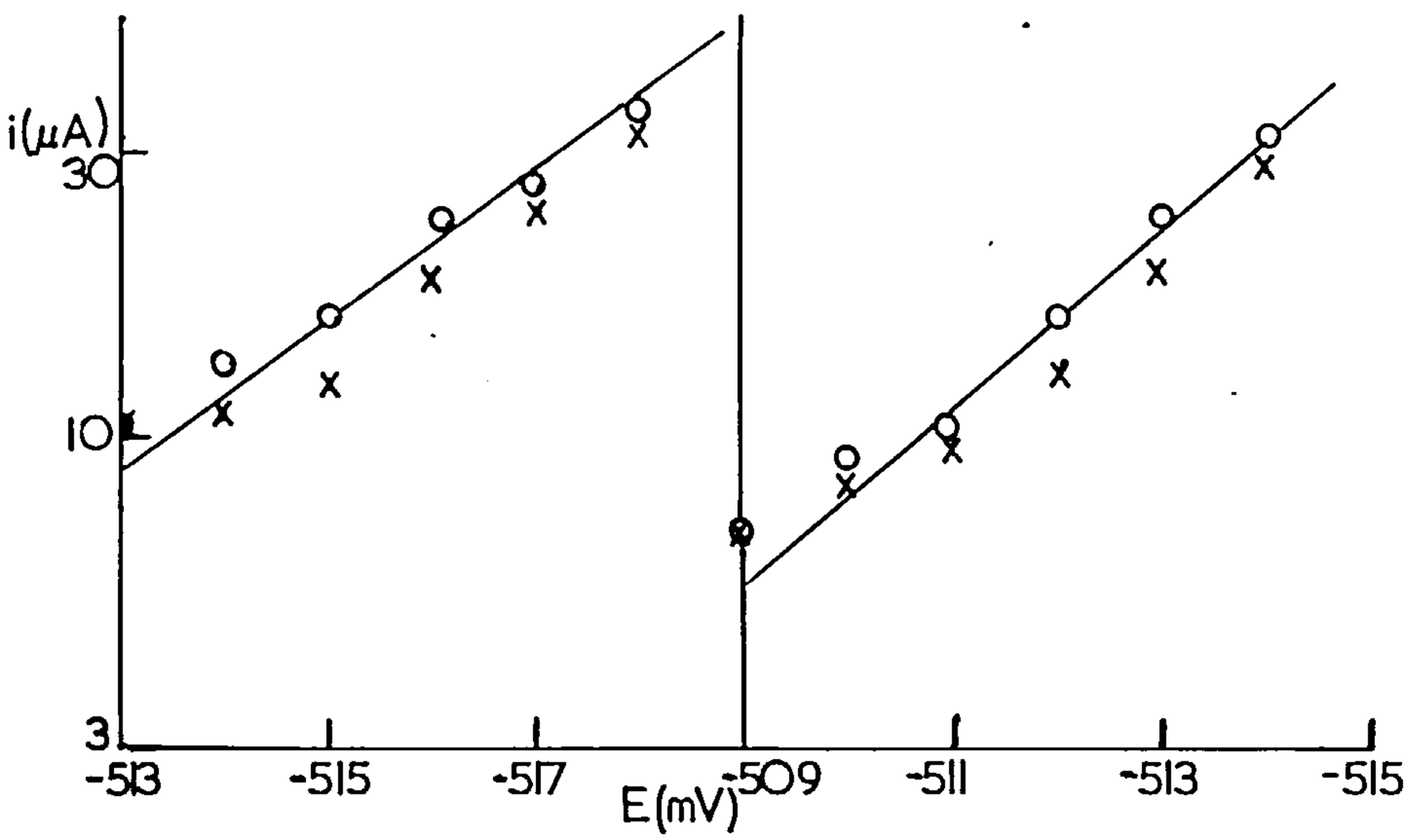

fig 71 O·0034M $PbCl_2$/1M KCl. elpd, polycrystalline Ag.
i(q) vs E for q = 200μC (o); q = 100μC (x).
prepulse -700mV, 10 msec (Ag/AgCl).

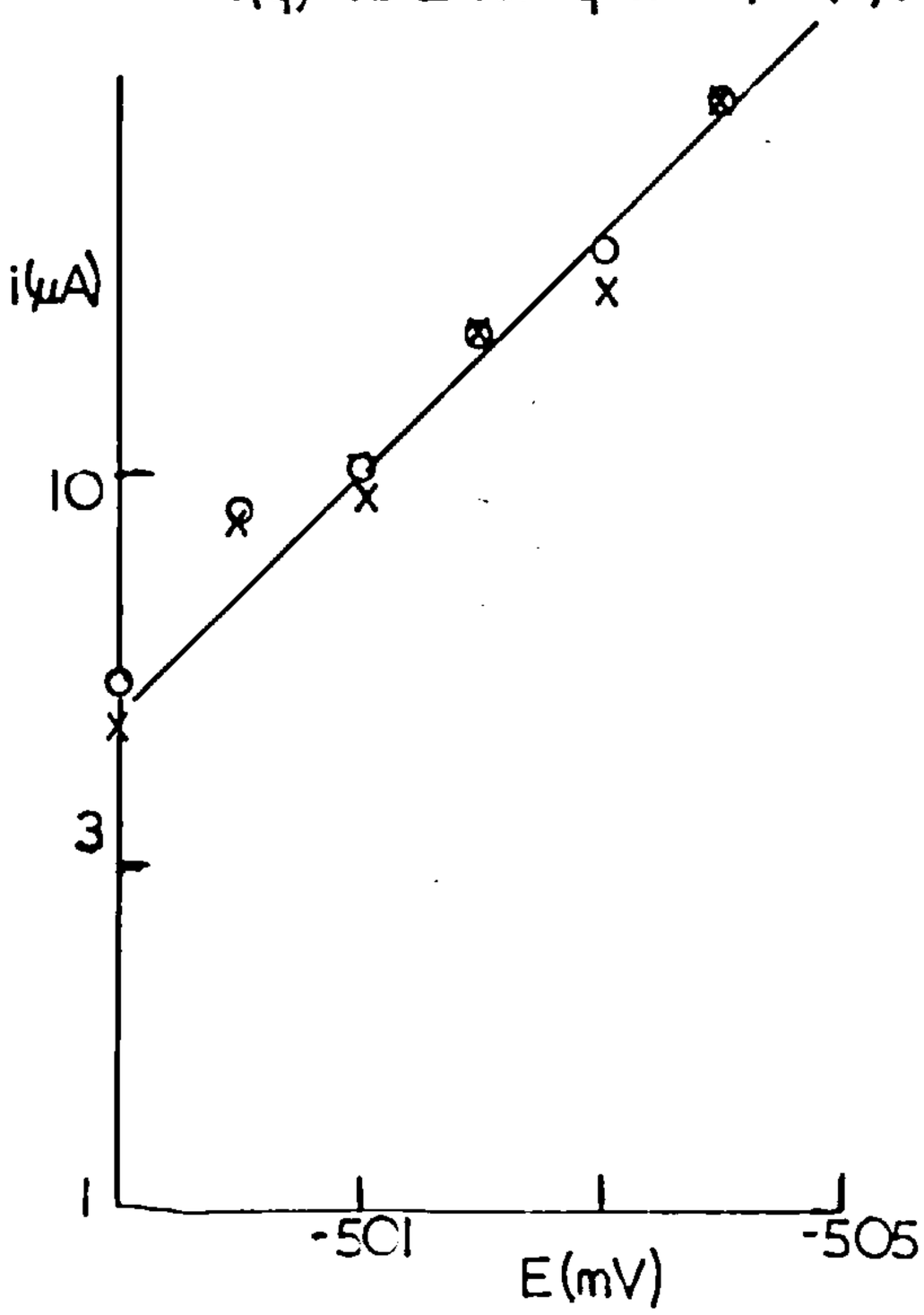

silver electrode is illustrated in the stereoscan micrographs shown as Fig.68, for a deposit grown at -800mV (Ag/AgCl) for 1 minute. The transmission electron diffraction pattern obtained for this deposit (Fig.69) showed d-spacings characteristic of lead (2.82 Å (experimental) ≡ 2.855Å (ASTM index); 2.52Å ≡ 2.475Å; 1.75Å ≡1.75Å). However there were some spacings close to PbO (2.95Å ≡ 3.03Å; 1.65Å ≡ 1.71Å).

In the belief that the extreme potential dependence of the transients observed may be due to nucleation processes, transients were observed after the application of large potential prepulses in an effort to nucleate all available sites and follow the growth of the nuclei at small overpotentials where essentially no more nucleation could occur. In this case prepulsing to 200mV more cathodic than the growing potential for a series of short times from 3 to 300 msec gave the unexpected result that prepulsing did not increase the growth current transients significantly, as in Fig.70. The potential dependence was also not very much affected. This is shown in Fig.67(b), for a plot of current at constant time against potential for a 3 x 10^{-3}M $PbCl_2$ solution onto the single silver crystal with a prepulse of -700mV, (Ag/AgCl), 30 msec (c.f. Fig.67(a)).

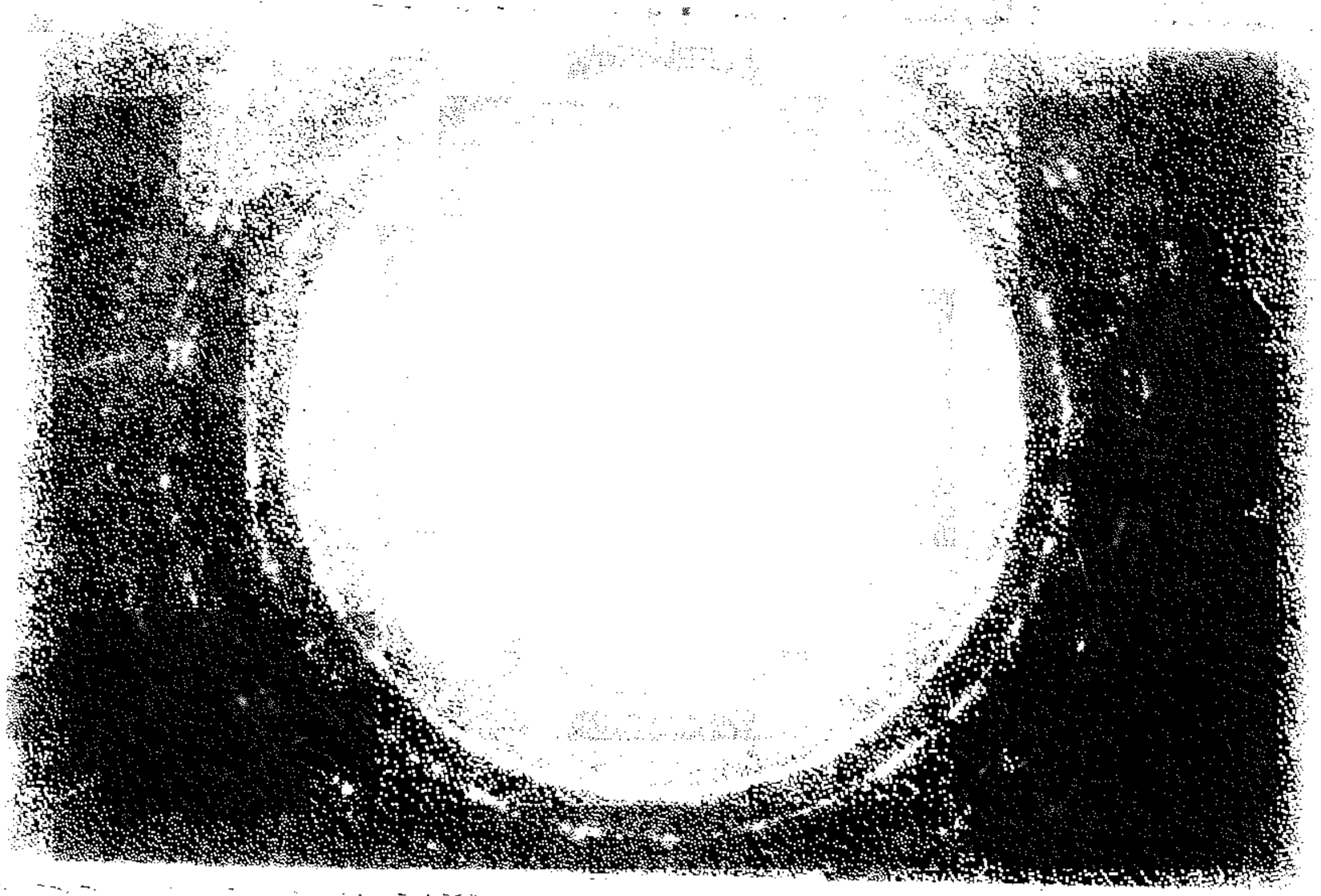

A similar plot of current at constant charge against potential is shown in Fig.71 for a 3.4×10^{-3}M $PbCl_2$ solution onto the polycrystalline electrode with a prepulse of -700mV (Ag/AgCl) for 10 msec. Similarly, prepulsing to the lower cathodic region in the fast peak regions in an attempt to produce a monolayer coverage, had no effect upon the potential dependence of the transients rising in the second peak regions.

It is impossible to explain such steep potential dependencies in terms of any clear electrochemical process. The steepest slope for a 2e process, without diffusion control, at the periphery of the nuclei, for the current plotted at fixed charge as a function of potential (this approximates to a planar electrode, i.e. constant interfacial area), being 30mV. Possible explanations which have been offered for such steep dependencies[135] include,

(a) Complications due to specific adsorption at the edge of the growing centres or on the electrode.

(b) The micropotential experienced by the ion in the rate determining step is substantially different from the micropotential.

(c) The centres are of such a size that the curvature of the edges changes the dependence of the lattice growth constant.

(d) There is considerable kinetic complexity at the reaction site.

Although any of these postulates could conceivably explain the results, none seem particularly appropriate explanations.

However, when diffusion in a Nernst diffusion layer of thickness δ controls the current,

$$i = \{nFAD/\delta\}\, C^{*}\left(1 - \exp\left[-nF\eta/RT\right]\right) \qquad (6.4.1.),$$

for a reversible electrochemical reaction at the surface, large potential dependence is possible near the reversible potential. Fig.72 shows the potential dependence of such a function as eqn. (6.4.1.), with n = 2e. Clearly for low η, the dependence is high, but the function levels off at ca. η = 14mV. It seems most probable that the nuclei do, in fact, grow from a Nernst diffusion layer. This would arise because the metal is dense and rapidly depletes the solution in its neighbourhood. The current into each nucleus is then independent of the nucleus geometry. This fits well with the observed $i \propto t$ time dependence which means progressive nucleation, each new nucleus bringing an equal increment in current. The fact that prepulsing has no effect must mean that the rate of nucleation is controlled

fig 72 $\{1-\exp(-2\eta F/RT)\}$ vs η

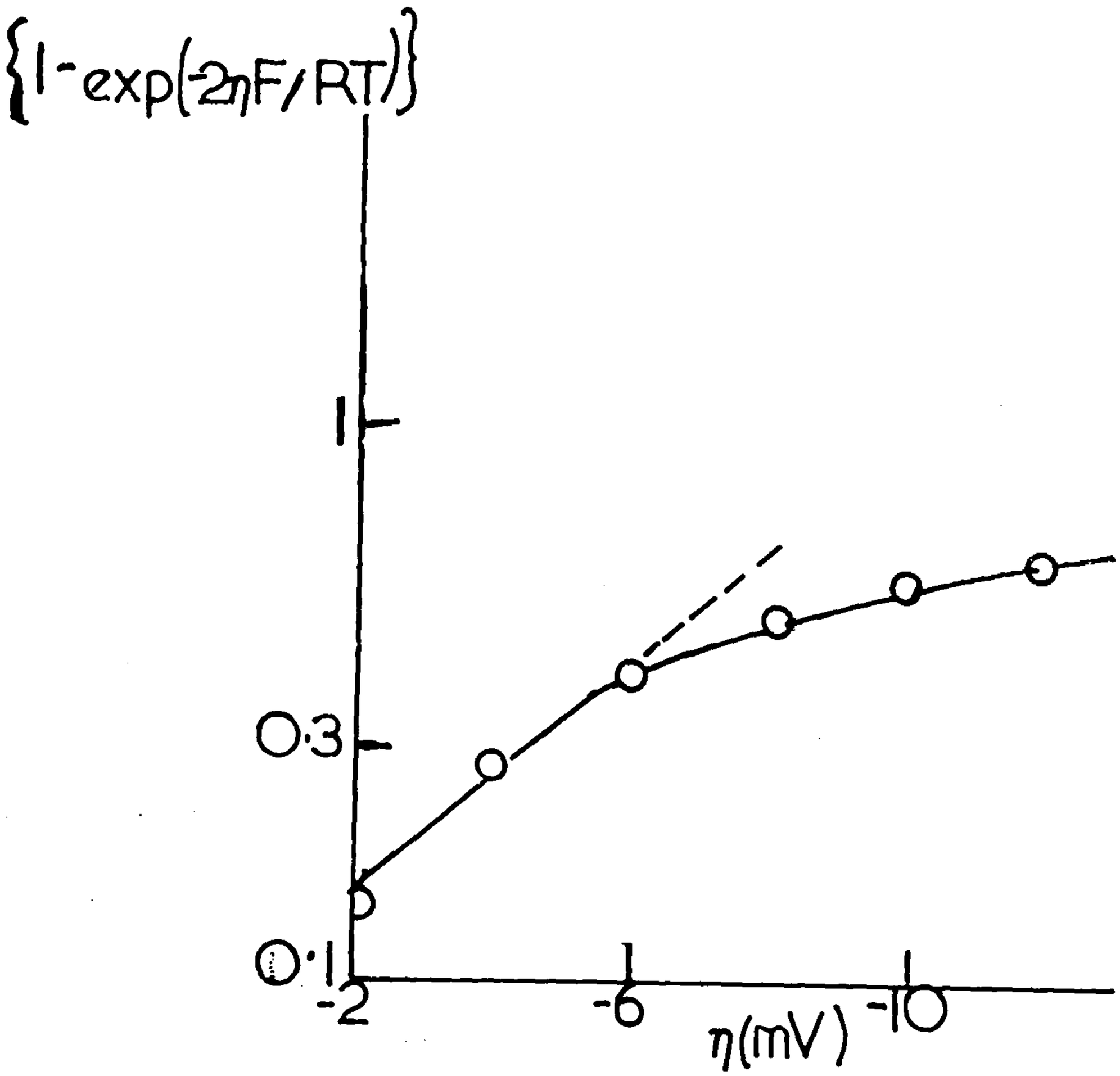

by the generation of defects in the surface of the deposited nuclei. A crude model in which the nucleus is considered as a growing hemisphere would give the surface area proportional to $t^{2/3}$ for constant flux. If it is assumed that the number of defects generated is directly dependent on the surface area then the rate of nucleation is just $t^{2/3}$. The volume will, however, be far from hemispherical and in practice $t^{2/3}$ would scarcely be distinguishable from $i \propto t$. The potential dependence can now be understood as arising from eqn. (6.4.1.).

The model of defect generation may account for the somewhat less steep potential dependencies obtained for the single silver crystal substrate. The smoother surface of the single crystal would produce a lower number of three-dimensional nuclei at a fixed time than those produced on the polycrystalline substrates where greater surface irregularities would tend to present a greater surface area for nuclei formation. The reduction of the number of nuclei and hence the number of defects at any time, would be reflected by lower potential dependencies.

6.5. A crystallographic explanation of the sweep behaviour

Since rising transients are observed under potentiostatic pulse conditions in the second peak region for Pb and Tl onto

Ag and for the peak region for Cd onto Pb, it seems evident that nucleation and growth of the new phase must be the controlling factors. An inspection of the unit cell dimensions and crystal habits for deposited metal/substrate metal systems investigated by Schmidt and Gygax[118] reveal the connection between the interplay of the crystallographic features and the number of peaks observed under sweep conditions. Table 3 displays such parameters for a number of systems investigated by Schmidt and Gygax.

Nothing is, in fact, known about the metal monolayer structure, but the charge suggests that it is a two dimensional layer. This is probably epitaxially fitted to the substrate metal. From Table 3 it seems that large differences in lattice dimension between the substrate and the metal film preclude the monolayer peak, as this is energetically unfavourable. This is in accord with Royer's ideas[19] on the growth of epitaxial deposits. There is some suggestion that positive $(a_D - a_S)$ values of some magnitude are more acceptable as far as the appearance of a monolayer peak is concerned, than negative values of any size. For example $(a_D - a_S) = +1.34\text{Å}$ for lead onto copper, but two peaks are observed; whereas an $(a_D - a_S)$ value only slightly larger in magnitude but negative in sign i.e. -1.57Å for cadmium

Table 3

A comparison of the crystallographic parameters for Deposit/Substrate investigated by Schmidt and Gygax[118]

No. of peaks	Deposited Metal	Crystal habit	Unit cell dimension a_D (Å)	Substrate Metal	Crystal habit	Unit cell dimension a_S (Å)	$(a_D - a_S)$ (Å)
2	Pb	Cubic	4.95	Ag	Cubic	4.09	+ 0.86
2	Pb	Cubic	4.95	Cu	Cubic	3.61	+ 1.34
2	Tl(α)	Cubic	3.88	Au	Cubic	4.08	- 0.2
2	Tl	Cubic	3.88	Ag	Cubic	4.09	- 0.21
2	Tl	Cubic	3.88	Cu	Cubic	3.61	+ 0.27
1	Tl	Cubic	3.88	Sn	Tetragonal	5.82	- 1.94
1	Cd	Hexagonal	2.96	Bi	Hexagonal	4.53	- 1.57
1	Cd	Hexagonal	2.96	Pb	Cubic	4.95	- 2
1	Cd	Hexagonal	2.96	Sn	Tetragonal	5.82	- 2.86

onto bismuth, corresponds to only one peak. This might be explained by considering that in the case of large positive $(a_D - a_S)$, the deposit structure could well bridge over the smaller lattice discontinuities of the substrate, whereas for large negative $(a_D - a_S)$ such a compromise is impossible. One would also expect epitaxy to occur more readily for like lattices and, in general, this seems to be borne out in the systems shown in Table 3 in so far as such deposit/substrate systems show the monolayer peak and systems of unlike crystal habit have but the one peak. In the cases where the monolayer forms some considerable potential difference is necessary before the layer can nucleate and grow further in a three dimensional nucleation which grows with the preferred lattice dimensions of the bulk metal.

Other systems using solid electrodes giving rise to two dissolution peaks under sweep conditions have been investigated in the literature. Nickel on platinum,[136,137] silver on graphite,[138] and copper on pyrolytic graphite[139] are such systems. In the case of copper on graphite,[139] three distinct dissolution peaks were observed, the two more anodic peaks being ascribed to monolayer deposits fitted to the substrate as described above, the bonding energies of which are different for two distinct electrode areas. The monolayers

were identified as covering the electrode surface uniformly by a microprobe technique.

The phenomenon of "undervoltage" i.e. deposition anodic to the thermodynamic equilibrium potential E^{o} for the bulk metal apparent in the positions of the first peaks for Pb/Ag and Tl/Ag, has also been observed in measurements of the deposition of trace amounts of Cu^{140} and Ag^{141} onto platinum and other electrodes under potentiostatic conditions. The amount deposited was measured using a radiotracer technique. Under-voltages of the order of 500mV have been observed for concentrations of depolariser ca. 10^{-9}M. The magnitude of the undervoltage observed was found to reflect the percentage misfit of deposit/substrate lattice dimensions in that larger misfits gave smaller undervoltages. A similar explanation as offered above was proferred for these results in that large undervoltages meant epitaxial deposition on the substrate.[140]

Chapter 7

The Electrocrystallisation of Cobalt on Mercury Substrates

7.1. Introduction

In view of the ideal properties of mercury as an inert substrate, e.g. ease of purification, reproducibility of the smooth surface; a metal was chosen for deposition which was ostensibly insoluble in mercury (nucleation of discrete centers possible), whose deposition potential was suitably cathodic to the Hg/Hg_2^{2+} potential, and whose ions did not react chemically with mercury. Such a system, nickel onto mercury from thiocyanate medium, has been investigated as mentioned in Chapter 1, section 4; potentiostatic pulse measurements were analysed in terms of the rate of discharge, surface diffusion and lattice growth.

The deposition of cobalt onto mercury fits the requirements above. Investigation of this system is also pertinent in view of work in the literature concerning double-wave behaviour of cobalt in thiocyanate medium at dropping mercury electrodes,[142,143] also the behaviour of stationary electrode polarograms for cobalt systems.[144]

7.2. The aqueous C_o^{2+} system

Cobaltous (C_o^{2+}) solutions were employed (10^{-2}M) made

up to 1M with KNO_3. Upon the application of a triangular potential profile current/voltage curves similar to that shown in Fig.73 were observed. A new Hg drop (area 0.1 cm^2) was upturned each time. The deposition peak began to rise at ca. -660mV (Ag/AgCl). The reversible potential for $C_o^{2+}/C_{o(s)}$ for this C_o^{2+} concentration is -560mV. The removal peak is shifted anodic to the deposition peak by a considerable margin, ca. 600mV. It was sometimes possible to observe the formation of two cathodic peaks (Fig.74), the second peak occurring at ca. -1,000mV. At fast sweep rates, the current/voltage curves degenerate into essentially parallelograms, with no peaks, formation or removal, present.

Pulse measurements at short times produced falling transients at various potentials throughout the sweep range. The initial (sitting) potential used was -500mV (Ag/AgCl). A plot of i vs. $t^{-1/2}$ for some of these potentials is shown in Fig.75. The curves do not appear to be truly diffusion controlled, especially at the lower potentials (up to ca. -1050mV). Some kind of reaction control in solution may be inferred. Pulse measurements at longer times produced rising transients. The transients rise then fall, and eventually rise once more (Fig.76). The charge under the maxima was ca. 13-15,000$\mu C.cm^{-2}$. The Tafel slope of the current (at constant time) vs. potential on the first

fig 73 0·01 M $Co(NO_3)_2$ / 1M KNO_3 on Hg. Sweep rate 100 mV/sec. (Ag /AgCl)

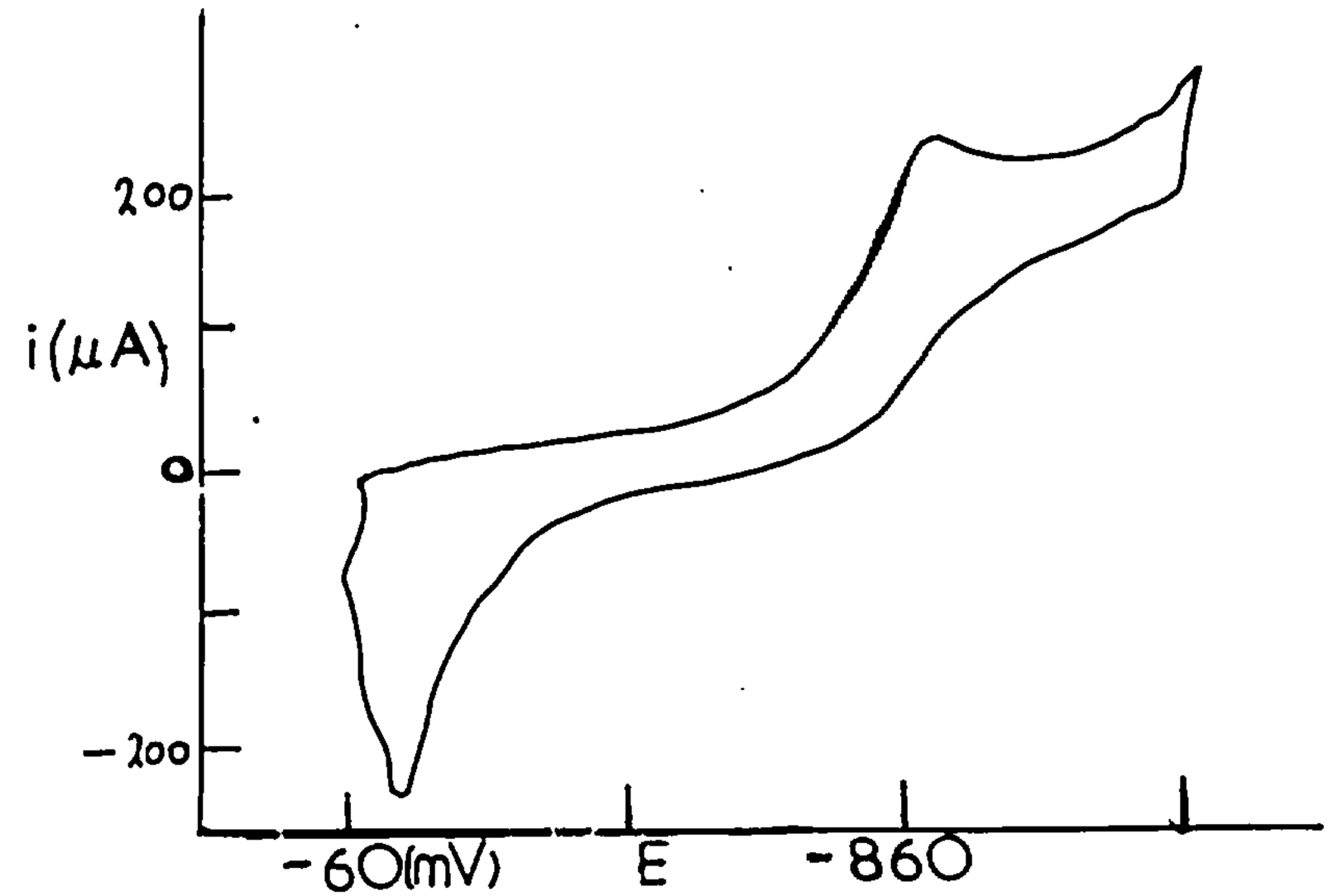

fig 74 0·01 M $Co(NO_3)_2$ / 1M KNO_3 on Hg. Sweep rate 10 V/sec.

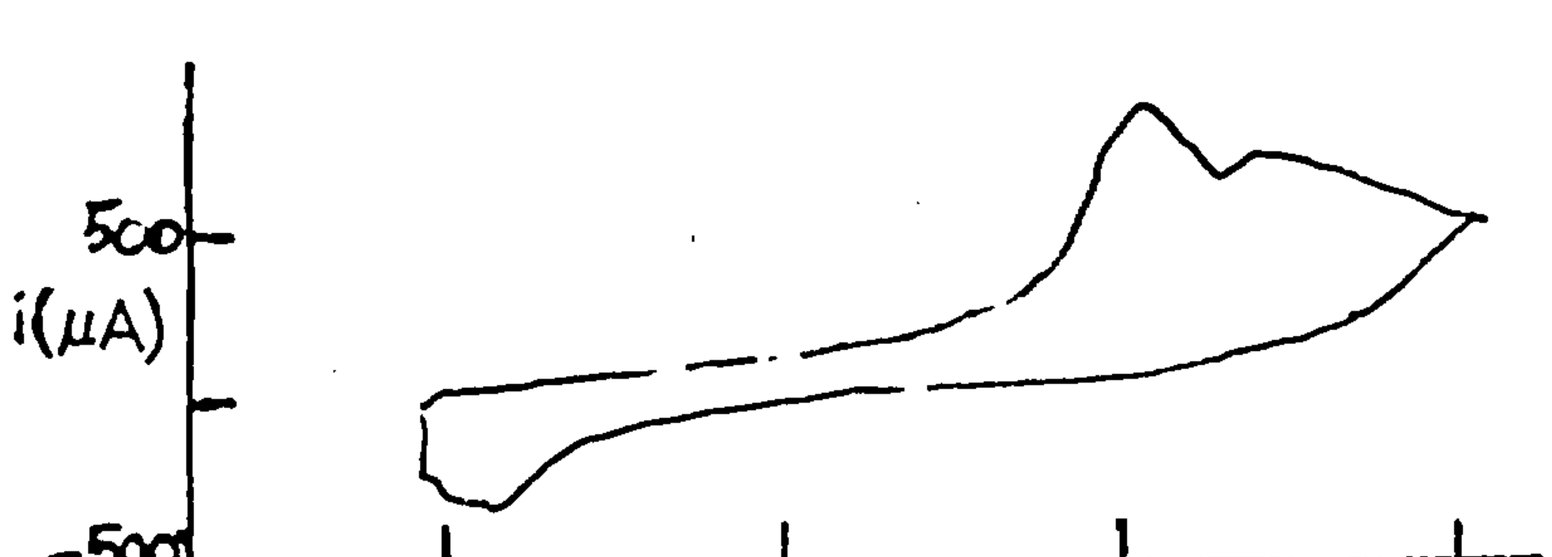

fig 75 0·01M $Co(NO_3)_2$ / 1M KNO_3 on Hg. i vs $t^{-1/2}$ for 1) -700 mV ; 2) -870 mV; 3) -900 mV ; 4) -1030 mV ; 5) -1090 mV ; 6) -1250 mV . (Ag/Ag Cl)

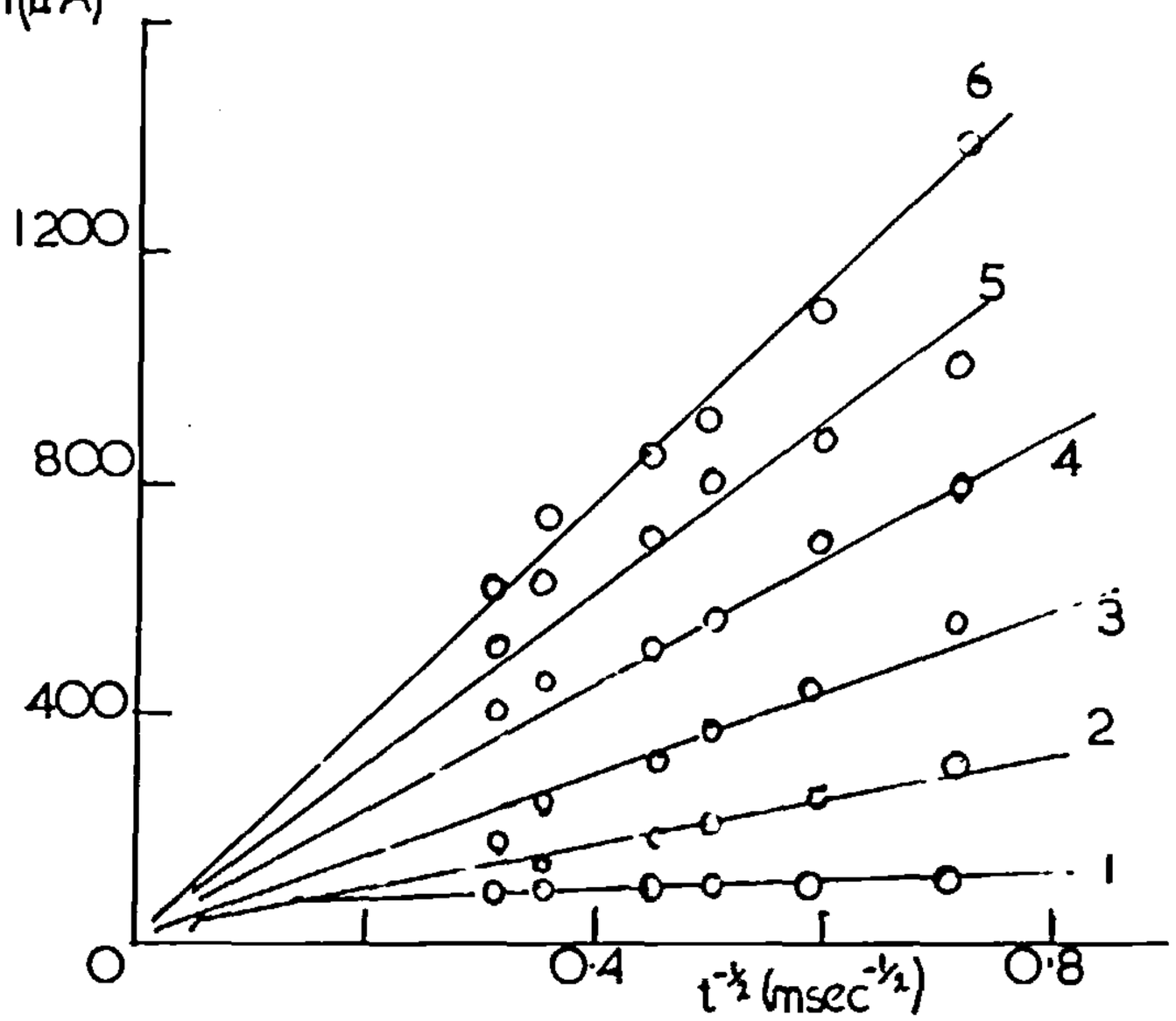

fig 76 0·01M $Co(NO_3)_2$/1M KNO_3 on Hg. i vs t , for E(ref-Ag/AgCl).

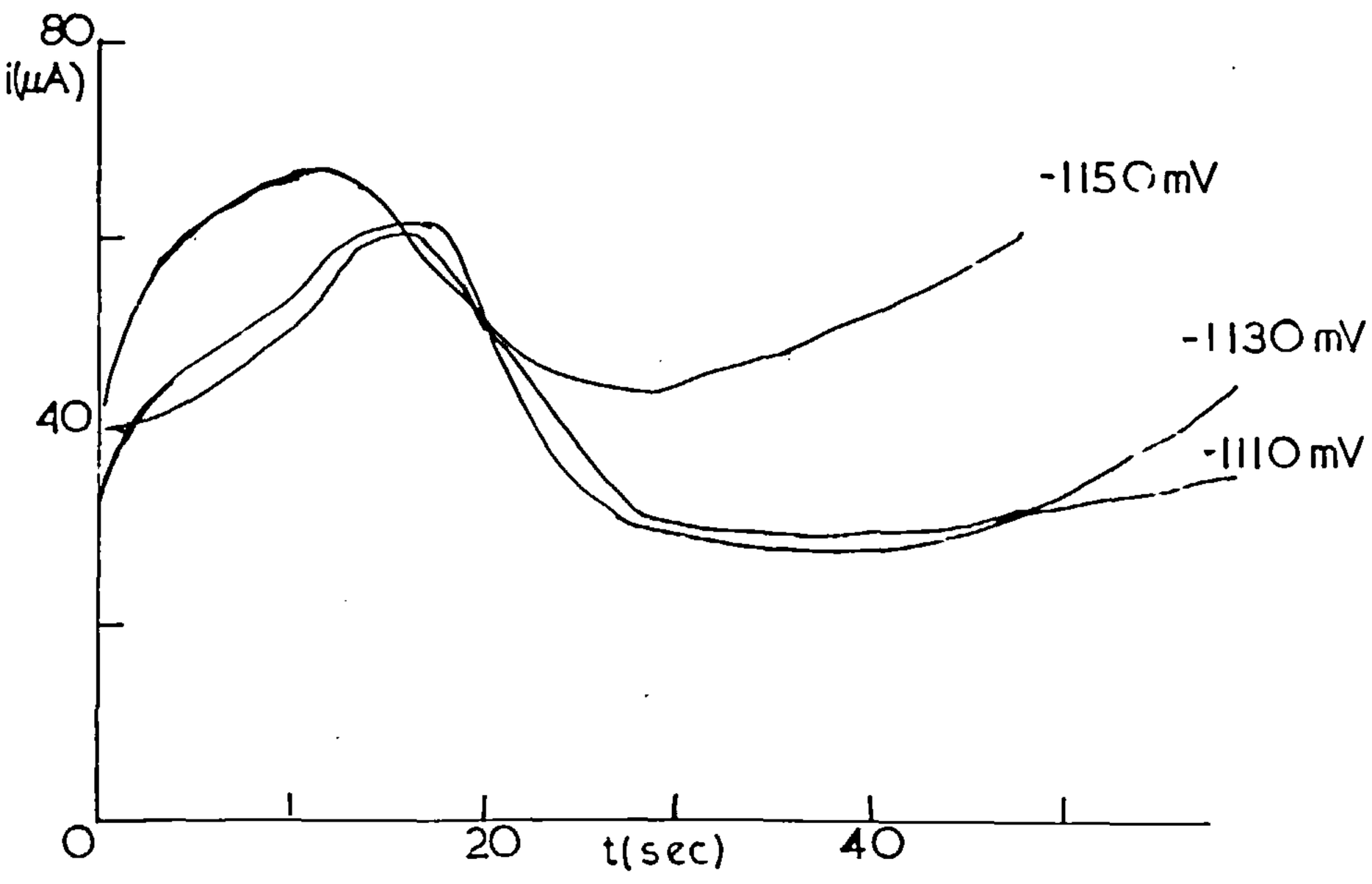

rising portion of such transients was low (ca. 200mV, Fig.77). This is another indication of reaction control in solution governing the rate of growth of the cobalt nuclei.

A possible scheme for the reduction path of Co^{2+} is,

$$Co^{2+} + H_2O \rightleftharpoons H^+ + CoOH^+ \xrightarrow{2e} Co + OH^-$$

$$Co^{2+} \swarrow \text{on the electrode surface} \qquad (7.2.1.)$$

$$Co(OH)_2 \text{ or } CoO$$

This mechanism depends on the fact that, due to the differing diffusion coefficients of H^+ and OH^-, a gradient of OH^- ions can exist in the region adjacent to the interface. The oxide(s) formed would cut off the initial growth transient for cobalt, and flatten off the sweep profiles for fast scans. Brdička[146,147] first postulated the reduction of $Co(OH)^+$ as a controlling step to explain the formation of a polarographic pre-wave observed for Co^{2+} in aqueous KCl medium. Similarly Verdier[148] reported two waves for Co^{2+} in KNO_3 medium with oxygen in the solution, attributing the first wave to reduction of a hydroxide species. The concentration of $CoOH^+$ in a 10^{-2}M Co^{2+} solution is calculated to be 2.5×10^{-9}M.[149]

The phenomenon of oxide formation may also be explained by considering by the process

$$H_2O \xrightarrow{e} \tfrac{1}{2}H_2 + OH^- \qquad (7.2.2.)$$

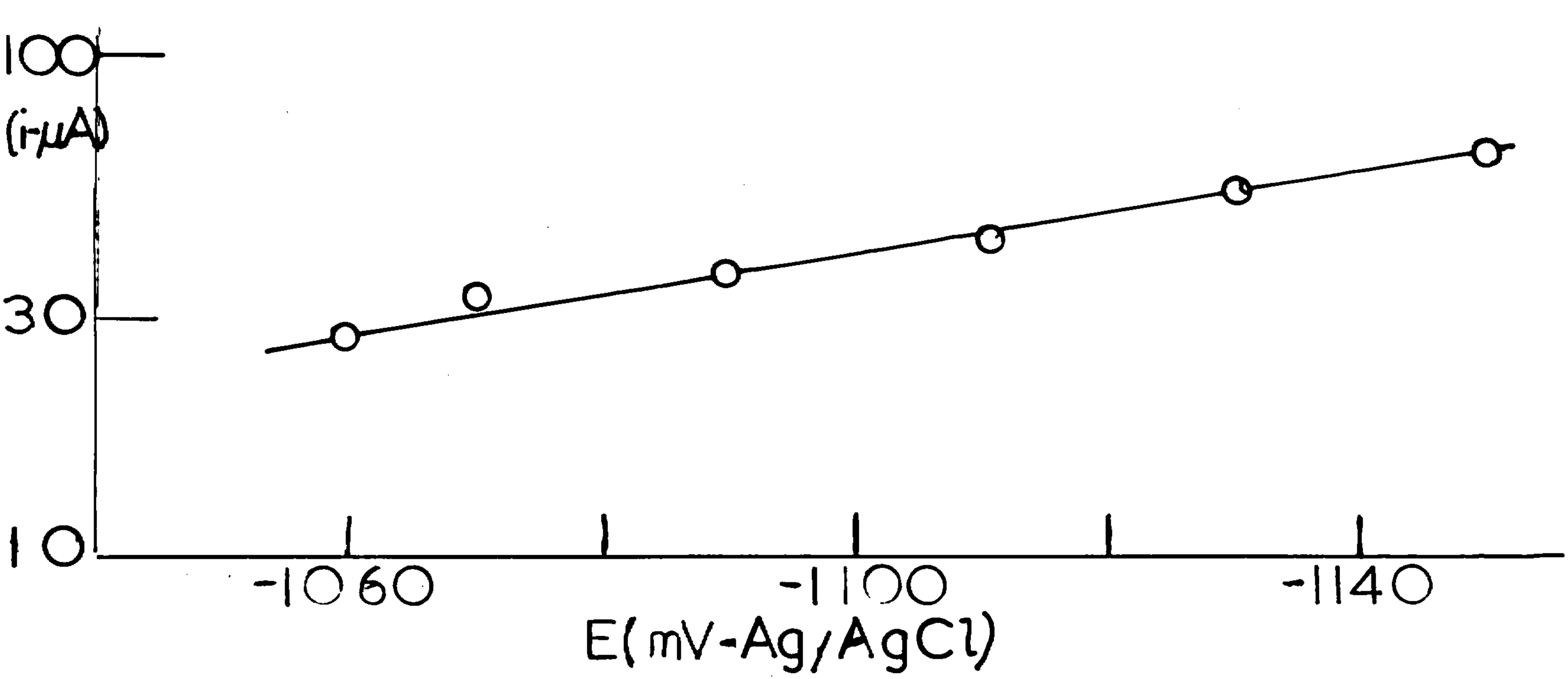

fig 77 0·01M $Co(NO_3)_2$/1M KNO_3 on Hg· i(10 sec) vs E.

This would mean the absorption of a hydrogen atom or molecule into the oxide film, as the production of gaseous hydrogen, even at high rates of formation of oxide, was not observed. There is evidence that in general cathodic oxide formation is greatly influenced by the amount of indifferent electrolyte present. In mechanism (7.2.1.) this could occur by changing the concentration of the reducible species C_oOH^+. Mechanism (7.2.2.) would allow these effects as an alteration of the activity of OH^- in the interfacial region. Similar phenomena of the formation of cathodic oxide or hydroxide occur during the reduction of the chromate anion.[150,151]

The further rising transient observed after the maxima under pulse conditions, and the second peak observed occasionally under sweep conditions might be attributed to the further reduction of the cobaltous oxide or hydroxide on the electrode surface. However there is also some evidence from the work of Babkin[152] that in the presence of some polyvalent cations (including C_o^{2+}), the reduction potential of nitrate ions is shifted anodic. From polarographic measurements shifts of up to 350mV have been observed, whilst the C_o^{2+} potential shifted cathodic by ca. 200mV. Such a process (presumably a catalytic reduction of NO_3^-

on the cobalt nuclei) may also account for the secondary effects observed for both pulse and sweep conditions.

7.3. The Cobalt/Thiocyanate System - sweep measurements

Because of the difficulties encountered in using uncomplexed cobaltous solutions; i.e. "passivation" effects - probably oxide formation, possibly nitrate reduction; measurements were made employing cobalt solutions in which the C_o^{2+} ions were strongly complexed. Thiocyanate was chosen as a suitable ligand. For a 10^{-2}M C_o^{2+} solution in 1M CNS^-, the various complex concentrations are calculated as;[153]

$\left[C_o^{2+}\ \text{free}\right] = 4.2 \times 10^{-6}$M, $\left[C_oSCN^+\right] = 4.2 \times 10^{-3}$M,

$\left[C_o(SCN)_2\right] = 4.2 \times 10^{-3}$M; $\left[C_o(SCN)_3^-\right] = 8.4 \times 10^{-4}$M,

$\left[C_o(SCN)_4^=\right] = 7.6 \times 10^{-4}$M. The predominant complexes are thus C_oSCN^+ and $C_o(SCN)_2$.

The reversible potential for the formation of mercurous thiocyanate in 1M CNS^- was calculated as -18mV (Ag/AgCl).[154] All measurements using this system were conducted cathodic to this potential. Upon the application of a potential sweep profile to a new mercury drop (area ca. 0.1 cm^2), current/voltage profiles similar to that shown in Fig.78 were observed. The deposition peak (occurring at ca. -1100mV (Ag/AgCl)) is shifted cathodic from the reversible potential for C_o^{2+}(free)/$C_{o(s)}$, i.e. - 661mV. The removal peaks are displaced about

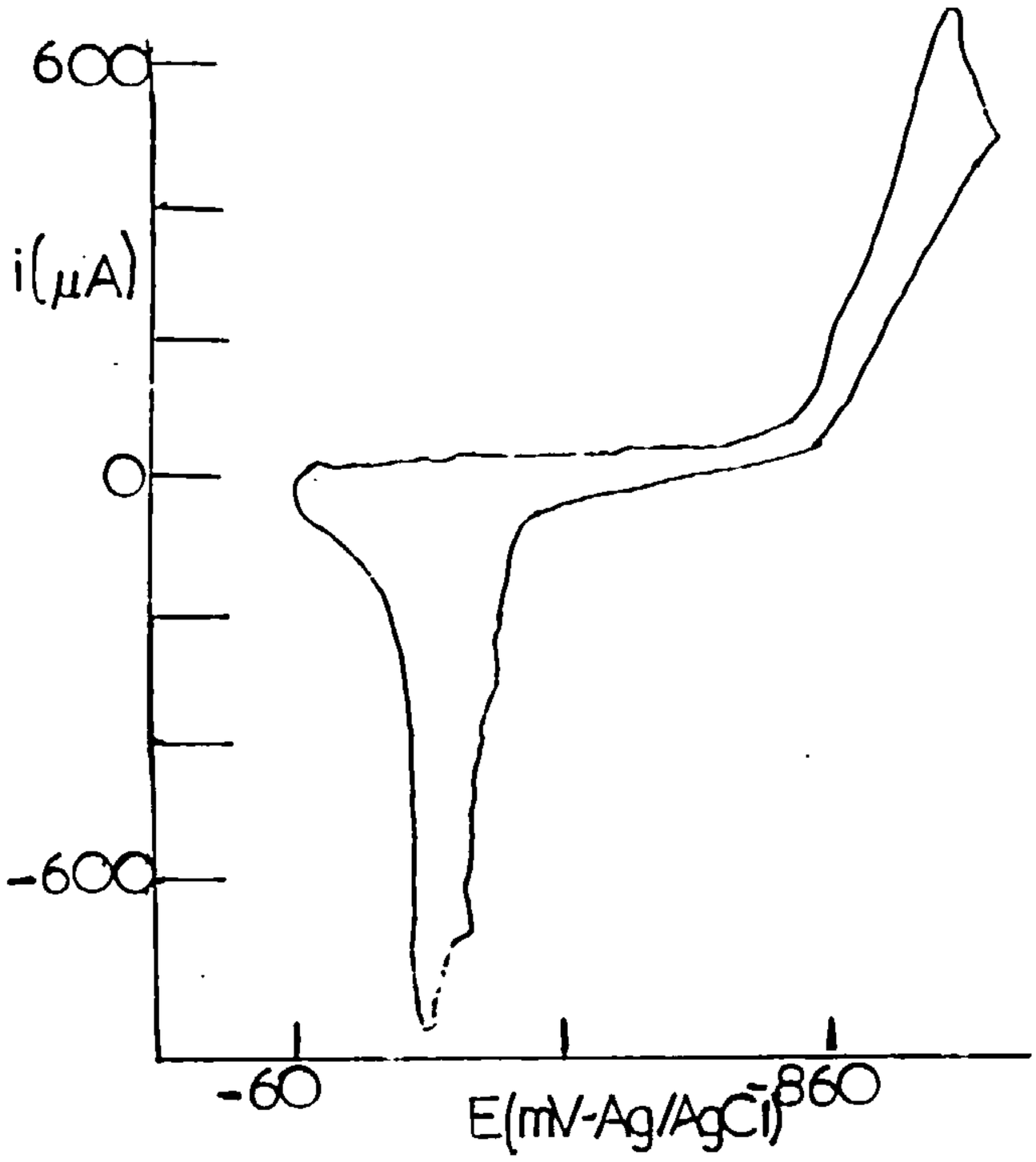

fig 78 0·01 M Co^{2+} / 1M KCNS on Hg. Sweep rate 300 mV / sec.

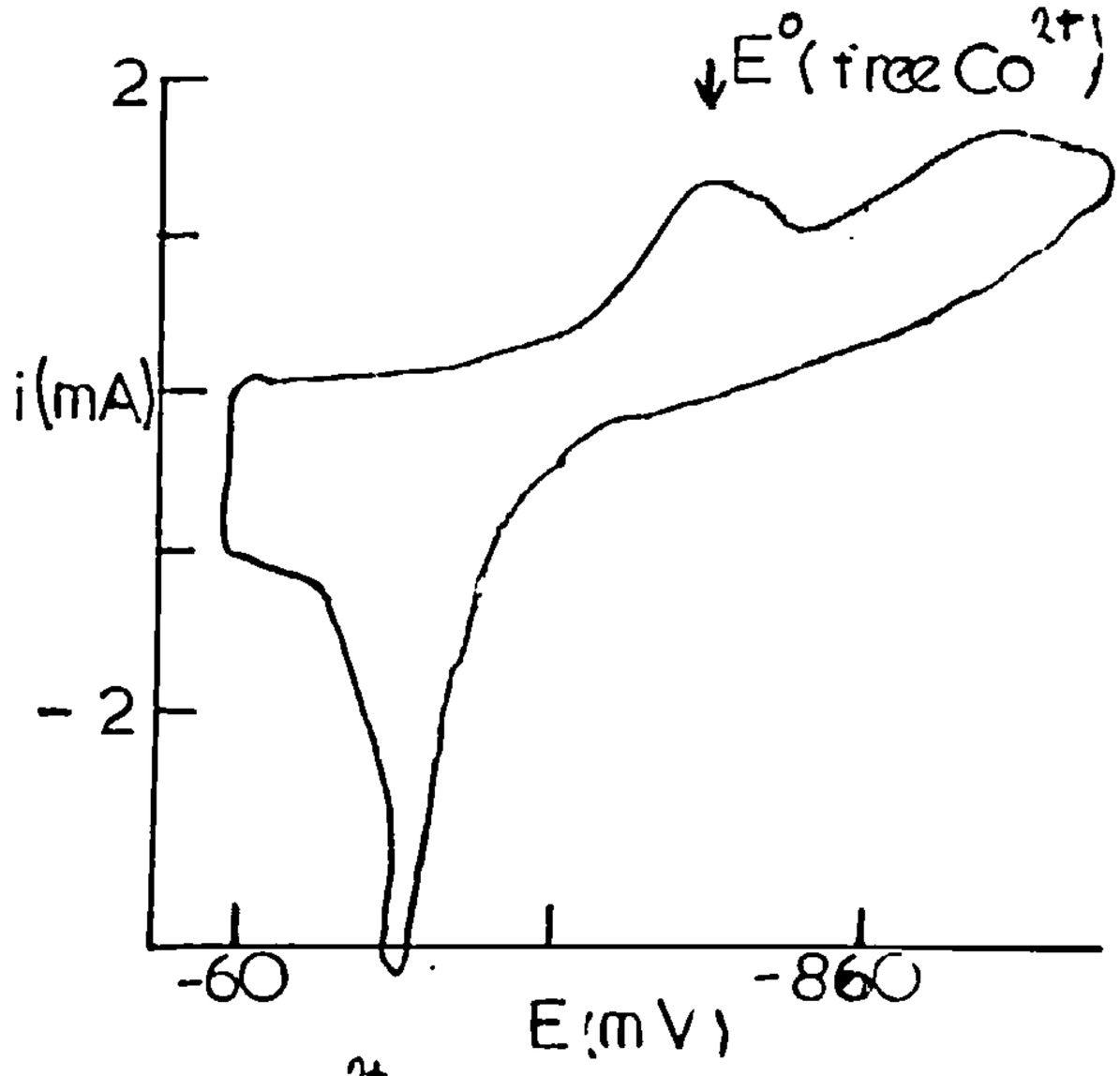

fig 79 0·01 M Co^{2+} / 1M KCNS on Hg. Sweep rate 10 V/sec.

After one cycle; sit at -60 mV, 30 sec.

1V anodic of the reduction peak. Two distinct parts of the removal peak are clearly visible. Such behaviour has also been observed by Housepian and Shain,[144] and Kemula and Galus[155] for cyclic scans on a hanging mercury drop electrode in solutions of cobalt (11) in pyridine-pyridinium chloride medium and chloride medium respectively. Similar behaviour has been reported for the Ni(11)-pyridine system.[156] Kemula and Galus postulated that the anodic peaks correspond to several stable forms of a cobalt-mercury amalgam.

Housepian and Shain[144] ascribed the form of the cyclic polarograms to a reversible charge transfer followed by an extremely rapid irreversible chemical reaction. They invoked the scheme

$$Co(II)\text{-complex} + \lambda e \rightleftharpoons Co(amalgam) \qquad (7.3.1.)$$

$$Co(amalgam) \xrightarrow{k_1} CoHg_X \qquad (7.3.2.)$$

and

$$CoHg_X + Co(amalgam) \underset{k_2 > k_1}{\xrightarrow{k_2}} Co_2Hg_X \qquad (7.3.3.)$$

Thus one may state the diffusion equation for $[C_o(amalgam)]$, C;

$$\text{i.e. } \partial C/\partial t = D\partial^2 C/\partial x^2 - k_1 C - k_2 C [C_{CoHg_X}] \qquad (7.3.4.)$$

It was argued that the loss of C_o(amalgam) through such

chemical reactions as (7.3.2.) and (7.3.3.) gave rise to the large anodic shift of the removal peak compared to the formation peak. As the concentration of C_o(amalgam) in solution rose so would the rate of process (7.3.3.), so that in the limit the concentration of $CoHg_x$ would tend to zero. Thus the rate of process (7.3.2.) would become limiting and the system would behave as if the succeeding chemical reaction were first order. Howsepian and Shain[3] experimentally observed that the shifts in the peak potentials became less at higher concentrations i.e. the loss of C_o(amalgam) became a first, rather than a second order process. It was pointed out that their data could not be adequately explained in terms of a conventional second-order reaction.

i.e. $$A + 2e \longrightarrow B \qquad (7.3.5.)$$

then $$B + C \xrightarrow{k_1} D \qquad (7.3.6.)$$

Thus $$\frac{\partial C_B}{\partial t} = D\left(\frac{\partial^2 C_B}{\partial x^2}\right) - k_1 C_B C_C \qquad (7.3.7.)$$

Eqn. (7.3.7.) predicts that the shift in peak potentials would always increase with concentration. There is evidence[157] from coulometric stripping experiments for the existence of a cobalt dimer as a stable form in the amalgams.

Comparison of the charges under the profiles (Fig.78) indicates that more charge is involved in deposition than corresponds to removal of the cobalt. The cobalt remaining may be a more stable $C_{o_n}-H_{g_x}$ compound. In fact after the completion of one cyclic scan upon a fresh mercury drop and waiting at the anodic potential for ca. 30 seconds; one obtains a further peak at ca. -660mV (Ag/AgCl) upon recycling (Fig.79). The extra peak (which is at about E^o for $C_o{}^{2+}/C_{o(s)}$) may correspond to deposition of cobalt onto surface cobalt (in the form of the undissolved $C_{o_n}Hg_x$ compound on the surface); the compound acting as a nucleation site. The second sweeps also only produce one removal peak (Fig.79). It is possible that the greater amount of C_o deposited (due to the peak at ca. -660mV) tends to accelerate the formation of C_o-Hg compounds so that little normal cobalt amalgam remains to give a definite removal peak.

7.4. $\underline{C_o(11)/\text{thiocyanate}}$ - reaction control

Potentiostatic pulse measurements at short times for various potentials, from an initial sitting potential of -500mV (Ag/AgCl), produced falling transients which did not plot as i vs. $t^{-1/2}$, (Fig.80). Control by a preceding chemical reaction is suggested by the plot of i vs. $t^{+1/2}$ (Fig.81). A plot of the initial current (obtained from the

fig 80 0·01M Co^{2+} / 1M KCNS on Hg. i vs $t^{\frac{1}{2}}$ for
1) -700 mV; 2) -900 mV; 3) -1030 mV; 4) -1050 mV; 5) -1070 mV;
6) -1090 mV; 7) -1110 mV; 8) -1180 mV; 9) -1200 mV; 10) -1300 mV.
(Ag/AgCl)

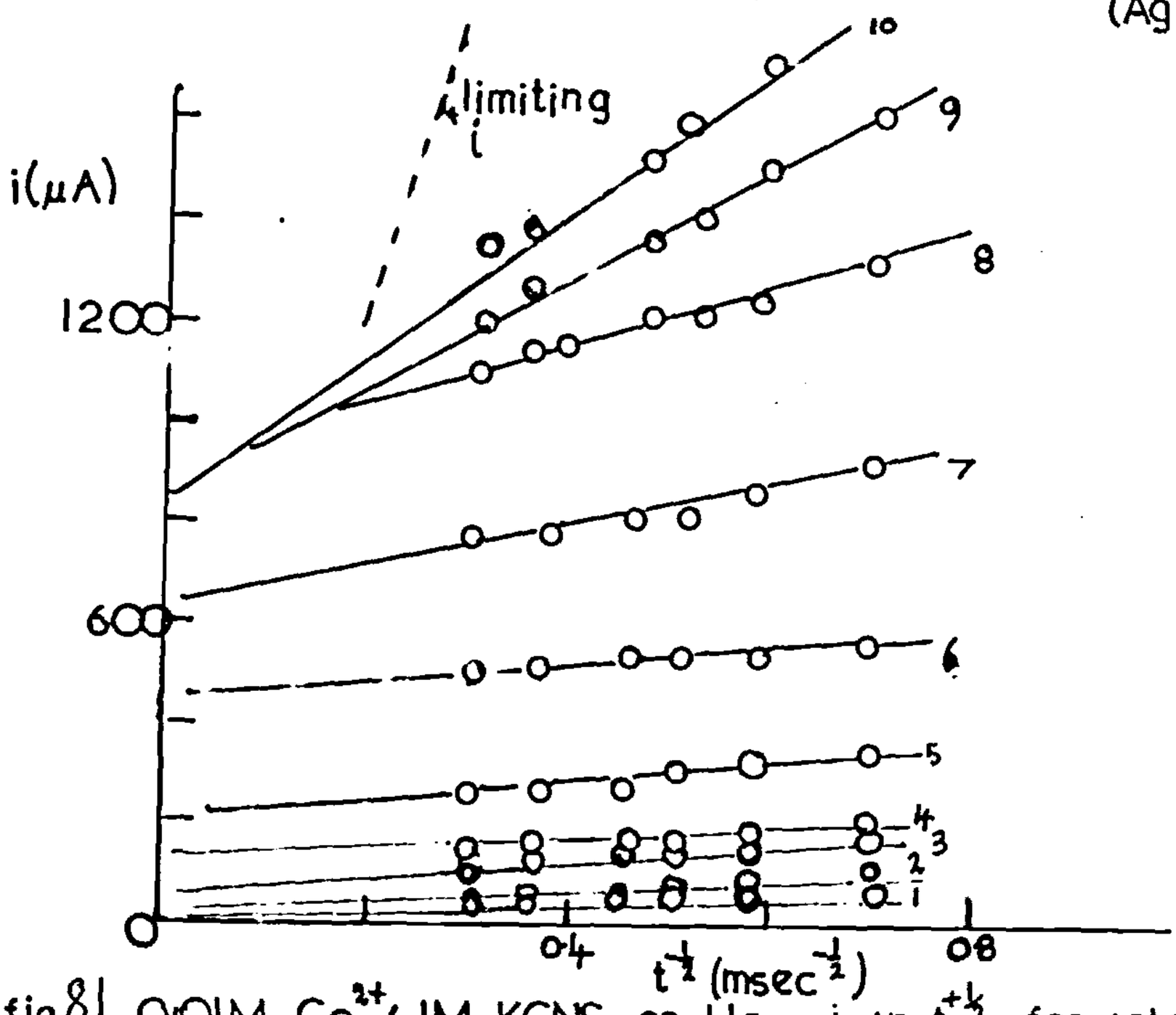

fig 81 0·01M Co^{2+} / 1M KCNS on Hg. i vs $t^{+\frac{1}{2}}$ for potentials (key above)

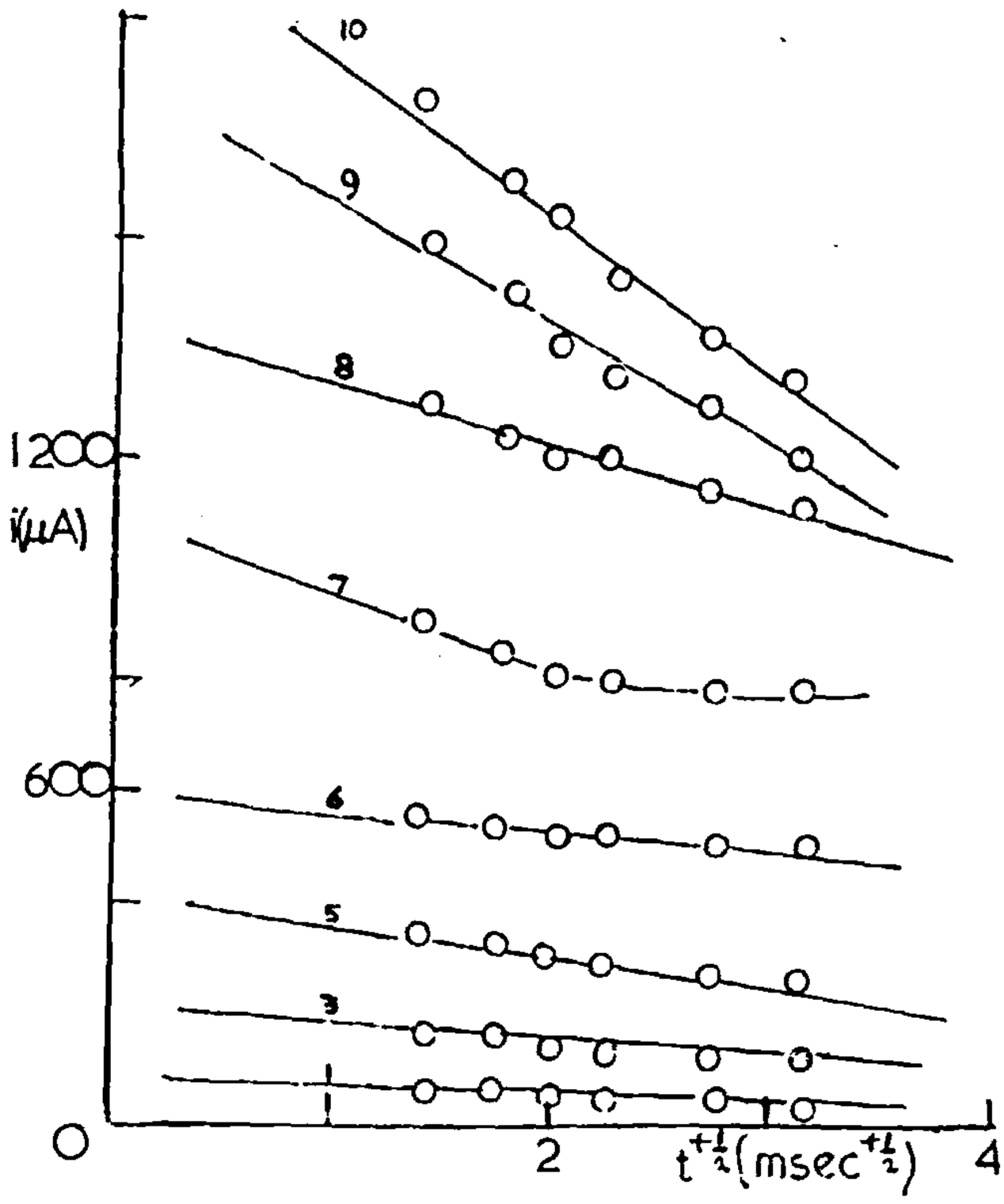

current intercepts on the $t^{+1/2} = 0$ axis) vs. potential (Fig.82), indicates first a potential dependent region, up to ca. -1150mV (Ag/AgCl), and then a limiting current plateau. The potential dependence of the former portion is ca. 90mV per current decade. This would correspond to simple electrochemical control for a λ electron transfer with $\alpha \approx 1/3$.

Consider a scheme,

$$A + B \underset{k_B}{\overset{k_f}{\rightleftharpoons}} X \xrightarrow{\lambda e} C_o/Hg \qquad (7.4.1.)$$

At lower potentials it is possible that the system may be limited by the electron transfer step. This would predict flat potentiostatic transients, the observed transients at potentials in the region -700mV to -900mV are fairly flat after the charging transient. At more cathodic potentials the system will become limited by the rate at which the preceding chemical reaction may supply the electro-active substance X. Even at ca. -1200mV on the initial current/voltage plateau, the plot i vs. $t^{+1/2}$ was still linear indicating that reaction control was still predominant.

It has already been stated in Chapter 6, section 3, that for a preceding reaction in which the equilibrium is far over to the left (in eqn. 7.4.1.), ignoring the back reaction k_B, and for an infinitely fast electrode process:

$$i = nFA C^* k_f \exp(k_f^2 t/D) \operatorname{erfc}(k_f (t/D)^{\frac{1}{2}})$$

fig 82 0·01M Co^{2+} / 1M KCNS on Hg. ic initial) vs E.

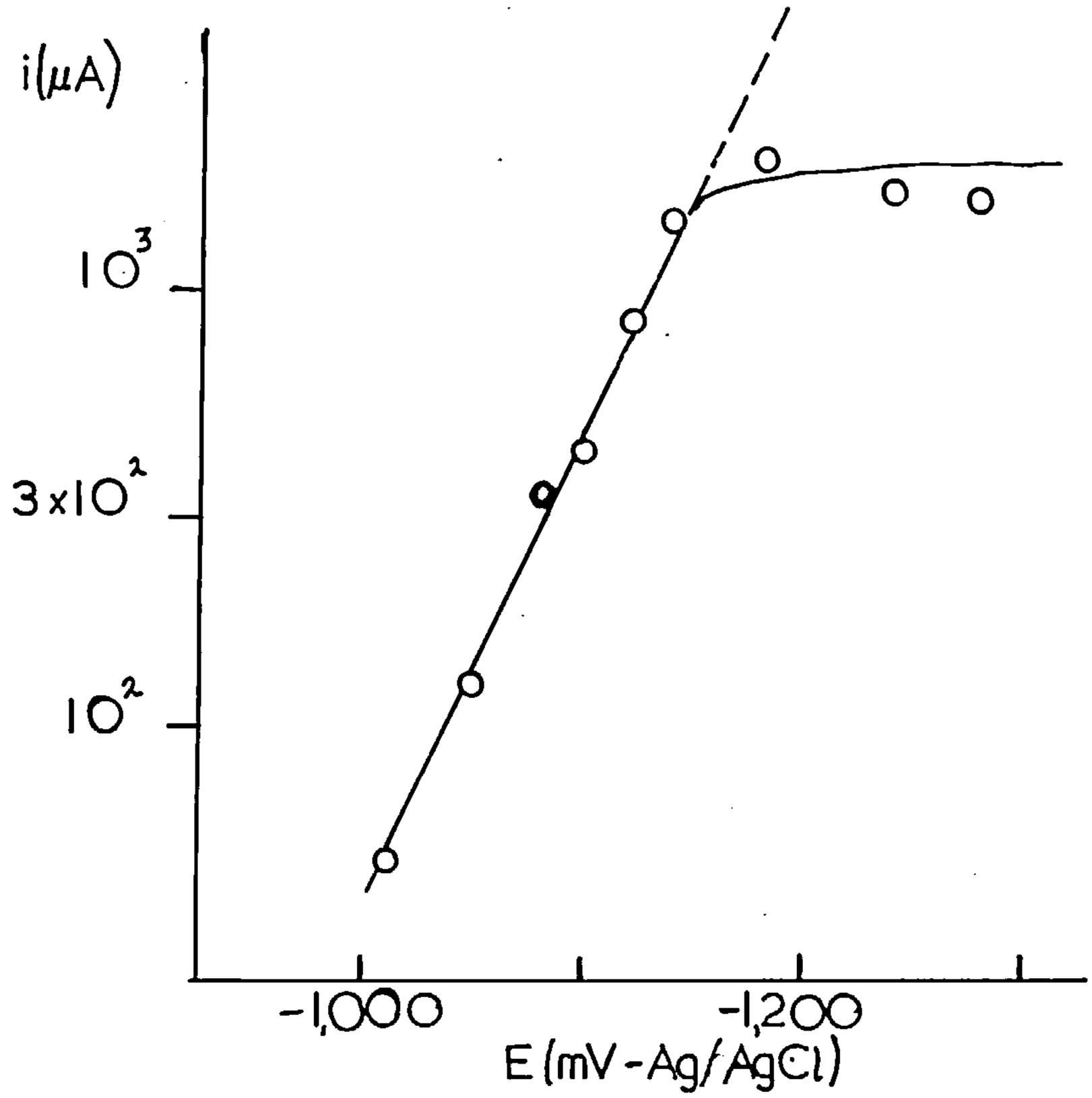

fig 83 0·05M Co^{2+} / 1M KCNS on Hg. i vs t. (E w.r.t. Ag/AgCl)

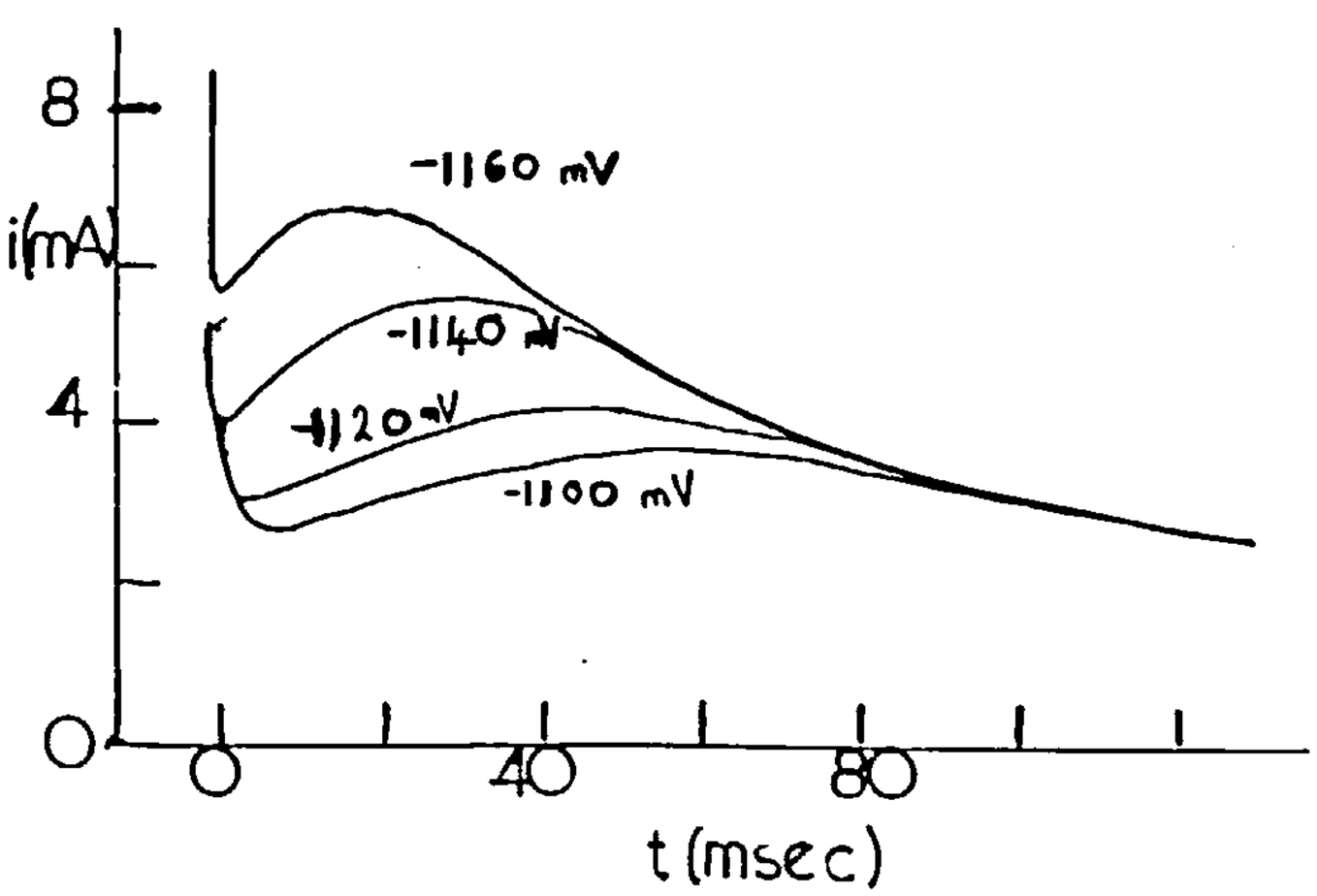

where C^* is the bulk concentration of A, k_f is in $cm.sec^{-1}$. B is considered in large excess so that its interfacial concentration is equivalent to its bulk concentration (1M CNS^- being used in this case). This plots as i vs. $t^{+1/2}$ at low times. Taking the initial currents as

$$i_{initial} = nFAC^* k_f \qquad (7.4.3.)$$

and relating k_f to the true bimolecular rate constant (k) in $litre.mole^{-1}sec^{-1}$ with the aid of the reaction layer thickness concept,

$$\text{i.e. } k = k_f / \mu C_{CNS^-} \qquad (7.4.4.)$$

one may obtain an estimate for k for the process considered. The reaction layer thickness corresponds to a layer adjacent to the electrode surface in which all molecules of X are formed and reduced. Koutecky and Brdička[158] obtained an estimate for μ by relating their equation derived by solving the diffusion equation for the conditions as for eqn. (7.4.2.), but not ignoring the back reaction,

$$\text{i.e. } i = nFAC^* D^{\frac{1}{2}} k_f^{\frac{1}{2}} K^{\frac{1}{2}} \exp(k_f K t) \operatorname{erfc}\left[(k_f K t)^{\frac{1}{2}}\right] \qquad (7.4.5.)$$

where k_f is in sec^{-1} and $K = [X]/[A][B]$; to the equation derived employing the reaction layer concept in the boundary condition

$$D_A \left(\partial C_A(x,t)/\partial x\right)_{x=0} = \mu k_f C_A(0,t) \qquad (7.4.6.)$$

where k_f is in sec^{-1},

$$\text{i.e.} \quad i = nFAC^{*}\mu k_f \exp\left(\frac{\mu^2 k_f^2 t}{D_A}\right) \operatorname{erfc}\left[\frac{\mu k_f t^{\frac{1}{2}}}{D_A^{\frac{1}{2}}}\right] \qquad (7.4.7.)$$

They thus obtained

$$\mu = \sqrt{D K / k_f} \qquad (7.4.8.)$$

Considering that A in this case is free C_o^{2+} (it seems that this would be unlikely in view of the greater concentration of complexed cobalt), and using eqn. (7.4.3.) i.e. back reaction ignored; along with eqns. (7.4.4.) and (7.4.8.), one obtains from the limiting current region, k for the reaction

$$C_o^{2+} + CNS^- \xrightarrow{k} C_oCNS^+ \xrightarrow{2e} C_o \qquad (7.4.9.)$$

as 5.3×10^4 $1.mole^{-1}$ sec^{-1}. Alternatively considering $C_o(SCN)_2$ to be reduced (this provides a more feasible reaction control as $\left[C_oSCN^+\right]$ and $\left[C_o(SCN)_2\right]$ are equal; also the equations are derived for conditions of equilibrium to the unreactive component),

$$\text{i.e.} \quad C_oSCN^+ + CNS^- \xrightarrow{k} C_o(SCN)_2 \xrightarrow{2e} C_o \qquad (7.4.10),$$

k becomes 4.5×10^1 $1.mole^{-1}$ sec^{-1}.

Employment of eqn. (7.4.5.) (back reaction considered),

gives k directly as 5×10^5 $1.mole^{-1}$ sec^{-1} for scheme (7.4.9.), and 5×10^1 $1.mole^{-1}$ sec^{-1} for scheme (7.4.10).

It is of interest to compare these figures with those derived by Turyan and Serova[159] for the nickel/thiocyanate system from polarographic measurements. They obtained k for the reaction for nickel identical to (7.4.9.) as 1.8×10^2 $1.mole^{-1}sec^{-1}$. The rate constants obtained here for scheme (7.4.9.) would seem to be rather high lending more support for scheme (7.4.10.) as rate limiting. In the case of the nickel system, free Ni^{2+} is only $^1/10$ of the $NiCNS^+$ concentration for an initial 0.01M Ni^{2+} solution in 1M CNS^-; $\left[Ni^{2+}\right] = 8.1 \times 10^{-5}M$; $\left[NiSCN^+\right] = 1.2 \times 10^{-3}M$; $\left[Ni(SCN)_2\right] = 3.5 \times 10^{-3}M$; $\left[Ni(SCN)_3^-\right] = 5.3 \times 10^{-3}M$.[160] This fact may allow a scheme as (7.4.9.) to control; for the cobalt system free C_o^{2+} is $^1/1,000$ of $\left[C_oSCN^+\right]$ (see section 7.3.), hence no such scheme may predominate.

7.5. C_o(11)/thiocyanate - crystal growth

Pulsing at longer times at lower potentials produced rising transients. Fig.83 illustrates transients at fairly short times at higher potentials measured oscillographically. It is noticeable that after the maximum all the transients follow the same curve as for diffusion control. The currents increased with pre-seeding but no significant change in

time dependence or potential dependence was observed.

Fig.84 shows transients for 10^{-2}M C_o^{2+}/1M CNS^- pre-seeded at -1V, 30msec (Ag/AgCl). Fig.85 illustrates the initial i vs. t^2 dependence observed. This probably corresponds to instantaneously nucleated growth of three-dimensional centres. Plots of $(i/t^2)^{1/3}$ vs. potential (Fig.86) corresponding to a lattice incorporation rate constant vs. potential plot, and current at constant time (Fig.87) and constant charge (Fig.88) vs. potential showed the same ca. 60mV slope. This corresponds to control by the lattice growth rate with rate constant determined by the simple $\frac{1}{2}$ electron transfer step. The potentials at which the transients were investigated were anodic to the initial current/voltage plateau observed i.e. well within the region when a similar potential dependence is observed for the initial currents.

It might be considered that a mercury surface would offer no nucleation points whence instantaneous nucleation could occur without prenucleation. It may be that adsorption of CNS^- on the mercury surface restricts the nucleation possibilities. In section 7.3., it was mentioned that sweeping once again after a cycle up to ca. -1100mV (Ag/AgCl) and back produced a further peak at ca. -660mV, attributed to

fig 84 0·01 M Co^{2+}/1M KCNS on Hg. i vs t. prepulse -1 V, 30 msec (Ag / AgCl).
1) -810 mV 2) -820 mV 3) -830 mV; 4) - 840 mV; 5) -850 mV; 6) - 860 mV.

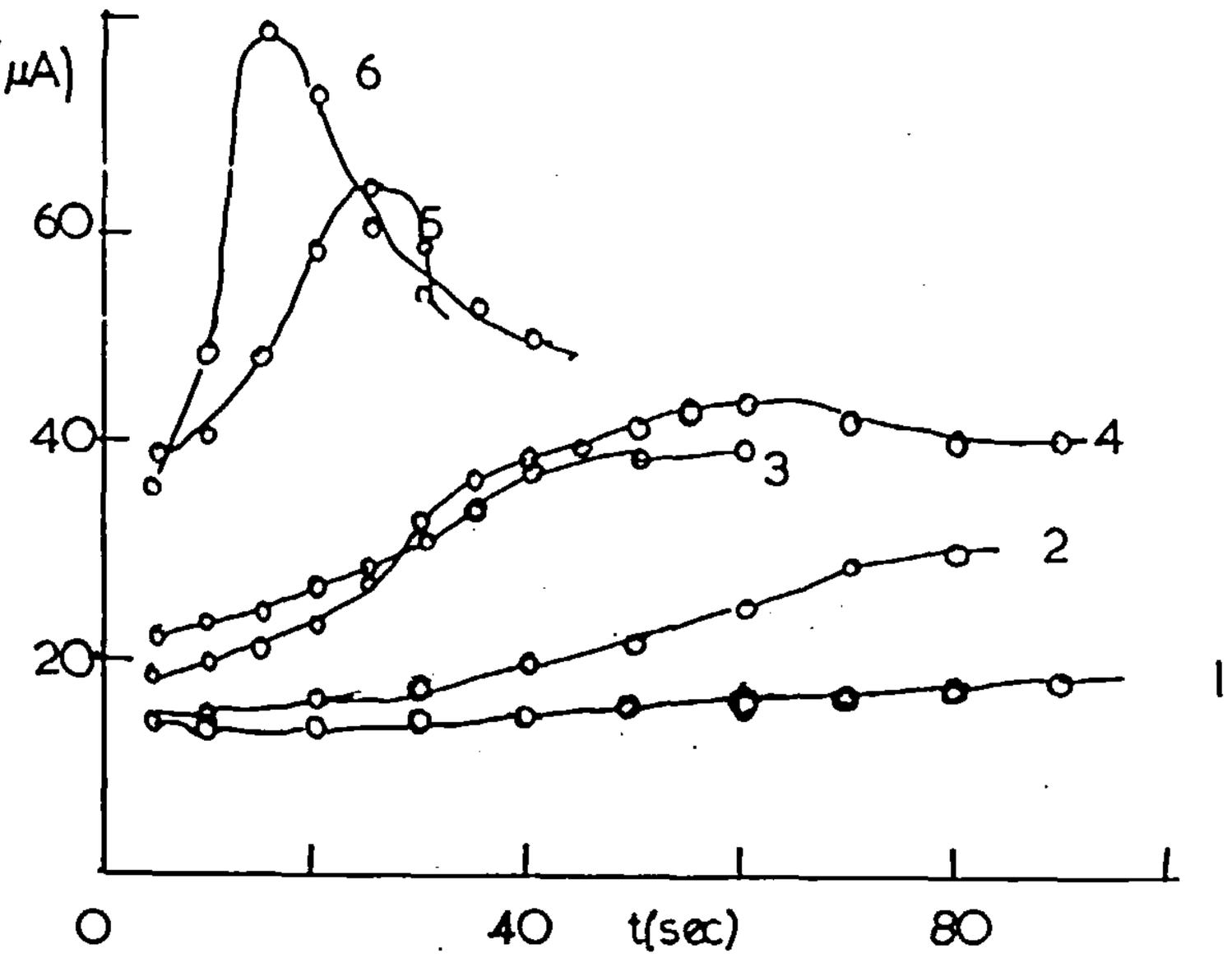

fig 85 As above. i vs t^2.

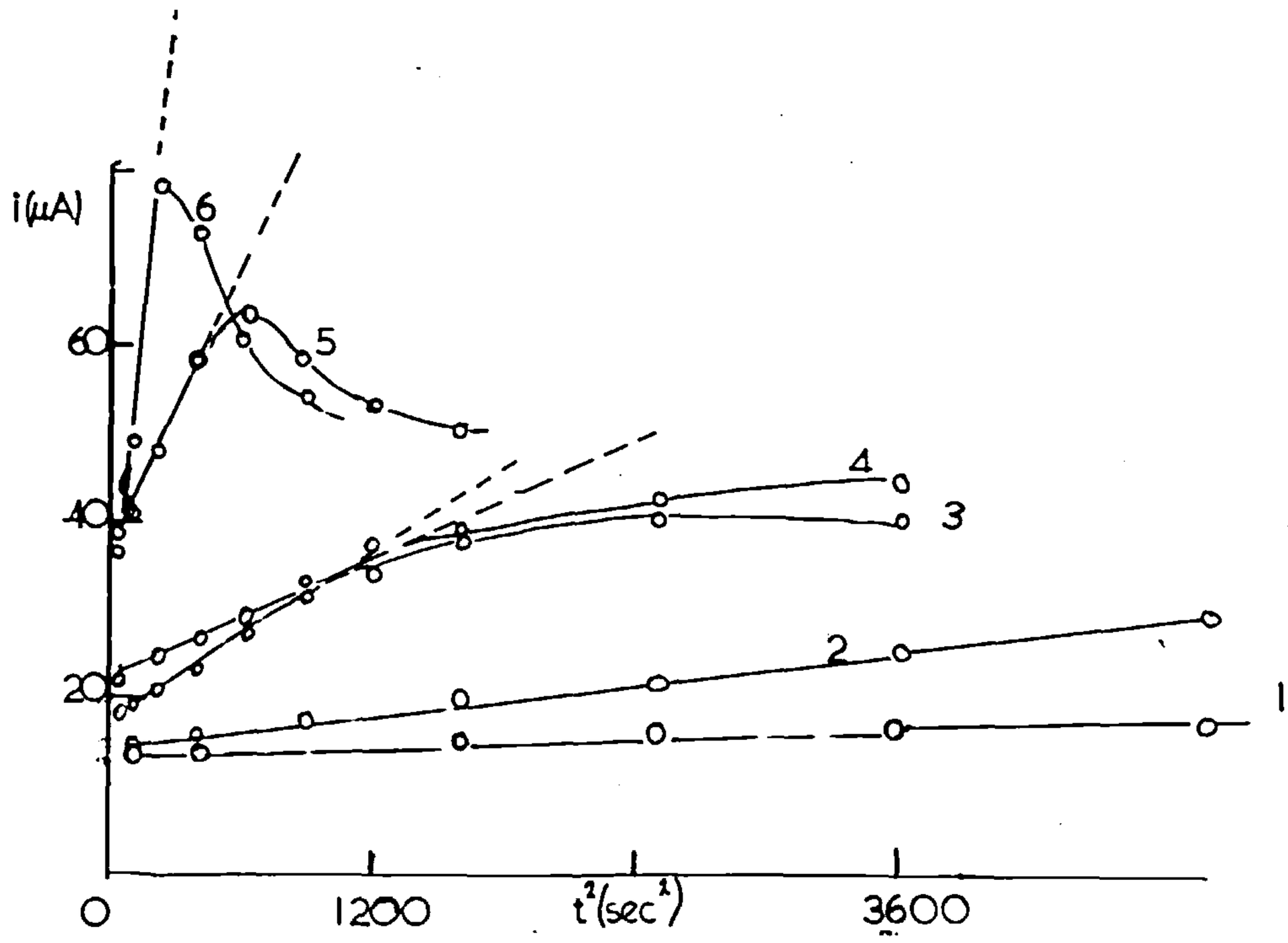

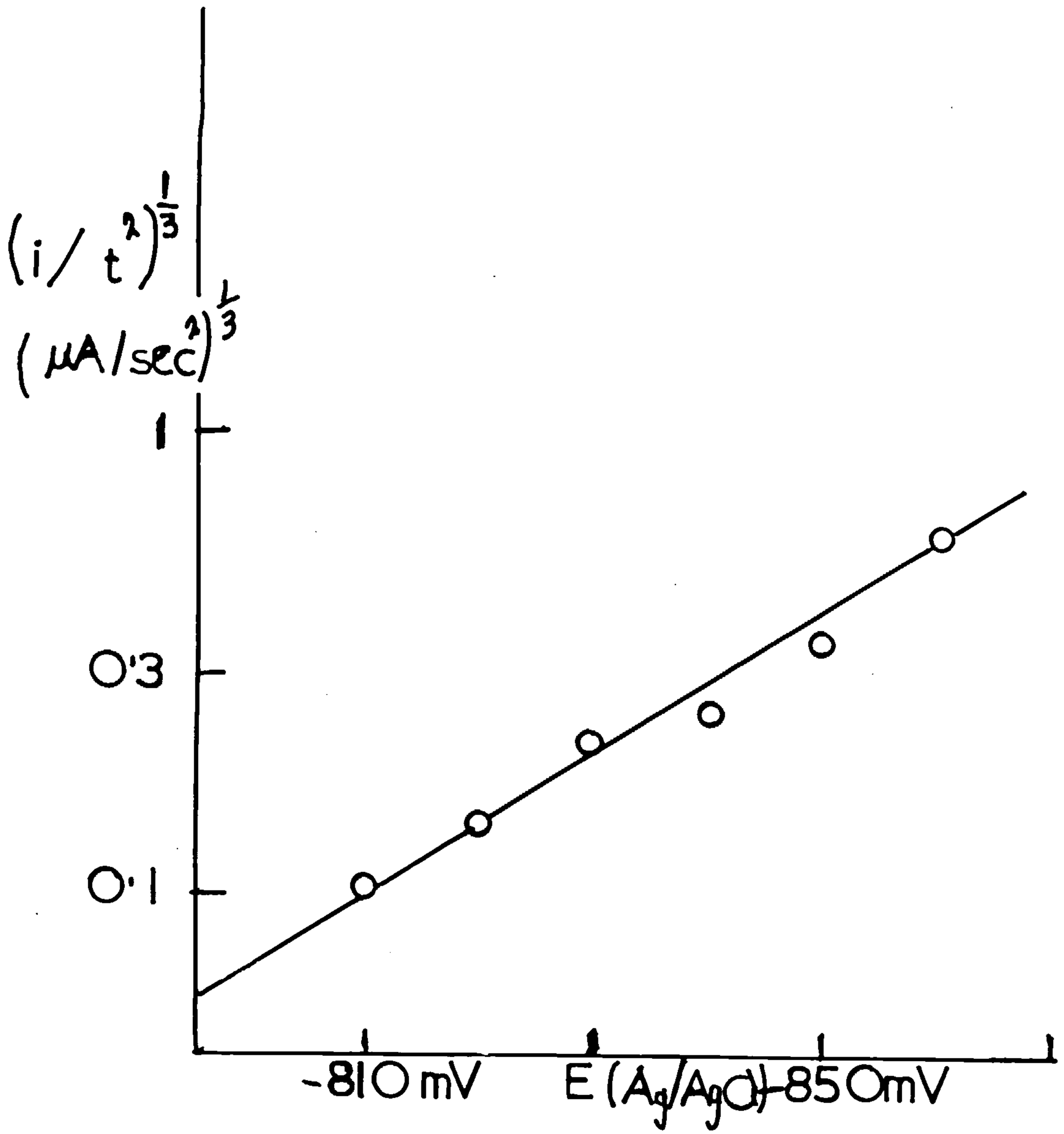

fig 86 0·01M Co^{2+} / 1M KCNS on Hg. $(i/t^2)^{\frac{1}{3}}$ vs E
prepulse -1V, 30msec.

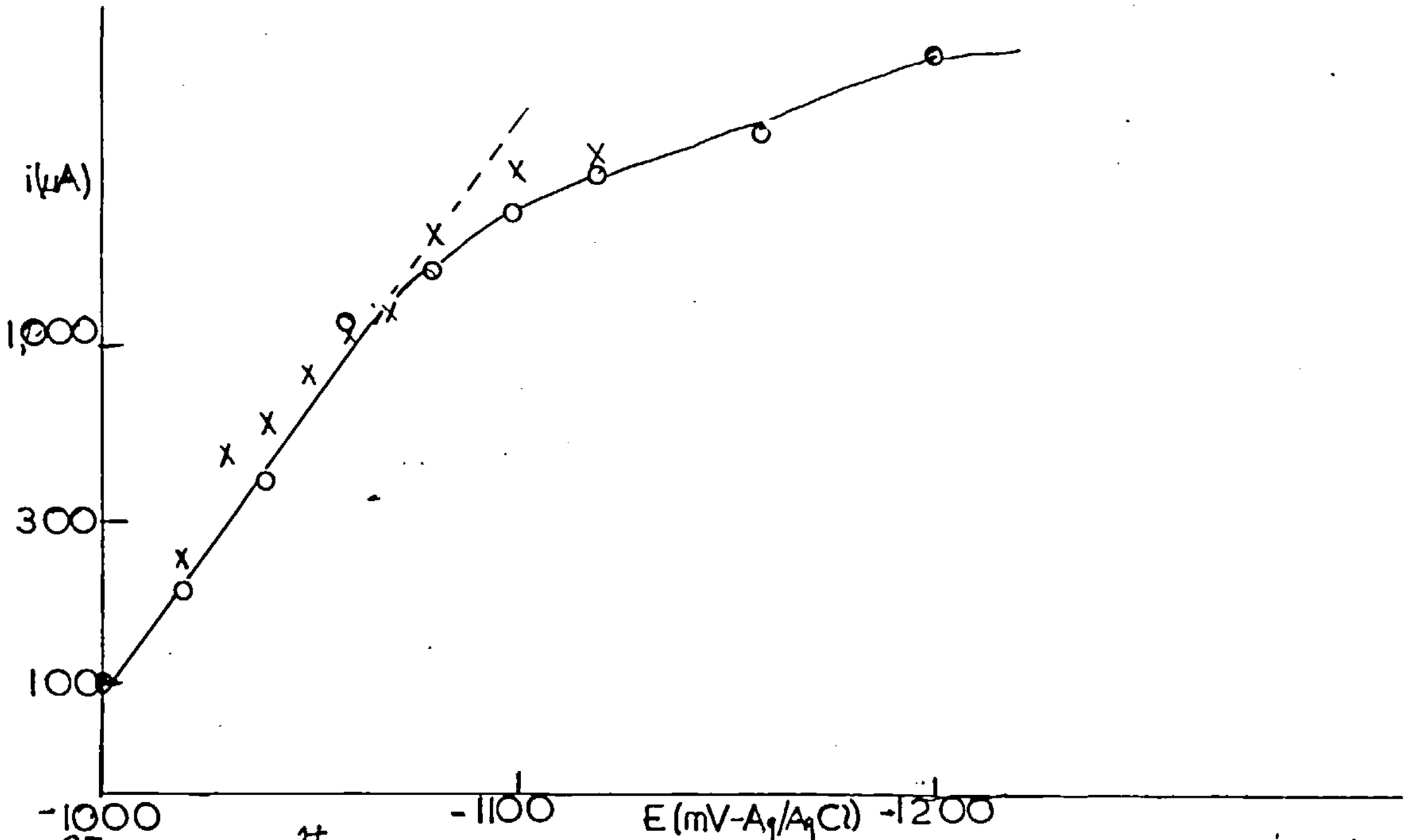

fig 87 0·05M Co^{2+} / 1M KCNS on Hg. i(t) vs E for, t=10 msec (o); t = 50 msec (x).

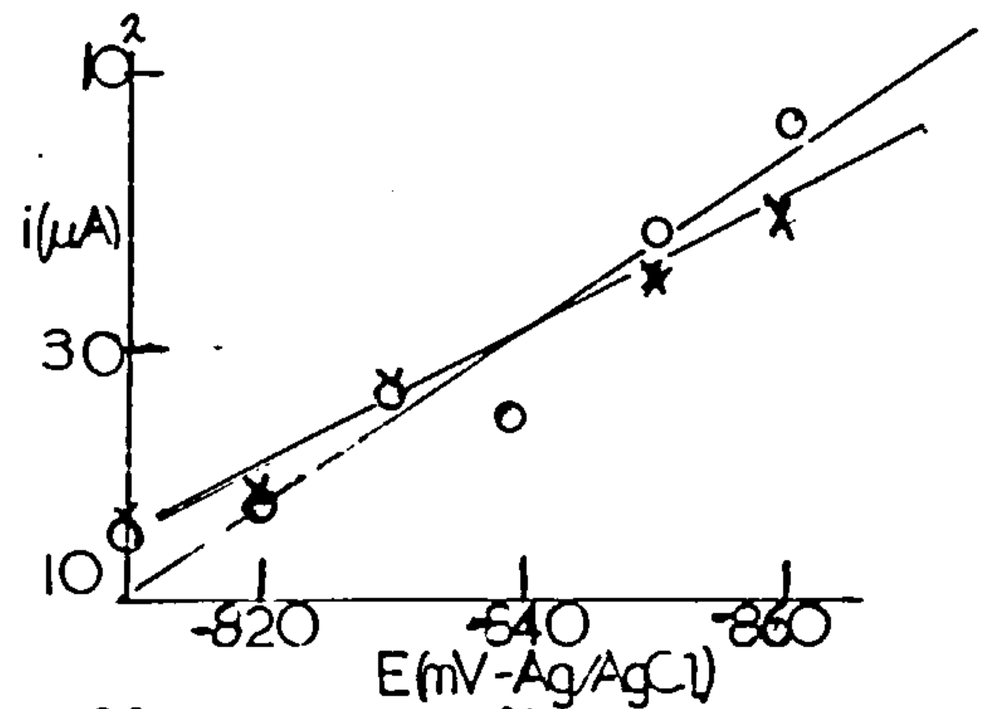

fig 88 0·01M Co^{2+} / 1M KCNS on Hg. i(t,q) vs E for, t= 15 sec (o); q=400 μC (x). prepulse -1V, 30 msec.

nucleation of C_o on remaining C_o-Hg surface compounds. It was not found possible to observe any growth under pulse conditions in the region observed, even after prenucleation at ca. 200mV more cathodic was employed. Growth transients are not observed under any conditions until ca. -800mV.

If amalgamation of the cobalt (section 7.3.) is a fast process, one would expect to see some evidence for the process in the potentiostatic transients. Considering three-dimensional centres, the reaction taking place over the hemispherical areas, rate constant k, and removal of deposit into the substrate through a cylinder radius r, height h; then

$$\frac{dV}{dt} = 2\pi r^2 \frac{dr}{dt} - 2\pi r h \frac{dr}{dt} = \left(\frac{M}{\rho}\right) k 2\pi r^2 \qquad (7.5.1.)$$

Thus $$dr - h\,dr/_{\rho} = \left(Mk/_{\rho}\right) dt \qquad (7.5.2.)$$

and $$r - h \ln r = t\left(Mk/_{\rho}\right) \qquad (7.5.3.)$$

As $i \propto r^2$ at any time then,

$$i^{\frac{1}{2}} - h/_2 \ln i \propto t \qquad (7.5.4.)$$

Eqn. (7.5.4.) means that at low times, $i \propto \exp t$ and later on $i \propto t^2$. No marked exponential time dependence was noted

during the transients so amalgamation may be a slow process.

Double-wave behaviour of cobalt (11) in thiocyanate medium has been observed at dropping mercury electrodes.[142,143] Kyriacov[142] proposed that the two waves resulted from two consecutive one-electron reductions. Perone and Gutknecht[143] attributed the first wave (occurring at ca. -1V. S.C.E.) to the reduction of an aquo-C_o(11) species, while the second was held to involve the reduction of a C_o(11)-SCN^- complex. The major C_o(11) species $C_o(SCN^+)$ was held to be reduced on the cobalt surface produced by the reduction of the aquo complex during the first wave; and the second wave was postulated as reduction of $C_o(SCN^+)$ on the mercury surface. Perone and Gutknecht also carried out potential sweep measurements on a hanging mercury drop electrode. They "pre-plated" their drop at a cathodic potential (-1,100mV, S.C.E.) for various durations of time and then cycled the drop cathodically from -800mV. It was found that the first wave was progressively shifted anodic as the duration of the "pre-plating" increased. This was stated as indicative that $C_o(SCN)^+$ may be reduced on the cobalt surface produced at -1,100mV., the later waves were attributed to reduction of the aquo species, and finally the thiocyanate complex on remaining exposed mercury. Potentiostatic pulse measurements

were made jumping from -810mV (S.C.E.) to various potentials. The rising transients obtained were erroneously attributed to an "induction period", corresponding to a slow build up of cobalt deposit at less cathodic potentials, followed by a sharp rise to the diffusion-limited reduction of $C_o(SCN)^+$ on the cobalt surface. Rising transients are evidence for nucleation and growth processes. It would seem more reasonable to explain the sweep measurements of Perone and Gutknecht in terms of nucleation of cobalt nuclei at the more cathodic potential, followed by their growth under sweep conditions at more anodic potentials. The number of polarographic waves encountered for this system is more probably due to the separate formation of the various C_o-Hg compounds mentioned in section 7.3. Indeed the anodic shift of the first wave observed by Perone and Gutknecht under sweep conditions for increasing "pre-plate" duration, is evidence for deposition of cobalt on a surface C_o-Hg compound as postulated from the sweep results in section 7.3.

Chapter 8

Summary

8.1. Introduction

It has been shown in Chapter 1, section 4 that information about metal electrocrystallisation processes can only really be obtained in the initial stages of metal growth upon inert substrates when nuclei are supposed reasonably free from dislocations. The potentiostatic pulse technique was employed in order to follow the initial growth of such nuclei, using two consecutive pulses of decreasing amplitude in order to control the nucleation in some cases. Some measurements were carried out employing the parent metal substrates (silver and mercury) in order to ascertain the relevance of certain models.

8.2. Electrocrystallisation of Silver on Silver

In Chapter 3, section 3.2. a model for the deposition of silver onto silver was suggested in which the process was controlled simply by diffusion of silver ions from the bulk, the concentration at the interface being maintained by the Nernst equation. The surface activity of 'adatoms' predicted by this model for the experimental pulse results was essentially the geometric area. Doubt was thereby thrown on any limiting 'adatom' step.

In order to clarify the experimental results of Krebs and Roe[103] who postulated a nucleation process for the deposition of silver onto silver from certain potential sweep measurements, the same model as above was postulated but starting from the condition of a linear concentration distribution, the interfacial concentration being shifted by the potential scan (section 3.3.). The current/voltage curves were computed on the basis of this model. Slight inflexions in the curves after the switches in scan direction were attributed to the concentration distribution lagging behind the linear distribution at fast sweep rates. No marked maxima were predicted (as found by Krebs and Roe) and the experimental measurements closely followed the computed curves. No evidence was therefore found for any nucleation process for the deposition of silver onto silver.

8.3. Electrocrystallisation of metals onto carbon substrates

In the case of the deposition of silver onto carbon (Chapter 3) under pulse conditions, an $i \propto t^2$ relationship was found which switched to $i \propto t$ upon adequate pre-seeding of nuclei. A model of nucleation and growth of two-dimensional centres, so growing as to form three-dimensional nuclei, was professed. This was in accord with the results of Budewski

et al,[92] who found that silver electrocrystallised in a two-dimensional nucleation on dislocation-free silver single crystal filaments. The Tafel dependence of the two-dimensional lattice growth constant was found to be 60mV. A mechanism involving an electrochemical pre-equilibrium controlled by the Nernst equation, followed by the slow lattice incorporation step involving the discharged silver surface atoms was invoked. It was pointed out that such a mechanism is in conflict with the usual electrochemical form of rate-constants involving α and i_o. It is postulated that such a scheme may occur in the electrocrystallisation of all the "softer" metals. A value for the lattice growth constant at the reversible potential ($\sim 5 \times 10^{-5}$ moles.cm^{-2} sec^{-1}) was given.

Palladium metal was deposited on carbon under pulse conditions (Chapter 4) and was found to follow an $i \propto t^3$ relationship, switching to $i \propto t^2$ upon pre-seeding. It was suggested that the form of such nuclei was hemispherical. The potential dependence of the three-dimensional lattice growth constant was found to be ca. 50mV. This was identified with a simple two electron process with $\alpha = 0.6$. A value for the lattice growth constant, $\sim 3 \times 10^{-9}$ moles.cm^{-2} sec^{-1}, was given for a 5×10^{-2}M Pd^{11} solution. The reduced complex was quoted as $PdCl_2$, as also predicted by Kravstov and Zelenskii.[111]

The differing palladium potentiostatic time dependence (compared to that of silver) was offered as evidence for rate-determining steps at the peripheries of growing nuclei of differing geometries.

Mercury was chosen as a metal for electrocrystallisation onto carbon (Chapter 5) in order to show that the absence of a lattice means that control by bulk diffusion processes for the growth of nuclei is involved. Mercurous ions were reduced at a mercury cathode under pulse conditions to demonstrate that the electrode process was fast and reversible. Nucleation and growth of mercury on carbon under pulse conditions was shown to be dependent upon the growth of hemispheres controlled by planar bulk diffusion. An $i \propto t^{3/2}$ dependence was observed, switching to $i \propto t^{1/2}$ upon pre-seeding, as predicted by the model. The seeded transients were found to be virtually independent of potential, as predicted for a reversible electrode process controlling the interfacial concentration at ca. 60mV from the reversible potential when growth was observed.

8.4. The formation of metal layers

Various metals were deposited onto inert metal substrates (Pb onto Ag, Tl onto Ag, and Cd onto Pb) in order to ascertain whether nucleation and growth processes were involved

in potential sweep phenomena observed by Schmidt and Gygax[118] for these and other systems which they attributed to adsorption processes (Chapter 6). Under potential sweep conditions the systems Pb/Ag and Tl/Ag gave rise to two formation and removal peaks, whereas Cd/Pb only one. The first peaks for Pb/Ag and Tl/Ag were ascribed to the formation of monolayers of the deposited metals, constrained to fit the substrate lattice. This is made possible by the small differences in the deposit/substrate lattice parameters. At more cathodic potentials for these two systems the deposit grows as its own preferred lattice in a three-dimensional manner to form the second peaks. In the case of Cd/Pb the larger difference in lattice parameters precludes the formation of the monolayer peak. The fact that such crystal growth processes are involved is justified by the appearance of only one peak for the deposition of lead on mercury, when an amalgam is formed.

Potential pulse measurements for these systems at short times gave rise to falling transients. The form of these transients in that plots of i vs. $t^{-1/2}$ at lower potentials cut the $t^{-1/2}$ axis at finite times and show some curvature, is explained in terms of the formation of partial monolayers of deposit. Some evidence for preceding chemical reaction

control was found in the case of the reduction of TlCl.

Crystal growth processes were identified in the multilayer (second peak) regions for Pb/Ag and Tl/Ag and the deposition peak region for Cd/Pb, by the observation of rising transients under pulse conditions. The explanation of Schmidt and Gygax in terms of adsorption was thereby discredited. The transients showed extreme potential dependence which was unchanged by pre-nucleation. An explanation was postulated in terms of growth of nuclei in a zone of constant Nernstian diffusion, the interfacial concentration being controlled by the Nernst equation. The rate of nucleation was assumed to be governed by the generation of defects on the surfaces of the deposited nuclei.

8.5. <u>The electrocrystallisation of cobalt on mercury</u>

Mercury was used assumed as an almost ideal inert substrate for this system (Chapter 7), but in view of the evidence for C_o-Hg compound formation this assumption is not justified. Uncomplexed C_o^{2+} gave rise to difficulties in that cathodic oxide formation shut off the deposition processes under both sweep and pulse conditions. Under pulse conditions a second rising transient was observed, and occasionally a second peak under sweep conditions. It was postulated that

either reduction of oxide or nitrate in solution would account for these phenomena. Evidence for chemical reaction control was obtained in the potential dependence of the rising transients and the form of the i vs. $t^{-1/2}$ plots. The formation of C_oOH^+ was postulated as the slow stage.

A thiocyanate medium was employed in order to eradicate the difficulties encountered in the use of uncomplexed C_o^{2+}. Sweep measurements produced formation and removal peaks which were widely separated, the removal peaks being split into two. Explanations were proferred in terms of the formation of cobalt mercury compounds. A further deposition peak at about the reversible potential for $C_o^{2+}/C_{o(s)}$ for a mercury drop already scanned cathodic was postulated as evidence for a surface cobalt-mercury compound. Short time pulse measurements indicated some degree of reaction control at more cathodic potentials. It was suggested that the slow stage was the formation of $C_o(SCN)_2$ from C_oSCN^+, for which a rate constant of ~ 50 $1.mole^{-1}$ sec^{-1} was found. Crystal growth transients were unchanged with pre-seeding, possibly due to thiocyanate adsorption. They showed i vs. t^2 initially, ascribed to the growth of three-dimensional centres. The potential dependence of such transients was ~ 60mV, identified with the simple two electron step. Evidence for amalgamation

from such transients was not obvious. The double-wave behaviour of polarograms observed for this system may be due to the separate formation of C_o-Hg compounds. The exact role and nature of such compounds, the amalgam and surface cobalt deposits is still to be identified in the polarographic, potential scan and pulse measurements.

Appendix 1

A finite difference method for obtaining cyclic current/voltage curves

The problem presented is to solve Fick's second law of diffusion

$$\partial C/\partial t = D\left(\partial^2 C/\partial x^2\right) \qquad \text{(A.1.1.)}$$

for conditions of reversible electron transfer under linear sweep conditions,

i.e. $$C^o = C^* \exp\left(-nF\left(\eta_i + \omega t\right)/RT\right) \qquad \text{(A.1.2.)}$$

where C^o is the interfacial concentration; C^* the bulk concentration, η_i the initial overpotential (positive for cathodic) and w the scan rate in volt/sec. In addition it is assumed that at η_i, conditions of diffusion from a Nernstian diffusion layer exist i.e. a linear concentration distribution from the interface to δ (the Nernst diffusion layer thickness).

Analytical solutions were found difficult under these conditions. The method of separating the variables and expanding as a Fourier series broke down when it was found that at t = 0, an infinite $\partial C/\partial x$ gradient ensued at x = 0. For a similar reason the method of direct solution of the

differential equation by the use of haplace transformations was inappropriate; inversion of the transform obtained presented a mathematical obstacle. It was thus decided to solve the problem by numerical means, facilitated by digital computation using an English Electric-Leo KDF 9 computer.

The concentration at a point x ($x = \delta/n$) along the perpendicular to the electrode surface at the initial potential is given by,

$$C(x, \eta_i) = C^* \exp\left(\frac{-nF\eta_i}{RT}\right) + \frac{x}{\delta}\left[C^* - C^* \exp\left(\frac{-nF\eta_i}{RT}\right)\right] \quad \text{(A.1.3.)}$$

assuming an initial linear concentration distribution.

When the electrode potential shifts by the scan in a time t, the surface concentration will follow by eqn. (A.1.2.). This means a redistribution of concentrations at various x by (A.1.1.). (A.1.1.) may be represented in terms of finite differences x and t,

$$\text{i.e. } \frac{\bar{C}_n - C_n}{t} = D\left\{\frac{(C_{n+1} - C_n)}{x^2} - \frac{(C_n - C_{n-1})}{x^2}\right\} \quad \text{(A.1.4.)}$$

Eqn. (A.1.4.) may be rearranged to give $\bar{C}_n$, the new C_n after time t.

$$\text{i.e. } \bar{C}_n = (tD/x^2)\left[C_{n+1} - 2C_n + C_{n-1}\right] + C_n \quad \text{(A.1.5.)}$$

Such an equation as (A.1.5.) can be shown to have a

difference between itself and the true diffusion equation which is bounded only if $^{tD}/_{x^2} \leqslant {}^{1}/_{6}$, the error growing exponentially with t when $^{tD}/_{x^2} \rangle {}^{1}/_{6}.10^{4}$ Such an insertion in eqn. (A.1.5.) leads to,

$$\overline{C}_n = {}^{1}/_{6}\left\{C_{n+1} + 4C_n + C_{n-1}\right\} \qquad \text{(A.1.6.)}$$

Thus the new concentration distribution with x may be calculated at given t intervals and the current at such times will be given by

$$i = \frac{FAD}{X}\left(\overline{C}[0] - \overline{C}[1]\right) \qquad \text{(A.1.7.)}$$

This procedure was programmed for the computer in KDF 9 ALGOL. The program appears below.

```
→ ESTABLISH CH24HDS00APU;
SWEEP DIFF LAYER;
O/P L→
begin library A0,A6;
real F,R,T,zed,eta,l,x,tau,D,t,c,y,grad,etar,zedar,fac;
integer f1,f2,z,n,zz;

open(20);open(30);
F:=9.6487₁₀4;
R:=8314.3;

T:=298.15;
n:=read(20);
zed:=read(20);
eta:=read(20);
l:=read(20);
x:=read(20);
tau:=read(20);
D:=read(20);
c:=read(20);
f1:=format([10s-d.dddddd₁₀-ndc]);
f2:=format([10sd.dddddd-nd]);
write text(30,[[3c]SWEEP**FIN**DIFF
[2c10s]SEC[19s]MA[2c]]);
t:=x↑2/6.0/D;

etar:=etaXF/R/T;zedar:=tXzedXF/R/T;
begin real array u[0:n] , v[0:n];
for y:=0step 1untilndo
      begin
      u[y]:=0.0;
      v[y]:=0.0;
      end;
for y:=0 step 1until n do
      begin
      u[y]:=cXexp(-etar)+cXyXx/l
            -cXyXx/lXexp(-etar);
      end;
fac:=DXFX1₁₀3/x;
grad:=(u[0]-u[1])Xfac;
write(30,f2,t);
write(30,f1,grad);
v[n]:=c;
z:=1;
```

```
SKIP:for y:=1step1until n-1 do
     begin
     v[y]:=1/6.0x(u[y-1]+4xu[y]+u[y+1]);
     end;
v[0]:=cxexp(-etar+zedarxz);
if z÷100x100=z then   begin
grad:=(v[0]-v[1])xfac;
write(30,f2,zxt);
write(30,f1,grad);    end;
for y:=0step1until n do
     begin
     u[y]:=v[y];
     end;
z:=z+1;
if zxt<tau then goto SKIP;
grad:=(v[0]-v[1])xfac;
write(30,f2,(z-1)xt); write(30,f1,grad);


z:=z-2;zz:=z+2;
JUMP:for y:=1 step 1 until n-1 do
     begin
          v[y]:=1/6.0x(u[y-1]+4xu[y]+u[y+1]);
     end;
v[0]:=cxexp(-etar+zedarxz);
if z÷100x100=z then
     begin
          grad:=(v[0]-v[1])xfac;
            write(30,f2,zzxt);
            write(30,f1,grad);
     end;
for y:=0 step 1 until n do
     begin
          u[y]:=v[y];
     end;
z:=z-1; zz:=zz+1;
if zxt>0then goto JUMP;
grad:=(v[0]-v[1])xfac;
write(30,f2,(zz-1)xt);
write(30,f1,grad);
close(20); close(30);
end;
end→
→
```

Appendix 2

Deposition of a metallic partial monolayer with reversible electron-transfer under potentiostatic conditions

In this appendix a solution of a model is presented for the reversible deposition of metal whose activity is allowed time-dependent under potentiostatic conditions.

The equations to be solved are:-

$$\partial C(x,t)/\partial t = D\left(\partial^2 C(x,t)/\partial x^2\right) \qquad \text{(A.2.1.)}$$

where $C_{(x,t)}$ is the concentration of metal ion at a distance x perpendicular to the electrode and at a time t.

The rate of change of activity (a) of the deposit will be related to the flux at the interface,

$$da(t)/dt = \left(AD/m\right)\left(\partial C(0,t)/\partial x\right) \qquad \text{(A.2.2.)}$$

where A is the electrode area and m is the number of moles of deposit at monolayer coverage. If one assumes a linearised Langmuir isotherm with the Nernst equation to apply to the electrode reaction,

$$C(0,t)/C^* = a(t)\exp\left(-nF\eta/RT\right) \qquad \text{(A.2.3.)}$$

where η is the overpotential, positive for a cathodic reaction, and C^* is the bulk concentration. The overpotential

is defined with respect to normal thermodynamic equilibrium with $a = 1$ and $C_{(o,t)} = C^{*}$.

The boundary conditions relevant to this model are:-

$$C_{(x,o)} = C^{*} \qquad \text{(A.2.4.)};$$

$$\lim_{x \to \infty} C_{(x,t)} = C^{*} \qquad \text{(A.2.5.)};$$

$$a(0) = 0 \qquad \text{(A.2.6.)}$$

Defining the Laplace transformation of a function $f_{(t)}$ as

$$\bar{f}(p) = \int_{0}^{\infty} f(t) \exp(-pt)\, dt \qquad \text{(A.2.7.)},$$

one may transform eqn. (A.2.1.) with respect to time,

$$-C(x,0) + p\,\bar{C}(x,p) = D\left(\partial^{2}\bar{C}(x,p)/\partial x^{2}\right) \qquad \text{(A.2.8.)}$$

Substituting for $C_{(x,o)}$ by eqn. (A.2.4.) in eqn. (A.2.8.), and solving the homogeneous second order equation in x,

$$\bar{C}(x,p) = A \exp\sqrt{\frac{p}{D}}\cdot x + B \exp -\sqrt{\frac{p}{D}}\cdot x + \frac{C^{*}}{p} \qquad \text{(A.2.9.)}$$

By eqn. (A.2.5.), $A = 0$ (for finite $C_{(x,t)}$).

Hence by (A.2.3.),

$$\bar{C}(0,p) = C^{*}\bar{a}(p) \exp\left(-nF\eta/RT\right) = B + C^{*}/p \qquad \text{(A.2.10.)}$$

Thus $$\bar{C}(x,p) = C^{*}\bar{a}(p) \exp\left(\frac{-nF\eta}{RT}\right) \exp -\sqrt{\frac{p}{D}}\cdot x - \frac{C^{*}}{p}\left\{\exp -\sqrt{\frac{p}{D}}\cdot x - 1\right\} \qquad \text{(A.2.11.)}$$

Upon differentiation with respect to x and taking $x = 0$,

$$\frac{\partial \bar{C}(0,p)}{\partial x} = C^* \bar{a}(p) \exp\left(-nF\eta/RT\right)\left(-\sqrt{\frac{p}{D}}\right) + \frac{C^*}{p}\sqrt{\frac{p}{D}} \qquad \text{(A.2.12.)}$$

Transforming eqn. (A.2.2.) with respect to time,

$$-a(0) + p\bar{a}(p) = \left(AD/m\right)\left(\partial \bar{C}(0,p)/\partial x\right) \qquad \text{(A.2.13.)}$$

Substitution of $\bar{a}(p)$ from eqn. (A.2.13.) into eqn. (A.2.12.), noting boundary condition (A.2.6.)

$$\frac{\partial \bar{C}(0,p)}{\partial x} = \frac{C^*}{D^{\frac{1}{2}}}\left\{1/\left(p^{\frac{1}{2}} + C^* D^{\frac{1}{2}}\left(A/m\right)\exp\left(-nF\eta/RT\right)\right)\right\} \qquad \text{(A.2.14.)}$$

The inversion of a function of the form $(p^{\frac{1}{2}} + \text{constant})^{-1}$ is given by,

$$L^{-1}\left\{1/\left(p^{\frac{1}{2}} + Z\right)\right\} = \frac{1}{\sqrt{\pi t}} - \left\{Z \exp Z^2 t \times \operatorname{erfc} Z\sqrt{t}\right\} \qquad \text{(A.2.15.)}$$

Hence by inversion of eqn. (A.2.14.) and noting that

$$i = nFAD\left(\partial C/\partial x\right)_{0,t} \qquad \text{(A.2.16.)}$$

$$i = nFAC^*\sqrt{\frac{D}{\pi t}} - \left[\left(\frac{nFA^2(C^*)^2 D}{m}\right)\left(\exp - \frac{nF\eta}{RT}\right) \times \exp\left[\left\{(C^*)^2 D\left(\frac{A^2}{m^2}\right)\exp\left(-2nF\eta/RT\right)\right\}t\right] \times \operatorname{erfc}\left\{\left[C^* D^{\frac{1}{2}}\left(A/m\right)\exp\left(\frac{-nF\eta}{RT}\right)\right]\sqrt{t}\right\}\right] \qquad \text{(A.2.17.)}$$

This expression may also be derived from the analysis of Delahay and Trachtenberg[131] for the kinetics of adsorption of

neutral substances on electrodes using the linearised isotherm. The linearisation assumption can only be justified at low concentrations of adsorbate. Their experimental results show that this simplification is only really justified with $C^{*} < $ ca. 10^{-4}M. However, an exact solution is not possible using the complete isotherm, though Reinmuth[132] produced a series solution. For low concentrations, Reinmuth found good agreement between the result predicted for the full and linearised isotherm up to 50% coverage. Actually the assumption of linear diffusion conditions is somewhat uncertain if separate nuclei are considered present on the electrode surface. Under these conditions hemispherical diffusion zones would spread out into the solution.

Appendix 3

Notation

d Bulk activity of ions in solution (section 1.4.).

a Activity of deposit.

a Arbitrary radius of atomic dimensions surrounding line sink (cm).

a_o Distance between neighbouring equilibrium surface positions (cm).

a_D Unit cell dimension of deposit (Å).

a_S Unit cell dimension of substrate (Å).

A Area of nucleus (cm^2).

A Geometric area of electrode surface (cm^2).

A_b Nucleation rate constant (sec^{-1}).

b Height of macroscopic surface electrode irregularity (cm).

c; C_a Adatom concentration (moles cm^{-2}).

co; C_a^o Equilibrium adatom concentration at step lines (moles cm^{-2}).

C_{Ag}^r Concentration of silver adatoms at the reversible equilibrium potential (moles cm^{-2}).

C^* Bulk concentration at ∞ (moles cm^{-3}).

C Bulk concentration at any distance from electrode (moles cm^{-3}).

C^o Surface concentration of depolariser (moles cm^{-3}).

C_o Surface concentration of atoms in electrode surface (atoms cm^{-2}).

C_{dl} Total double layer differential capacity ($\mu F\ cm^{-2}$).

C^i Differential capacity of the inner layer ($\mu F\ cm^{-2}$).

C^d Differential capacity of the diffuse layer ($\mu F\ cm^{-2}$).

C_ρ Concentration of reactant in "pre-electrode layer" (moles cm^{-3}).

Pd Spacing between crystal planes (Å).

d_1 Crystal spacing in surface plane of substrate (Å).

d_2 Crystal spacing in epitaxial overgrowth parallel to d_1 (Å).

D Bulk diffusion coefficient ($cm^2\ sec^{-1}$).

D_S Surface diffusion coefficient ($cm^2\ sec^{-1}$).

E.e.c.m. Potential of electrocapillary maximum (volt).

$E^r; E^o$ Equilibrium electrode potential (volt).

E Electrode potential (volt).

F Faraday (coulomb $equiv^{-1}$).

ΔG_{max} Free energy of formation of critical nucleus (erg).

h Height of two-dimensional growth centres (cm).

i Current (A); current density (Amp. cm^{-2}).

i_p Potential sweep peak current (Amp.).

i_o Exchange current density (Amp. cm^{-2}).

J Nucleation rate (nuclei sec^{-1}).

k Boltzmann's constant (erg deg^{-1}).

k Lattice incorporation rate constant (moles cm^{-2} sec^{-1}).

k_o Lattice growth constant at reversible potential (moles cm^{-2} sec^{-1}).

k_1 Lattice growth constant for uncharged silver adatoms (moles cm^{-2} sec^{-1}).

k_2^o Anodic reaction rate constant at the standard electrode potential (sec^{-1}).

k_f Forward homogeneous rate constant ($cm.sec^{-1}$).

k_B Backward homogeneous rate constant ($cm.sec^{-1}$).

K Dislocation density (cm^{-2}).

K Complex association constant.

$l; l'$ Distance between neighbouring dislocations (cm).

m Number of moles of deposit.

M Interfacial misfit.

M_c Critical interfacial misfit.

M Molecular weight (gm $mole^{-1}$).

n Charge on an ion.

n Fraction of sites occupied by kinks in a step line.

n_s Concentration of surface sites occupied by adsorbed molecules (cm^{-2}).

n_o Total number of crystal surface sites.

N_o Total number of surface nucleation sites.

N_o Total concentration of surface positions.

q_m Charge on metal electrode ($\mu C.cm^{-2}$).

q_1 Specifically adsorbed charge ($\mu C.cm^{-2}$).

Q_{jq} Charge (μC).

Q_c Charge at t = 0 (section 3.3) (μC).

r Radius of nucleus (cm).

r Radius of hemicylindrical diffusion zone (cm).

R Gas constant (erg deg^{-1} $mole^{-1}$).

S Surface area of crystal (cm^2).

S_o Area per molecule in a two-dimensional layer (cm^2).

t Time (sec).

t_o Induction period for nucleation (sec).

T Absolute temperature (deg).

u Age of nucleus (sec).

v Rate of advance of a spiral step ($cm.sec^{-1}$).

v_o Rate of advance of a straight step ($cm.sec^{-1}$).

v Flux of adions into growth steps (cm^{-2}).

V Molar volume of metal ($cm^3 mole^{-1}$).

w Energy of formation of kink (erg).

W_s Energy of evaporation from a kink site to the crystal surface (erg).

$\frac{1}{2} W_1$ Amplitude of potential field ($\mathring{A}$).

x Distance parallel or perpendicular to surface from growth position (cm).

x_s Mean free path of adatom (cm).

y Distance perpendicular from electrode surface (cm).

y Surface concentration of deposited metal (section 6.1.) (moles cm^{-2}).

Z Rate of arrival of molecules at surface lattice sites (sec^{-1}).

α Ratio of applied pressure p, to the equilibrium pressure p_o.

α Fraction of overpotential assisting deposition.

γ_e Specific edge free energy (erg. cm^{-2}).

δ Nernst diffusion layer thickness (cm).

ε Dielectric constant.

η Overpotential (volt).

η_i Initial overpotential (volt).

μ Force constant ($\mathring{A}^{-1}$).

μ Reaction layer thickness (cm).

ρ Metallic density ($gm.cm^{-3}$).

ρ Radius of curvature of step line (cm).

ρ_c Radius of critical nucleus (cm).

ϕ_s Potential of bulk solution (volt).

ϕ_1 Potential of inner Helmholtz plane relative to bulk solution (volt).

ϕ_2 Potential of outer Helmholtz plane relative to bulk solution (volt).

ϕ_p Potential of "pre-electrode layer" referred to that in bulk (volt).

σ Surface energy of nucleus (erg. cm^{-2}).

τ_s Lifetime of adatom (sec).

ω Linear voltage scan rate (volt sec^{-1}).

References

1. J.W. Gibbs, Collected Works, Longmans Green and Co., London, 1928, p.325.

2. W.K. Burton and N. Cabrera, Disc. Farad. Soc., 5, 33, (1949).

3. W. Kossel, Nachr. Ges. Wiss. Gottingen, 135 (1927).

4. J. Frenkel, J. Phys., Moscow, 9, 392 (1945).

5. W.K. Burton, N. Cabrera and F.C. Frank, Phil. Trans. Roy. Soc. A243, 299 (1951).

6. M. Volmer, Z. Phys. Chem. 102, 267 (1922).

7. J. Frenkel, Kinetic Theory of Liquids, Clarendon Press, Oxford, 1946.

8. M. Volmer, Z. Phys. Chem. 119, 277 (1926).

9. R. Kaischew and Z.N. Stranski, Z. Phys. Chem. B26, 317 (1934).

10. R. Becker and W. Doring, Ann. Physik. 24, 719 (1935).

11. M. Volmer, Kinetik der Phasenbildung, Steinkopff, Dresden and Leipzig, 1939.

12. M. Volmer and W. Schutze, Z. Phys. Chem. A156, 1 (1931).

13. F.C. Frank, Advances in Physics, 1, 91 (1952).

14. F.C. Frank, Disc. Farad. Soc., 5, 48 (1949).

15. J.M. Burgers, Proc. Acad. Sci. Amst. 42, 293 (1939).

16. A.R. Verma, Crystal Growth and Dislocations, Butterworths, London, 1953.

17. S. Amelinckx, The Direct Observation of Dislocations, Solid State Physics Supp. 6, Academic Press, New York, 1964.

18. E. Budewski, Electrochim. Metallorum 1., 131 (1966).

19. L. Royer, Bull. Soc. franc. Min. 51, 7 (1928).

20. D.W. Pashley, Advances in Physics, 5, 173 (1956).

21. J.H. van der Merwe, Disc. Farad. Soc., 5, 201 (1949).

22. I.N. Stranski, Z. Phys. Chem. A142, 453 (1929).

23. F.C. Frank and J.H. van der Merwe, Proc. Roy. Soc. A198, 205, 216 (1949); A200, 125, 261 (1949).

24. M. Smollett and M. Blackman, Proc. Phys. Soc. A64, 683 (1951).

25. G.I. Finch and A.G. Quarrell, Proc. Roy. Soc. A141, 398 (1939); Proc. Phys. Soc. A46, 148 (1934).

26. L.N.D. Lucas, Proc. Phys. Soc. A64, 945 (1951).

27. R.C. Newman and D.W. Pashley, Phil. Mag. 46, 917 (1955).

28. J.H. van der Merwe, J. Appl. Phys. 34, 117, 123 (1963).

29. J.H. van der Merwe, Single Crystal Films, M.H. Francombe and H. Sato (eds.), Pergamon Press, Oxford, 1964, p.139.

30. M. Gouy, J. de Phys. 9, 457 (1910).

31. D.L. Chapman, Phil. Mag. (6) 25, 475 (1913).

32. O. Stern, Z. Elektrochem. 30, 508 (1924).

33. D.C. Grahame, J. Amer. Chem. Soc. 76, 4819 (1954).

34. D.C. Grahame, J. Amer. Chem. Soc. 79, 2093 (1957).

35. J.R. MacDonald, J. Chem. Phys. 22, 1857 (1954).

36. D.C. Grahame, J. Chem. Phys. 18, 903 (1950).

37. D.C. Graham, J. Chem. Phys. 23, 1725 (1955).

38. R.J. Watts-Tobin, Phil. Mag. 6, 133 (1961).

39. J.R. MacDonald and C.A. Barlow, J. Chem. Phys. 36, 3062 (1962).

40. N.F. Mott and R.J. Watts-Tobin, Electrochim. Acta. 4, 79 (1961).

41. R.D. Armstrong, W.P. Race and H.R. Thirsk, J. Electroanal. Chem. 14, 143 (1967).

42. D.C. Grahame, Chem. Revs. 41, 441 (1947).

43. R. Parsons, Modern Aspects of Electrochemistry No. 1, J. O'M. Bockris (ed.), Butterworths, London, 1954, p.103.

44. O.A. Esin and B.F. Markov, Acta Physico chim. U.R.S.S., 10, 353 (1939).

45. O.A. Esin and V. Shikov, Zhur. fiz. Khim. 17, 236 (1943).

46. B.V. Erschler, Zhur. fiz. Khim. 20, 579 (1946).

47. D.C. Grahame, Z. Elektrochem., 62, 264 (1958).

48. J.R. MacDonald and C.A. Barlow, Proc. 1st Aust. Conf. on Electrochemistry, 1963. Pergamon Press, London, 1965, p.199.

49. V.G. Levich, V.A. Kiryanov and V.S. Krylov. Dokl. Akad. Nauk. S.S.S.R. 135, 1425 (1960).

50. G.A. Barlow and J.R. MacDonald, J. Chem. Phys. 40, 1535, (1964).

51. F.P. Buff and F.H. Stillinger, J. Chem. Phys. 39, 1911 (1963).

52. G.M. Bell, J. Mingins and S. Levine, Trans. Farad. Soc. 62, 949 (1966).

53. S. Levine, G.M. Bell and D. Calvert, Can. J. Chem. 40, 518 (1962).

54. S. Levine, J. Mingins and G.M. Bell, Can. J. Chem. 43, 2834 (1965).

55. D.C. Grahame, J. Electrochem. Soc. 98, 343 (1951).

56. D.C. Grahame, A.E. Higinbotham and F.R.M. Deane, Proc. Symp. Electrode Processes 1959, ed. Yeager, Wiley, New York (1961). p.197.

57. A.N. Frumkin, Ibid. p.207.

58. A.N. Frumkin, Electrochimica Acta 5, 265 (1961).

59. A. Obruscheva, Doklady. Akad. Nauk. S.S.S.R., 120, 1072 (1958).

60. A.N. Frumkin and A. Titevskaya, Zhur. fiz. Khim. 31, 485 (1957).
A.N. Frumkin and N. Polianovskaya, Zhur. fiz. Khim. 32, 157 (1958).

61. V.G. Levich, Dokl. Akad. Nauk, S.S.S.R., 67, 309 (1949).

62. K.J. Sparnaay, Trans. Farad. Soc. 53, 306 (1957).

63. A.N. Frumkin, Trans. Farad. Soc. 55, 156 (1959).

64. A.N. Frumkin, Z. physk. Chem. 164, 121 (1933).

65. J. Horiuti and M. Polanyi, Acta Physicochim U.R.S.S., 2, 505 (1935).

66. J.A.V. Butler, Proc. Roy. Soc. A157, 423 (1936).

67. R. Parsons and J. O'M. Bockris, Trans. Farad. Soc. 47, 914 (1951).

68. B,E. Conway and J. O'M. Bockris, Can. J. Chem. 35, 1124 (1957).

69. idem. Proc. Roy. Soc. A248, 394 (1958).

70. idem. Electrochimica Acta 3, 340 (1961).

71. R. Parsons, Modern Aspects of Electrochemistry (ed. J.O'M. Bockris) Vol.I, Butterworth London (1954), p.170.

72. E. Mattson and J.O'M. Bockris, Trans. Farad. Soc. 55, 1586 (1959).

73. W. Lorenz, Z. Naturforschung 750 (1952), Z. physik. Chem. 202, 275 1953), Z. Elektrochem 57, 382 (1953), Z. Naturforschung 9A, 716 (1954).

74. D.A. Vermilyea, J. Chem. Phys. 25, 1254 (1956).

75. R. Piontelli, Proc. 2nd Reunion of C.I.T.C.E. Tamburini, Milan (1950) p.136.

76. M. Fleischmann and H.R. Thirsk, Electrochimica Acta 2, 22 (1960).

77. M. Volmer and A. Weber, Z. phys. Chem. 119, 277 (1926).

78. H. Gerischer and R.P. Tischer, Z. Elektrochem, 61, 1159 (1957).

79. M. Fleischmann and J.A. Harrison, Electrochimica Acta, 11, 749 (1966).

80. C. Kasper, Trans. Electrochem. Soc. 77, 353 (1940).

81. M. Fleischmann and J.A. Harrison, Trans. Farad. Soc. 61, 2742 (1965).

82. M. Fleischmann and H.R. Thirsk, Advances in Electrochemistr and Electrochemical Engineering, (ed. P. Delahay) Vol.3, Interscience, New York (1963).

83. M. Fleischmann and J.A. Harrison, J. Electroanal. Chem, 12, 183 (1966).

84. M. Fleischmann, S.K. Rangarajan and H.R. Thirsk, Trans. Farad. Soc. 63, 1240 (1967).

85. M. Fleischmann, S.K. Rangarajan and H.R. Thirsk, Trans. Farad. Soc. 63, 1256 (1967).

86. J. O'M. Bockris, H. Kita and M. Enyo, Can. J. Chem. 39, 1670 (1961).

87. J. O'M. Bockris and M. Enyo, Trans. Farad. Soc., 58, 1187 (1962).

88. J.O'M. Bockris and H. Kita, J. Electrochem. Soc. 109, 928 (1962).

89. J.O'M. Bockris and W. Mehl, J. Chem. Phsy. 27, 818 (1959).

90. idem. Can. J. Chem. 37, 190 (1959).

91. J.O'M. Bockris and A.R. Despic, J. Chem. Phys. 32, 389 (1960).

92. E. Budewski, W. Bostanoff, T. Vitanoff, Z. Stoinoff, A. Kotzewa and R. Kaischew, Phys. Stat. Sol., 13, 577 (1966).

93. H. Gerischer and M. Krause, Z. Physik. Chem. NF10, 264 (1957).

94. idem, ibid NF14, 184 (1958).

95. J.A. Harrison, S.K. Rangarajan and H.R. Thirsk, J. Electrochem. Soc., 113, 1120 (1966).

96. A. Bewick, A. Bewick, M. Fleischmann and M. Liles, Electrochim. Acta. 1, 83 (1959).

97. A. Bewick and M. Fleischmann, Electrochim Acta, 8, 89 (1963).

98. A. Bewick and O.R. Brown, J. Electroanal. Chem. 15, 129 (1967).

99. O.R. Brown Electrochim Acta, 13, 317 (1968).

100. R. Shuttleworth, R. King and B. Chalmers, Metal Treatment, 14, 161 (1957).

101. A.W. Moulen, J. Electrochem. Soc., 99, 1330 (1952).

102. R. De Levie "Advances in Electrochemistry and Electrochemical Engineering" Ed. P. Delahay. Interscience Publishers, Vol.6, 329 (1967).

103. W.M. Krebs and D.K. Roe, J. Electrochem. Soc. 114, 892 (1967).

104. "Numerical Methods", A.D. Booth, Butterworths (1955) p.114.

105. T. Berzins and P. Delahay, J. Amer. Chem. Soc. 75, 555 (1953).

106. O.R. Brown, Ph.D. Thesis, University of Durham (1963).

107. M. Fleischmann and M. Liler, Trans. Farad. Soc., 54, 1370 (1958).

108. Yu.M. Polukarov and G.A. Feklistov, Electrokhimiya, 3, 323 (1967).

109. H.A. Droll, Ph.D. Thesis (Penn. State University) (1956) Univ. Microfilms 16705.

110. D.H. Templeton, G.W. Watt and C.S. Garner, J. Amer. Chem. Soc. 65, 1608 (1943).

111. V.I. Kravstov and M.I. Zelenskii, Elektrochimiya, 2, 1138 (1966).

112. M. Sluyters-Rehbach and J.H. Sluyters, Rec. Trav. Chim. 83, 983 (1964).

113. H. Imai and P. Delahay, J. Phys. Chem. 66, 1108 (1962).

114. H. Matsuda, S. Oka and P. Delahay, J. Amer. Chem. Soc. 81, 5077 (1959).

115. H. Gerischer and K.E. Staubach, Z. Phys. Chem. NF6, 118 (1956).

116. C. Berecki-Biedermann, G. Biedermann and L.G. Sillen, Report to Analytical Section, IUPAC, July (1953).

117. S. Hietanen and L.G. Sillén, Arkiv. Kemi, 10, 103 (1956)

118. E. Schmidt and H.R. Gygax, J. Electroanal. Chem., 12, 300 (1966).

119. idem, Helv. Chim. Acta, 49, 733 (1965).

120. idem, ibid. 48, 1178 (1965).

121. idem, ibid. 48, 1584 (1965).

122. J.M. Hale and R. Greef, Electrochim. Acta 12, 1409 (1967)

123. S. Srinivasan and E. Gileadi, ibid. 11, 321 (1966).

124. M.W. Breiter, Trans. Farad. Soc. 62, 2887 (1966).

125. A. Bewick, M. Fleischmann and H.R. Thirsk, Trans. Farad. Soc. 58, 2200 (1962).

126. M. Fleischmann, J. Pattison and H.R. Thirsk, Trans. Farad. Soc. 61, 1256 (1965).

127. I. Dugdale, M. Fleischmann and W.F.K. Wynne-Jones, Electrochim. Acta, 5, 229 (1961).

128. C.A. Streuli and W.D. Cooke, Anal. Chem. 25, 1691 (1953)

129. R.D. Armstrong, M. Fleischmann and J.W. Oldfield, J. Electroanal. Chem., 14, 235 (1967).

130. V.J. Veselovsky, Acta. physicochim, U.R.S.S. 11, 815 (1939).

131. P. Delahay and I. Trachtenberg, J. Amer. Chem. Soc., 79, 2355 (1957).

132. W.H. Reinmuth, J. Phys. Chem., 65, 473 (1961).

133. P. Delahay, J. Amer. Chem. Soc. 73, 4944 (1951).

134. S. Bordi, Ann. Chim. (Italy) 48, 811 (1958).

135. R.D. Armstrong, Ph.D. Thesis, University of Newcastle upon Tyne (1965).

136. M.M. Nicholson, Anal. Chem., 32, 1058 (1960).

137. idem, J. Amer. Chem. Soc., 79, 7 (1957).

138. S.P. Perone, Anal. Chem. 35, 2091 (1963).

139. B.H. Vassos and H.B. Mark, J. Electroanal. Chem. 13, 1 (1967).

140. R.C. De Geiso and L.B. Rogers, J. Electrochem. Soc., 106, 433 (1959).

141. L.B. Rogers, D.P. Krause, J.C. Griess and D.B. Ehrlinger, J. Electrochem. Soc. 95, 33 (1949).

142. D. Kyriacov, Anal. Chem., 37, 1036 (1965).

143. S.P. Perone and W.F. Gutknecht, Anal. Chem., 39, 892 (1967).

144. B.K. Hovsepian and I. Shain, J. Electroanal. Chem., 12, 397 (1966).

145. W.M. Latimer, "Oxidation Potentials", 2nd Edn. Prentice-Hall, New York, (1952).

146. R. Brdička, Coll. Czech. Chem. Comm., 2, 489 (1930)

147. idem, Ibid, 3, 396 (1931).

148. E.T. Verdier and G. Baptiste, J. Electroanal.Chem., 10, 42 (1965).

149. J.J. Polestá, Rev. Fac. Cienc. Quim. La Plata 30, 61 (1957).

150. J.J. Tondeur, A. Drombret and L. Gierst., J. Electroanal. Chem., 3, 225 (1962).

151. J.H. Green and A. Walkley, Aust. J. Chem., 8, 51 (1955).

152. G.N. Babkin, Russ. Phys. Chem. 1, 73 (1965).

153. M. Lehné, Bull. Soc. Chim. France, 76 (1951).

154. A.E. Brodsky, Z. Elektrochem. 35, 833 (1929).

155. W. Kemula and Z. Galus, Bull. Acad. Polon. Sci., Ser. Sci. Chim. Geol. Geograph., 7, 729 (1959).

156. W. Kemula, L. Jeftić and Z. Galus, J. Electroanal. Chem., 10, 387 (1965).

157. H.K. Ficker and L. Meites, Anal. Chim. Acta. 26, 172 (1962).

158. J. Koutecky and R. Brdička, Coll. Czech. Chem. Comm., 12, 337 (1947).

159. Y.I. Turyan and G.F. Serova, Russ. Phys. Chem. 34, 480 (1960).

160. S. Fronaeus, Acta. Chem. Scand. 7, 21 (1953).

ACKNOWLEDGEMENTS

I wish to thank Professor H.R. Thirsk for initiating and supervising this work. I am greatly indebted to Dr. J.A. Harrison for his continued advice and guidance throughout the course of this work.

My thanks are due to Mr. E.H. Boult for assistance with the electron microscopy and to the Science Research Council for the provision of a Research Studentship.